DETERMINING THE FUNCTIONAL IMPACT OF KSHV INFECTION OF ENDOTHELIAL CELLS

By

HANNAH CLAIRE JEFFERY

A thesis submitted to The University of Birmingham for the degree of

DOCTOR OF PHILOSOPHY

Schools of Cancer Sciences and Clinical and Experimental Medicine

College of Medical and Dental Sciences

The University of Birmingham

May 2012

ABSTRACT

Kaposi's sarcoma-associated herpesvirus (KSHV) is the aetiologic agent of Kaposi's sarcoma (KS), a malignancy characterised by spindle-shaped tumour cells with an endothelial phenotype that line primitive vascular structures. This thesis examines the concept that KSHV infection of primary endothelial cells alters their migration, supporting development of the extensive aberrant angiogenesis seen in KS.

Primary human umbilical vein endothelial cells were infected with KSHV and their migration examined at time points between one and ten days post-inoculation. Infected cells transmigrated preferentially across porous filters compared to untreated or non-infected cells, and wounds in inoculated monolayers closed more rapidly compared to untreated cultures. Several cellular properties which might regulate cell migration rates were altered by KSHV inoculation. The virus modulated the laminin profile of the sub-endothelial matrix by reducing laminin-P1 deposition but increasing that of the laminin-α4 chain. No effect on deposition of either fibronectin or collagen IV was found. An increase in cell-surface expression of the laminin-binding integrin-α6 subunit was also detected with infection. Furthermore, KSHV infection partitioned actin stress fibres to the cell cortex and reduced the size and number of focal adhesions per cell. These results support a pro-migratory, pro-angiogenic effect of KSHV on endothelial cells that might be targeted to treat KS.

DEDICATION

I dedicate this thesis to my mother, sister and late father who have provided continual support and encouragement throughout my education.

ACKNOWLEDGEMENTS

The work described in this thesis was funded by the Medical Research Council (MRC) and carried out in the Schools of Cancer Sciences and Clinical and Experimental Medicine at The University of Birmingham, during the period October 2007 to March 2012. Except where stated, it is the original work of Hannah C. Jeffery. This thesis has not been submitted, in part or in totality to any other university.

Firstly, I would like to thank my supervisors, Professors David Blackbourn and Gerard Nash, for their guidance throughout my studies and for proof-reading and advising on my end-of year reports, abstracts that I have submitted for attendance at conferences and this thesis. I am extremely grateful for all that they have taught me on my journey to becoming a scientist.

Secondly I would like to thank Dr Lynn Butler for all of her input in the design of my experiments and for being a great friend and support throughout my studies. Her encouragement helped me to 'soldier on' during the low times.

Thirdly I would like to thank Miss Rachel Wheat and the late Mr Philip Stone for their assistance as laboratory technicians and especially for showing me the techniques of virus culture and HUVEC isolation respectively when I first joined the lab.

Fourthly I thank all my other lab colleagues for the advice that they have provided on their individual techniques of expertise and for their friendship in making the working environment a pleasant place to be each day. Special acknowledgement to Dr Clara Yates who performed the Luminex on a set of supernatants I collected in this study.

Finally, outside of my lab groups, I acknowledge the following people for their contributions during my studies: Dr. Jeffrey Vieira (University of Washington, USA) for his generous gift of the VK219 cell line used for production of rKSHV.219 in these studies; Professor Paul Kellam (Wellcome Trust, Sanger Institute, UK) for his generous gift of a panel of PCR primers for amplification of KSHV mRNAs including vFLIP used in this study; Dr. Sukhbir Kaur (University of Birmingham, UK) for her advice on the immunofluorescence assay protocol (Chapter 6) to analyse F-actin and vinculin distribution in HUVEC; Dr. David Kelly (Wellcome Trust Centre for Cell Biology, University of Edinburgh, UK) who worked with me to write a macro in Image-Pro for analysis of F-actin distribution; and all the mothers attending the Birmingham Women's hospital who consented to donate the umbilical cords from their babies for research.

CONTENTS

Chapter One: Introduction 0

1.1 Kaposi's sarcoma-associated herpesvirus (KSHV) 1

1.1.1 Classification 1

1.1.2 Structure of the KSHV virion 3

1.1.3 The KSHV genome 4

1.1.4 The KSHV lifecycle 7

1.1.5 Incidence and transmission of KSHV infection 7

1.1.6 Cell types infected by KSHV 10

1.1.7 The mechanism of KSHV infection 10

1.1.8 Diseases associated with KSHV infection 13

1.1.8.1 Primary Effusion Lymphoma (PEL) 13

1.1.8.2 Multicentric Castleman's Disease (MCD) 13

1.2 Kaposi's sarcoma (KS) 14

1.2.1 Histology of KS lesions 14

1.2.2 The epidemiologic forms of KS 16

1.2.3 Risk factors for KS 19

1.2.4 Identification of KSHV as the aetiologic agent for KS 23

1.3 Endothelial cells 25

1.3.1 Overview of endothelial cell functions 25

1.3.2 Mechanisms of tumour angiogenesis 31

1.3.2.1 Sprouting angiogenesis 33

1.3.3 The mechanism of cell migration 37

1.3.4 Integrins 38

1.3.5 Focal adhesions 44

1.4 The extracellular matrix (ECM) 50

1.4.1 Laminins 51
1.4.2 Collagens 54
1.4.3 Fibronectin 57
1.4.4 Extracellular matrix proteins as chemotactic and haptotactic stimuli 59
1.5 Effects of KSHV infection on endothelial cell identity 61
1.6 Impact of KSHV infection upon endothelial cell motility 64
1.7 Objectives of this thesis 66
Chapter Two: Methods 68
2.1 Cell Culture 69
2.1.1 Maintenance of cell lines 69
2.1.1.1 BCBL-1 cells 69
2.1.1.2 HEK293 cells 69
2.1.1.3 VK219 cells 70
2.1.1.4 Human dermal lymphatic endothelial cells (LEC) 71
2.1.1.5 Isolation of neutrophils from whole blood 71
2.1.2 Production of KSHV 72
2.1.2.1 Production of KSHV from BCBL-1 cells 72
2.1.2.1.1 Sucrose cushion method for harvest of KSHV from supernatants of reactivated BCBL-1 cells 73
2.1.2.1.2 Standard method for harvest of KSHV from supernatants of reactivated BCBL-1 cells 74
2.1.2.2 Production of rKSHV.219 from VK219 cells 74
2.1.2.3 Production of Baculovirus K50 (BacK50) 75
2.1.2.4 Determination of BacK50 titre 76
2.1.2.5 Determination of rKSHV.219 titre 77
2.1.3 Isolation and culture of human umbilical vein endothelial cells (HUVEC) 78
2.1.3.1 Isolation of HUVEC from umbilical cord veins 79
2.1.3.2 Detachment of HUVEC from 25cm^2 flasks 80

2.1.3.3 Detachment of HUVEC from 24-well plates 80
2.1.3.4 Freezing HUVEC for storage in liquid nitrogen 81
2.1.3.5 Reviving HUVEC from storage in liquid nitrogen 81
2.1.4 Inoculation of HUVEC with rKSHV.219 82
2.2 Flow cytometry 82
2.2.1 Antibodies 82
2.2.2 Determining the percentage infection of rKSHV.219-inoculated cell cultures 83
2.2.3 Staining surface antigens 83
2.2.4 Staining intracellular antigens 85
2.2.4.1 Staining intracellular antigens using the Fix and Perm Kit by Invitrogen 85
2.2.4.2 Staining phospho-p38 MAPK 85
2.3 Migration assays 90
2.3.1 Transmigration assay 90
2.3.2 Transmigration assay to determine percent transmigration of KSHV-infected and non-infected HUVEC individually 91
2.3.3 Wound recovery assay 92
2.3.3.1 Wound recovery assay on 24hour sub-endothelial matrices deposited by KSHV-inoculated and untreated HUVEC 93
2.3.4 Tracking the migration of HUVEC in isolation 94
2.3.5 Tracking the migration of HUVEC during wound recovery 95
2.4 Analysis of basement membrane composition by enzyme-linked immunosorbent assay (ELISA) 101
2.5 Luminex 102
2.6 RNA isolation and Polymerase Chain Reaction (PCR) 104
2.6.1 RNA isolation 104
2.6.2 cDNA synthesis 105
2.6.3 PCR 105
2.7 Immunofluorescence assay 109

2.7.1 Immunofluorescence assay for LANA-1 following inoculation of HUVEC with BCBL-1 derived KSHV 109
2.7.2 Immunofluorescence assay for analysis of LANA-1 dots and coincident GFP expression in rKSHV.219-infected HUVEC 110
2.7.3 Immunofluorescence assay for analysis of actin cytoskeleton organisation and focal adhesion (vinculin) distribution in KSHV infected HUVEC 111
2.8 siRNA transfection of HUVEC 113
2.8.1. Sources and preparation of siRNA. 113
2.8.2 Assay to examine the impact of laminin-α4 knockdown on the transmigration of HUVEC and their intracellular synthesis and deposition of the laminin-α4 chain. 114
2.9 Immunofluorescence Image analysis 117
2.9.1 Measurement of cell shape parameters 117
2.9.2 Concentric ring analysis of F-actin distribution 117
2.9.3 Concentric ring analysis of F-actin distribution based on intensity line profiles for rhodamine-phalloidin 119
2.9.4 Analysis of focal adhesion size, number and distribution based on immunofluorescence assay for vinculin. 119
2.10 Analysis of the effect of KSHV-inoculation upon cell density over time 123
2.11 Assay to examine horizontal transmission of infection through KSHV-inoculated HUVEC monolayers 126
2.12 Microscopes used: 128
2.13 Statistics 128
2.14 Suppliers of the reagents, equipment and software used in these studies 129

Chapter Three: Development and characterisation of an *in vitro* system to study the functional effects of KSHV infection of primary endothelial cells 132

3.1 Introduction 133

3.2 Results 134

3.2.1 Infection of HUVEC with BCBL-1 derived KSHV 134

3.2.2 Production of rKSHV.219 for use in infection studies 134

3.2.3 Infection of HUVEC with rKSHV.219 139

3.3 Discussion 152

Chapter Four: Effect of KSHV infection upon endothelial cell motility.....162

4.1 Introduction 163

4.2 Results 164

4.2.1 Development of a transmigration assay 164

4.2.2 The effect of KSHV infection upon endothelial cell transmigration 165

4.2.3 Development of a wound recovery assay 171

4.2.4 The effect of KSHV infection upon endothelial cell wound recovery 175

4.2.5 The effect of KSHV infection upon the motility of isolated endothelial cells 182

4.3 Discussion 187

Chapter Five: Effect of KSHV infection upon endothelial cell deposition of basement membrane proteins and surface expression of integrin receptors.....194

5.1 Introduction 195

5.2 Results 196

5.2.1 Establishment of a suitable cell removal method for subsequent analysis of the sub-endothelial matrix by ELISA. 196

5.2.2 The effect of KSHV infection on the production and secretion of basement membrane components by endothelial cells 198

5.2.3 The effect of deposited matrices on endothelial cell migration 214
5.2.4 The effect of reducing laminin-α4 chain expression on endothelial cell migration 216
5.2.5 The effect of KSHV infection on the expression of endothelial cell surface integrins 222
5.3 Discussion 226

Chapter Six: Effect of KSHV infection upon the endothelial cell actin cytoskeleton and focal adhesions 238

6.1 Introduction 239
6.2 Results 239
6.2.1 The effect of KSHV infection on the size and shape of HUVEC 241
6.2.2 The effect of KSHV infection on the organisation of F-actin in HUVEC 241
6.2.3 The effect of KSHV-infection on the distribution of focal adhesions in HUVEC 252
6.3 Discussion 258

Chapter Seven: Effects of KSHV-induced chemokines and growth factors on enhanced migration of KSHV-infected endothelial cells 264

7.1 Introduction 265
7.2 Results 266
7.2.1 The impact of KSHV inoculation on the secretion of IL-6, IL-8 and IP-10 by HUVEC 266
7.2.1.1 Investigating a role for IL-8 in the enhanced transmigration of KSHV-infected HUVEC 268
7.2.1.2 Investigating a role for IP-10 in the enhanced transmigration of KSHV-infected HUVEC 270
7.2.2 The impact of KSHV infection on the pro-angiogenic VEGFC/VEGFR3 axis 272
7.2.3The impact of KSHV infection on p38 MAPK activity 274
7.3 Discussion 278

Chapter Eight: General Discussion 285

Chapter Nine: Appendix **302**

References **304**

LIST OF FIGURES

Chapter One

Figure 1.1: Phylogenetic dendrogram of the taxonomic family *Herpesviridae*. 2

Figure 1.2: The three-layered architecture of herpesvirus virions. 3

Figure 1.3: The KSHV genome. 6

Figure 1.4: The macroscopic and cellular appearance of KS lesions. 16

Figure 1.5: The process of sprouting angiogenesis. 36

Figure 1.6: The major steps in cell migration. 38

Figure 1.7: Diagrammatic representation of a universal integrin receptor. 42

Figure 1.8: The integrin receptor family. 43

Figure 1.9: Diagrammatic representation of a focal adhesion. 48

Figure 1.10: Diagrammatic representations of laminins 411 and 511. 53

Figure 1.11: Diagrammatic representation of collagen IV network formation. 56

Figure 1.12: Diagrammatic representation of a fibronectin subunit. 58

Chapter Two

Figure 2.1: Schematic diagram of the rKSHV.219 genome 71

Figure 2.2: Assessment of percent KSHV infection by flow cytometry quantifying GFP expression. 87

Figure 2.3: Transmigration assay set up and analysis. 96

Figure 2.4: Wound recovery assay set up. 97

Figure 2.5: Method for analysis of wound recovery. 99

Figure 2.6: Strategy for analysis of isolated cell migration. 100

Figure 2.7: The principle underlying the macro devised in Image-Pro for concentric ring analysis of F-actin distribution. 118
Figure 2.8: Strategy for concentric ring analysis of F-actin distribution based on intensity line profiles of rhodamine-phalloidin staining. 120
Figure 2.9: Strategy for analysis of focal adhesion size and number. 122
Figure 2.10: Strategy for analysis of viable and lytic cell densities. 125

Chapter Three

Figure 3.1: Comparison of BCBL-1 derived KSHV preparations for infection of HUVEC. 136
Figure 3.2: Effect of storage time upon KSHV titre. 137
Figure 3.3: Effect of storage temperature upon KSHV titre. 138
Figure 3.4: Effect of KSHV titre on infection of HUVEC. 140
Figure 3.5: Effect of HUVEC density upon KSHV infection efficiency. 141
Figure 3.6: Effect of time post KSHV inoculation on cell morphology, GFP expression and RFP expression. 142
Figure 3.7: Effect of time post-inoculation on the extent of KSHV infection within HUVEC monolayers. 143
Figure 3.8: Quantification of the extent of horizontal transmission of KSHV infection through HUVEC monolayers. 146
Figure 3.9: Quantification of the extent of horizontal transmission of KSHV infection through HUVEC monolayers. 148
Figure 3.10: Quantification of the number of KSHV LANA-1 dots in the nuclei of GFP positive and GFP negative HUVEC from KSHV-inoculated cultures at 24hours post-inoculation. 149

Figure 3.11: Effect of KSHV inoculation upon HUVEC monolayer densities.....150
Figure 3.12: Poisson distributions for the proportion of cells in a population that are expected to be infected with k infectious units when inoculated with virus at multiplicities of infection (MOIs) between 0.1 and 10. 159
Figure 3.13: Poisson distribution for the proportion of cells in a population that are expected to be infected with k infectious units when inoculated with virus at a multiplicity of infection (MOI) of 1.6. 160

Chapter Four

Figure 4.1: Effect of pore size and duration of assay upon the endpoint percent transmigration of HUVEC.....167
Figure 4.2: Effect of duration of KSHV infection upon the transmigration of HUVEC. 168
Figure 4.3: Comparison of transmigration by KSHV-infected, non-infected and untreated HUVEC. 169
Figure 4.4: Effect of culture supernatants from KSHV-inoculated HUVEC on HUVEC transmigration.....170
Figure 4.5: Developmment of a wound recovery assay to examine the effect of KSHV on HUVEC migration at day-seven post-inoculation. 173
Figure 4.6: Effect of KSHV infection on HUVEC wound recovery. 176
Figure 4.7: Effect of cell density on KSHV-enhanced wound recovery. 177
Figure 4.8: Effect of KSHV inoculation on start and endpoint cell numbers in fields analysed in the wound recovery assay. 180
Figure 4.9: Comparison of the distances migrated by infected and non-infected cells at the edges of wounded monolayers. 181

Figure 4.10: Effect of KSHV infection on the distances migrated by sparsely distributed HUVEC. 183
Figure 4.11: Effect of KSHV infection on the migration pathways of sparsely distributed HUVEC. 184
Figure 4.12: Effect of KSHV on the persistence of migration of sparsely distributed HUVEC. 186

Chapter Five

Figure 5.1: Comparisons of cell removal methods to expose the sub-endothelial matrix for analysis by ELISA. 197
Figure 5.2: Effect of KSHV inoculation on the protein content of sub-endothelial matrix. 200
Figure 5.3: Relationship between cell density and matrix protein deposition. 201
Figure 5.4: Effect of long-term KSHV inoculation on the protein content of sub-endothelial matrix. 203
Figure 5.5: Effects of culture supernatants from KSHV-inoculated cultures on the composition of previously deposited sub-endothelial matrix. 205
Figure 5.6: Effects of inhibitors of matrix-metalloproteinases or serine proteases on KSHV-induced suppression of laminin deposition in the sub-endothelial matrix. . 206
Figure 5.7: Effect of KSHV inoculation on intracellular levels of laminin. 208
Figure 5.8: Effect of the number of PCR amplification cycles upon the resolution of a cDNA titration when analysed by ethidium bromide gel electropheresis. 209
Figure 5.9: Effect of KSHV inoculation on transcript levels of endothelial laminin subunits. 210

Figure 5.10: Effect of KSHV inoculation on the laminin-alpha chain content of sub-endothelial matrix. 212
Figure 5.11: Effect of KSHV inoculation on intracellular levels of the laminin-α4 chain. 213
Figure 5.12: Effects of matrix proteins, deposited by KSHV-inoculated (KSHV-EC) or untreated (UT-EC) HUVEC cultures, upon HUVEC migration. 215
Figure 5.13: Comparison of the efficiency of siRNA duplexes in knockdown of the laminin-α4 chain in HUVEC. 218
Figure 5.14: Comparison of the efficacy of siRNA duplexes used singly and in combination in knockdown of the laminin-α4 chain in HUVEC. 219
Figure 5.15: Effects of laminin-α4 chain siRNA on laminin-α4 content and deposition, and on transmigration for KSHV-inoculated (KSHV-EC) and untreated (UT-EC) HUVEC. 220
Figure 5.16: The effect of KSHV inoculation upon the HUVEC surface-integrin expression profile. 223
Figure 5.17: The effect of KSHV inoculation upon the HUVEC surface-integrin expression profile. 224
Figure 5.18: Effect of blocking integrin α6 on KSHV-enhanced transmigration of HUVEC. 225

Chapter Six

Figure 6.1 Effect of KSHV infection on the organization of F-actin and the distribution of focal adhesions in HUVEC. 240
Figure 6.2: Effect of KSHV infection on the size and shape of HUVEC. 244
Figure 6.3: Effect of KSHV infection on the organisation of F-actin in HUVEC. ... 246

Figure 6.4: Effect of KSHV infection on the amount of F-actin in HUVEC.....248
Figure 6.5: Concentric ring analysis of the effect of KSHV infection on the distribution of F-actin in HUVEC. 249
Figure 6.6: Line profile analysis of the effect of KSHV infection on the distribution of F-actin in HUVEC. 250
Figure 6.7: Effect of KSHV infection on the size, number and distribution of focal adhesions in HUVEC. 253
Figure 6.8: Patterns of phalloidin and anti-vinculin staining in HUVEC. 255
Figure 6.9: Effect of KSHV infection on the number and size of focal adhesions in HUVEC. 256

Chapter Seven

Figure 7.1: Effect of KSHV inoculation on the secretion of IL-6, IL-8 and IP-10 by HUVEC. 267
Figure 7.2: Effect of KSHV infection on cell surface expressions of CXCR1 and CXCR2.....269
Figure 7.3: PCR for KSHV-vGPCR. 271
Figure 7.4: Effect of blocking IP-10 activity upon KSHV-enhanced transmigration of HUVEC. 271
Figure 7.5: Effect of KSHV inoculation of HUVEC on cell surface expression of VEGFR3. 273
Figure 7.6: Effect of inhibition of p38 MAPK activity on KSHV enhanced transmigration of HUVEC.....276
Figure 7.7: Effect of KSHV-infection on baseline p38 MAPK activity. 277

LIST OF TABLES

Table 1.1: Proteins present in focal adhesions and their functions. 49

Table 2.1: Antibodies used in the studies reported in this thesis 88

Table 2.2: Primer sequences and conditions for PCR 108

Table 2.3: siRNA duplexes 114

Table 2.4: Addresses for the suppliers of equipment, reagents and software used in these studies 129

Table 9.1: Determination of the percentage transmigration of KSHV-infected (V) and non-infected (NI) HUVEC by calculation from the results of parallel 48hour transmigration assays with microscopic and flow cytometry readout. 303

ABBREVIATIONS

AIDS	Acquired Immunodeficiency Syndrome
ANG	Angiopoietin
AP-1	Activator protein 1
ARP	Actin related protein
BacK50	Baculovirus K50
BEC	Blood vascular endothelial cells
bFGF	Basic fibroblast growth factor
BM	Basement membrane
BSA	Bovine serum albumin
cAMP	Cyclic adenosine monophosphate
CAS	Crk-associated substrate
CD	Cluster of differentiation molecule
cGMP	Cyclic guanosine monophosphate
CRP	Cysteine-rich protein
Csk	Carboxy-terminal src kinase
CXCR	C-X-C chemokine receptor
DC-SIGN	Dendritic cell-specific intercellular adhesion molecule-3-grabbing non-integrin
DLL4	Delta-like ligand 4
DMSO	Dimethyl sullfoxide
dsDNA	Double-stranded deoxyribonucleic acid
EBNA	Epstein-Barr virus nuclear antigen
EBV	Epstein-Barr virus
EC	Endothelial cell
ECM	Extracellular Matrix
EDTA	Ethylene diaminetetracetic acid
EGF	Epidermal growth factor
EHS	Engelbreth-Holm-Swarm
ELSA	Enzyme-linked immunosorbent assay
ERK	Extracellular signal-regulated kinase
ERM	Ezrin-radixin-moesin
F-actin	Filament actin
FAK	Focal adhesion kinase
FBS	Foetal bovine serum
FCGR3A	Fc Fragment of the IgG low affinity IIIa receptor
FCS	Foetal calf serum
Fc	Fragment crystallisable
FGF	Fibroblasr growth factor
GAP	GTPase activating protein
gB	Glycoprotein B
GEF	Guanine nucleotide exchange factor
GFP	Green fluoresecent protein

GlyCAM-1	Glycosylation dependent cell adhesion molecule 1
Grb	Growth factor receptor-bound protein
Gro-a	Growth regulated oncogene-alpha
GTP	Guanosine triphosphate
HAART	Highly active anti-retroviral therapy
HCMV	Human cytomegalovirus
HEV	High endothelial venules
HHV8	Human herpesvirus eight
HIV	Human immunodeficiency virus
HLA	Human leukocyte antigen
HRP	Horseradish peroxidase
HSV	Herpes simplex virus
HUVEC	Human umbilical vein endothelial cells
HVS	Herpesvirus Saimiri
IARC	International Agency for Research on Cancer
IFNg	Interferon gamma
IL	Interleukin
ILK	Integrin-linked kinase
IP-10	Interferon gamma-induced protein 10
KS	Kaposi's sarcoma
KSHV	Kaposi's sarcoma-associated herpesvirus
KSHV-EC	KSHV-inoculated HUVEC
LANA-1	Latency associated nuclear antigen-1
LAR	Leukocyte common antigen receptor
Lay	Layilin
LEC	Lymphatic endothelial cells
LMP	Latent membrane protein
LYVE-1	Lymphatic vessel endothelial hyaluronan receptor
MAdCAM-1	Mucosal addressin cell adhesion molecule-1
MAPK	Mitogen-activated protein kinase
MCD	Multicentric Castleman's Disease
MCP-1	Monocyte chemotactic protein-1
MHC	Major histocompatability complex
MHV-68	Murine gammaherpesvirus 68
MLEC	Mouse lung endothelial cells
MMP	Matrix metalloproteinases
mRNA	Messenger ribonucleic acid
NC1	Carboxy-terminus non-collagenous
NI	Non-infected HUVEC from KSHV-EC culture
NPC	Nasopharyngeal carcinoma
ORF	Open reading frame
PAF	Platelet activating factor

PAK	p21-activated kinase
Pall	Palladin
PBMC	Peripheral blood mononuclear cells
PBS	Phosphate buffered saline
PBSA	PBS supplemented with BSA
PCR	Polymerase chain reaction
PDGF	Platelet derived growth factor
PEL	Primary Effusion Lymphoma
PI3K	Phosphatidylinositol 3-kinase
PIPKγ	Phosphatidylinositol phosphate kinase-γ
PIX	PAK-interacting exchange factor
PKB	Protein kinase B
PKL	Paxillin kinase linker
PlGF	Placenta-derived growth factor
PMA	Phorbal myristate acetate
PROX-1	Prospero homeobox protein-1
PtdIns	Phosphatidylinositol
$PtdIns(4,5)P_2$	Phosphatidylinositol 4,5 bisphosphate
RFP	Red fluorescent protein
RGD	Arginine-Glycine-Aspartate
RNA	Ribonucleic acid
RRV	Rhesus monkey Rhadinovirus
RTA	Lytic switch and transcription activator protein
SH2	Src homology-2
SH3	Src homology-3
SHIP-2	SH2-containing inositol 5-phosphatase-2
SHP-2	SH2-containing phosphatase-2
SHPS-1	SHP-2 substrate-1
siRNA	Small interfering RNA
Src	Src-family kinases
Syn-4	Syndecan-4
Synd	Syndesmos
Synt	Syntenin
TGFb	Transforming growth factor beta
Th	T-helper
TIME	Telomerase immortalized microvascular endothelial
TNFa	Tumour necrosis factor alpha
uPAR	Urokinase plasminogen activator receptor
UT-EC	Untreated HUVEC
UV	Ultra violet
UV-KSHV-EC	UV-irradiated KSHV-inoculated HUVEC

V	KSHV-infected HUVEC
VASP	Vasodilator-stimulated phosphoprotein
VCAM-1	Vascular cell adhesion molecule-1
VEGF	Vascular endothelial growth factor
VEGFR	Vascular endothelial growth factor receptor
vFLIP	Viral FLICE inhibitory protein
vGPCR	Viral G protein-coupled receptor
WASP	Wiscott-Aldrich Syndrome Protein
WAVE	Wiscott-Aldrich family verprolin homologous protein
xCT	Cysteine/glutamate exchange transporter system

Throughout this thesis, which involves the inoculation of HUVEC with KSHV, the cell types generated are defined in the figures by the following abbreviations (see also section 2.2):

Untreated (UT-EC) or (UT): Control cells inoculated with blank culture medium

KSHV-inoculted (KSHV-EC): Cells inoculated with infectious KSHV

UV-irradiated KSHV-inoculated (UV-KSHV-EC): Cells inoculated with KSHV that had been inactivated by UV irradiation

KSHV-infected (V): Cells wthin the KSHV-inoculated culture that on the basis of their positivity for GFP expression were concluded infected with KSHV at the timepoint of study

Non-infected (NI): Cells within the KSHV-inoculated culture that on the basis of their negativity for GFP expression were concluded not infected with KSHV at the timepoint of study

Uninfected: Any cell from either an untreated or KSHV-inoculated culture that did not appear infected at the timepoint of study.

CHAPTER ONE

INTRODUCTION

1.1 KAPOSI'S SARCOMA-ASSOCIATED HERPESVIRUS (KSHV)

1.1.1 Classification

Kaposi's sarcoma-associated herpesvirus (KSHV) was first identified in 1994 by the method of representational difference analysis (Chang et al., 1994) **(section 1.2.4)**. The virus has a double-stranded deoxyribonucleic acid (dsDNA) genome and was classified by phylogenetic sequence-based analysis to be a herpesvirus. It was the eighth and most recent human herpesvirus discovered; hence its alternative assignation HHV8 (human herpesvirus eight) (Chang et al., 1994).

Mammalian herpesviruses, together with avian and reptilian herpesviruses, are grouped in the taxonomic family, '*Herpesviridae*' of the order '*Herpesvirales*'. This family is further subdivided into subfamilies of *Alpha* (α), *Beta* (β) and *Gammaherpesvirinae* (γ) (reviewed by Davison et al., 2009) according to biological properties including: host range, replication cycle and cell tropism (reviewed by Wen and Damania, 2010)

Of the human herpesviruses, KSHV is most closely related to HHV4, which is commonly referred to as the Epstein-Barr virus (EBV). Both KSHV and EBV are gammaherpesviruses although the genome of KSHV shows greater homology to those of the prototype rhadinovirus, Herpesvirus Saimiri (HVS) (Russo et al., 1996), and Rhesus monkey Rhadinovirus (RRV) (Alexander et al., 2000). Subsequently, KSHV has been assigned to the γ2 or *Rhadinovirus* genus whilst EBV is classified in the genera γ1 or *Lymphocryptovirus* (reviewed by Davison et al., 2009) **(Figure 1.1)**.

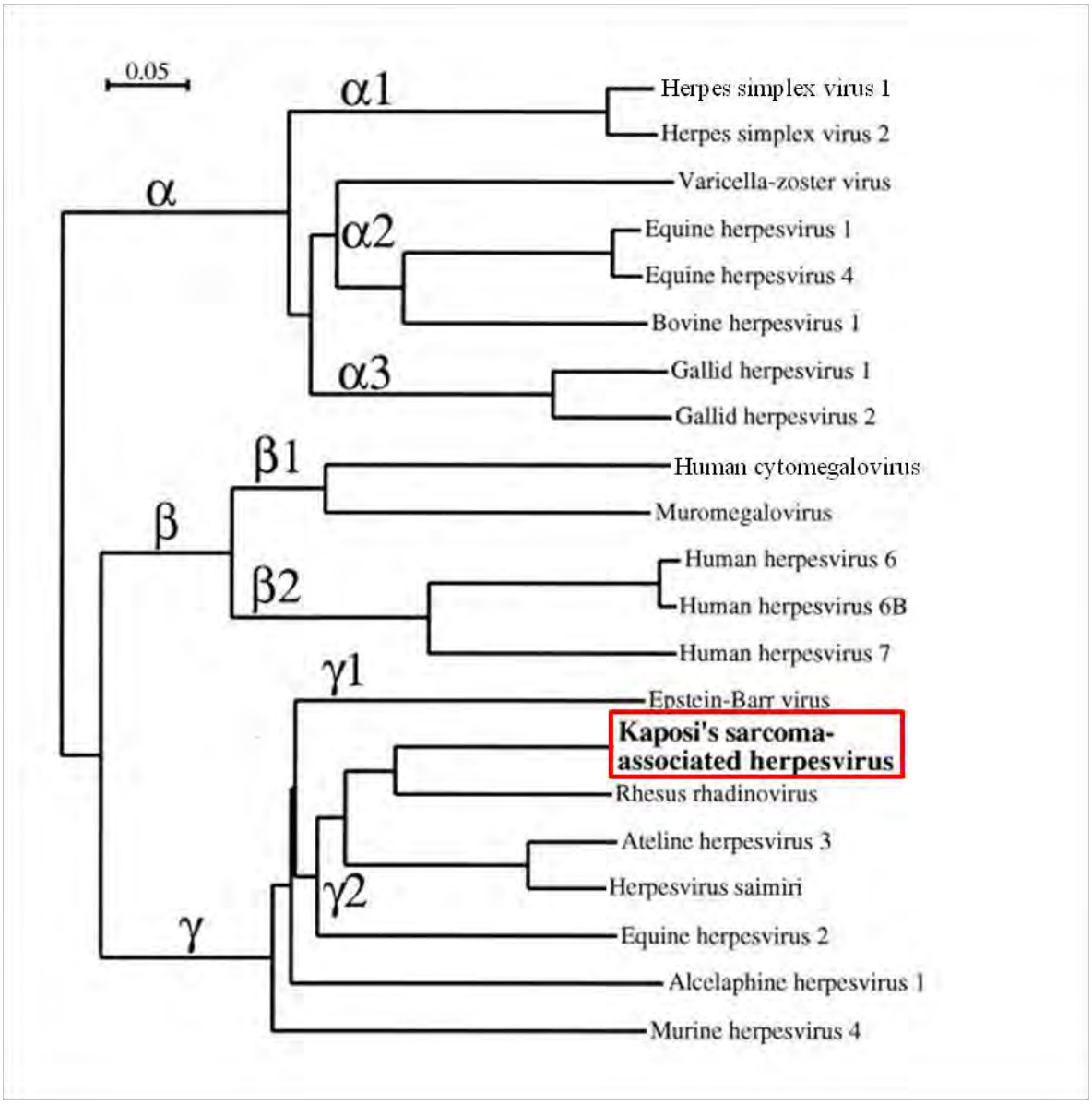

Figure 1.1: Phylogenetic dendrogram of the taxonomic family *Herpesviridae*.

The dendrogram was calculated based on the sequences of the herpesvirus major basic capsid proteins (section 1.1.2) The relationships between 21 herpesviruses across the three subfamilies (α, β and γ) are shown. The location of KSHV within the γ2 subgroup is highlighted (red box) showing its close phylogenetic relationship to the Rhesus rhadinovirus and Herpesvirus saimiri. Modified from Trus et al (2001).

1.1.2 Structure of the KSHV virion

KSHV virions share the three-layered architecture distinct to herpesviruses (McGeoch et al., 2006; Said et al., 1997; Trus et al., 2001; Wu et al., 2000). This is evident from negative stain electron microscopy and electron cryomicroscopy with image reconstruction. The three structural layers that surround the dsDNA core include: (1) an innermost icosahedral capsid built of four principal protein subunits including: major capsid protein, triplex α-subunit, triplex β-subunit and the small basic capsid protein (the triplexes are αβ2 heterotrimers); (2) a middle protein-rich tegument; (3) an outer glycoprotein-impregnated lipid envelope. The glycoproteins that decorate the outer envelope are thought to mediate KSHV entry by acting as ligands to specific receptor proteins on the host cell **(section 1.1.7) (Figure 1.2)**.

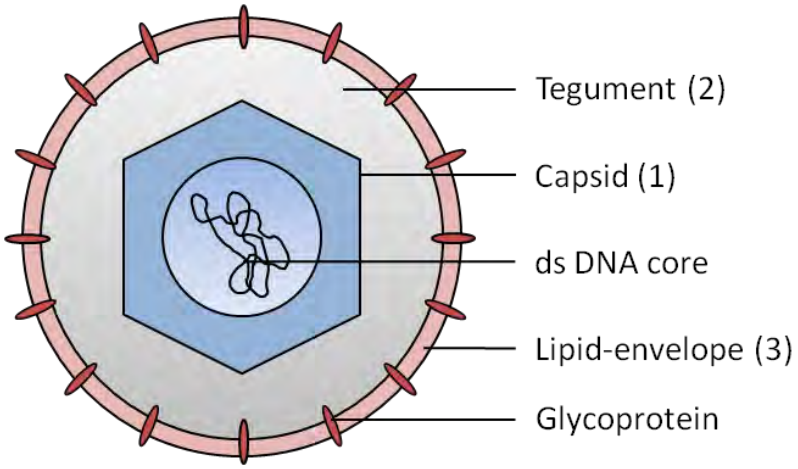

Figure 1.2: The three-layered architecture of herpesvirus virions.
Numbers indicate the three main structural layers that surround the dsDNA core.

In contrast to the capsid, the composition and architecture of the tegument layer is less well defined and appears to include both viral and host cell proteins (Bechtel et al., 2005b; Zhu et al., 2005). Messenger RNAs (mRNAs) have also been detected (Bechtel et al., 2005a). It is suggested that the tegument proteins, when they are released into the cell during virus entry, coordinate fundamental processes of the virus lifecycle that are necessary for *de novo* infection to establish, such as: translocation of the viral capsid to the nucleus, modulation of the cell cycle, viral gene activation and host gene inactivation (Bechtel et al., 2005a; Bechtel et al., 2005b; Zhu et al., 2005).

1.1.3 The KSHV genome

The dsDNA genomes of herpesviruses range in size from 124 to 295kbp (reviewed by McGeoch et al., 2006). The KSHV genome **(Figure 1.3)** is approximately 170kbp (Rezaee et al., 2006). When packaged within the capsid, the DNA is linear. Unpaired, complementary nucleotides are found at each terminus and support episome formation upon circularisation of the genome during infection **(section 1.1.4)**. Genes involved in virion replication or structure are conserved among members of the *Herpesviridae* and are organised into seven genomic blocks located predominantly within the central region. The order of arrangement of these genes is the same across viruses of the same subfamily but differs between subfamilies. Despite this gene conservation, herpesviruses from within the same genera do not necessarily use homologous genes for the same processes in their lifecycle.

The non-core genes are mostly situated toward the termini. It is thought that many new gene functions have arisen through mechanisms of gene duplication and lateral transfer from either the

host cell or other viruses. Many of those thought to have been acquired from the host might aid survival of the virus in the host cell through immunomodulatory and anti-apoptotic functions (reviewed by McGeoch et al., 2006).

The central protein-coding region of the KSHV genome is 140.5kbp and encodes eighty-six genes of which at least twenty-two have predicted immunomodulatory functions (see Rezaee et al., 2006). Sixty-six KSHV genes show homology to those of HVS and are designated open reading frames (ORFs) 4 to 75 accordingly. Those unique to KSHV are notated with the letter 'K' to distinguish them from HVS homologues (Russo et al., 1996).

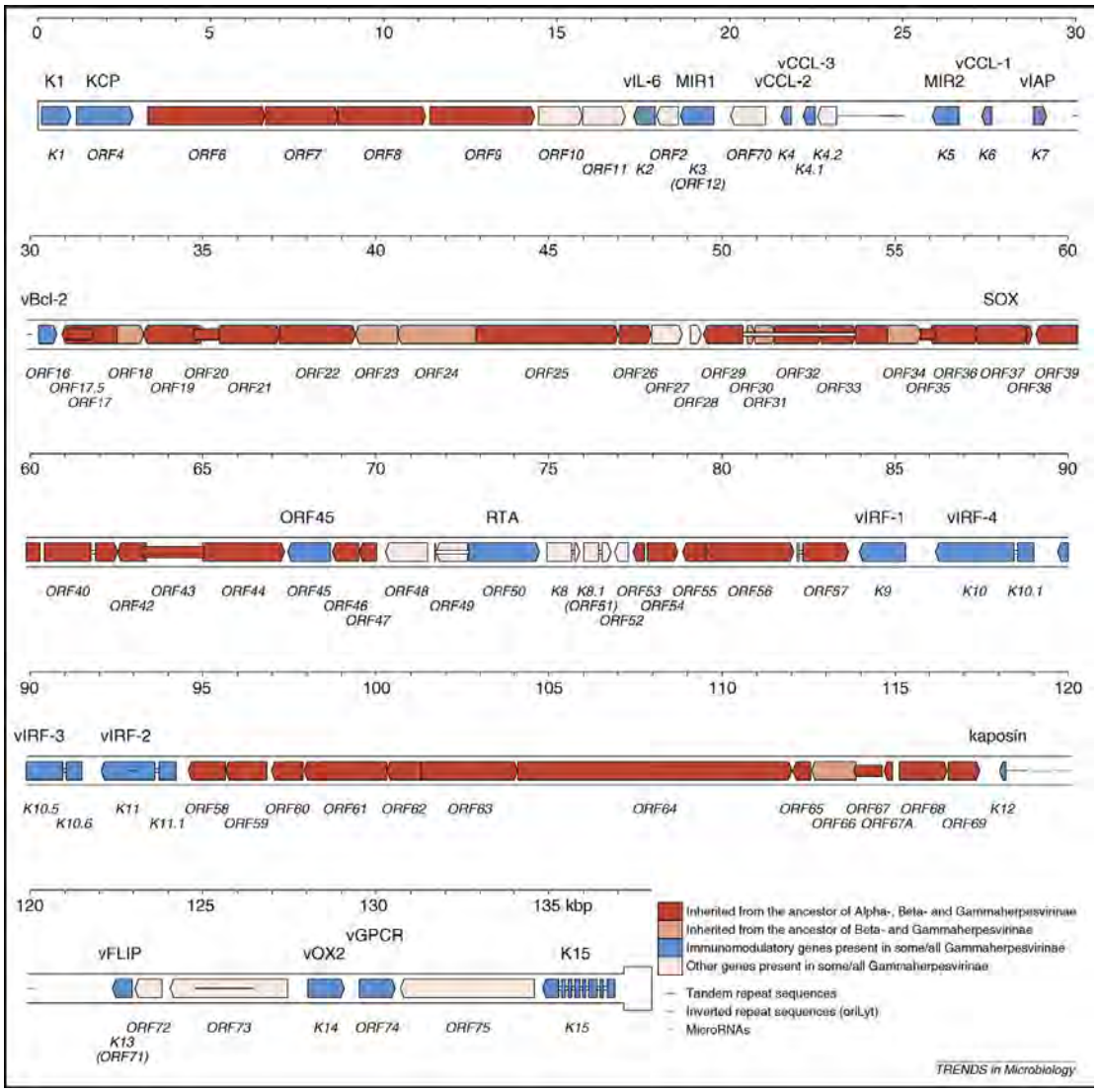

Figure 1.3: The KSHV genome.

The dsDNA KSHV genome totals approximately 170kbp and consists of a central unique region (U) flanked at each end by a sequence of direct repeats (TR) that mediate circularisation of the linear genome into the viral episome. The sequence shown is of U followed by a single copy of TR (widened bar). Coloured arrows indicate protein coding regions with phylogenetic relationships as defined by the key. Narrow white bars indicate introns. Gene nomenclature is given below the bar and the names of the encoded proteins are stated above. Taken from Rezaee (2006).

1.1.4 The KSHV lifecycle

In order to survive, viruses need to replicate and assemble new progeny. They are absolutely dependent upon their host cell and subvert its molecular machinery to support processes of DNA replication, transcription and translation.

Herpesviruses demonstrate two alternative reproductive programs namely episomal latency and lytic replication. Latency is a period of dormancy during which viral gene expression is heavily restricted and new viral particles are not assembled. The genome is maintained as a circular episome and is propagated between daughter cells at low copy number. By contrast lytic replication describes an active phase of new virion production during which the majority of viral genes are expressed according to a temporally regulated cascade. The 'immediate early genes' are expressed first followed by the 'delayed early genes' and finally the 'late genes'. Such orderly changes in gene expression ensure that host anti-viral immune responses are subverted for maintenance of the infected cell and viral DNA is replicated to attain a high copy number before the structural proteins, required for new virion assembly, are synthesized (reviewed by Ganem, 2007)

KSHV infection, both *in vivo* and *in vitro* is typically latent. The study of the lytic cycle typically requires chemical-induced reactivation or ectopic expression of the KSHV lytic switch and transcription activator protein (RTA/K50) (Ganem, 2007).

1.1.5 Incidence and transmission of KSHV infection

KSHV infection occurs worldwide; however, prevalence varies between populations and even within regions as reported for Italy (Whitby et al., 1998) and Africa (Mbulaiteye et al., 2005).

Countries within Asia, Northern America and Northern Europe have low overall prevalence. Mediterranean, Middle Eastern and Caribbean countries have intermediate prevalence and high prevalence is seen in Africa and parts of the Amazon basin (reviewed by Dukers and Rezza, 2003; Mbulaiteye et al., 2004).

Phylogenetic studies have defined a number of KSHV subtypes: A, B, C, D, E and N. Sequence variation between subtypes is below 3% and resides almost exclusively in ORF K1; thus the subtype categorization is based primarily upon K1 sequence. Geographical differences in subtype prevalence are reported, suggesting that subtypes may have originated via different selective pressures operating alongside different human populations. For example subtypes B, D, E and N have been associated with people of African, Old Asian and Polynesian, Amerindian and South African populations respectively. Population associations have not been described for subtypes A and C but both are found in Northern Europe, the Americas and Asia (reviewed by Dukers and Rezza, 2003; Schulz, 2006).

Relationships between rates of KSHV infection and demographic factors including gender or age vary. Therefore, it appears that the principal modes of transmission differ with geographical region. While this may be due to variability in assays it suggests that social, economic and environmental conditions are important determinants (see Mbulaiteye et al., 2005). In non-endemic countries such as Northern Europe and North America, seroprevalence is generally higher among men than women and may in part reflect a disproportionately high incidence of infection found among the male homosexual community in these regions. Indeed the increased occurrence in male homosexuals implies that facets of male homosexual practice potentiate transmission. A lack of infection during childhood in low prevalence regions is further supportive

of a sexual route of transmission. Conversely, however, in Africa, where disease is endemic, seropositivity is equal among men and women and increases during childhood, reaching 40-70% by adulthood (Corey et al., 2002); hence non-sexual modes of KSHV infection are also possible. Close contact, a lack of hygienic practices such as regular bathing and washing of hands, and overcrowding might aid transmission in these populations (Mbulaiteye et al., 2004; Mbulaiteye et al., 2003).

KSHV replication is thought to occur primarily at the oropharynx and saliva is typically the only mucosal secretion positive for KSHV DNA in seropositive persons. Studies investigating KSHV shedding in genital secretions concluded a low and inconsistent presence and there is limited evidence to suggest that replication of the virus occurs at genital sites (see Corey et al., 2002; Koelle et al., 1997; Pauk et al., 2000) hence saliva is likely to mediate most of KSHV transmission in both the homosexual (Blackbourn et al., 1998; Koelle et al., 1997; Pauk et al., 2000; Vieira et al., 1997) and non-homosexual setting (Dedicoat et al., 2004; Mbulaiteye et al., 2004). Such is consistent with the common practices of oral-genital sex and deep kissing performed by homosexual men and also with childhood behaviors and parent-child interactions such as the use of saliva to clean children's faces (see Dedicoat et al., 2004; Dukers and Rezza, 2003; Mbulaiteye et al., 2004; Mbulaiteye et al., 2003; Pauk et al., 2000). Nonetheless, if salivary contact is the major route of transmission, it is somewhat surprising that KSHV prevalence and incidence of associated disease is not higher and that KSHV is not transferred efficiently within heterosexual relationships.

Blood is unlikely to mediate much of KSHV transmission, particularly in low prevalence areas, since the isolation of KSHV DNA from peripheral blood mononuclear cells (PBMC) is

minimal among either healthy (Blackbourn et al., 1997) or seropositive individuals without KSHV-related disease (Cannon et al., 2003). Furthermore, KSHV infection occurs at similar rates in human immunodeficiency virus (HIV)-positive individuals acquiring HIV parenterally and HIV-negative blood donors (Kedes et al., 1996) and in contrast to viral infections including: HIV-1, hepatitis B and hepatitis C, which spread readily among intravenous drug users, efficient transmission does not occur for KSHV (Renwick et al., 2002).

1.1.6 Cell types infected by KSHV

In vitro and *in vivo* studies have demonstrated that KSHV has a broad cellular tropism in its natural human host. This work implies that KSHV entry receptors must have a fairly ubiquitous expression. *In vivo*, KSHV DNA and transcripts have been identified in human B cells, monocytes, macrophages, keratinocytes, and endothelial cells and *in vitro*, infection of endothelial, epithelial and fibroblast cell lineages has been successful. In addition, infection of a number of animal cells has been reported (see Akula et al., 2003).

1.1.7 The mechanism of KSHV infection

The paradigm for herpesvirus infection implicates steps of: (1) adsorption and binding to the host cell; (2) fusion of the viral envelope with the host cell membrane (plasma membrane or intracellular endosomal membrane); (3) release of the capsid to the cytosol; (4) translocation of the capsid to the nuclear envelope; (5) delivery of the genome into the nucleus (Akula et al., 2003; Kaleeba and Berger, 2006a).

Many microorganisms bind to their host cell through interaction of their surface proteins with host cell proteoglycans. As demonstrated for a number of alpha, beta and gammaherpesviruses,

as well as other types of virus such as: HIV-1, vaccinia virus, sindbis virus, adeno-associated virus, foot and mouth disease virus and respiratory syncytial virus, KSHV exploits heparan sulfate-like moieties for adsorption (see Akula et al., 2001b). The role of heparan in KSHV-binding appears specific but dispensable since soluble heparin (≤100μg/ml) inhibited, but did not completely abolish the binding and uptake of the virus and caused displacement of KSHV when added to virus-cell mixtures. In contrast, pre-treating KSHV with either chondroitin sulfates A or C (1000μg/ml) failed to reduce either step or to induce displacement of pre-adsorbed virus. Treatment with heparinases I and III also afforded 65% reduction in infection (Akula et al., 2001b).

Overall, KSHV is expected to exploit additional host cell surface molecules besides heparan for adsorption to the host cell. It is suggested that interactions with heparan sulfate provide the initial ligand-receptor interactions during the adsorption phase, serving to concentrate KSHV at the host cell and facilitate its binding to other cell-surface receptors that act as adsorption or entry receptors and/or signal transducers during the infection process (Akula et al., 2001b).

Studies have indicated that KSHV-glycoprotein B (gB/ORF8) (Akula et al., 2001a) and K8.1 (Wang et al., 2001) mediate binding of KSHV to heparan-sulfate moieties. The encoding of two or more glycoproteins for heparan binding appears typical among herpesviruses and reflects the importance of heparan sulfate moieties as host-cell receptors. gB has counterparts in other herpesvirus (for example Herpes simplex virus (HSV)-1; HSV-2; Human cytomegalovirus (HCMV); HHV-7 (see Wang et al., 2001) which also function in heparan sulfate binding. In contrast K8.1 is unique to KSHV but is a positional homologue of the EBV and Murine

gammaherpesvirus 68 (MHV-68) envelope glycoproteins gp350/220 and gp150 respectively, which have roles in virus infectivity (see Wang et al., 2001).

Electron microscopy images of the early events following KSHV entry into microvascular endothelial cells indicate that KSHV enters endothelial cells by fusion of the virion envelope with the plasma membrane (Dezube et al., 2002), although the same study also identified virions enclosed within vacuoles which is suggestive of endocytic uptake. Consistently, entry to human fibroblasts involved pH-dependent, clathrin-mediated endocytosis (Akula et al., 2003) but entry to 293L cells, while pH acidification dependent, proved clathrin and caveolae independent (Inoue et al., 2003). Overall, the mechanism of KSHV entry might be cell-type specific (Kaleeba and Berger, 2006a). Equally, direct and endocytic mechanisms might participate depending upon virus titre. The mechanism by which virions are routed into the cell might further dictate whether either latency or productive infection occurs (Dezube et al., 2002).

The host cell receptors critical for entry are not well established and might differ according to cell type. *In vitro* studies have identified a number of candidate molecules including the Arg-Gly-Asp (RGD)-binding integrins $\alpha 3\beta 1$ (Akula et al., 2002) and $\alpha v\beta 3$ (Garrigues et al., 2008), Dendritic cell-specific intercellular adhesion molecule-3-grabbing non-integrin (DC-SIGN) (Rappocciolo et al., 2006), and the 12-transmembrane light chain of the human cysteine/glutamate exchange transporter system, xCT (Kaleeba and Berger, 2006b). Interestingly, KSHV gB contains an RGD motif at its amino terminus, which is highly conserved among KSHV strains (Meng et al., 1999) and is a likely mediator of the interaction of KSHV with integrin receptors (Akula et al., 2002). The cognate KSHV ligands for xCT and DC-SIGN are not

known but in support of a role for xCT, KSHV fusion correlates with xCT expression (Kaleeba and Berger, 2006b).

1.1.8 Diseases associated with KSHV infection

In 2009 the International Agency for Research on Cancer (IARC) assigned KSHV as the aetiologic agent for the endothelial neoplasm Kaposi's sarcoma (KS) and for the rare, non-Hodgkin B-cell lymphoma, Primary Effusion Lymphoma (PEL). Although not the formal causative agent for Multicentric Castleman's Disease (MCD), KSHV infection is also associated with the plasmablastic form of this lymphoproliferative disease (Bouvard et al., 2009). Both B-cell disorders are generally linked to an underlying state of immunodeficiency and primarily affect HIV-seropositive Aquired Immunodeficiency Syndrome (AIDS) patients.

1.1.8.1 Primary Effusion Lymphoma (PEL)

PEL (also referred to as body cavity lymphoma) is an aggressive, usually fatal, non-Hodgkin's lymphoma that is thought to arise by the clonal proliferation of post-germinal B-cells given the hypermutation of their immunoglobulins and the presence of late stage B-cell differentiation markers. The tumour typically localises to the body cavities including the pleural space or pericardium; however, lymphomas of solid mass in the lymph nodes, lungs or gastrointestinal tract are observed in some patients. In approximately 80% of cases, co-infection of KSHV with EBV is seen (reviewed by Verma and Robertson, 2003).

1.1.8.2 Multicentric Castleman's Disease (MCD)

KSHV is associated with approximately 50% of plasmablastic MCD cases in which KSHV DNA is detected in around 30% of B-cells in the mantle zones surrounding the germinal centres.

The alternative hyaline-vascular form of MCD is generally KSHV negative. MCD is an aggressive, systemic, non-malignant illness. Symptoms include sustained fever and sweats, weight loss, lymphadenopathy and splenomegaly. Lesions develop at multiple sites and are polyclonal. The lymphoproliferation incurred is attributed to hypersecretion of interleukin (IL)-6. In KSHV infected lesions, the KSHV homologue of IL-6, vIL-6, may also contribute. In contrast to PEL, co-infection with EBV has not been noted for MCD (reviewed by Verma and Robertson, 2003) .

The work contained in this thesis is with regard to the role of KSHV in KS pathogenesis. Therefore, the following section in this introduction provides an overview to KS and the identification of KSHV as the aetiologic agent for that disease.

1.2 KAPOSI'S SARCOMA (KS)

1.2.1 Histology of KS lesions

KS was first described in 1872 by the Hungarian dermatologist, Moritz Kaposi as 'idiopathic multiple pigmented sarcoma of the skin'. It was not until 1891 that the eponymous name, Kaposi's sarcoma, was assigned (see Boshoff and Weiss, 1997). KS lesions are multifocal and typically cutaneous, although in more aggressive disease they also affect the viscera. The lesions have a distinct raised and purplish appearance (reviewed by Restrepo and Ocazionez, 2011) **(Figure 1.4)**.

The lesions originate as flat maculae (patch stage) and progress through a plaque to nodular stage (Ensoli et al., 2001) increasing in granularity and cell type by the infiltration of

inflammatory cells, including: dendritic cells, macrophages, plasma cells and lymphocytes and the extravasation of erythrocytes (reviewed by Ensoli et al., 2001; Mesri et al., 2010; Pantanowitz et al., 2009; Restrepo and Ocazionez, 2011). An abnormal, primitive vasculature of slit-like vessels is formed by the proliferation of activated endothelial cells and as the tumour progresses the stroma surrounding the vascular spaces becomes increasingly filled with cells of spindle morphology which represent the main proliferative component (see Ensoli et al., 2001; Restrepo and Ocazionez, 2011). These spindle cells have an endothelial phenotype and feature latent KSHV infection; only 2-5% of cells are lytically infected (Moses et al., 1999; Orenstein et al., 1997; Staskus et al., 1997; Zhong et al., 1996) **(Figure 1.4)**. The proliferation of these tumour cells is believed to contribute to the aberrant neoangiogenesis and neolymphangiogenesis (see Colman and Blackbourn, 2008; Mesri et al., 2010) that is a hallmark of KS. Infiltrating B-cells and neovascular endothelial cells also harbour the virus (Antman and Chang, 2000).

There is some debate concerning whether KS is a true sarcoma. This is in view of the simultaneous appearance of multiple lesions across the body, their polyclonality and an absence of chromosomal changes. Nonetheless, in advanced disease, clonality of spindle cells has been reported (Rabkin et al., 1995) and nuclear and chromosomal abnormalities typical of malignancy identified (Bedi et al., 1995; Dictor et al., 1991; Ensoli et al., 2001).

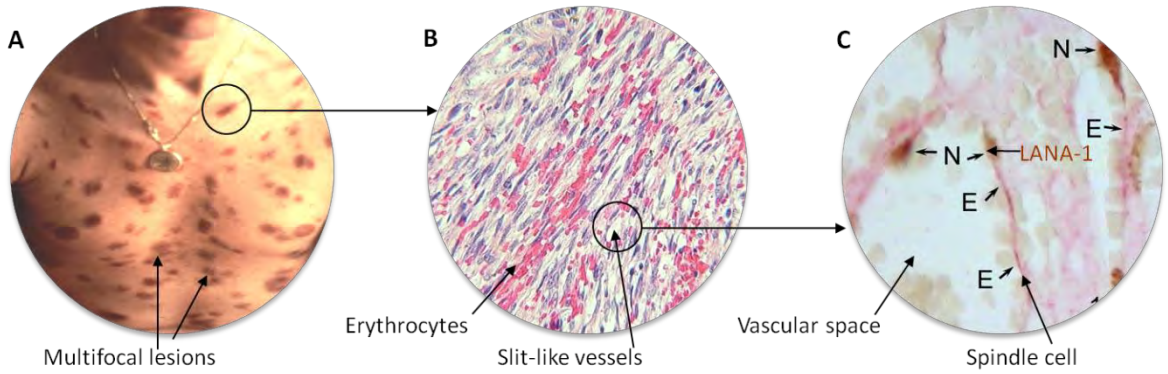

Figure 1.4: The macroscopic and cellular appearance of KS lesions.
(A) Photograph of the chest of a patient with AIDS-related KS illustrating the multifocal, cutaneous nature of the lesions and their raised purplish appearance. **(B)** Haematoxylin (nucleus) and eosin (cytoplasm) stained section of a KS lung lesion viewed with a 25x objective lens illustrating an abundance of abnormal slit like vessels and extravasated erythrocytes (Blackbourn unpublished data). **(C)** Paraffin-embedded KS skin section dual stained for nuclear-expressed KSHV latency associated nuclear antigen-1 (LANA-1) and vascular endothelial growth factor C (VEGFC), which is expressed in the cytoplasm of KSHV-infected cells of KS lesions. The image illustrates the spindle-shape of KSHV-infected endothelial cells and their localisation lining the aberrant vasculature. Adapted from Colman and Blackbourn (2008).

1.2.2 The epidemiologic forms of KS

To date four epidemiologically distinct forms of KS have been described (classic, endemic, epidemic and iatrogenic) that are histopathologically identical indicating a similar mechanism of development. KSHV is the aetiologic agent for all (reviewed by Mesri et al., 2010; Restrepo and Ocazionez, 2011) **(section 1.2.4).**

'Classic' also termed 'sporadic' KS was the form originally identified by Moritz Kaposi. It is a rare, slow growing, indolent disease observed primarily among elderly men, between 50 and 70 years of age, who are of Mediterranean, Eastern European and Jewish descent (Boshoff et al., 1995a; Oriel, 1997). Lesions are generally restricted to the skin of the lower limbs. Internal organs are rarely affected. Secondary malignancies, typically non-Hodgkin lymphomas, are also seen in up to 30% of patients (Escalon and Hagemeister, 2006)

'Endemic' otherwise known as 'African' KS was first reported in the early 1900s among populations in subequatorial Africa, such as countries including: The Congo Republic, The Congo, Burundi, Uganda and Zambia. It is a chronic nodular disease that primarily affects the legs and feet (Ziegler, 1993). Interestingly, incidence is five times more common in males than females even though seropositivity for KSHV is high and similar in males and females in this population (Boshoff and Weiss, 1997). Endemic KS is the most prevalent cancer among men in this area, representing, up to 10% of malignancies in men (see Parkin, 2006). A highly fatal lymphadenopathic disease variant that affects the viscera is also seen in this region among children prior to adolescence: it accounts for up to 25% of childhood cancers (see Restrepo and Ocazionez, 2011).

'Iatrogenic' or 'transplant-associated' KS describes disease arising in patients who are receiving immune suppression therapy or who have undergone solid-organ transplantation and are consequently receiving immunosuppressive drugs to prevent rejection of the donated organ by their body's immune system (Penn, 1988, 1991). There is no apparent association between KS and congenital immune deficiency states. The withdrawal of immunosuppressive regimens can

lead to regression of this disease (Wen and Damania, 2010) suggesting that immune suppression is a key contributor to the establishment of KS in KSHV-infected individuals.

The risk of KS increases 1000 to 5000 fold in subjects infected with HIV compared to the general population and 50% of HIV-infected individuals develop KS. In fact KS is the most common malignancy associated with AIDS and is therefore one of the recognised AIDS-defining diseases (reviewed by Parkin, 2006).

The HIV/AIDS epidemic and coincident rise in cases of KS saw the description of the fourth form of KS as 'Epidemic' or 'AIDS-related' KS. It is clinically the most aggressive form of KS and affects populations globally; although, with the introduction of highly active anti-retroviral therapy (HAART), incidence in the western world has been much reduced (Sarwar et al., 2007). The limited availability of such therapy in developing countries means that KS continues to be a major clinical concern in those countries. In the western world, the disease is mainly seen among HIV-infected male homosexuals but also bisexual men and female sexual partners of bisexual men, while in Africa and developing countries it is common in heterosexual adults. The higher incidence of KS among homosexuals in the western world is consistent with the increased seroprevalence of KSHV in that population **(section 1.1.5)**.

1.2.3 Risk factors for KS

This section provides a summary of some of the additional risk factors that have been suggested for KS (see also Colman and Blackbourn, 2008; Dukers and Rezza, 2003).

Environment: The incidence of KS is higher in rural regions and is increased among persons in agricultural occupations such as cereal cultivation (Cottoni et al., 1997). Associations with altitude and climate are not clearly defined and may differ between countries. Studies examining incidence rates of KS across Africa reported highest frequencies near to the equator and at altitudes over 2000ft where humidity was moderate to high (Cook-Mozaffari et al., 1998; Ziegler, 1993). This was however in contrast to the geographic patterns noted in Italy where decreasing risk of Classic KS with increasing altitude was described (Ascoli et al., 2009; Geddes et al., 1995). Red clay, limestone and volcanic soils have also been associated with the disease in both Africa (Cook-Mozaffari et al., 1998; Ziegler, 1993) and Italy (Ascoli et al., 2009) but the fact that KS occurs at low frequency in areas such as Ethiopia, which have volcanic soils, suggests additional cofactors modulate risk (Ziegler, 1993).

Gender and genetics: There is a predilection of KS for men. Genetic polymorphisms also influence susceptibility to a number of viral infections. Tentative associations with allele genotypes of the Fc fragment of the IgG low affinity IIIa receptor (FCGR3A) (Brown et al., 2005; Lehrnbecher et al., 2000), human leukocyte antigen (HLA) (Dorak et al., 2005; Gaya et al., 2004; Masala et al., 2005) and IL-6 promoter (Foster et al., 2000) have been postulated but require further clarification.

HIV-1 Tat protein: HIV-1 infection increases tendency to develop epidemic KS ten-fold compared to HIV-2 infection in populations where KSHV seroprevalence is identical (Horenstein et al., 2008). These data suggest that a factor peculiar to HIV-1 potentiates KS progression in ways other than by immune suppression. *In vitro* studies have implicated a role for the HIV-1 protein Tat that is released by acutely infected T-cells. Once extracellular, Tat induces the adhesion, growth, migration and invasive properties of normal and KS endothelial cells through binding of its RGD sequence to integrin receptors and its basic sequence to heparan sulphates. The latter supports angiogenesis through competitive liberation of basic fibroblast growth factor (bFGF). Tat also induces upregulated expression of cytokines, adhesion molecules and matrix metalloproteinases (MMPs) that have angiogenic and invasion promoting effects (reviewed by Ensoli et al., 2001).

Immune suppression: Reduced immune control over KSHV leading to increased viral load might explain instances of epidemic and iatrogenic KS. Weakening of the immune system occurs with age, other neoplasms and concurrent infections; thus immune suppression might also trigger onset of Classic KS. In support, a Greecian study of Classic KS observed that CD4+ T-cell counts were significantly lower in cases compared to controls (Touloumi et al., 1999).

Socioeconomic: Overcrowding in countries burdened by endemic KS is speculated to contribute to transmission of KSHV in these communities (Dukers and Rezza, 2003); moreover, KSHV seropositivity is associated with either surface water or a communal standpipe as the source for drinking water compared to a private supply (Mbulaiteye et al., 2005). However, whilst overcrowding is generally greater among families of low economic status and consistently KSHV seropositivity was associated with lower maternal education and income and low status

father's occupation for a cohort of 600 Ugandan children (Mbulaiteye et al., 2005), other case control studies in Uganda have reported incidence to be higher among individuals with improved educational and professional level and increased earning capacity. It is speculated that wealthy land owners in developing countries might spend longer toiling the land and thus incur greater exposure to risk from possible cofactors such as soil or water and livestock (Ziegler et al., 2003; Ziegler et al., 1997).

Co-infection: Co-infection of the host with other viruses or parasites might be important in various forms of KS. For example HHV6 and HHV7 have been noted to infect the monocyte population of KS lesions (Kempf et al., 1997) and HCMV infection is frequently observed in KS. Moreover, *in vitro* studies demonstrate that HCMV is capable of reactivating KSHV from latency into lytic replication (Vieira et al., 2001).

A role for malaria infection was suggested from observations that incidence of KS was high in areas that were or had been endemic for malaria (see Geddes et al., 1995; Ruocco et al., 2011). It is hypothesised that parasites, such as malaria, might serve as cofactors for KS by inducing reactivation of the virus and/or enhancing susceptibility to infection by the virus. The downregulation of T helper (Th)-1 cellular responses and upregulation of Th-2 humoral responses might limit host cell control of KSHV infection (Lin et al., 2008). While two epidemiologic studies conducted in northern (Cottoni et al., 2006) and north-eastern Sardinia (Cottoni et al., 1997) did not find statistical association between Classic KS and malaria, evidence of a link between KSHV seroprevalence and malaria parasitaemia was reported among women in Uganda (Wakeham et al., 2011). Moreover, the finding that anti-mosquito strategies to eradicate malaria in Sardinia led to a reduction in KSHV seroprevalence (Ascoli ref Colunzzi,

2003) provided further support for malaria as a possible cofactor for KS. Other parasite infections that have been linked to KS include: *Mansonella perstans*, hookworm (Wakeham et al., 2011) and *Stronglyoides stercoralis* (Lin et al., 2008). Frequencies of infection with intestinal parasites including: *Schistosoma mansouri*, *Giardia lamblia*, *Trichomonas hominis* and *Entamoeba histolytica* were also higher in KS patients compared to other cancer patients but the differences were not statistically significant (Lin et al., 2008). Contrary to Wakeham et al (2011), Lin et al (2008) reported an inverse association between KS and hookworm; however, Lin et al (2008) did not control for HIV infection: HIV-infection might have caused a decrease in parasite egg production and subsequent detection in stools, thereby accounting for the inverse or insignificant association between KS and a number of the parasites studied.

The distribution of promoter arthropods, which are blood sucking insects that cause irritating bites (Ascoli et al., 2009; Coluzzi et al., 2002), has also been found to correlate with the incidence of KS in Sardinia (Ascoli et al., 2009). Interestingly, as for parasites, the promoter arthropods were at their highest densities under environment conditions previously highlighted as potential risk factors for KS, for example areas with past malaria prevalence, limestone, acid volcanic soil, lower altitude and cereal cultivation. Thus, the non-uniform distribution of KS globally but also within small geographic regions might be explained by the geographic variation in parasite and insect distributions. Roles for these organisms as cofactors might help to explain some of the environmental links to KS (Ascoli et al., 2009). It is suggested that by piercing the skin and injecting their saliva, promoter arthropods stimulate KSHV reactivation, leading to increased transmission through shedding of the virus in human saliva. Their saliva also induces

itching and inflammatory responses in the host that might underlie KS development (Ascoli et al., 2009).

1.2.4 Identification of KSHV as the aetiologic agent for KS

As already introduced, KSHV is the recognised aetiologic agent of KS. The hypothesis that KS was caused by a viral pathogen was first presented during the 1960s, in view of the geographic variation in incidence of KS. At the identification of herpesvirus-like particles in short term cultures of KS biopsies, a role for HCMV infection was initially proposed but HCMV DNA failed to be detected in samples of KS tumours and the hypothesis was quashed. The HIV pandemic in the 1980s with subsequent AIDS epidemics and a correlated rise in AIDS-related KS revived the search for viral causation. HIV was not a candidate since Classic KS predated epidemic KS and the incidence of epidemic KS differed considerably between different populations infected with HIV.

In 1994, the genome sequences of a KS lesion and normal tissue for a single AIDS-KS patient were compared by method of representational difference analysis (Chang et al., 1994). This work identified two short DNA fragments (330bp and 631bp) with homology to herpesviral capsid and tegument components respectively that were present in the lesions but not normal tissue (Chang et al., 1994). The sequences were found to be for a novel herpesvirus, KSHV.

A number of PCR based studies have since amplified Chang's herpesviral capsid 233bp sequence in DNA isolated from non AIDS-KS biopsies (Boshoff et al., 1995b; Dupin et al., 1995; Moore and Chang, 1995; Schalling et al., 1995; Su et al., 1995), providing strong support for KSHV as the putative KS aetiologic agent for all forms of KS as opposed to a mere

contaminating opportunistic virus in the tumours of immunosuppressed AIDS patients. That sequences were amplified from lesions in different tissues (Schalling et al., 1995) but remain largely undetected in normal skin (Dupin et al., 1995; Moore and Chang, 1995; Schalling et al., 1995) provides additional persuasion for KSHV as the causative factor and this conclusion is strengthened by converse observations for the quantification of HIV pro-viral DNA in AIDS patients where no difference between abundance of HIV-pro-viral DNA in tumour and unaffected tissues is reported (Dupin et al., 1995). KSHV sequences have also been detected in peripheral blood mononuclear cells (PBMC) of HIV positive KS patients (Boshoff et al., 1995b), specifically CD19+ B-cells (Ambroziak et al., 1995) and prospective studies among HIV positive populations that analysed KSHV infection of PBMCs concluded that infection precedes tumour development and is a predictor of risk (Moore et al., 1996).

As described above (**section 1.2.1**), KSHV-infected spindle cells, are the main tumour cells of KS lesions. Moreover, their distribution lining the aberrant vascular spaces suggests a major role in the process of tumour angiogenesis that is a prominent hallmark of KS.

The overall aim of this thesis was to further current understanding of how KSHV infection drives development of KS lesions. Since the infected spindle cells of KS lesions have an endothelial character, suggesting an endothelial cell origin, it was decided to focus specifically upon the impact of KSHV infection on endothelial cell functions. Moreover, as the migration of endothelial cells is a central process in angiogenesis **(sections 1.3.2 and 1.3.3)**, the effect of KSHV infection on functions that might regulate the migration of endothelial cells was principally examined.

As relevant background for these studies, the following sections provide an overview to endothelial cells and their functions with a particular focus on their role in angiogenesis. Subsequently, the process of endothelial migration is described and factors that regulate endothelial cell migration discussed.

1.3 ENDOTHELIAL CELLS

Endothelial cells are simple squamous cells that arise from the splanchnopleuric mesoderm (reviewed by Sumpio et al., 2002). Monolayers of endothelial cells surrounded by a thin protein basement membrane form the innermost lining (*tunica intima*) of all structures within the circulatory system, including the heart and all blood and lymphatic vessels. In an adult this totals $1\text{-}6x10^{13}$ cells forming an organ with mass of about 1kg (reviewed by Sumpio et al., 2002). Vascular capillaries which join arterioles and venules in the closed circulatory system, and lymphatic capillaries which drain to the larger collecting lymphatics, have only a *tunica intima* whereas the endothelia of arteries, arterioles, venules, veins and larger lymphatics are surrounded by a middle layer (*tunica media*) of smooth muscle and elastic tissue (elastin and collagen) and an outer layer (*tunica adventitia*) made from collagenous connective tissue. The *tunica media* is very thick at the site of the arteries to enable the vessels to withstand the high blood pressure as blood leaves the heart but this layer becomes thinner with distance from the heart.

1.3.1 Overview of endothelial cell functions

The endothelium has several roles within the circulatory system. It helps to reduce turbulence of blood flow, enabling fluid to be pumped further and acts as a selective permeability barrier to regulate the exchange of small and large molecules between the blood and the tissues.

Furthermore, via the action of secreted paracrine and endocrine mediators, and their regulated expression of certain surface receptors, endothelial cells influence both underlying smooth muscle cells and circulating cells, including platelets and leukocytes, to control blood pressure and processes of haemostasis, inflammation and immune responses.

Regulation of vessel permeability: The extent of endothelial permeability varies between endothelia at different anatomical sites according to the organization and specialization of the endothelial cells. For example, the blood brain barrier (endothelium lining the brain microvasculature) is continuous and of low permeability due to a specialized system of tight junctions between the cells. This ensures that uptake of molecules into the brain is selective and the entrance of cells and pathogens from the blood into brain extracellular fluid is prevented. Small hydrophobic molecules can cross the blood brain barrier but nutrients, primarily glucose and amino acids, are specifically transported. The tight junctions establish polarity to the endothelium which aids in this selective uptake and similarly the regulated release of toxic waste products away from the brain (reviewed by Abbott et al., 2010; Garlanda and Dejana, 1997).

In contrast, sinusoidal vessels are found at sites including the liver, lymphoid tissue, bone marrow, spleen and endocrine organs. The endothelium of sinusoids is discontinuous with large intercellular clefts and few tight junctions between cells; thereby allowing the free passage of small and medium-sized proteins and also the transmigration of leukocytes into the tissues. Pores in endothelial cells called fenestrae act as additional filters of fluids, solutes and particles in some vascular beds such as the liver sinusoids, the kidney and gastrointestinal tract (reviewed by Aird, 2007).

Control of blood flow: Endothelial cells regulate vascular tone through the production and release of vasoconstrictors including endothelin and platelet activating factor (PAF) and vasodilators including: nitric oxide and prostacyclin. In the physiologic homeostatic state, the endothelium also helps to maintain blood flow by preventing platelet adhesion and activation and the generation of thromboses. Firstly, the endothelium presents a negatively charged surface that repels platelets from the vessel wall. Secondly, factors synthesised including nitric oxide and prostacyclin are inhibitory to platelet activation by stimulating an increase in intracellular levels of each of: cyclic guanosine monophosphate (cGMP) and cyclic adenosine monophosphate (cAMP); ecto-ADPase which catabolises extracellular AMP to guard against activation of the vessel wall; thrombomodulin and tissue factor inhibitor which inhibit the prothrombotic effects of α-thrombin. Components of the endothelium-associated matrix also activate antithrombotic factors. For example, heparan sulfate and related glycosaminoglycans activate antithrombin III, and dermatan sulfate activates heparin cofactor II. Under conditions of injury, these protective mechanisms break down and the endothelium changes from an anti to prothrombotic surface. Endothelial cells become activated and express PAF and tissue factor, and platelets become exposed to sub-endothelial matrix proteins including: von Willebrand factor, fibrillar collagens, fibronectin and laminins to which they can bind, become activated and aggregate (reviewed by Cines et al., 1998; Jackson, 2011).

Role in inflammation and immune responses: The adaptive immune response requires activation of antigen specific lymphocytes involving the binding of antigen presented by major histocompatability complex (MHC) molecules on the antigen presenting cell to the cognate T-cell receptor. Naïve T-cells primarily encounter antigen presented by antigen presenting cells in

secondary lymphoid tissue. Endothelial cells of high endothelial venules (HEV) at the sites of lymphoid tissue are adapted to facilitate continuous patrol of the tissue by lymphocytes. Approximately 25% of lymphocytes passing through HEV will bind and transmigrate into the lymphoid tissue (Girard and Springer, 1995). HEV support this recruitment through their constitutive expression of mucin ligands (glycosylation dependent call adhesion molecule 1 (GlyCAM1), mucosal addressin cell adhesion molecule 1 (MAdCAM-1) and CD34) which bind to the transmembrane glycoprotein, L-selectin, that is expressed by most leukocytes and also through their presentation, possibly following transcytosis, of the chemokine CCL21. CCL21 signals via its cognate receptor CCR7 on the leukocytes to mediate activation of leukocyte integrins, firm adhesion and cell spreading ahead of emigration from the vasculature into the lymphoid tissue (Carlsen et al., 2005; Forster et al., 2008; Girard and Springer, 1995). Under inflamed conditions, cytokines including tumour necrosis factor-alpha (TNFα), IL-1β and interferon gamma (IFNγ) induce upregulation of adhesion receptors, notably vascular cell adhesion molecule-1 (VCAM-1) and P and E-selectin, by vascular endothelium thereby establishing a surface for the recruitment of effector lymphocytes (Springer, 1995). Once tethered, the lymphocytes receive further chemokine and prostanoid (e.g. prostaglandin D2 (PGD_2)) signals that direct their stable adhesion and the process of diapedesis (Ahmed et al., 2011). Passage across endothelium and receipt of a PGD_2 signal also enhances the propensity of lymphocytes to exit the tissue entering the lymphatic system for return to the blood (Ahmed et al., 2011). Similar processes support the recruitment of neutrophils from the blood into inflamed tissue as part of the initial innate immune response (Tull et al., 2009).

Role in formation of the blood and lymphatic vasculature: Endothelial cells have central roles in the formation of new blood and lymphatic vessels in the processes of vasculogenesis, lymphatic vascular morphogenesis, angiogenesis and lymphangiogenesis. Vasculogenesis is the process of vascularisation of the embryo. It involves the fusion of blood islands (aggregates of endothelial precursor cells that have differentiated from mesodermal cells) into primary capillary plexi which then organise into the vascular network of arterioles, arteries, capillaries, venules and veins (see Adams and Alitalo, 2007; Lamalice et al., 2007). Subsequently, vascular smooth muscle cells associate with the arteries and veins while pericytes surround the capillaries. Lymphatic vascular morphogenesis is the formation of the early lymphatic vessels from the blood vasculature in the embryo. Lymphatic endothelial cells (LEC) sprout from the embryonic vein and assemble into lymph sacs that separate from the blood vascular system in a mechanism involving platelet aggregation and continue to sprout into the lymphatic primary plexus. In turn this plexus remodels into the collecting, pre-collecting and capillary vessels of the lymphatic system (see Adams and Alitalo, 2007; Albrecht and Christofori, 2011; Schulte-Merker et al., 2011). Angiogenesis is the formation of new blood vessels from preexisting ones. During embryogenesis, angiogenesis and lymphangiogenesis extend the early vascular and lymphatic trees respectively. In adulthood, angiogenesis is important for wound healing and tissue regeneration (Lamalice et al., 2007). Angiogenesis and lymphangiogenesis also occur in tumourigenesis being fundamental for the continued growth and increased stage of the lesion. Lymphangiogenesis and the enlargement of the lymph vessels also facilitates metastasis (reviewed by Achen and Stacker, 2008; Alitalo, 2011; Karnezis et al., 2012; Weis and Cheresh, 2011). In contrast to the tightly regulated processes of physiological vessel formation, wherein vessels mature to a specific type and then become quiescent, new vessels grow without stopping

during tumour angiogenesis. This results in a disorganised network of leaky, dilated, tortuous vessels in which flow is often slow and irregular (see Bergers and Benjamin, 2003).

Since an extensive aberrant vasculature is a hallmark of KS lesions, the molecular mechanisms of tumour angiogenesis are overviewed in the following section. Lymphangiogenesis has been less well characterized than blood vascular angiogenesis but similar signaling pathways appear to be involved; therefore the following description is primarily in the context of blood vascular angiogenesis but the major differences between the triggers for the two processes are highlighted.

1.3.2 Mechanisms of tumour angiogenesis

Sprouting angiogenesis **(section 1.3.2.1)**, the growth of new vessels out of pre-existing ones, is the main mechanism of growth of the blood and lymphatic vasculature during embryogenesis and adulthood. It is also considered to be the predominant mechanism of tumour angiogenesis; however, recent evidence suggests roles for two further angiogenic processes that are seen in physiologic vasculogenesis, in tumour angiogenesis including: (1) the recruitment of endothelial progenitor cells and their assembly into new vessels; (2) intussusception angiogenesis, which is the splitting of pre-existing vessels into two daughter vessels. In addition, tumours may achieve sufficient neovascularisation to assist their growth through the co-option of existing vessels or the process of 'vasculogenic mimicry' wherein tumour cells dedifferentiate to an endothelial phenotype and assemble into tube-like structures (reviewed by Carmeliet and Jain, 2011; Hillen and Griffioen, 2007). It is becoming increasingly apparent that in addition to endothelial cells, mural cells called pericytes, which form direct and indirect interactions with capillary endothelial cells, have important roles throughout angiogenesis and vessel stabilistion (reviewed by Gerhardt and Betsholtz, 2003; Raza et al., 2010).

Pericytes: Pericytes are elongated contractile cells that ensheath the capillary wall on the abluminal endothelial surface. The association between endothelial cells and pericytes is so close that they share a common basement membrane: both cells contribute to the synthesis of this matrix and attach to its proteins via integrin heterodimers (section 1.3.4). Where there are holes in the basement membrane, tight junctions, adherens junctions and gap junctions form between the two cell types to facilitate the transmission of contractile force between their actin cytoskeletons and the exchange of nutrients, metabolites, secondary messengers and ions; thereby

supporting cross regulation between the two cell types (reviewed by Gerhardt and Betsholtz, 2003; Raza et al., 2010).

Pericytes are phenotypically plastic with the potential to differentiate into other mesenchymal cell types including: smooth muscle cells, fibroblasts and osteoblasts (see Gerhardt and Betsholtz, 2003). While a pan pericyte marker has not been defined, the most common markers include: desmin, α-smooth muscle actin, regulator of G-protein signaling 5, PDGFR and chondroitin sulfate proteoglycan (see Raza et al., 2010). Dependent upon the capillary bed, pericytes are found either as individual cells or as a monolayer: the extent of coverage of the endothelial abluminal surface ranges between 10 and 50%. Generally pericyte coverage is higher at capillary branch sites while surfaces involved in gas or nutrient exchange are devoid of pericytes (see Gerhardt and Betsholtz, 2003). Pericytes appear to have a fundamental role in the central nervous system for the maintenance of the integrity and function of the blood brain barrier. This is reflected by a significantly higher pericyte coverage of brain compared to peripheral capillaries (reviewed by Winkler et al., 2011). Angiogenesis is driven by a panoply of pro-growth factors (vascular endothelial growth factors (VEGF); FGF, angiopoietins (ANG), epidermal growth factor (EGF), platelet derived growth factor (PDGF), transforming growth factor beta (TGFβ), placenta-derived growth factor (PlGF), TNFα, interleukins, ephrins, soluble adhesion molecules, PAF and angiogenin) of which VEGFs and ANGs are of major importance (reviewed by Carmeliet and Jain, 2011; Conway et al., 2001).

VEGFs: The mammalian VEGF family includes five members (VEGFA, B, C, D and PlGF) and their splice variants. VEGFs function as dimers and bind in an overlapping pattern to three

receptor tyrosine kinases (VEGFR1, 2 and 3). VEGFA, B and PlGF bind VEGFR1, VEGFA binds VEGFR2 and VEGFC and D bind VEGFR3. Proteolytic processing of VEGFC and D also facilitates their binding to VEGFR2 (reviewed by Olsson et al., 2006). Ligand binding leads to the homo or heterodimerisation of their receptors and subsequent receptor activation. Activity is also regulated by co-receptors such as heparin sulfate proteoglycan and neuropilins which bind to both VEGFs and VEGFRs (see Adams and Alitalo, 2007; Olsson et al., 2006). VEGFA signaling via VEGFR2 is particularly associated with angiogenesis while VEGFC and D which signal via VEGFR3 expressed on lymphatic endothelial cells (LEC) are the main stimulants of lymphangiogenesis (reviewed by Achen and Stacker, 2008; Olsson et al., 2006) although VEGFA through VEGFR2, also expressed by LEC, may contribute (see Achen and Stacker, 2008).

ANGs: The human ANG family includes three members (ANG-1, 2 and 4) that bind competitively to the TIE-2 receptor. ANG-1 functions as a TIE-2 agonist and promotes endothelial quiescence and vessel stabilisation through the establishment of cell-cell junctions, pericyte coverage and basement membrane deposition. ANG-2 functions as a competitive ANG-1 antagonist, promoting pericyte detachment and vascular permeability and favouring endothelial cell sprouting. ANG-4 has not been well characterized but is believed to act similarly to ANG-1 (reviewed by Carmeliet and Jain, 2011).

1.3.2.1 Sprouting angiogenesis

Sprouting angiogenesis is a consecutive process **(Figure 1.5)** initiated when angiogenic stimulatory factors, in particular VEGF, induce an increase in the permeability of the endothelial cell layer and plasma proteins, such as fibrinogen and fibronectin, extravasate forming a matrix on which endothelium can migrate. It has been suggested that VEGF released by pericytes in

response to the paracrine action of NO secreted by activated endothelial cells is the principal source of VEGF in some tissue beds (Reynolds et al., 2000). ANG-2 subsequently released by activated endothelial cells functions as a competitive ANG-1 antagonist at the TIE-2 receptor; this promotes a loss of interactions between endothelial cells and surrounding pericytes and destablises the existing vasculature. Activated endothelial cells and pericytes secrete proteases such as MMPs that degrade the basement membrane and extracellular matrix locally releasing angiogenic factors and clearing a route for growth of the new endothelial sprout into the perivascular space (Carmeliet and Collen, 2000).

In this process of sprouting, disintegration of the vasculature by non-selective sprouting along the vessel length is prevented by NOTCH-receptor-ligand pathways that establish one cell, termed the 'tip cell,' to lead the sprout and cause neighbouring cells to assume a subsidiary role as stalk cells. The tip cell continuously extends and retracts filopodia to sense the environment. Semaphorins and ephrins are key guidance molecules. The stalk cells elongate, proliferate and migrate behind the tip cell to extend the sprout. These regulating events of tip-cell selection are linked to the proangiogenic VEGF axis: VEGFA induces Delta-like ligand 4 (DLL4) expression by the tip cell and DLL4 binds to its cognate NOTCH receptor on the neigbouring cell. Activation of NOTCH suppresses the expression of VEGFR2 by the stalk cell and leads to upregulation of VEGFR1; thus stalk cells become less sensitive to the sprout promoting VEGFA stimulus and more responsive to PlGF. Ultimately, where adjacent sprouts and vessels meet and interact positively, continuous lumens establish allowing perfusion of the new vessel. The vessels become stabilized by the reformation of cell-cell junctions, coverage of the vessel by pericytes and the deposition of basement membrane (reviewed by Adams and Alitalo, 2007; Carmeliet and

Jain, 2011; Hillen and Griffioen, 2007; Weis and Cheresh, 2011). It is proposed that the secretion of PDGF-B by endothelial cells and the subsequent activation of PDGFR-β on pericytes stimulates pericyte recruitment (reviewed by Gerhardt and Betsholtz, 2003). Factors including Ang1, sphingosine-1-phosphate and MMPs might also promote pericyte recruitment and the expression of tissue inhibitors of matrix metalloproteinases by both pericytes and endothelial cells contribute to vessel stabilistion (Raza et al., 2010).

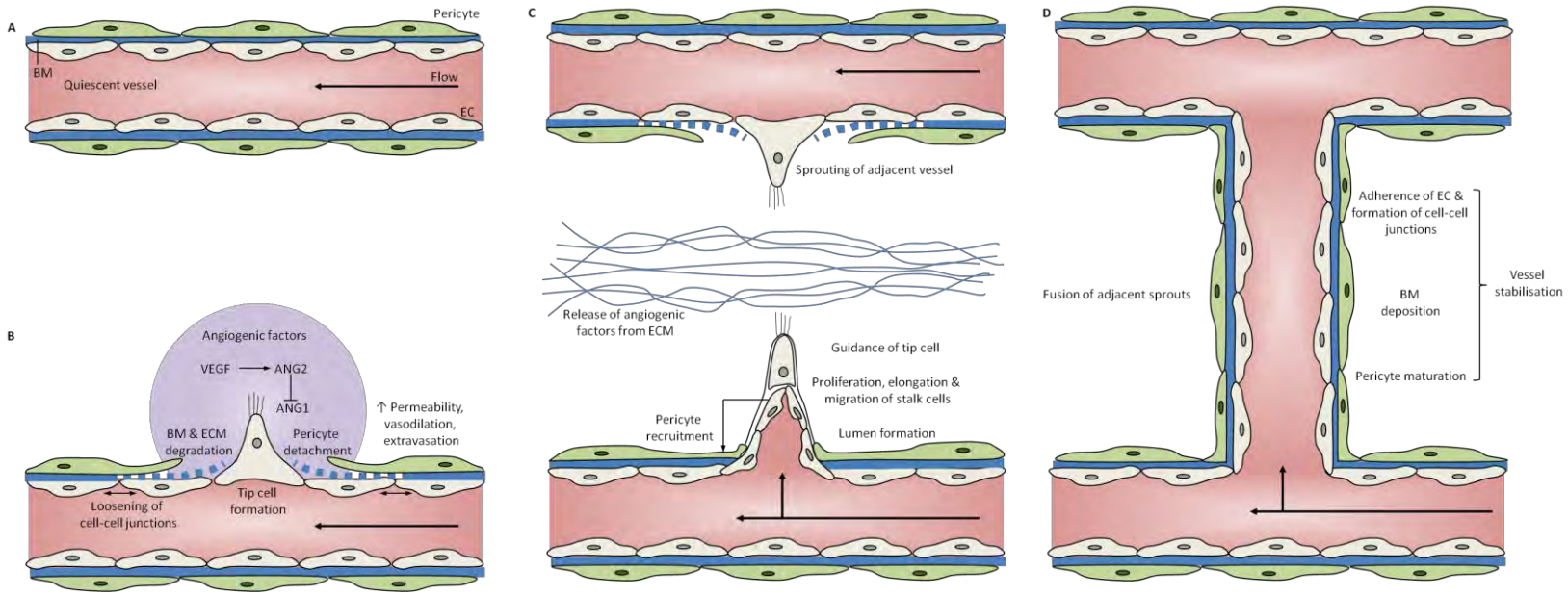

Figure 1.5: The process of sprouting angiogenesis.

Angiogenic factors (e.g. vascular endothelial growth factors (VEGF) and angiopoietins (ANG)) released by tumours cause a quiescent vessel **(A)** to become destabilized and a tip cell to form in a NOTCH-receptor-ligand pathway **(B)**. Proteases secreted by activated endothelial cells (EC) degrade the basement membrane (BM) and extracellular matrix (ECM) locally releasing angiogenic factors and creating a path for the stalk cells to proliferate, elongate and migrate into the perivascular space guided by the tip cell which senses the environment through receptors on its filiopodial projections. A lumen forms in the sprouting vessel **(C)**. Sprouts from adjacent vessels fuse allowing perfusion of the neovessel. The new vessel is stabilized by the formation of EC-EC junctions, coverage by pericytes and BM deposition by both EC and pericytes **(D)**. Adapted from Carmeliet and Jain (2011).

1.3.3 The mechanism of cell migration

The migration of endothelial cells during angiogenesis is the product of three migratory mechanisms: chemotaxis (migration toward a gradient of soluble chemoattractants); haptotaxis (migration toward a gradient of immobilised ligands) and mechanotaxis (migration induced by mechanical forces experienced at the blood vessel inner face). Stimulants for these processes include: soluble growth factors, extracellular matrix (ECM) components and sheer stress, respectively. Endothelial cells sense these signals via receptors on their filopodial extensions and migrate in the direction coordinated by the sum of the received signals. A cycle of stepwise changes to the organisation of the cell's actin cytoskeleton underlies the process.

After a stimulus is detected by sensing filopodial projections, a lamelipodium is extended from the leading edge. Surface adhesion receptors called integrins **(section 1.3.4)** cluster beneath and mediate attachment of this extension to the underlying substratum, which *in vivo* is the ECM **(section 1.4)**. Activation of the integrins promotes the assembly of protein complexes called focal adhesions **(section 1.3.5)** at these sites and the formation of actin stress-fibres. Subsequent contraction of the cell body achieves forward progression of the cell. This is followed by release of the rear of the cell and the cycle completes with the recycling of the adhesive and signalling molecules (reviewed by Gardel et al., 2010; Lamalice et al., 2007) **(Figure 1.6)**. A host of cellular and extracellular proteins are thus important mediators of cell migration and their abundance, organisation and activation states are potential modifiers of cell motility.

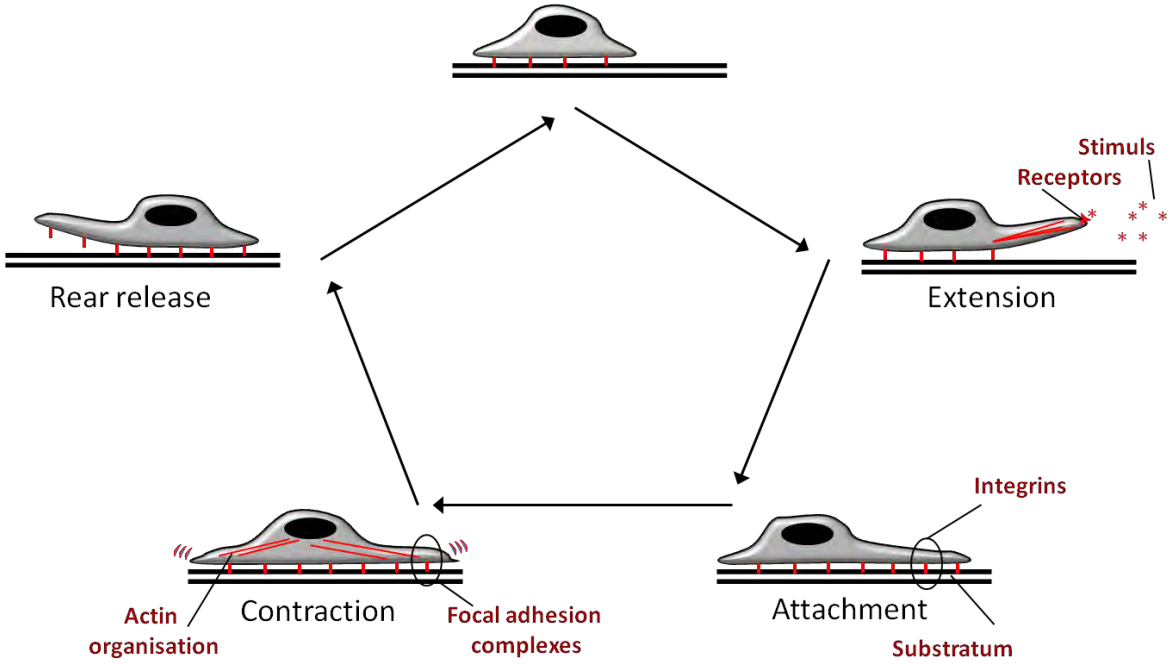

Figure 1.6: The major steps in cell migration.
In response to a motility stimulus (soluble chemoattractant (e.g. growth factor), immobilised ligand (e.g. extracellular matrix component) or sheer stress) cells extend a lamellipodium toward the stimulus. Focal adhesions link the cytoskeleton to the extracellular matrix and contraction of actin stress fibres pulls the cell body forward. The rear of the cell detaches and adhesive and signalling proteins are recycled. Adapted from Lamalice et al (2007).

1.3.4 Integrins

Integrins are a family of adhesion molecules that together with proteins including cadherins, immunoglobulin super family cell adhesion molecules, selectins and syndecans are critical mediators of cell-cell and cell-ECM interactions (Alberts et al., 2002). Integrins synergize with other cell surface receptors, such as G-protein coupled and kinase receptors, that respond to soluble chemokines or growth factors, to regulate the shape, polarity and motility and also the survival and proliferation of cells (see Hynes, 2002).

Integrins are heterodimeric proteins composed of non-covalently associated α and β subunits both of which are highly glycosylated single-pass transmembrane proteins (90-160kDa) (Anthis and Campbell, 2011; Hynes, 1992) **(Figure 1.7).** Eighteen α and eight β subunits have been identified to date with further variants generated by differential splicing. These subunits are arranged into at least twenty-four αβ heterodimers (see Anthis and Campbell, 2011; Hynes, 2002) making the integrins a highly diverse family both structurally and functionally **(Figure 1.8).** Despite a similarity in primary structure (Springer and Wang, 2004) the phenotypes of knockout mice indicate that each integrin subunit has a specific and non-redundant function (reviewed by Hynes, 2002).

The different integrin heterodimers recognise distinct ligands, although there is some overlap **(Figure 1.8)**, and relay signals bidirectionally across the membrane conveying information concerning the extracellular environment into the cell (termed 'outside-in' signalling) but also regulating integrin adhesiveness according to intracellular conditions (termed 'inside-out' signalling). Integrin cytoplasmic tails lack enzymatic or actin binding activity but support signalling as they present domains for the recruitment of complexes of enzymatic and adaptor proteins with signalling capacity. The β-tails are the main platforms for these intracellular interactions while the α-subunits are the principal determinants of extracellular ligand binding specificity (Anthis and Campbell, 2011).

A given cell type presents a distinct array of integrins. The main endothelial integrins include: α1β1; α2β1; α3β1; α5β1; α6β1; αvβ3 (Stupack and Cheresh, 2002). Overall, integrins have roles in a broad spectrum of biological processes including development, tissue repair, innate and adaptive immunity, haemostasis and angiogenesis; thus the deregulation of

integrins is implicated in many diseases such as autoimmune conditions, vascular disease and cancer (reviewed by Humphries, 2000; Hynes, 2002; Rathinam and Alahari, 2010).

The binding of integrins to their ligands involves the shared coordination of a divalent cation, either calcium or magnesium, between the integrin and its ligand. Accordingly, a carboxylate residue, either an aspartate or glutamate residue, is key in the ligand binding site. The I domains, present in about half of α subunits, and the I-like domains of β subunits are important for ligand binding because they contain a metal ion dependent adhesion site that binds the critical cation: the ion becomes fully coordinated by interaction with the ligand. Herein magnesium and calcium can have opposite effects upon the binding of different integrins to their ligands (Mizejewski, 1999). In the presence of the α subunit I domain, the β-subunit I-like domain assumes an indirect role in ligand binding, regulating the activity of the I domain through contacts with the α subunit β-propeller domain (see Humphries, 2000; Springer and Wang, 2004).

Studies suggest two extremes of integrin activation state, an "active/on" state and "inactive/off" state, which lie in conformational equilibrium (Anthis and Campbell, 2011). Intracellular and extracellular conditions impinge upon this equilibrium and dictate where the balance lies. Many integrins appear to retain an adhesion competent state whilst others, such as the β2 integrins that regulate leukocyte extravasation from circulation and the major platelet integrin, αIIbβ3, which directs haemostasis, are necessarily maintained in an inactive state until cells are appropriately activated (see Hynes, 2002). A bent, closed conformation is suggested for the inactive receptor: the structure is stabilized by extensive interactions between buried surfaces of the integrin head and tailpieces. In contrast, from an extended conformation, an open, active conformation that is capable of high affinity interaction with its

ligand can be accessed. This form is stabilised by ligand binding (reviewed by Anthis and Campbell, 2011; Hynes, 2002; Springer and Wang, 2004).

With the exception of integrin $\alpha 6\beta 4$, which connects to intermediate filaments, integrin cytoplasmic domains link via a plethora of sub-membrane adaptor proteins to the actin-based microfilament system of the cell's cytoskeleton. The assembly of such protein complexes generally requires integrin clustering (see Hynes, 2002). The following section provides an overview to the focal protein assemblies that form at cell-substratum attachment sites.

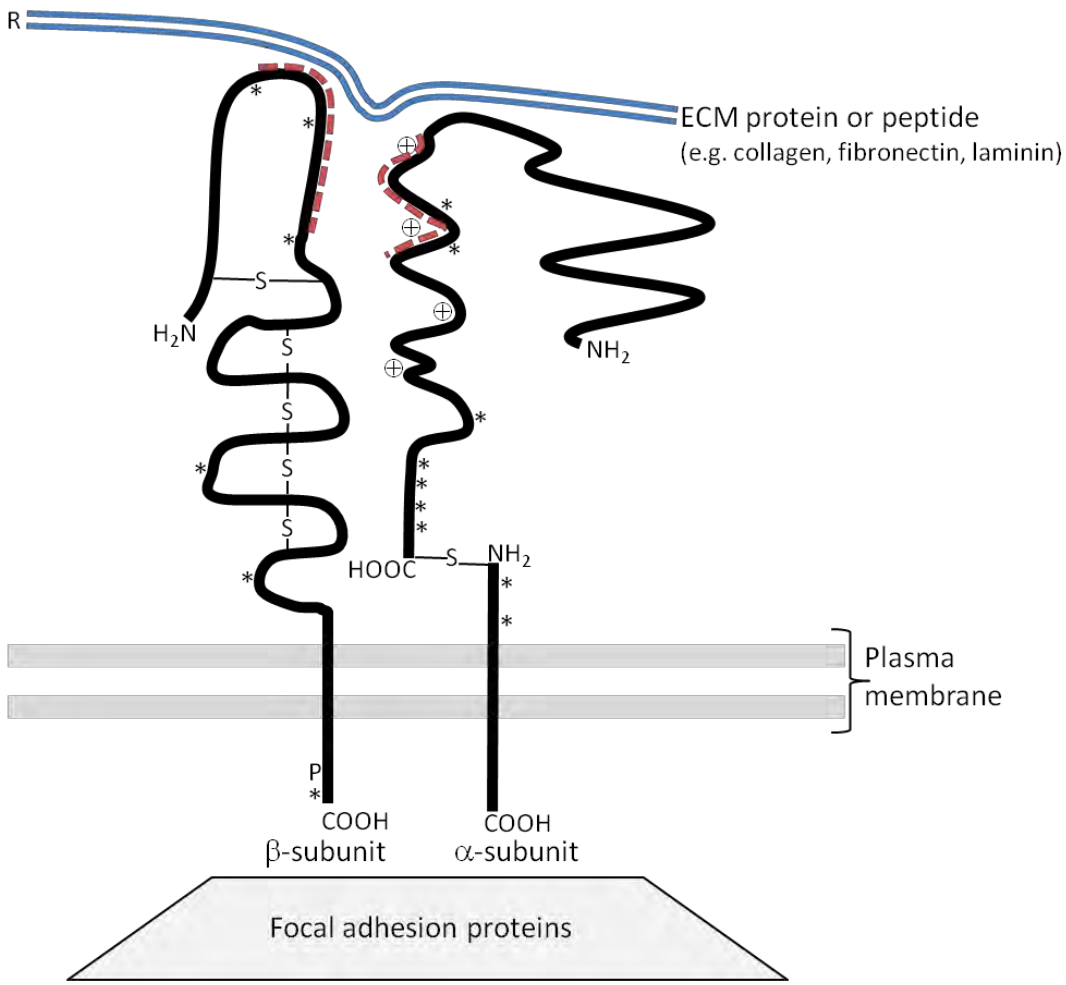

Figure 1.7: Diagrammatic representation of a universal integrin receptor.

Integrin receptors are heterodimers formed by the non-covalent association of one α and one β subunit. Both subunits are single pass transmembrane proteins with a long extracellular domain compared to cytoplasmic domain. On the extracellular side they bind to molecules of the extracellular matrix. On the intracellular side they recruit molecules of focal adhesions which provide a physical link to the actin cytoskeleton. The tertiary structures of both subunits are maintained through disulfide bridges (-S-S-) and non-activated integrins contain divalent cation salt bridges that are extruded upon ligand binding (⊕). Both subunits contribute to the ligand binding pocket (dotted red line). Both subunits are heavily glycosylated (*). Phosphorylation site (P). Adapted from Mizejewski (1999).

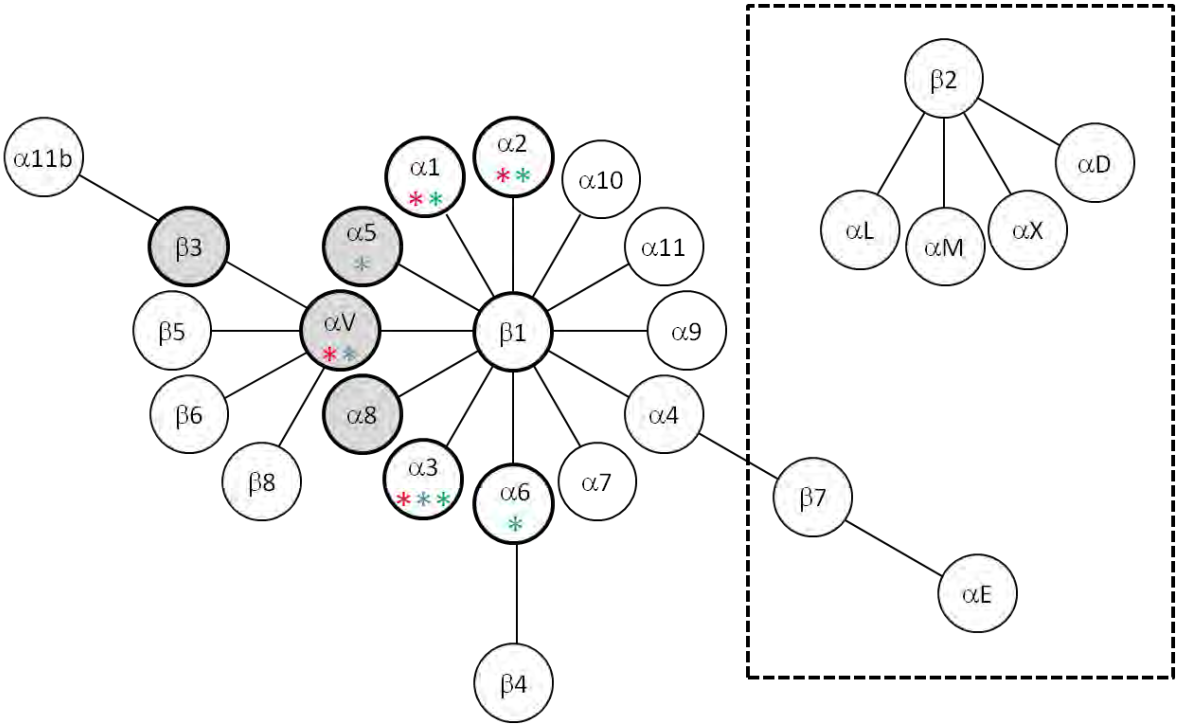

Figure 1.8: The integrin receptor family.

Eight β subunits are known to assort with eighteen α subunits in the formation of 24 different integrin heterodimers. Among these, expression of a subgroup is restricted to leukocytes (dotted box). Subunits with bold surrounds indicate those expressed by endothelial cells. The ligand binding specificities of the subunits expressed by endothelial cells are indicated: collagen (red star (*)); fibronectin (blue star (*)); laminin (green star (*)) and Arg-Glu-Asp (RGD) (grey shading). Adapted from Hynes (2002).

1.3.5 Focal adhesions

The physical connection of the ECM to the ends of actin stress fibres means that the structures formed are adhesive and the cell is brought close to its substratum at these sites. The nascent complexes, which generally form beneath the lamellipodia of migrating cells, are small dot-like structures termed 'focal complexes'. These complexes are usually immobile and short-lived, either dissembling or elongating into mature 'focal adhesions' within seconds. In contrast, focal adhesions can exist for tens of minutes before gradually disappearing or maturing further into stable fibrillar adhesions (reviewed by Gardel et al., 2010; Geiger et al., 2001; Parsons et al., 2010; Wolfenson et al., 2009)

Focal adhesion assembly is driven by tension forces that are either generated intracellularly by myosin-II driven contraction of the cytoskeleton or are provided by an extracellular applied force (Geiger et al., 2001). In this way, focal adhesion formation reflects the contractile state of the cell and also the pliability of the matrix (see Parsons et al., 2010; Wolfenson et al., 2009). By acting as anchorage sites for bundles of stress fibres, focal adhesions support the generation of traction forces within the cell and their transduction to the matrix, mediating cell adhesion, manipulation of matrix protein organisation and the forward movement of migrating cells (reviewed by Parsons et al., 2010; Wolfenson et al., 2009).

Relaxation of the cytoskeleton generally leads to focal adhesion disassembly. In the cycle of events underlying cell migration, focal adhesions disassemble when they become localised to the rear of the cell. This allows forward movement of the rest of the cell **(Figure 1.6)** (see Ridley et al., 2003). The mechanism for disassembly is uncertain but suggested triggers include: down regulation of myosin II contractility by a high density of microtubules (Elbaum et al., 1999; Small et al., 2002), activity of the focal adhesion protease calpain (Bhatt et al.,

2002) and microtubule-dependent endocytosis activated by the Focal Adhesion Kinase (FAK)-dynamin pathway (Burridge, 2005; Ezratty et al., 2005; Wolfenson et al., 2009).

Current estimates suggest that over 125 different proteins function at focal adhesions (see Deakin and Turner, 2008) although not all are necessarily present simultaneously in all complexes. Integrins are the central components of most focal adhesions, binding to ECM molecules (mainly fibronectin, vitronectin and collagens) via their extracellular domain and plaque proteins via their cytoplasmic domain. However, other non-integrin membrane-bound protein and glycoprotein components are involved such as: syndecan-4 (Syn-4) (Echtermeyer et al., 1999; Okina et al., 2009); layilin (Lay) (Borowsky and Hynes, 1998; Wegener et al., 2008); urokinase plasminogen activator receptor (uPAR) (Chapman and Wei, 2001; Wei et al., 1999), leukocyte common antigen receptor (LAR) (Serra-Pages et al., 1995) and SHP-2 substrate-1 (SHPS-1) (Tsuda et al., 1998), as well as signalling lipids, for example phosphatidylinositol 4,5 bisphosphate (PtdIns $(4,5)P_2$), which can regulate actin polymerisation (reviewed by Geiger et al., 2001)

Most cytosolic focal adhesion proteins are multi-domain proteins and have several possible binding partners. Competition for binding is apparent among these partners; thus the specific combinations of proteins recruited provide regulation of focal adhesion functions. Many protein docking sites are generated by phosphorylations catalysed by tyrosine, and serine-threonine kinases that are recruited to the adhesions. For example, phosphotyrosines are sites for Src homology-2 (SH2)-domain-containing proteins. Proline rich sequences are similarly docking sites for SH3-domain-containing proteins (see Zamir and Geiger, 2001).

Among the plethora of proteins there are some which connect the integrins directly to the actin cytoskeleton. These are the main structural scaffolds of the complexes. Other proteins

with adaptor or enzymatic functions associate only with the integrin tails; while others bind to the actin filaments. Additional adaptor proteins and enzymes bind to these integrin or actin binding proteins and function in completing multi-protein, intracellular connections between the ECM and the actin cytoskeleton and in signalling **(Table 1.1 and Figure 1.9)** (see Geiger et al., 2001; Zamir and Geiger, 2001).

FAK is recognised to be a principal regulator of focal adhesion dynamics through its actions as both a kinase and a scaffold protein (see Mitra et al., 2005). Studies suggest that it has important roles in the assembly but also the disassembly of focal adhesions as phosphorylation of FAK was associated with focal adhesion formation (Parsons, 2003) but equally focal adhesion formation was increased in FAK-null fibroblasts (Ilic et al., 1995).

FAK becomes localised at forming adhesions through the binding of its focal adhesion targeting (FAT) domain to paxillin and talin at the sites of integrin clusters. Subsequent autophosphorylation of FAK at Tyr397 creates a binding site for Src kinase and a dual-activated FAK-Src signalling complex is formed. Src phosphorylation of additional phosphotyrosines on FAK maximises its catalytic (Tyr576 and Tyr577) and adaptor (Tyr861 and Tyr925) activity: pTyr861 potentiates SH3-domain mediated binding of p130Cas to the C-terminal proline rich region and pTyr925 recruits Growth factor receptor-bound protein (Grb)-2 via its SH2-domain. These interactions lead to the respective activation of the Rho-family small guanosine triphosphate (GTP)-binding protein RacGTPase and the RasGTPase-extracellular signal-regulated kinase-2 (ERK2)/mitogen-activated protein kinase (MAPK) cascade with impacts upon migration (reviewed by Frame et al., 2010; Mitra et al., 2005).

Other Rho-family GTPases: Cdc42, RhoG and RhoA also have roles in modulating the establishment of cell polarity and controlling migration; their regulators are likewise controlled by FAK (see Frame et al., 2010).

Cdc42, RhoG and Rac regulate lamellipolia and filopodia formation at the leading edge. The polymerisation of the branched actin network of lamellipodia is mediated by the actin related protein (Arp)2/3 complex which is activated by the Wiskott-Aldrich Syndrome Family Proteins WAVE (Wiscott-Aldrich family Verprolin homologous protein) and WASP (Wiscott-Aldrich Syndrome Protein) that are Rac and Cdc42 effectors. WAVE and WASP proteins themselves also feedback to positively and negatively regulate Rac and Cdc42 through binding to guanine nucleotide exchange factors (GEFs) and GTPase activating proteins (GAPs). Furthermore, FAK associates with Cdc42 activated-N-WASP to promote cell motility through retaining N-WASP in the cytosol (see Mitra et al., 2005). FAK also binds directly to Arp2/3 (Serrels et al., 2007).

RhoA typically functions at the sides and rear of the cell. The mechanism of zonal Rho-family GTPase activity within a polarised migrating cell is not fully defined. FAK has also been implicated in the regulation of RhoA through binding and phosphorylating p190RhoGEF (Tomar and Schlaepfer, 2009). Finally, gradients of phosphoinositides (PtdIns) are generated in cells that are migrating in response to chemoattractant and provide intracellular amplification of the shallow chemokine gradient across the cell. They also bind to and recruit certain focal adhesion proteins (e.g. α-actinin, vinculin and talin). Several of the PtdIns kinases in this cascade interact with and are activated by FAK such as Type I PtdIns phosphate kinase-γ (PIPKγ), which converts PtdIns(4)P to PtdIns(4,5)P_2 and PtdIns 3-kinase (PI3K), which converts PtdIns(4,5)P_2 to PtdIns(3,4,5)P3 (see Mitra et al., 2005)

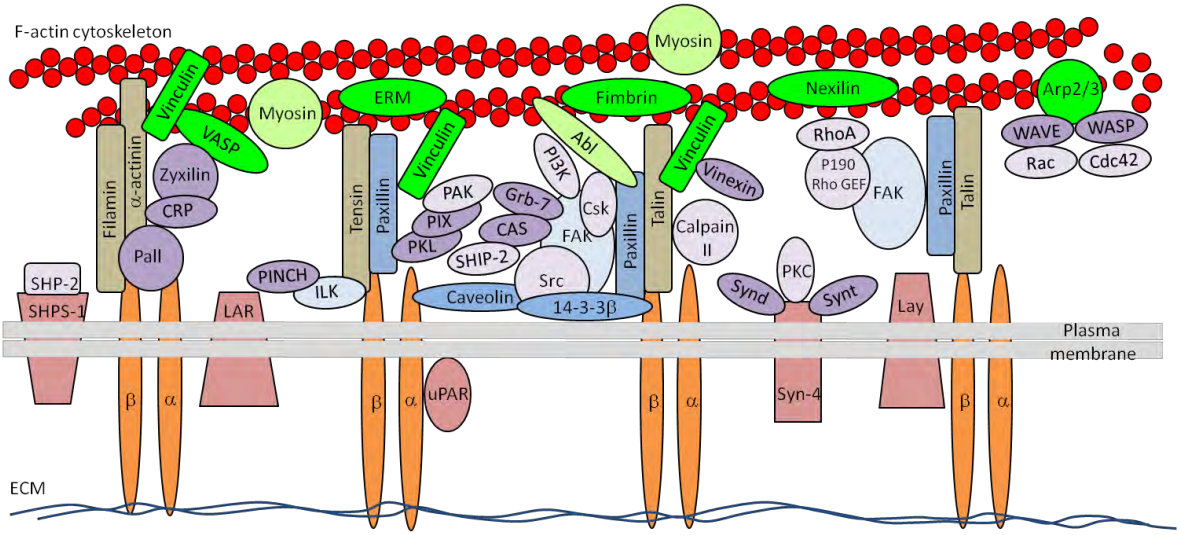

Figure 1.9: Diagrammatic representation of a focal adhesion.

Focal adhesions are multi-protein complexes that assemble at sites of integrin (orange) activation and link the cytoplasmic actin cytoskeleton to the extracellular matrix (ECM). Bi-directional signalling occurs enabling the cytoskeleton to exert force on the ECM but also the ECM to influence the cell's contractility. Other non-integrin membrane bound proteins are also found (pink). On the inside of the cell there are: scaffolding proteins that link integrins to the cytoskeleton (brown); integrin binding (blue) and actin binding (green) adaptors and enzymes; as well as additional adaptors and enzymes (purple) [adaptors are indicated by darker shades, enzymes by light shades]. Refer to text and Table 1.1 for definition of acronymns. Adapted from Geiger (2001).

Table 1.1: Proteins present in focal adhesions and their functions.

Protein function	Examples
Connect integrins directly to the actin cytoskeleton	α-actinin filamin talin tensin
Integrin binding	caveolin integrin-linked kinase (ILK) paxillin 14-3-3
Actin binding	ezrin-radixin-moesin proteins (ERM) fimbrin nexilin parvin vasodilator-stimulated phosphoprotein (VASP) vinculin
Adaptor proteins	Crk-associated substrate (CAS) cysteine-rich protein (CRP) Grb-7 PAK-interacting exchange factor (PIX) palladin (Pall) paxillin kinase linker (PKL) syndesmos (synd) syntenin (synt) vinexin zyxin
Enzymes	Abl kinase calpain II carboxy-terminal src kinase (Csk) focal adhesion kinase (FAK) p21-activated kinase (PAK) phosphatidyl inositol 3-kinase (PI3K) SH2-containing phosphatase-2 (SHP-2) SH2-containing inositol 5-phosphatase-2 (SHIP-2) Src-family kinases (Src)

1.4 THE EXTRACELLULAR MATRIX (ECM)

Similar to a number of other tissues including epithelial, nerve, muscle and fat, the endothelium is interfaced on its subluminal side by a thin, highly organized dense meshwork of protein fibres called the basement membrane (see Kruegel and Miosge, 2010; Sund et al., 2004). This protein matrix is deposited by endothelial and supporting cells and maintains separation of the endothelium from the more porous, fibrillar connective tissue beneath (Schwarzbauer, 1999). Together, basement membrane and connective tissue constitute the ECM.

The ECM is a dynamic substance being continuously secreted and remoulded. The specific composition and organization of the ECM differs according to the tissue type, stage of development and location (see Kruegel and Miosge, 2010; Schwarzbauer, 1999; Sund et al., 2004).

The ECM has a critical role in the assembly, stabilization and properties of the vasculature since endothelial cells bind to components of the ECM via their surface integrins and non-integrin receptors and receive signals that regulate their proliferation (see Assoian and Schwartz, 2001; Meredith and Schwartz, 1997; Roovers and Assoian, 2000; Vinals and Pouyssegur, 1999), survival (Meredith and Schwartz, 1997) and migration **(section 1.4.4)** and which establish and maintain their organization into blood vessel structures (see Davis and Senger, 2005).

During vascular morphogenesis endothelial cells from distant sites can organize into multicellular structures by the generation of contractile forces through the ECM (Davis and Senger, 2005). In sprouting angiogenesis, ECM fibres aligned by traction forces might provide the pathways for the follow-the-leader behavior of endothelial cells (see Vernon and

Sage, 1995). Overall it has been suggested that the role of the ECM in endothelial cell migration, proliferation and survival is equal to or greater than that of angiogenic growth factors. Furthermore, by immobilizing angiogenic growth factors, the ECM may assist in their actions (see Davis and Senger, 2005).

Although the structures of interstitial connective tissue and the basement membrane differ, they comprise similar proteins. The major components of the endothelial basement membrane include laminins, collagen IV and fibronectin; additional accessory components include perlecan, nidogens, entactin, heparin sulphate proteoglycans and collagen XVIII. It is not clear whether endothelial cells *in vivo* can generate a complete functional basement membrane or whether this is dependent upon supporting cells such as pericytes to contribute accessory components such as nidogens (see Davis and Senger, 2005). The following paragraphs provide a description of each of the three major protein types present in endothelial basement membrane.

1.4.1 Laminins

Laminins are a family of large heterotrimeric proteins (500-900kDa) that appear to be the principal determinants of basement membrane assembly (Davis and Senger, 2005).

Each laminin trimer is comprised of one α, one β, and one γ chain assembled into a cross-shape with two or three short arms and one long arm **(Figure 1.10).** Five α, three β and three γ chains have been identified and demonstrate some tissue specificity. Overall, when splice variants are also considered, sixteen different laminins have been identified. Individual chains contain several conserved domains **(Figure 1.10)**. These have structural and functional importance. Furthermore, the specific patterns with which laminin molecules are deposited in the matrix can influence the matrix function (reviewed by Hamill et al., 2009).

Laminin trimers are assembled intracellularly and are then secreted. Sequences in the C-terminus of the coiled-coil, alpha helical domains of each chain are implicated in the process of trimerisation. Initially, disulfide bonds form between the β and γ chains, creating an acidic pocket that is subsequently stabilised by the interaction of a basic site on the α chain. Trimerisation, by the binding of the α chain also drives secretion (Nomizu et al., 1996). Laminin deposition and the formation of laminin matrices is regulated by cell surface receptors including: integrins, dystroglycan, 32/67kDa laminin receptor, 67kDa elastin-laminin receptor, galactoside-binding lectin, galactosyltransferase, heparan sulphate proteoglycans, and Ig-related basal cell adhesion molecule (see Patarroyo et al., 2002).

Several integrins have been found to interact with laminins including: α1β1, α2β1, α3β1, α6β1, α6β4, αvβ3 and α7β1. They demonstrate distinct and overlapping specificities (reviewed by (Patarroyo et al., 2002; Tzu and Marinkovich, 2008). Most of the characterised sites of integrin-laminin binding are within the G-domain and domain VI of the laminin α chains but some interactions with laminin β and γ chains have been described. Proteolysis of laminin α, β and γ chains might also expose additional sites for integrin binding (reviewed by Patarroyo et al., 2002; Tzu and Marinkovich, 2008).

The predominant laminins expressed in endothelial basement membranes are thought to include laminin-411, and laminin-511, but there is some additional contribution from laminin-421 and laminin-521. During development laminin-411 appears to predominate over laminin-511 in the vascular bed but in adult tissues there is a switch and laminin-511 becomes the more abundant. While laminin-511 is capable of self-polymerisation, laminin-411 lacks the necessary globular LN domain at the N terminus of its α4 chain. Subsequently, it may be unable to drive the assembly of the laminin matrix but might still establish connections with

other matrix constituents such as collagens, nidogens, and perlecan (reviewed by Davis and Senger, 2005).

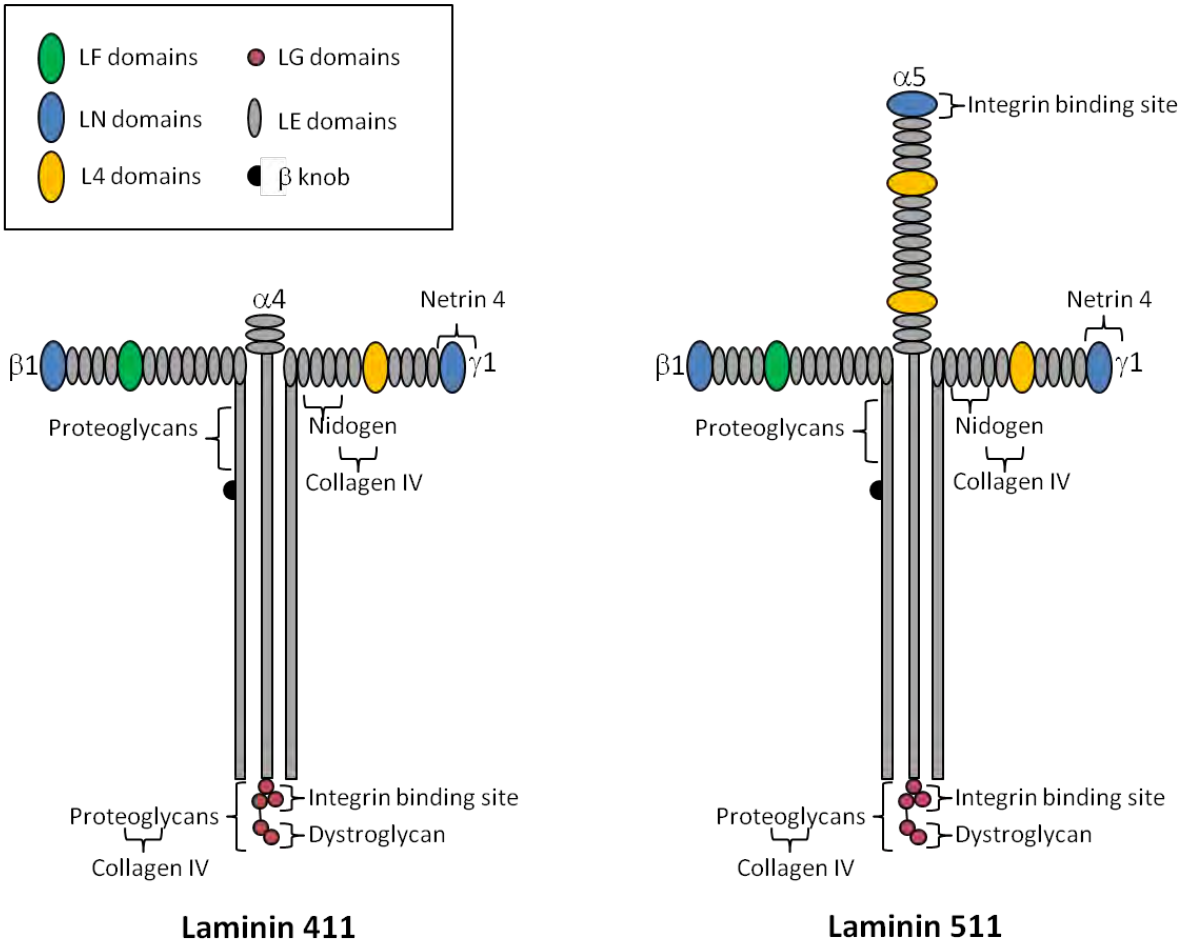

Figure 1.10: Diagrammatic representations of laminins 411 and 511.

Laminins are heterotrimeric molecules in which the three chains (α, β and γ) are organised into a cross shape. 5α, 3β and 3γ chains are known. Endothelial laminins are composed of assortments of α4, α5, β1, β2 and γ1 chains and include laminins 411, 511, 421 and 521. Each chain features a number of functionally important domains including LN, L4 and LF globular domains that are interspersed among laminin-type epidermal growth factor-like LE domains. An α-helical domain follows the LE repeats. In the heterotrimer these stretches wind around each other forming a coil-coil. The α-helical region of the β-chain is interrupted by a stretch of amino acids called the β-knob. Five globular LG domains follow the α-helical domain of the α-chain. Domains LG1-LG3 adopt a clover leaf shape. The LG4-LG5 domain

may be proteolytically cleaved from the α4 chain following secretion. The α4 chain also lacks the amino-terminal LN domain found in most other α chains, this may impact polymerisation. Binding sites for matrix molecules (proteoglycans, collagen IV, netrin and nidogen) and cell surface receptors (integrins and dystroglycan) are indicated. Adapted from Hamill et al (2009).

1.4.2 Collagens

Collagens are large macromolecules which in vertebrates serve as one of the major extracellular scaffolds, providing mechanical strength and organisation to the extracellular matrix. Twenty-eight different collagens have been identified to date (types I-XXVIII). Their basic building units are collagen α-chains that self-assemble, according to the chains present, into several supramolecular structures including: fibrils, microfibrils, networks and transmembrane proteins. Other macromolecules such as laminins, perlecan, and proteoglycans attach to these scaffolds in the construction of the multimolecular ECM and cells adhere to the ECM by the binding of certain integrin (primarily of the β1 subgroup of integrins (α1β1, α2β1)) and non-integrin receptors (heparin sulphate proteoglycans, glycoprotein VI, mannose receptor family and discoidin domain receptors) to specific sites within collagen structures (reviewed by Khoshnoodi et al., 2006; Khoshnoodi et al., 2008; Leitinger and Hohenester, 2007)

The assembly of collagens first involves the homo or hetero-trimerisation of three type-specific α-chains which intertwine forming triple helical protomers. Following their secretion from the cell, these protomers oligomerise into the 'encoded' supramolecular structure. The constituent α-chains of collagens have a common structure. They feature a central collagenous domain, characterised by triplet repeats of the residues Gly-X-Y, which is

flanked by non-collagenous domains at both the N and C termini. The excision or processing of these terminal domains is important for the assembly of some collagens (see Khoshnoodi et al., 2006).

Collagen IV **(Figure 1.11)**, a network collagen, is of particular interest to this study as it is an exclusive collagen of basement membrane where it influences the behaviours, such as adhesion, migration and differentiation, of many cell types including: endothelial cells, hepatocytes, keratinocytes, pancreatic cells, platelets and tumour cells (see Khoshnoodi et al., 2008). Up to six α-chains (α1-α6) have been identified in collagen IV networks from across different tissues and developmental stages. While seventy-six trimers are theoretically possible using these six chains, only three heterotrimers (α1α1α2, α3α4α5, α5α5α6) are observed in vertebrate basement membranes illustrating the high degree of encoded specificity that exists in collagen trimer formation. Studies suggest that the C-terminal non-collagenous regions of collagen IV α-chains (~230 residues) control the chains incorporated into the triple helices through a three-dimensional domain swapping mechanism (reviewed by Khoshnoodi et al., 2006).

The central collagenous domains of collagen IV α-chains (~1400 residues) contain between 21 and 26 short non-collagenous sequence interruptions. These contribute flexibility to the collagen IV network, potentiate interchain crosslinking and serve as cell binding sites (Khoshnoodi et al., 2008). High resolution electron microscopy of collagen IV networks has revealed an irregular polygonal structure that is maintained by lateral interactions along the length of the helix and between end terminal domains (Yurchenco and Ruben, 1987). Twisting into a supercoil also stabilises the structure (Yurchenco and Ruben, 1987). The collagen molecules are also extensively modified co-and post-translationally by a number of

specific and non-specific enzymes. Examples of processing and modifications include: the removal of signal peptide in the endoplasmic reticulum, addition of hydroxylate to proline and lysine residues, glycosylation of hydroxylysines and the addition of mannose rich oligosaccharides (reviewed by Khoshnoodi et al., 2006; Khoshnoodi et al., 2008).

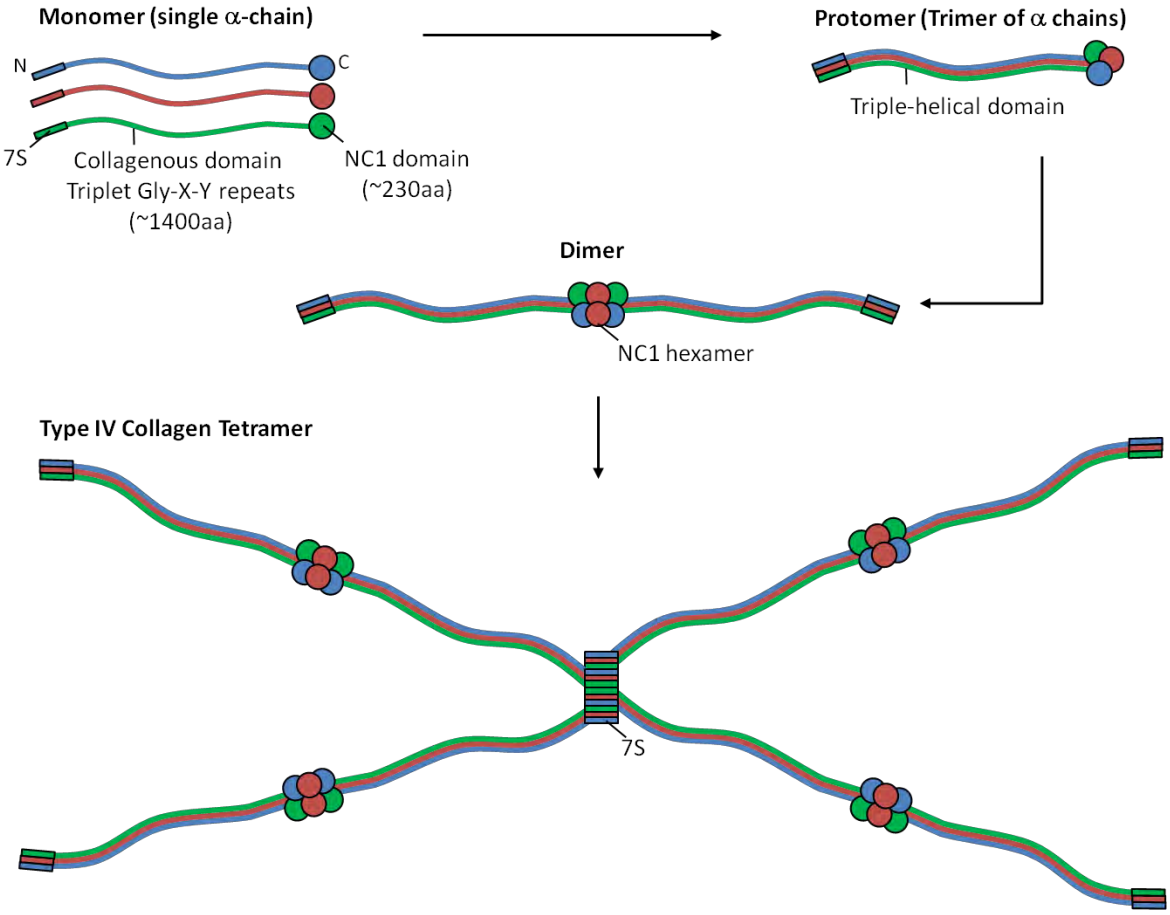

Figure 1.11: Diagrammatic representation of collagen IV network formation.
Three collagen monomers each comprising an amino terminal glycosylated 7S domain, central collagenous Gly-X-Y domain and carboxy-terminus non-collagenous (NC1) domain trimerise to form a protomer with central helical domain in a mechanism that is initiated by the NC1 domains. Two protomers dimerise by end-to-end interaction of the two NC1 trimers forming an NC1 hexamer. Subsequent interaction of four dimers at the amino terminal forms the tetramer. Tetramers can assemble into higher order supramolecular organisations and three dimensional networks.

1.4.3 Fibronectin

Fibronectin is a large multidomain, dimeric glycoprotein **(Figure 1.12)** that is one of the main non-collagen scaffolding proteins of the extracellular matrix. It is present in all tissues where it has an essential role throughout all stages of life. The constituent monomers are joined end-to end in the dimer by disulfide bonds. Maturation of the fibronectin matrix involves further clustering of individual fibrils into thicker bundles, a process that is directed by the actomyosin cytoskeleton.

Unlike collagens, fibronectin fibrils do not self assemble. Rather, additional cell-surface proteins assist with their polymerisation. In particular, the fibronectin binding integrin, $\alpha5\beta1$, associates with fibronectin fibrils at sites called fibrillar adhesions (fibrillar adhesions are distinct from focal adhesions and involve a different array of adaptor proteins) and links fibronectin to the actin cytoskeleton. Contraction of the actin cytoskeleton stretches the fibrils exposing hidden binding sites for the clustering of fibrils.

Fibronectin monomers comprise several domains that are connected by lengths of flexible polypeptide chain. These domains are further subdivided into a number of repeated modules that have different functions. The main modular units include types I, II and III fibronectin **(Figure 1.12)**. Several domains of the protein have been identified to have roles in the assembly of fibronectin fibrils and in their binding to other components of the extracellular matrix, such as collagen, heparin and syndecans. For example, the RGD motif in module III10 and the synergy site in III9 are important for cell mediated assembly of the fibronectin matrix via integrin $\alpha5\beta1$ binding (reviewed by Alberts et al., 2002; Singh et al., 2010).

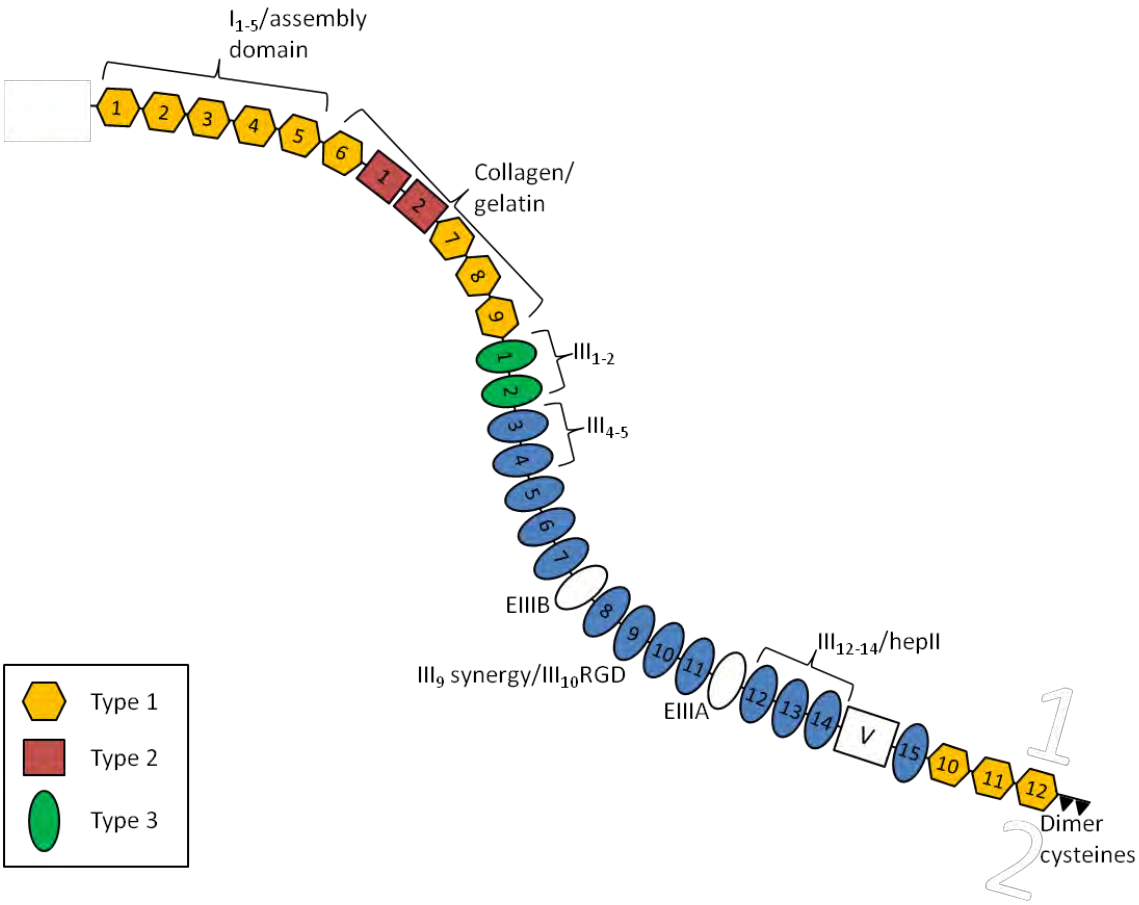

Figure 1.12: Diagrammatic representation of a fibronectin subunit.

Fibronectin is a 500kDa dimeric molecule formed through the interaction of two subunits via a pair of antiparallel disulfide bonds between the C-termini. Each subunit comprises three types of repeating unit (type 1 (hexagon); type 2 (rectangle); type 3 (oval) that follow a curved contour similar to the shape illustrated. Assembly involves domains I1-5 and the III1-2 domains. Other modules provide binding sites for collagen/gelatine (I6-9), integrin α5β1 (synergy site in III9 and RGD sequence in III10), fibronectin (II1-2, III4-5 and III12-14/hepII), heparin and syndecans (III12-14/hepII) and other extracellular molecules. Alternative splicing at EIIIA and EIIIB and exon subdivision at V generates multiple isoforms of fibronectin (20 in humans). Adapted from Singh (2010).

1.4.4 Extracellular matrix proteins as chemotactic and haptotactic stimuli

The individual contributions of ECM components to chemotactic and haptotactic migration are incompletely understood and appear to be cell-type dependent but several studies, summarised in this section, have demonstrated the potential of ECM molecules to influence the migratory behaviours of cells in response to gradients of growth factors and to themselves act both as chemoattractants and haptotactic signals.

Boyden chamber, checkerboard analysis of the effect of fibrinogen on endothelial cell migration indicated both chemoattractant and chemokinetic effects of this interstitial ECM component (Dejana et al., 1985) and dermal microvascular endothelial cells migrated in an integrin $\alpha1\beta1$ and integrin $\alpha2\beta1$ dependent fashion in both a gradient of immobilised collagen I and in a uniform collagen I matrix toward VEGF (Senger et al., 2002).

The study by Dejana et al (1985) did not observe a chemotactic effect of fluid-phase fibronectin (5-300μg/ml) on endothelial cell migration; however, haptotactic properties of fibronectin on endothelial cells have been demonstrated using a novel method involving the cross diffusion of functionalisable alkanethiols to generate gradients of fibronectin between 0 and 1.23ng fibronectin/mm^3 (Smith et al., 2006; Smith et al., 2004). Fibronectin gradients supported a higher drift speed of both bovine aortic and human microvascular endothelial cells than uniform fibronectin when cells were either migrating away from a confluent monolayer or were growing as individual 'free' cells (Smith et al., 2004). The increase in drift speed increased with increasing gradient slope between 0 and 1.23ng/mm^3 (Smith et al., 2006)

Similar to fibrinogen in the work by Dejana et al (1985), collagen IV, when added to the lower chamber of a Boyden chamber, stimulated the directional migration of aortic endothelial cells in a concentration gradient dependent fashion. An insoluble substratum

adsorbed gradient of collagen IV mirrored this effect of fluid phase collagen IV in promoting migration, indicating that collagen IV acts as a haptotactic stimulus. Laminin was less effective on a molar basis at promoting endothelial cell migration in the study (Herbst et al., 1988). Nonetheless, the lack of observation of an effect for laminin might have been due to the particular laminin isoforms predominating in the Engelbreth-Holm-Swarm (EHS) mouse sarcoma that was used as the source of laminin (laminin 111 as opposed to laminins 411 or 511), as cells do not demonstrate uniformity in their capacity to bind and migrate on different laminins (Cherepanova et al., 2002; Kalmykova et al., 2002).

Most of the more recent studies looking at the effects of laminin on cell migration have focussed on laminin 332, the laminin underlying skin, rather than endothelium. Nonetheless these studies indicate that the processing of laminin subunits and/or the patterns in which they are deposited in the matrix may be important in regulating the potential of laminin to influence cell migration. For example processing of the α3 chains of laminin-332 was found to underlie hemidesmosome formation while intact α3 chains supported migration (Goldfinger et al., 1998). This might be because processing exposes an internal binding site for the α6β4 integrin which supports hemidesmosome formation and inhibits migration (Hintermann et al., 2005). Certain fragments released upon cleavage by proteases might also promote migration. For example, DIII fragments cleaved from the laminin γ2 chain of laminin 322 by membrane type-1 MMP promoted breast cancer cell migration through ligation of the EGF receptor (Koshikawa et al., 2005).

There is considerable variation in the patterns in which different cells deposit laminins in culture. A rosette-like pattern of laminin-322 was found for non-migratory human keratinocytes whereas actively migrating keratinocytes had laminin-322 assembled into trails

(Sehgal et al., 2006). Whether, the degree of variation in arrangement extends to intact basement membranes *in vivo* is nonetheless unclear (Hamill et al., 2009). However, the importance of basement membrane organisation in governing migration is supported by observations that integrin β4-deficient skin cells, which migrate in an abnormal circular pattern *in vitro*, show processive migration when plated onto a laminin-322 matrix deposited by wildtype cells (Sehgal et al., 2006).

1.5 EFFECTS OF KSHV INFECTION ON ENDOTHELIAL CELL IDENTITY

As mentioned previously, this study aimed to extend current knowledge on KS pathogenesis by furthering understanding of the impact of KSHV infection upon endothelial cell functions. The effect of the virus on endothelial cell behaviour was of interest because the tumourigenic spindle cells of KS lesions have endothelial characteristics, notably they express the markers: cluster of differentiation molecule (CD)-34, C-X-C chemokine receptor (CXCR)-4, VEGFR3, lymphatic vessel endothelial hyaluronan receptor-1 (LYVE-1) (Dupin et al., 1999; Regezi et al., 1993; Weninger et al., 1999).

Prior to the work in this thesis, studies observing the infection of endothelial cells, both primary (Ciufo et al., 2001; Flore et al., 1998; Grossmann et al., 2006) and cell lines (Milligan et al., 2004; Moses et al., 1999) had affirmed the induction of a characteristic spindle cell shape following KSHV infection; thus supporting an endothelial origin for the KS spindle cell which is infected with KSHV *in vivo* (Boshoff et al., 1995a; Colman and Blackbourn, 2008*)*. Furthermore, ectopic expression of the single KSHV gene, viral FLICE inhibitory protein (vFLIP), in endothelial cells had generated a spindle morphology providing additional evidence that KSHV infection of endothelial cells underlies induction of the spindle shape and the possible modulated properties of these cells. NFκB activation downstream of vFLIP was

implicated in this morphological transformation (Grossmann et al., 2006). However, in view of the mixed blood vascular (CD34, CXCR4) and lymphatic (VEGFR3, LYVE-1) endothelial phenotype of KS spindle cells (Dupin et al., 1999; Regezi et al., 1993; Weninger et al., 1999); (Carroll et al., 2004; Hong et al., 2004; Wang et al., 2004a) and the fact that both types of endothelial cell are equally susceptible to KSHV infection (Wang et al., 2004a), it continues to be debated whether the spindle precursor cell during KS pathogenesis is of either vascular or lymphatic lineage.

Studies addressing the effect of KSHV infection upon the transcription profile of endothelial cells have highlighted that the dual blood vascular and lymphatic phenotype might have arisen because the virus reprogrammed the transcriptome of the infected cell. Using gene expression microarrays, Wang et al (2004a) observed a drift in the transcriptomes of both LEC and blood vascular endothelial cells (BEC) following infection with KSHV, such that the gene expression profiles of infected LEC and BEC were closer than those of untreated cells. In agreement, Hong et al (2004) reported KSHV-induction of (~70%) lymphatic lineage specific genes in human dermal microvascular endothelial cells and similar responses in human umbilical vein endothelial cells (HUVEC). Concurrently they also noticed the downregulation of several blood vascular genes (CXCR4, CD44, intercellular-adhesion molecule-1, laminin, neuropilin-1, PlGF and VEGFC).

Prospero homeobox protein-1 (PROX-1) is a master regulator of lymphatic vessel development and differentiation and is not expressed by BEC. It was down regulated in LEC by KSHV infection (Wang et al., 2004a), which might explain the loss of lymphatic phenotype and increased blood vascular character in these cells. KS tumour cells and KSHV-infected BEC both express PROX-1. However, while PROX-1 might contribute to the KSHV-

induced drift in phenotype toward that of lymphatic vasculature, transfection with small interfering ribonucleic acid (siRNA) to inhibit PROX-1 upregulation in BEC infected with KSHV only partially inhibited the upregulation of lymphatic genes suggesting that additional transcriptional regulators are involved (Hong et al., 2004). Recent work has demonstrated that the reprogramming of LEC toward a BEC phenotype might involve KSHV-encoded micro-RNAs, notably miR-K12-11 and miR-K12-6, which silence the transcription factor musculoaponeurotic fibrosarcoma oncogene homolog (MAF) thereby inhibiting its role in the differentiation of LECs (Hansen et al., 2010).

Several lines of evidence reported by Wang et al (2004a) support LEC as the spindle-cell precursor: (1) using gene expression microarray the neoplastic cells of KS lesions were found to resemble lymphatic endothelial cells; (2) although susceptibility to infection was equal across BEC and LEC, LEC supported a higher KSHV genome copy number; (3) KS lesions arise at sites that are rich in lymph vessels (e.g. skin, lymph nodes and mucosa) but not in organs that are without lymphatics (e.g. brain). Nonetheless, the genetic drift of BEC toward a lymphatic phenotype provides support that BEC or an endothelial progenitor (Wang et al., 2004a) could be the precursor of spindle cells. Accordingly, both BEC, in particular HUVEC and LEC continue to provide current models for investigating the effects of KSHV infection on endothelial cells. Dermal microvascular endothelial cells are also often used and these represent mixed populations of BEC and LEC. In view of the expertise of Professor Nash's lab in the culture of primary HUVEC and the availability of multiple donor umbilical cords from the local maternity department within the Birmingham Women's Hospital it was decided to use primary HUVEC as the target endothelial cell type for these studies.

1.6 IMPACT OF KSHV INFECTION UPON ENDOTHELIAL CELL MOTILITY

To my knowledge, prior to the studies presented in this thesis, no work had been published on the effect of whole virus infection on the motility of primary endothelial cells. Literature on the association between KSHV and cell migration had only considered the influence of single KSHV gene products by methods of ectopic overexpression. Genes that had been examined included the viral G protein-coupled receptor (vGPCR) (Couty et al., 2009); the M type K15 transmembrane protein (K15M) (Tsai et al., 2009) and the transmembrane ubiquitin ligase K5/MIR2 (Mansouri et al., 2006). Different effects upon cell migration are reported according to the gene of study highlighting the importance of studying the effect of infection by the whole virus in order to resolve what the overall effect of KSHV infection is on cell motility.

Tsai et al (2009) reported that the K15M protein had pro-migratory and pro-invasive effects. This was demonstrated in assays across several cell types. Ectopic K15M expression increased the transmigration of NIH-3T3 cells through transwell filters and transfection of BC-1 cells with K15M specific siRNA to silence endogenous K15M suppressed BC-1 transmigration through transwell filters compared to BC-1 cells transfected with a siGFP control oligonucleotide. In addition, co-transfection with siRNA oligonucleotides to either miR-21 or miR-31 inhibited the K15M induced increase in migration through transwell filters of cells of the human microvascular endothelial cell line HMEC-1.

In contrast to K15M, Mansouri et al (2006) demonstrated that Adenovirus-K5-transduced HUVEC immortalised with the human papilloma virus E6 and E7 proteins were slower at closing scratch wounds compared to AdGFP-transduced control cells (Mansouri et al., 2006).

This the authors attributed to downregulation of CD31 by K5. CD31 has been demonstrated by others to have a role in the recovery of scratch wounds (Gratzinger et al., 2003).

Finally, studies by Couty et al (2009) which investigated the effects of vGPCR on migration, found that basal signalling by the viral receptor inhibited the migration of immortalised mouse lung endothelial cells (MLEC) in a transwell assay. When considering that vGPCR-transgenic mice present lesions that resemble those of human KS (featuring prominent angiogenesis and vascular permeability) (Jensen et al., 2005; Montaner et al., 2003), and ectopic vGPCR expression *in vitro* induced expression of angiogenesis-related genes (Ma et al., 2010), this result seems somewhat counterintuitive. Instead, a migration-enhancing effect of the viral receptor might have been expected. However, interferon gamma-induced protein-10 (IP-10), which acts as an inverse agonist to vGPCR (Geras-Raaka et al., 1998; Rosenkilde et al., 1999), countered the suppressive effects of vGPCR on MLEC migration, improving wound recovery of vGPCR-expressing cells and stimulating the directed migration of vGPCR-expressing cells compared to controls by 237% in a transwell chemotaxis assay. IP-10 also had slight chemokinetic effects on vGPCR-expressing cells but the chemokine had no regulatory impact upon the behaviour of mock transfected cells.

Overall the work by Couty et al (2009) indicates that the interaction between viral genes and the chemokine milieu, possibly governed by the effects of additional viral gene products, is likely to be important in dictating the influence of individual viral genes on host cell functions. Thus it strengthens the importance of the study in this thesis which set out to interrogate the effect of whole virus infection on endothelial cell migration.

1.7 OBJECTIVES OF THIS THESIS

The research presented in this thesis set out to determine the overall impact of KSHV infection on the motility of primary endothelial cells and to investigate the effect of the virus on properties of endothelial cells that if altered might underlie changes in their migratory behaviour. The underlying hypothesis for this work was that alterations in endothelial cell motility imposed by the virus KSHV might support the generation of the extensive aberrant vasculature that is a hallmark of KS. Determining the mechanisms involved might lead to the identification of suitable targets for novel prophylactic or therapeutic drugs against KS.

The main specific objectives included:

- To establish a protocol for high efficiency *in vitro* infection of primary endothelial cells (HUVEC) with KSHV.
- To characterise the temporal changes in percent infection within inoculated cultures over ten–days and assess the extent of sideways transmission of infection occurring from infected to non-infected cells within inoculated cultures.
- To develop *in vitro* assays to test the effect of KSHV infection on rates of HUVEC migration.
- To examine the effect of KSHV infection on the relative amounts of each of the major basement membrane proteins deposited by HUVEC including: collagen IV, fibronectin and laminin.
- To examine the effect of KSHV infection on the profile of integrin receptors expressed on the surfaces of HUVEC.

- To characterise the effect of KSHV infection on the F-actin cytoskeleton and on the formation of focal adhesion structures in HUVEC.

- To investigate the roles of chemokines and growth factors in KSHV-induced changes to HUVEC migratory behaviours.

CHAPTER TWO

METHODS

2.1 CELL CULTURE

2.1.1 Maintenance of cell lines

All cells were cultured in a humidified incubator at 37°C, 5%CO_2 except where stated. Their media and other cell-type specific methods are detailed in the following sections.

2.1.1.1 BCBL-1 cells

BCBL-1 cells were cultured in RPMI medium (Sigma) supplemented with: 10% (v/v) foetal bovine serum (FBS) (PAA Laboratories), 2mM glutamine (Gibco, Invitrogen), 50U/ml penicillin (Gibco, Invitrogen), 50μg/ml streptomycin (Gibco, Invitrogen). Cells were passaged 1:5 every 3-4 days or plated at 0.2×10^6 cells/ml.

2.1.1.2 HEK293 cells

HEK293 cells were cultured in Dulbecco's Modified Eagle Medium (Gibco, Invitrogen) supplemented with: 10% (v/v) FBS (PAA Laboratories), 2mM glutamine (Gibco, Invitrogen), 50U/ml penicillin (Gibco, Invitrogen), 50μg/ml streptomycin (Gibco, Invitrogen) and 1% (v/v) non-essential amino acids (Sigma, catalogue number M7145). Cells were cultured in 25cm^2 (or 75cm^2) flasks and passaged 1:6 every 3-4 days.

To passage, culture medium was removed, cells washed once with phosphate buffered saline (PBS) and incubated with 0.05% (w/v) trypsin-ethylene diaminetetraacetic acid (EDTA) (Gibco, Invitrogen, catalogue number: 25300054) (room temperature) until detached. Trypsin was quenched with culture medium and an appropriate volume of cell suspension transferred to the

culture flask. The volume was made to 5ml (25cm^2 flask) or 15ml (75cm^2 flask) with culture medium.

2.1.1.3 VK219 cells

The VK219 cell line is a Vero cell line latently infected with the recombinant KSHV strain, rKSHV.219 (Vieira and O'Hearn, 2004). This virus expresses the green fluorescent protein (GFP) gene from the EF-1α promoter as a marker of latent infection and the Ds red fluorescent protein (RFP) gene from the PAN RNA promoter as a lytic cycle marker. The puromycin N-acetyltransferase (pac) gene for puromycin resistance is also included as a selectable marker. Ectopic expression of the KSHV lytic switch replication and transactivator (RTA) protein, encoded by ORF50, induces reactivation of rKSHV.219 from latent to lytic replication **(Figure 2.1)**.

Cells were cultured in Minimum Essential Medium Eagle-AQmedia™ (Sigma) supplemented with: 10% (v/v) FBS (PAA Laboratories), 10U/ml penicillin (Gibco, Invitrogen), 10μg/ml streptomycin (Gibco, Invitrogen), 5μg/ml puromycin (Sigma) and 1% (v/v) non-essential amino acids (Sigma). Cells were cultured in 175cm^2 flasks and passaged 1:5 every 3-4 days.

To passage, culture medium was removed, cells washed once with 10ml PBS, incubated with 7ml 0.02% (w/v) EDTA (Sigma) (5mins, 37°C) followed by 0.05% (w/v) trypsin-EDTA (Gibco, Invitrogen) (5mins, 37°C). Trypsin was quenched with 10ml culture medium and cells pelleted (5mins, 500 x *g*). Cells were resuspended in 5ml medium and 1ml added to 20ml medium in a 175cm^2 flask.

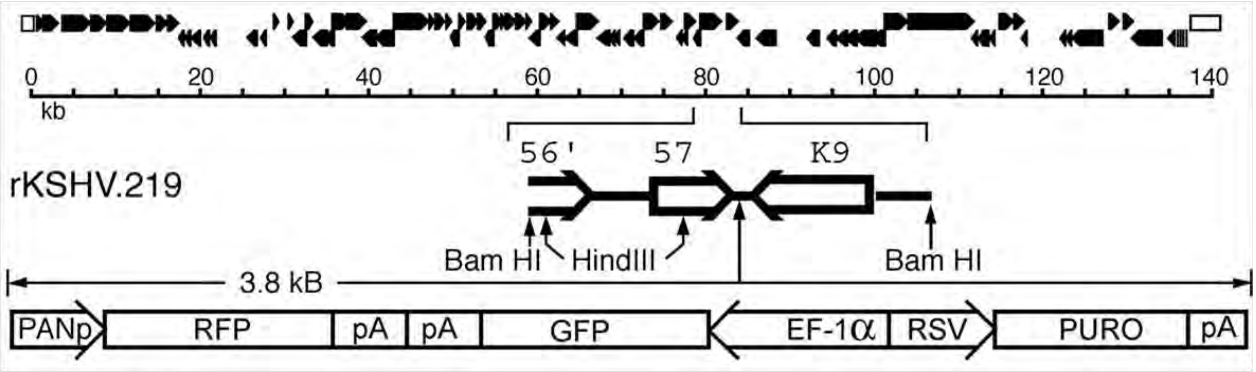

Figure 2.1: Schematic diagram of the rKSHV.219 genome

Recombinant rKSHV.219 was generated by recombination of the 4.8kb BamHI fragment of the KSHV genome into the wildtype KSHV genome of JSC-1 cells. This fragment contains the RFP/GFP/PURO cassette inserted in a non-coding region between ORFK9 and ORF57. GFP is expressed under the control of the human elongation factor 1α promoter, which is active in all cells, and RFP is under the control of the lytic PAN RNA promoter which is activated in cells undergoing lytic reactivation. The pac gene is included to confer puromycin resistance (PURO) on infected cells and therefore provides a selectable marker. Taken from Vieira and O'Hearn (2004).

2.1.1.4 Human dermal lymphatic endothelial cells (LEC)

Primary human dermal lymphatic endothelial cells (LEC) (PromoCell) were cultured in MV2 basal medium supplemented with: 50µl/ml foetal calf serum (FCS), 5ng/ml recombinant human EGF, 10ng/ml recombinant human bFGF, 20ng/ml insulin-like growth factor, 0.5ng/ml recombinant human $VEGF_{165}$, 1µg/ml ascorbic acid and 0.2µg/ml hydrocortisone (all from PromoCell).

2.1.1.5 Isolation of neutrophils from whole blood

Whole blood was collected in an EDTA-containing tube (Sarstedt). For isolation of neutrophils from 5ml whole blood, 2.5ml Histopaque 1119 (Sigma) was added to a 10ml tube

and 2.5ml Histopaque 1077 (Sigma) layered on top. 5ml EDTA-blood was layered on top of the Histopaque gradient and centrifuged (40mins, 1400 x *g*). The upper plasma and PBMC bands were discarded. The neutrophil band was transferred to a clean tube and washed twice with Ca^{2+} and Mg^{2+}-containing PBS (Sigma) supplemented with 0.5% (w/v) bovine serum albumin (BSA) (Sigma) (5mins, 500 x *g*).

2.1.2 Production of KSHV

2.1.2.1 Production of KSHV from BCBL-1 cells

Two weeks prior to KSHV harvest, two T225 cell culture flasks were plated with BCBL-1 cells at 0.2×10^6/ml and cultured for four days. Cultures were pooled and six T225 flasks plated at 0.2×10^6/ml. After three days, cell suspensions were decanted into wide-necked straight centrifuge pots and cells pelleted using a Sorvall RC5B Plus centrifuge fitted with an SLA3000 rotor (10mins, 500 x *g*). Cells were re-plated at 0.5×10^6/ml in eight T225 (100ml per flask) and reactivated by the addition of Phorbal Myristate Acetate (PMA) (Sigma) (final concentration 20ng/ml) and sodium butyrate (Sigma) (final concentration 300μM). Cells were cultured for five to six days. For reactivation, 300mM sodium butyrate solution (dissolved in sterile distilled water) was prepared fresh, filter sterilised and 100μl added to each 100ml culture. PMA was kept as a frozen stock of 1mg/ml in Dimethyl sulfoxide (DMSO) (Sigma) and diluted in culture medium to give a 1μg/ml working solution on the day of reactivation. 2ml of the working PMA solution (1μg/ml) was added to each 100ml culture.

On the day of virus harvest, cell cultures were transferred to wide-necked straight centrifuge pots and pelleted using a pre-chilled Sorvall RC5B Plus centrifuge fitted with SLA3000 rotor (20mins, 1500 x *g*, 4°C). The supernatant was decanted into sterile, wide-necked, straight centrifuge pots for harvest of KSHV by the sucrose cushion method or into side-opening, 400ml centrifuge pots for harvest by the standard method.

2.1.2.1.1 Sucrose cushion method for harvest of KSHV from supernatants of reactivated BCBL-1 cells

8ml 25% (w/v) sucrose in TNE buffer (150mM NaCl, 10mM Tris pH8, 2mM EDTA) pH8 were aliquoted to each of six Ultra Clear 1×3.5inch (25×89mm) tubes (Beckman) and overlain with 29ml virus-containing supernatant. Tubes were placed into Beckman SW32 rotor buckets and balanced by adding or removing virus-containing supernatant. Virus was pelleted from the supernatant by centrifugation using a Beckman Optima LE-80K Ultracentrifuge (2hours, 133668 x *g*, 4°C). Supernatants were discarded and the tubes inverted on tissue to drain remaining supernatant. 300µl EBM-2 medium (without heparin) (PromoCell) were aliquoted onto each pellet and incubated on ice overnight in the cold room (4°C) to resuspend. To complete resuspension, virus preparations were pipeted gently and pooled in 1.5ml microfuge tubes. Microfuge tubes were centrifuged to pellet any debris (30secs, 16,000 x *g*). The cleared supernatant was transferred to clean microfuge tubes and either used immediately or aliquoted and stored at -80°C.

2.1.2.1.2 Standard method for harvest of KSHV from supernatants of reactivated BCBL-1 cells

Virus was pelleted from the supernatant in side-opening centrifuge pots using a pre-chilled Sorvall RC5B Plus centrifuge fitted with SLA3000 rotor (3hours, 16927 x *g*, 4°C). The supernatant was discarded and virus resuspended in culture medium on ice in the cold room overnight. The volume of medium added was just below that required for 100-fold concentration of the virus compared to the original culture supernatant volume. The next day suspensions were gently pipeted to ensure complete resuspension of the pellet. The suspension was transferred to a 15ml tube and the volume made to that required for 100-fold concentration of the virus using culture medium. The resulting preparation was filter sterilised using a 0.45μm-pore filter and either used immediately or aliquoted and stored at -80°C.

Before using a virus preparation to prepare an inoculum, it was allowed to thaw, if frozen, and was mixed thoroughly. Before inoculating the cells, the diluted virus was warmed in a 37°C water bath for 10 minutes.

2.1.2.2 Production of rKSHV.219 from VK219 cells

Three days prior to expansion for reactivation, two stock 175cm^2 flasks were plated. On the day of expansion, cells were detached from the two culture flasks and ten 175cm^2 flasks plated at 2-3×10^6 cells per flask in complete medium (containing puromycin). Cells were cultured overnight or until ~60% confluent.

To reactivate rKSHV.219 from its latent to lytic cycle, culture medium was removed, cells washed with 10ml PBS to remove traces of puromycin, and 20ml medium without puromycin

added. 'Reactivation mixture' containing BacK50 at the dilution determined by titration **(section 2.1.2.4)** and sodium butyrate was prepared in culture medium without puromycin and 2.27ml added to each flask. The final sodium butyrate concentration was 1.25mM. Cells were cultured for 48hours before harvesting rKSHV.219 from the culture supernatant.

On the day of harvest, RFP fluorescence and cell death confirmed reactivation. Supernatants were transferred to 50ml tubes, cleared of cellular material by centrifugation (15mins, 500 x *g*, 4°C) and decanted to six ultracentrifuagtion Ultra Clear 1×3.5inch (25×89mm) tubes (Beckman). Tubes were balanced in SW32 rotor buckets and virus pelleted from the supernatant by ultracentrifugation in a Beckman Optima LE-80K Ultracentrifuge (4hours, 31,073 x *g*, 4°C). Supernatant was decanted and tubes inverted on tissue to drain fully. Virus pellets were covered with 50µl EBM-2 medium (without supplements) and left to resuspend overnight at 4°C. Pellets were pooled in a 1.5ml microfuge tube and cleared of debris by centrifugation using a bench top microfuge (4mins, 1520 x *g*). Supernatant was transferred to a fresh microfuge tube and stored at 4°C unless otherwise stated.

2.1.2.3 Production of Baculovirus K50 (BacK50)

BacK50 is a recombinant baculovirus engineered to express the KSHV lytic switch protein RTA that is encoded by ORF50. Baculovirus is an insect virus that is unable to replicate within mammalian cells but which will infect and express encoded proteins. BacK50 was used in this system to ectopically express RTA within VK219 thereby reactivating rKSHV.219.

BacK50 was produced in insect SF9 cells that were grown in either 500ml or 1litre flasks shaken at 27°C, 5%CO_2. Growth medium was Sf-900 II medium (Gibco, Invitrogen)

supplemented with 10% (v/v) FBS (PAA Laboratories), 50U/ml penicillin (Gibco, Invitrogen), 50μg/ml streptomycin (Gibco, Invitrogen). For BacK50 production, SF9 cells were expanded to four 1litre flasks. Once cells reached a viable density of 2×10^6 cells/ml they were inoculated with BacK50 and returned to the shaker. Three-to-four days post-inoculation, cells were decanted to 50ml tubes and centrifuged (20mins, 450 x *g*). Supernatants containing BacK50 were pooled, filtered through a 0.45μm-pore filter and stored at 4°C.

2.1.2.4 Determination of BacK50 titre

The BacK50 titre was determined by titration on VK219 cells. VK219 cells were plated in a 24-well plate at 2×10^4 cells/well and incubated overnight to reach ~60% confluence. Reactivation solutions containing 1.25mM sodium butyrate were prepared in VK219 culture medium without puromycin. BacK50 was titrated between 1:5 and 1:50. Untreated and sodium butyrate–only controls were included and for standardization purposes, the previous BacK50 batch was also tested in parallel. To reactivate the VK219 cells, the culture medium, containing puromycin, was removed, cells washed once with 500μl PBS and 300μl reactivation solution added. Each condition was set up in duplicate. Cells were returned to culture. The following day, HEK293 cells were plated in a 96-well plate at 2×10^4 cells/well and cultured overnight.

48hours post-reactivation, the reactivation supernatants were collected into 1.5ml microfuge tubes, centrifuged (15mins, 1000 x *g*, 4°C) to remove debris and diluted 1:200 and 1:400 in EBM-2 medium without supplements. Medium was removed from HEK293 cells and 100μl of each diluted VK219 supernatant aliquoted in duplicate. Cells were centrifuged in the presence of the virus (30minutes, 328 x *g*), then the virus incubated with the cells for a further 90minutes

(37°C, 5%CO_2) before removal. Cells were washed once with culture medium then returned to incubation for 48hours during which time infected cells transcribed GFP. Two days post-inoculation the number of GFP positive HEK293 cells per well was counted and the RTA titre calculated assuming that one infectious unit generates one GFP positive HEK293 cell in 48hours.

2.1.2.5 Determination of rKSHV.219 titre

HEK293 cells were plated in a 96-well plate at 2×10^6 cells/well and incubated overnight. Immediately before inoculation, serial dilutions of rKSHV.219 were prepared between 1:100 and 1:80000 using EBM-2 medium without supplements. Culture medium was removed and replaced with 100µl inoculum. Each dilution was tested in duplicate. Cells were centrifuged in the presence of the virus (30minutes, 328 x *g*), then the virus incubated with the cells for a further 90minutes (37°C, 5%CO_2) before removal. Cells were washed once with culture medium then returned to incubation for 48hours during which time infected cells transcribed GFP. The plate was viewed on a fluorescence microscope and a dilution selected that gave a countable number of GFP expressing cells in the entire well. The total number of GFP positive cells per well was counted and the titre calculated (infectious units per mililitre) assuming that one infectious unit generates one GFP positive HEK293 cell in 48hours. Throughout the studies reported in this thesis, multiplicities of infection (MOIs) for KSHV inoculations, where stated, refer to the number of infectious units supplied per cell (as determined by titration of the virus on HEK293 cells). MOI was based on KSHV infection of HEK293 because HEK293 were found to be permissive to KSHV. Inter-donor variability in infectability was seen among HUVEC; thus to ensure use of a constant MOI would have required titration of the virus on cells from each donor prior to the use of the donor in an assay. This was not feasible due to the limited availability of

cells for each donor, inability to expand HUVEC cultures across multiple passages and the need to infect HUVEC for use in an assay within one week of their isolation. The decision was therefore taken to keep the amount of KSHV added per cell constant as opposed to inoculating with virus according to its titre on each donor. 2.1.2.6 UV irradiation of rKSHV.219

Ultraviolet (UV) irradiated preparations of rKSHV.219 were made at the time of the assay so that the UV-irradiated and non-UV irradiated virus were of the same batch. 50-70µl volumes of rKSHV.219 were aliquoted into wells of a 96 well plate and the plate put into the GS Gene Linker UV Chamber (BIO RAD) with its lid removed. The sterilization (Str) program was selected and the virus exposed to 400mJ radiation for two consecutive periods of 10minutes. In between the irradiations the plate was swirled gently. In the preparation of the inoculums the UV irradiated virus was diluted equivalently to the non-irradiated sample from which it derived so that cells received either productively infectious or inactive virus originally at the same MOI.

2.1.3 Isolation and culture of human umbilical vein endothelial cells (HUVEC)

Primary HUVEC were isolated and sub-cultured in Medium 199 (M199) (Gibco, Invitrogen) supplemented with 20% (v/v) FCS, 2.5µg/ml amphotericin B, 50U/ml penicillin, 50µg/ml streptomycin, 1ng/ml EGF, 28µg/ml gentamycin and 1µg/ml hydrocortisone (all from Sigma).

Each experiment used a separate HUVEC donor.

2.1.3.1 Isolation of HUVEC from umbilical cord veins

Umbilical cords still attached to their placentas were received from the Birmingham Women's Hospital with donor consent. Cords were cut from their placentas, and after clearing surface blood, were inspected for clamp marks, punctures or sites of large hemorrhage. The vein of each cord was cannulated and flushed with PBS (Sigma) until the through flow was clear. Each volume (20ml) of PBS was followed by a full syringe of air (20ml) to expel all PBS.

Next, the opposite end of the vein was cannulated and the vein filled with 1X collagenase type 1a (1mg/ml) (Sigma) that was diluted in PBS from 100X or 10X frozen stocks stored at -20°C. The cord was incubated (15mins, 37°C, 5%CO_2) to allow digestion of collagen in the extracellular matrix and thus detachment of endothelial cells. The cord was then massaged and flushed with 30ml PBS and the flow through collected in a 50ml tube. Cells were pelleted (5mins, 500 x *g*), re-suspended in culture medium and aliquoted to 25cm^2 flasks, 4ml per flask (~10cm of cord were allowed for each 25cm^2 flask). Cells were allowed to settle and adhere for a minimum of 2hours or overnight before the medium was changed. Culture medium was changed every two or three days until cells were confluent (typically within four to six days). Cells were then passaged for experiment.

During a period of limited HUVEC availability it was necessary to expand the cell stocks. Cells were passaged for expansion when ~80-90% confluent, frozen and stored in liquid nitrogen. Cells isolated in-house were cultured in M199-based culture medium and frozen at P2 or P3. Cells purchased from PromoCell were expanded in supplemented EBM-2 medium (PromoCell), transferred from 25cm^2 to 75cm^2 flasks at first passage and frozen at P3.

2.1.3.2 Detachment of HUVEC from 25cm^2 flasks

Culture medium was removed, cells washed once with 2ml 0.02% (w/v) EDTA (Sigma) then incubated with 2ml 0.25% (w/v) trypsin (Sigma, catalogue number: T4424) diluted 1:1 with 0.02% (w/v) EDTA (Sigma) (Sigma) at room temperature until cells rounded and detached. Trypsin was quenched with 7ml culture medium and cells pelleted (5mins, 500 x *g*).

For expansion of the culture, the cell pellet was resuspended in culture medium and divided between two 25cm^2 flasks or transferred to a 75cm^2 culture flask (HUVEC purchased from PromoCell).

To plate cells for an experiment, the cell pellet (from one 25cm^2 flask) was resuspended in 400-600µl culture medium and the live cell density determined by trypan blue staining. A four-factor dilution of the HUVEC was suitable for counting. Cells were diluted to an appropriate number of cells/volume and aliquoted into plasticware.

2.1.3.3 Detachment of HUVEC from 24-well plates

To detach cells from 24-well plates the culture medium was removed, cells in each well were washed once with 500µl 0.02% (w/v) EDTA then incubated (room temperature) with 200µl 0.25% (w/v) trypsin (Sigma) diluted 2:5 with 0.02% (w/v) EDTA (Sigma) (trypsin-EDTA) (room temperature) until rounded and detached. Trypsin was quenched with 500µl culture medium. To encourage complete cell detachment, the cell suspension was gently pipeted. Cells were transferred to 1.5ml microfuge tubes (or 15ml tube if pooling cells from a large number (10-12) wells) and pelleted (5mins, 425 x *g*). Pellets were resuspended in an appropriate volume for counting the density and/or replating.

2.1.3.4 Freezing HUVEC for storage in liquid nitrogen

Cells were detached from the culture flask and the cell pellet resuspended in ice-cold Cryo-SFM freezing medium (PromoCell) (1ml/25cm^2 flask). The resulting cell suspension was aliquoted to ice-cold cryovials (1ml/vial) and placed in a cell cryopreservation container at -80°C to freeze gradually. The following day, cells were transferred to storage in liquid nitrogen.

2.1.3.5 Reviving HUVEC from storage in liquid nitrogen

9ml supplemented EBM-2 medium was warmed to 37°C. A vial of frozen HUVEC was warmed between the hands until the cell suspension had almost thawed then was added to the EBM-2 medium and cells pelleted (5mins, 500 x *g*). The cell pellet was resuspended in 4ml EBM-2 medium and transferred to a 25cm^2 flask. Cells were cultured until a confluent monolayer was attained. The culture medium was changed to M199-based culture medium either one day prior to use (if cells were to be infected on the day of plating) or at the time of plating (if cells were to be infected following overnight incubation). It was necessary to revive cells in EBM-2 culture medium since pilot studies revealed poor recovery in M199-based medium. For successful infection and functional assays however, cells needed to acclimate to M199-based medium since infection efficiency in EBM-2 is low, possibly due to inclusion of heparin as a supplement. HUVEC functions might also be altered by differences in the nutrient/growth factor availability and balance between the two media.

2.1.4 Inoculation of HUVEC with rKSHV.219

HUVEC were plated in culture medium at the required density required for the experiment the day before inoculation unless otherwise stated. Following overnight culture, cells were washed once with culture medium to remove non-adhered cells and inoculums prepared by diluting the required volume of virus (to give MOI10 unless otherwise stated) in EBM-2 medium without supplements to a total volume of 100µl (96 well plate) or 420µl (24 well plate) or 60µl (µ-slides) (for µ-slides, 30µl were required to fill the channel and an extra 30µl to fill the ports in order to prevent the cells from drying out during centrifugation). Cells were centrifuged in the presence of the virus (30minutes, 328 x *g*), then the virus incubated with the cells for a further 90minutes (37°C, 5%CO_2) before removal. Cells were washed once with culture medium and then cultured until the timepoint of interest post-inoculation. The medium was changed throughout this period every two or three days (plates) or every one or two days (µ-slides).

2.2 FLOW CYTOMETRY

2.2.1 Antibodies

All antibodies used in this thesis for applications including: flow cytometry, enzyme linked immunosorbent assay (ELISA), immunofluorescence assay and functional assays are listed in **Table 2.1**. Details of their working concentration/dilution, isotype, clone and source are given.

2.2.2 Determining the percentage infection of rKSHV.219-inoculated cell cultures

Cells were removed by trypsinisation and fixed in 1ml 4% (w/v) formaldehyde (Sigma) diluted in PBS (15mins, room temperature), pelleted (5mins, 500 x *g*), washed with 2ml PBS (5mins, 500 x *g*) and resuspended in 300µl PBS for data acquisition on a Dako Cyan flow cytometer. A minimum of 3000 events were counted. Data were analysed using FlowJo (Tree Star) or Dako Summit 4.3 software. Cells were considered infected if their GFP fluorescence intensity was greater than that of 99% of untreated cells **(Figure 2.2)**.

2.2.3 Staining surface antigens

To detach HUVEC from 24-well tissue culture plates (~7-9x10^4 cells/well), the culture medium was removed and the cells in each well were washed once with 500µl 0.02% (w/v) EDTA (1min) then covered with 500µl enzyme free cell dissociation buffer (Gibco, Invitrogen) and incubated (37°C, 5%CO_2) until rounded and detached. 1ml cold culture medium was added and the cell suspension gently pipeted to encourage complete cell detachment. The cell suspension was transferred to FACS tubes (BD Falcon) (~4-9x10^4 cells/tube), 2ml ice-cold 2% (w/v) BSA in PBS (2%PBSA) added and the cells pelleted (5mins, 500 x *g*, 4°C). The supernatant was aspirated and the cell pellet resuspended in 50µl primary antibody **(Table 2.1)** diluted in 2%PBSA (30-40mins, on ice, dark**)**. For staining of VEGFR3, in accordance with the manufacturer's instructions, cells were blocked in 40µl 2% (v/v) goat serum in 0.5%PBSA (20mins, room temperature) prior to addition of the antibody (in 10µl) into the cell suspension and incubation on ice (30-40mins, dark).

Excess antibody was washed out in 3ml ice-cold 2%PBSA (5mins, 500g, 4°C). Samples stained with fluorophore-conjugated primary antibodies were washed a second time (3ml 2%PBSA, 5mins, 500 x *g*, 4°C) then resuspended in 200µl 4% (w/v) formaldehyde to fix (15mins, room temperature). Samples to stain with a secondary antibody were resuspended in 50µl secondary antibody (30-40mins, on ice, in dark). Excess antibody was washed out in two 3ml-volumes of ice-cold 2%PBSA before resuspension in 200µl 4% (w/v) formaldehyde to fix (15mins, room temperature). Fixative was washed out in 2ml PBS (5mins, 500 x *g*) and cells resuspended in 300µl PBS for data acquisition on a Dako Cyan flow cytometer. A minimum of 3000 events were collected. Data were analysed using FlowJo (Tree Star) or Dako Summit 4.3 software.

2.2.4 Staining intracellular antigens

2.2.4.1 Staining intracellular antigens using the Fix and Perm Kit by Invitrogen

Cells to be stained were detached from 24-well plates using trypsin-EDTA and transferred to FACS tubes (3.5-7x10^4 cells). 2ml wash buffer (PBS supplemented with 5% (v/v) FCS) were added and cells pelleted (5mins, 500g). Cells were fixed and stained using the Invitrogen Fix and Perm Kit according to the manufacturer's instructions. Cells were resuspended in 50µl Medium A (15mins, room temperature, in dark) to fix. The fixative was washed out in 2ml wash buffer, and cells resuspended in 50µl primary antibody **(Table 2.1)** diluted in Medium B (1hr, 37°C, dark). Excess antibody was washed out in 3ml wash buffer (5mins, 500 x *g*) and cells resuspended in 50µl secondary antibody **(Table 2.1)** diluted in Medium B (40mins, 37°C, dark). Excess antibody was washed out in 3ml wash buffer followed by 1ml PBS then resuspended in 300µl PBS for analysis on a Dako Cyan flow cytometer. A minimum of 3000 events were collected. Data were analysed using FlowJo (Tree Star) or Dako Summit 4.3 software.

2.2.4.2 Staining phospho-p38 MAPK

Cells (~8x10^4) to be stained were detached from 24-well plates using trypsin-EDTA, quenched with 500µl medium and 77µl 16% (w/v) formaldehyde added immediately to fix. 2ml PBS were added and cells pelleted (5mins, 500 x *g*). To complete fixation, cells were resuspended in 500µl 2% (w/v) formaldehyde (10mins, room temperature). Cells were then washed with 4ml ice-cold PBS (5minutes, 500 x *g*) followed by a second 1ml ice-cold PBS wash (5mins, 500 x *g*). Cells were permeabilised in 100µl 100% (v/v) methanol (30mins, 4°C). The methanol was removed by one wash in 2ml ice-cold PBS followed by one wash in 2ml ice-cold 2% (w/v) BSA in PBS

(2%PBSA). Cells were resuspended in 30µl primary antibody **(Table 2.1)** diluted in 2%PBSA (1h, room temperature, dark). Excess antibody was removed by two washes with 2ml 2%PBSA (5mins, 500 x *g*). Cells were resuspended in 300µl PBS and analysed immediately after staining on a Dako Cyan flow cytometer. A minimum of 10000 events were collected. Data were analysed using FlowJo (Tree Star) or Dako Summit 4.3 software.

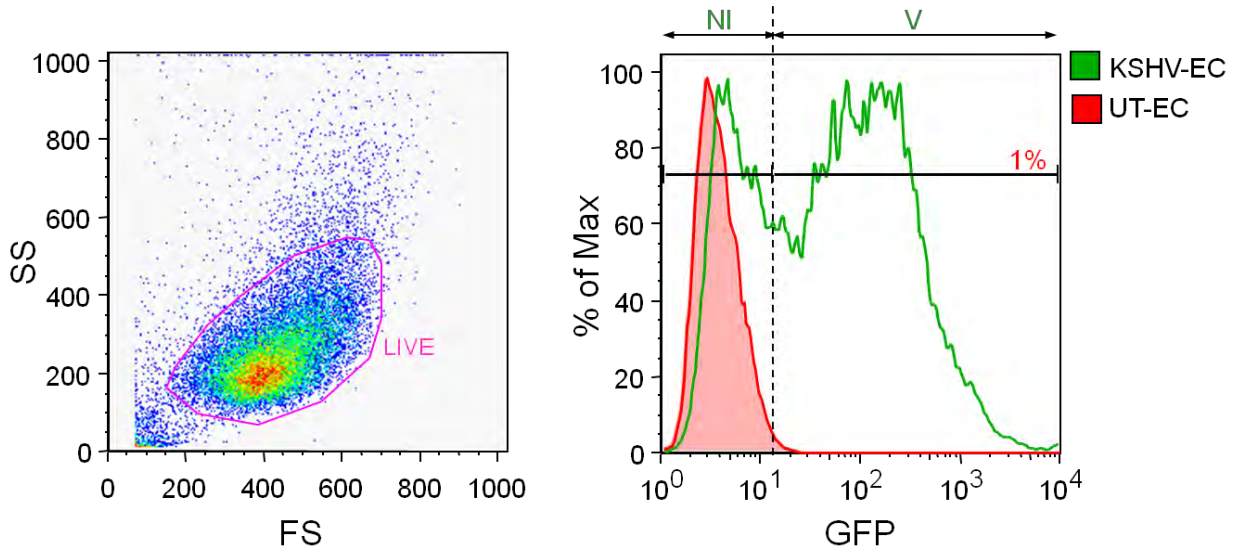

Figure 2.2: Assessment of percent KSHV infection by flow cytometry quantifying GFP expression.

The expression of GFP under the human elongation factor-1α promoter in the rKSHV.219 genome meant that cells infected by rKSHV.219 expressed GFP. The 'live' HUVEC population, identified from its scatter on the forward scatter (FS) v side scatter (SS) flow cytometry plot was examined for its GFP fluorescence. Cells were concluded to be infected with the virus (denoted V) if their GFP fluorescence exceeded that of 99% of untreated (UT-EC) cells. If their fluorescence was not greater than that of 99% of untreated cells, and thus they fell within the subset of UT-EC negative for GFP signal, they were concluded to be non-infected (NI).

Table 2.1: Antibodies used in the studies reported in this thesis

Antibody	Clone	Isotype	Company	Catalogue number	Conjugation	Application	Dilution/ concentration
Primary antibodies							
Collagen IV	COL-94	Mouse IgG1	Sigma	C1926	Unconjugated	ELISA	1/5000 (0.02μg/ml)
CXCR1	42705	Mouse IgG2a	R&D Systems	FAB330P	PE	Flow cytometry	1/20
CXCR2	48311	Mouse IgG2a	R&D Systems	FAB331P	PE	Flow cytometry	1/20
Fibronectin	FN-3E2	Mouse IgM	Sigma	F6140	Unconjugated	ELISA	1/5000 (0.02μg/ml)
Integrin α2	HAS3	Mouse IgG2a	R&D Systems	BAM1233	Biotinylated	Flow cytometry	1/20
Integrin α3β1	P1B5	Mouse IgG1	Dako	M0608	Unconjugated	Flow cytometry	1/20
Integrin αvβ3	23C6	Mouse IgG1			Unconjugated	Flow cytometry	1/400
Integrin α6	GoH3	Rat IgG2a	R&D Systems	FAB13501P	PE	Flow cytometry	1/50
Integrin α6	NKI-GoH3	Rat IgG2a,κ	AbDSerotec	MCA699EL	Unconjugated low endotoxin	Function block	10μg/ml
Integrin β1	P5D2	Mouse IgG1	R&D Systems	FAB17781P	PE	Flow cytometry	1/50
Integrin β3	PM6/13	Mouse IgG1	AbDSerotec	MCA728	Unconjugated	Flow cytometry	1/50
IP-10/CXCL10	33036	Mouse IgG1	R&D Systems	MAB266	Unconjugated	Function block	2μg/ml
Laminin-α4	3H2	Mouse IgG1	Santa Crutz	Sc-130540	Unconjugated	Flow cytometry ELISA	1/20 1/1000
Laminin-α5	4B12	Mouse IgG1	Santa Crutz	Sc-130542	Unconjugated	ELISA	1/50
Laminin-P1	HL-4H3	Mouse IgG1	Calbiochem	IF10L	Unconjugated (100μg/ml)	Flow cytometry ELISA	1/20 (5μg/ml) 1/1000 (0.1μg/ml)
LANA-1	LN53	Rat IgG	Advanced Biotechnologies	13-210-100	Unconjugated	IFA	

LANA-1	LN25	Mouse IgG	Gift from Dr Ian Milton		Unconjugated	IFA	1/50
p38MAPK pT180/pY182	36/p38	Mouse IgG1	BD Pharmingen	BD612595	Alexa Fluor 647	Flow cytometry	1/4
VEGFR3	54733	Mouse IgG1	R&D Systems	FAB3492A	APC	Flow cytometry	1/20
Vinculin	hVIN-1	Mouse IgG1	Sigma	V9264	Unconjugated	IFA	1/500
Isotype control antibodies							
Mouse IgG1	DAK-GO1	Mouse IgG1	Dako	X0931	Unconjugated	Flow cytometry IFA	1/20 1/100
Mouse IgG1	PPV-06	Mouse IgG1	Immunotools	21275514	PE	Flow cytometry	1/50
Mouse IgG2a	20102	Mouse IgG2a	R&D Systems	IC003P	PE	Flow cytometry	1/20
Mouse IgG1	MOPC-21	Mouse IgG1	Biolegend	400122	APC	Flow cytometry	1/20
Rat IgG2a	eBR2a	Rat IgG2a	Ebioscience	16-4321-82	Unconjugated	Function block	10μg/ml
Secondary antibodies							
Anti-Mouse IgG AF594	-	Goat IgG	Invitrogen MP	A21125	Alexa Fluor 594	IFA	1/100
Anti-Mouse IgG AF633	-	Goat IgG	Invitrogen MP	A21050	Alexa Fluor 633	Flow cytometry IFA	1/1500 1/500
Anti-Rat IgG AF633	-		Invitrogen MP		Alexa Fluor 633	IFA	
Anti Mouse IgG RPE	-	Rabbit F(ab')2	AbD Serotec	STAR12A	RPE	Flow cytometry	1/20
Streptavidin Conjugate	-	-	Invitrogen MP	S11222	Pacific blue	Flow cytometry	1/100
Anti mouse IgG HRP	-	Goat IgG	Dako	P0447	HRP	ELISA	1/2000

MP stands for Molecular Probes AF stands for Alexa Fluor

2.3 MIGRATION ASSAYS

2.3.1 Transmigration assay

At the time point of interest post-inoculation (day-seven unless otherwise stated), KSHV-inoculated and untreated HUVEC were detached from wells of the 24-well inoculation plate using trypsin-EDTA, pelleted in 1.5ml microfuge tubes (5mins, 425 x g) and re-suspended in culture medium at a density of 1.4×10^5cells/ml (2.7×10^4 cells/200µl). In preparation, 3 or 8µm-pore transwell chambers (BD Falcon) had been set out in a 24-well plate and 700µl culture medium aliquoted to the lower chamber. 200µl cell suspension was added to the upper chamber and cells incubated at 37°C for 48hours.

The medium was removed, the upper and lower surfaces of the filter washed once with PBS (200µl) and cells on both surfaces fixed with 2% (w/v) formaldehyde (PFA) containing bisbenzimide (2µg/ml) (Sigma) (15mins, room temperature, dark) (200µl upper and 700µl lower). The fixative was removed and the chambers filled with PBS. The filters were cut from their inserts using an 11-gauge scalpel and mounted using Vectashield mountant (Vector Laboratories Inc) on a glass microscope slide (76x26mm) (Thermo Scientific) beneath a 22×22mm glass coverslip (Menzel Glaser, Thermo Scientific). Filters were stored at 4°C for analysis by fluorescence microscopy.

Filters were viewed using a 20x objective lens and the number of cells on the top and bottom of the filter in each of 14-18 fields counted **(Figure 2.3)**. The average percentage transmigration

was calculated. Two or three filters were prepared for each condition in each experiment and the average transmigration calculated.

2.3.2 Transmigration assay to determine percent transmigration of KSHV-infected and non-infected HUVEC individually

In parallel to the standard transmigration assay **(section 2.3.1)** filters were set up for analysis of the percentage of GFP positive cells in the cultures removed from the top and bottom surfaces of the filters after 48hours transmigration. At the 48hour timepoint, medium was removed from the upper and lower chambers and the surfaces of the filters washed with PBS. The chambers were filled with 0.02% (w/v) EDTA (200µl upper and 700µl lower) and incubated (10mins, 37°C). Washings were transferred to FACS tubes and 0.25% trypsin (w/v) (Sigma) diluted 2:1 with 0.02% EDTA (Sigma) added to the chambers (200µl upper and 700µl lower) and incubated (10mins, 37°C). Trypsin was quenched with an equivalent volume of culture medium and the cells removed to FACS tubes, pooling them with those recovered in the wash. In the process, the bottom of the filter was carefully flushed by gentle pipeting to remove all cells. After removing the cell suspension from the upper chamber, the top surface of the filter was washed with 200µl PBS to ensure total recovery of cells. Cells were pelleted (5mins, 500 x *g*) and fixed in 300µl 2% (w/v) formaldehyde for data acquisition on on a Dako Cyan flow cytometer. The percentage of GFP positive cells in each culture was determined. These data were used together with the standard transmigration data to calculate the percent transmigrations of KSHV-infected and non-infected HUVEC separately. The calculation strategy, illustrated by the raw data for this study is given in the appendix **(Table 9.1)**.

2.3.3 Wound recovery assay

On day-six post-inoculation, KSHV-inoculated and untreated HUVEC were detached from wells of the 24-well inoculation plate, pelleted in 1.5ml microfuge tubes (5mins, 425 x *g*) and re-suspended in culture medium at densities of 2.1×10^5cells/ml. In advance, a graph paper grid had been photocopied onto acetate and strips of grid of size 25mm x 75mm cut. A window (2mm wide) was cut lengthwise down the centre of each strip and the strips secured to the backs of 6-well plates such that the central windows ran down the centre of the wells. A culture insert for wound recovery assays (Ibidi, Thistle Scientific) was placed in the centre of each well such that the central divider of the insert was contained within the window. 70µl cell suspension were seeded into each well of the insert, on either side of the central divider, and incubated overnight (unless otherwise stated) **(Figure 2.4A)**. Inserts were removed to reveal the 'wounded monolayers' and the cells washed once with culture medium to remove cells that had not adhered to the plate. Monolayers were covered with 2ml culture medium and three phase contrast images along the length of each wound taken using a 4x objective lens. The grid positions for the sites photographed at the start were recorded and returned to at the end of the recovery period of 32hours **(Figure 2.4B)** The area of the wound at the start and end of the recovery period was measured using ImageJ software for each site of observation along the wound and the average percentage recovery calculated **(Figure 2.5)**. Where possible, conditions were set up in duplicate and the average of those repeats calculated.

To determine wound-recovery in relation to cell density, images were divided into thirds using the rectangular selection tool together with the draw command. The area of the wound in each third was measured for paired start and end images and the number of cells in each region of

the monolayer surrounding the wound was counted at the start and end. The average cell density across the wound was calculated for each third and plotted against the percent wound-recovery for that portion of the wound. The decision to divide images into thirds was taken because it was noticed that a gradation in density sometimes occurred along the length of the wound attributable to the well edge effect (cells tend to pool at the two ends of the insert wells giving higher density toward the ends).

2.3.3.1 Wound recovery assay on 24hour sub-endothelial matrices deposited by KSHV-inoculated and untreated HUVEC

On day-seven post-inoculation, KSHV-inoculated and untreated HUVEC were detached from wells of the 24-well inoculation plate, transferred to 1.5ml microfuge tubes, pelleted (5mins, 425 x *g*) and re-suspended in culture medium to a density of 2.1×10^5cells/ml. Culture inserts for wound recovery assays were placed into the centres of 6-well plate wells with an acetate grid behind and 70µl cell suspension (KSHV-inoculated or untreated) or culture medium seeded into each well of each insert. Inserts were set up in duplicate. Cells were allowed to adhere and deposit sub-endothelial matrix proteins for 24hours after which the monolayers were washed once with 70µl PBS per side of the insert and the cells stripped from the sub-endothelial matrix by incubation in 70µl pre-warmed detergent lysis buffer (37°C) (PBS containing 0.5% (v/v) Triton X-100; 20mM NH_4OH). To remove all traces of lysis buffer, the monolayers were washed four times with 100µl PBS followed by 100µl culture medium. 70µl first passage allogenic untreated HUVEC were seeded onto the sub-endothelial matrices at a density of 2.1×10^5 cells/ml. After 6hours the inserts were removed, the monolayers washed once with culture medium and the start images taken. The grid positions of the imaged sites were recorded and returned to after

18hours of wound recovery. The area of the wound at the start and end of the recovery period was measured using ImageJ software for each of three sites of observation along the length of each wound and the average percentage wound recovery calculated across the duplicate wounds.

2.3.4 Tracking the migration of HUVEC in isolation

HUVEC were plated in 12-well plates at 3×10^4 cells/well in 1ml culture medium. Seeding at this density created patches of isolated cells. Cells were allowed to adhere for 24hours then time-lapse images recorded for 150minutes observing cells using a 10x objective lens. 8-bit Tiff images were saved at 10minute intervals. To avoid problems of pH change, the culture medium was changed immediately before imaging from complete M199-based culture medium to pre-warmed cell imaging medium, (9.7g/l Hanks's Balanced Salts Solution without sodium bicarbonate and phenol red (Sigma) supplemented with 10μM HEPES (Sigma) and 20% (v/v) FCS, pH 7.4). Cells were incubated at 37°C throughout recording.

Cells to track were selected at random by assigning each cell in the view at the start a number and including those whose numbers were generated in a set of random numbers. The (x,y) coordinates of the cell centroids at each timepoint were determined using ImageJ software and the distance migrated between each timepoint calculated according to Pythagoras' theorem ($h=\sqrt{(a^2+b^2)}$), where 'h' is the distance migrated, and 'a' and 'b' are the differences between the x and y coordinates for the centroid at the timepoint of interest and those of the cell at the previous timepoint of measurement **(Figure 2.6)**. KSHV-infected cells were identified from a GFP fluorescence image overlain at the start.

2.3.5 Tracking the migration of HUVEC during wound recovery

KSHV-inoculated HUVEC were plated into a culture insert for wound recovery placed in the centre of a 6-well plate. At the start of wound recovery the insert was removed, the monolayer washed once with pre-warmed cell imaging media and covered with 2ml cell imaging media. Cells were imaged using a 6x objective lens and incubated at 37°C throughout recording. 8-bit Tiff images were saved at 15minute intervals for a total of 8hours. KSHV-infected cells were distinguished using a GFP fluorescence image overlain at the start and cells to track, both infected and non-infected, were selected at random. The distance migrated between each timepoint was calculated according to Pythagoras' theorem **(section 2.3.4)**; however, in this study, the centroid used was that of the cell nucleus as opposed to the total cell surface area, since for cells in a confluent monolayer at low power magnification, nuclei were clearly defined but cell contacts prohibited accurate visualisation of the cell perimeter.

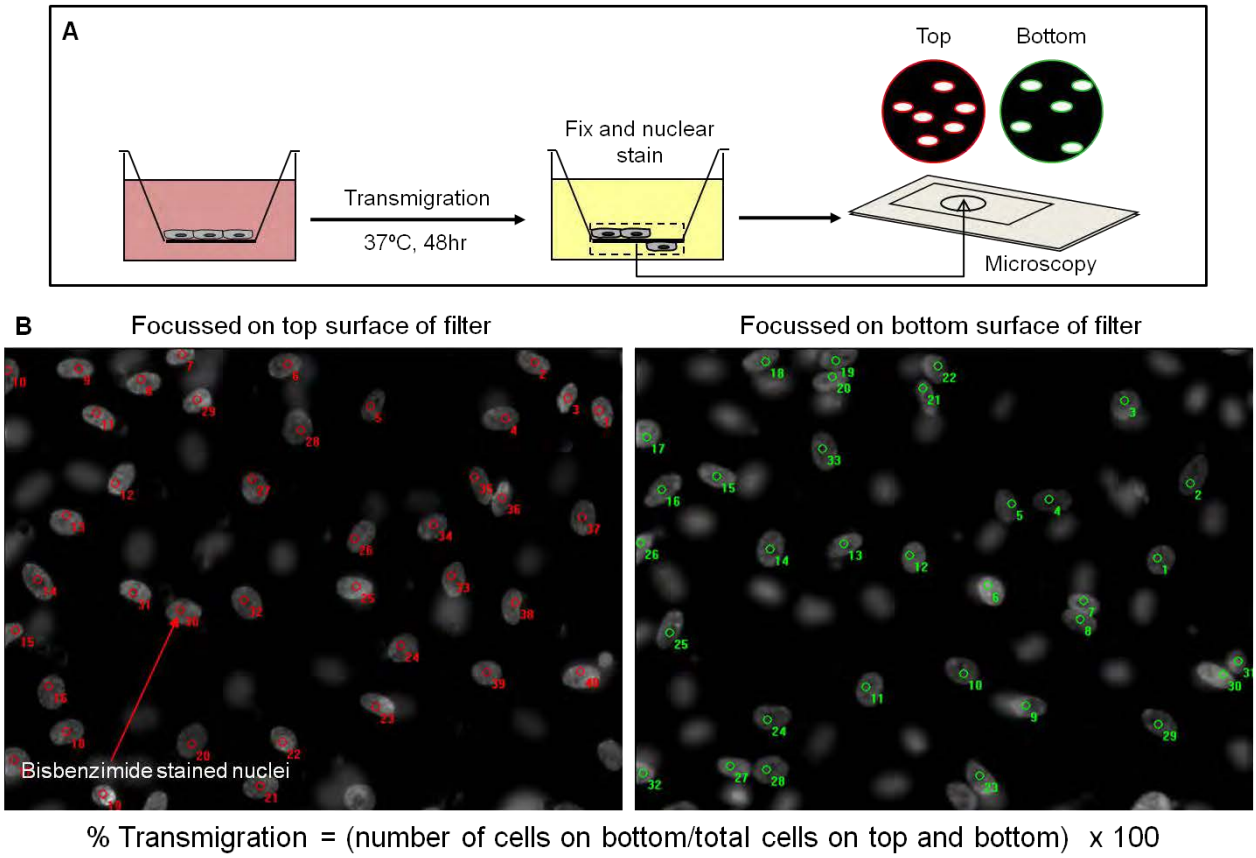

Figure 2.3: Transmigration assay set up and analysis.

(A) HUVEC were allowed to transmigrate across 8µm pore filters of 24-well size transwell chambers. After 48hours the cells were fixed on the filters and their nuclei stained. The filters were then cut out of the chambers and mounted on microscope slides. **(B)** Cells on the top and bottom surfaces of the filter were focused onto separately for the same field of view and the number of cells on each surface counted. The percentage of cells in the field that had transmigrated to the bottom of the filter was calculated according to the equation stated. Percent transmigration for each filter was the average percent transmigration of 14-18 fields.

Figure 2.4: Wound recovery assay set up.

(A) Strips of grid on acetate were secured to the bases of 6-well plates to enable the same fields of cells imaged at the start to be re-imaged at the end. A window (2mm wide) had been cut in the centre of each strip to accommodate the wound. The wound recovery inserts were set in the centre of each well such that their central divisions were within the window. Each chamber was filled with 70µl cell suspension ($1.5x10^4$ cells). Once cells had adhered, the inserts were removed to reveal the wounds. **(B)** The microscope (using 4x objective lens) was focused onto the grid at the edge of the window. The microscope was fitted with a tool that gave a series of concentric rectangles in the field of view when looking through the microscope eyepiece. A corner of a square on the acetate grid at the edge of the window was aligned with the corner of a selected rectangle (white circle). The rectangle and grid square combination was recorded so that the site could be found again at the end of the recovery period. Without moving the x,y position of the microscope stage the microscope was focused onto the monolayer and a picture taken. The picture was saved in Tiff format.

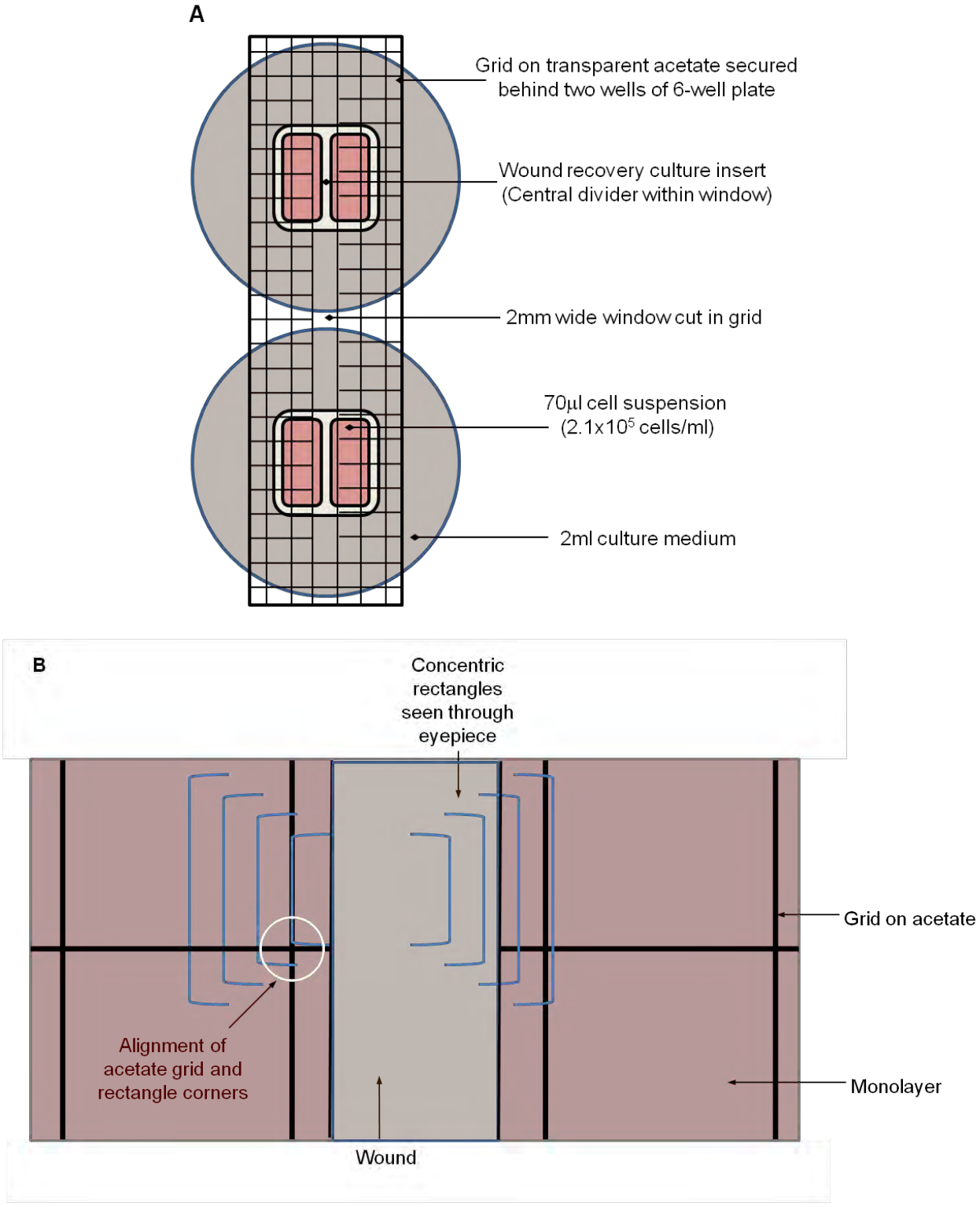
A
Grid on transparent acetate secured behind two wells of 6-well plate
Wound recovery culture insert (Central divider within window)
2mm wide window cut in grid
70µl cell suspension (2.1x10^5 cells/ml)
2ml culture medium
B
Concentric rectangles seen through eyepiece
Grid on acetate
Alignment of acetate grid and rectangle corners
Monolayer
Wound

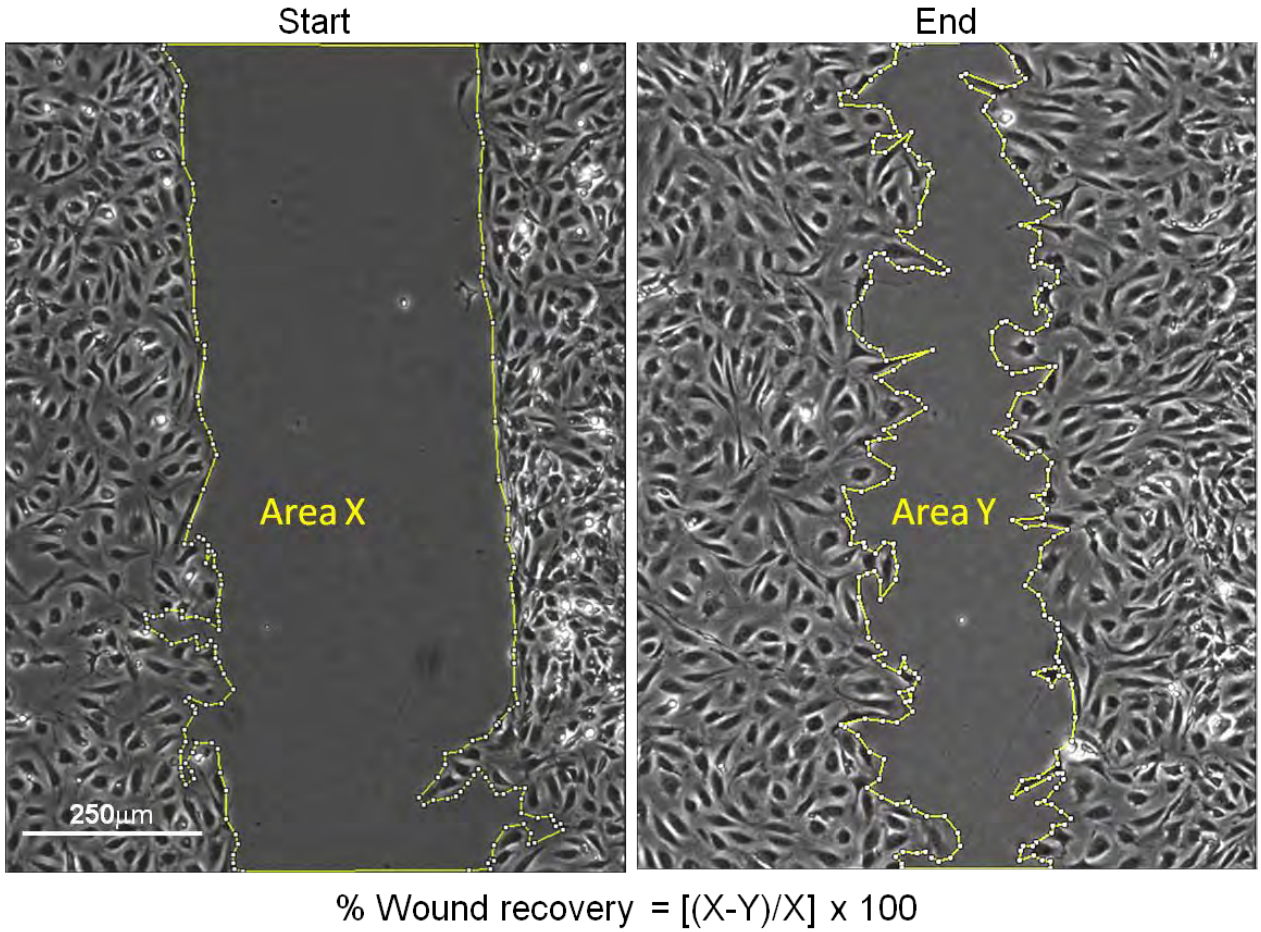

Figure 2.5: Method for analysis of wound recovery.

Images of the wound at the start and end of the recovery period were opened in ImageJ and the polygon tool used to draw around the perimeters of the wounds. The areas of the shapes created were measured and the percent wound recovery calculated according to the equation stated.

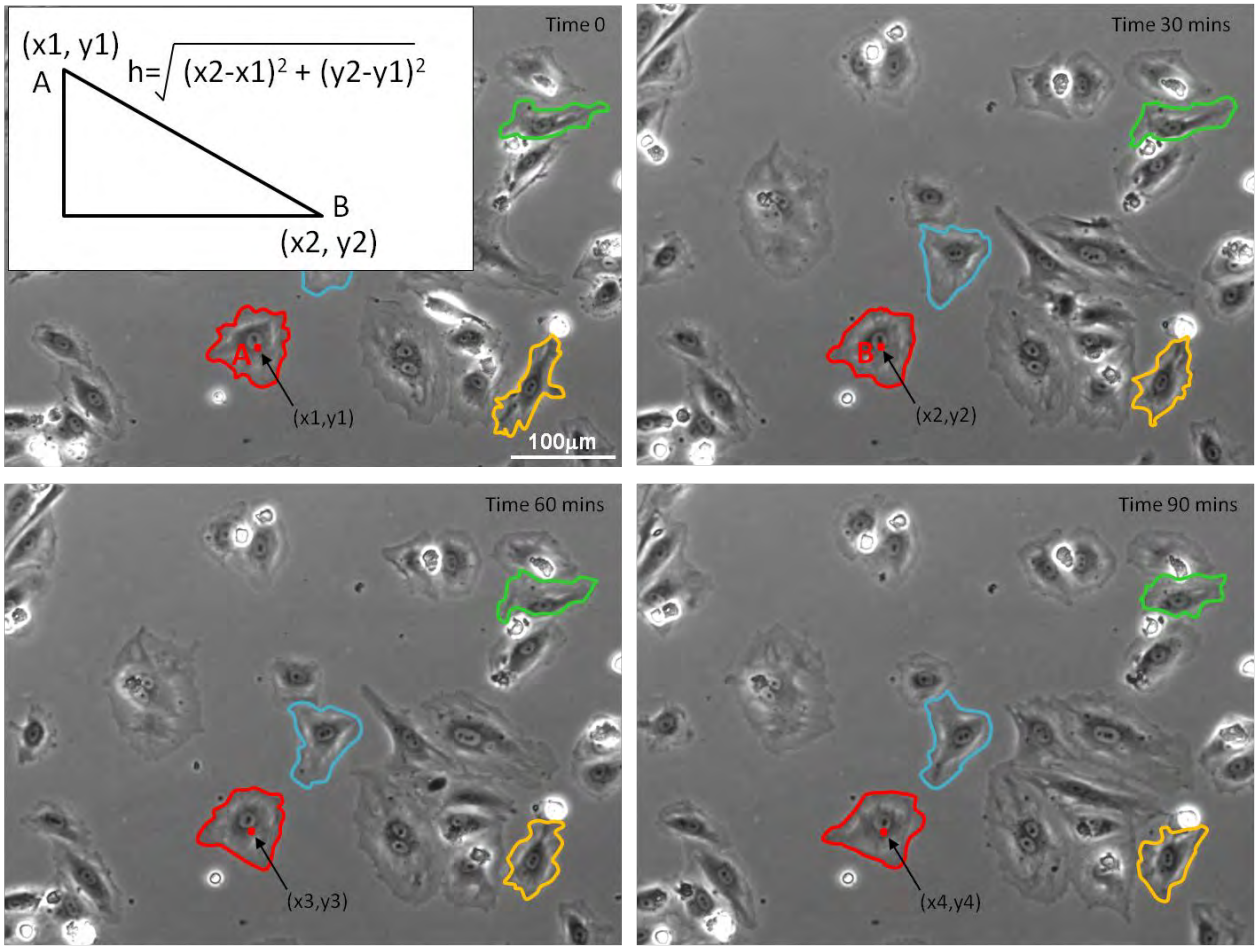

Figure 2.6: Strategy for analysis of isolated cell migration.

Sequences of images captured during a timelapse recording of 2.5hours were opened in ImageJ and the polygon tool used to draw around the perimeters of the cells (selected at random) at 10minute intervals. The (x,y) coordinates for the midpoint of each cell under analysis (as shown for the red cell) were recorded at each timepoint and the overall distance migrated calculated according to Pythagoras' Theorem, where total distance travelled was the sum of the hypotenuses (Σh). Estimates of migration distance were also made for intervals of 30, 50 or 150minutes between measurement of the cell midpoint. Pictures shown illustrate for four cells, at 30minute intervals over the first 90minutes, how the movement of cells was followed by drawing around their perimeters.

2.4 ANALYSIS OF BASEMENT MEMBRANE COMPOSITION BY ENZYME-LINKED IMMUNOSORBENT ASSAY (ELISA)

For deposition assays between days zero and four post-inoculation, cells were plated at 3×10^4 cells/well of 96 well plate in 100µl culture medium for 4-6hours then were inoculated with KSHV, UV-inactivated KSHV or non-supplemented EBM-2 (untreated control). For deposition assays between days seven and eleven post-inoculation, cells were detached from the inoculation plate on day-seven and replated at 3×10^4 cells/well of 96 well plate. Medium was changed on day-two post-plating.

On day-four post-plating, cells were stripped from the underlying basement membrane. To strip the cells, the monolayer was rinsed once with 100µl PBS then incubated with 100µl pre-warmed (37°C) detergent lysis buffer (PBS containing 0.5% (v/v) Triton X-100; 20mM NH_4OH) for 2minutes or until cells had lysed. The lysis buffer was removed and membranes washed four times with 200µl PBS then blocked with 1% (w/v) BSA in PBS (1%PBSA) (1.5-2h, 37°C) before incubation with 50µl primary antibodies **(Table 2.1)** diluted in 1%PBSA containing 2% (v/v) goat serum (2h, 37°C). Membranes were washed five times with 1%PBSA then incubated with an HRP-conjugated secondary antibody, goat anti-mouse HRP **(Table 2.1)** diluted in 1%PBSA (1.5h, 37°C). Excess antibody was removed through five washes with 1%PBSA before development at room temperature with 100µl SIGMAfast OPD (Sigma) solution prepared according to manufacturer's instructions. The reaction was quenched after 10minutes by addition of 100µl 2N sulfuric acid and the endpoint absorbance read at 490nm using a BioTek synergy HT plate reader. The average of three technical repeats was calculated and absorbance for stained

wells that had contained medium only, as opposed to cells, subtracted as background. This background had been validated to be equivalent to staining basement membrane with an isotype control antibody but allowed conservation of cells.

In some development assays, cells were removed by 4hour incubation (37°C) in 100µl 0.02% (w/v) EDTA as opposed to lysis buffer.

2.5 LUMINEX

A Luminex kit was purchased (Chemicon, Millipore) for analysis of the following cytokines in a single sample (50µl) of supernatant: IL–1α; IL-1β; IL-4; IL-6; IL-8; IL-10; IFN-γ; IP-10, monocyte chemotactic protein-1 (MCP-1); TNFα and TNFβ. For each cytokine, the kit included 125µl of microparticle beads coated with capture antibody and 125µl of biotinylated detection antibody. The beads were dyed with differing concentrations of two fluorophores to generate distinct bead sets that could be differentiated by the Luminex 100 plate reader (Luminex Corporation, USA).

The beads were vortexed for 30seconds to separate them into singlets then 125µl volumes of all beads were mixed together with 4ml 'bead buffer'. The resulting bead suspension was stored (on ice, dark) until required.

100µl BSA/Tween buffer (1% (w/v) BSA in 0.05% (v/v) Tween in PBS) was added to each well of the Luminex plate to moisten the bottom of the plate. The plate was attached to a

Millipore vacuum pump to remove the wash through the bottom of the plate. 50µl of sample (or standard) were added to the plate followed by 25µl of the bead suspension. The plate was covered and shaken for 2hours at room temperature.

During the incubation period, the biotinylated antibody solutions were mixed and diluted in 22ml 'assay buffer'. The solution was kept on ice until required. After the 2hour incubation the plate was washed six times using the Millipore vacuum pump. 100µl antibody solution were then added to each well and the plate shaken for 1hour. During the incubation period, the streptavidin-phycoerythrin (S-PE) solution was prepared by dilution of the stock supplied in 22ml BSA/Tween buffer. Following the 1hour incubation, the plate was washed four times and 100µl S-PE solution added to each well. The plate was shaken for 30minutes then analysed using the Luminex 100 machine which distinguished the analytes according to their microparticle bead fluorescences and measured the amount of analyte bound on the basis of PE median fluorescence intensity (MFI).

2.6 RNA ISOLATION AND POLYMERASE CHAIN REACTION (PCR)

2.6.1 RNA isolation

Total ribonucleic acid (RNA) was isolated by TRizol® chloroform extraction with isopropyl alcohol precipitation of RNA. At the timepoint of interest post-inoculation, cells in 24-well plates ($8x10^4$ cells/well), were washed once with PBS and harvested in 1ml TRizol® reagent (Invitrogen) per well into 1.5ml RNase free microfuge tubes. Samples were either stored at -80°C or RNA isolated immediately. If processed on a different day, samples of cell lysates in TRizol® were first thawed and equilibrated to room temperature. To isolate RNA, 200µl chloroform (Sigma) were added, the mixture vortexed for 15seconds then incubated (2-3min, room temperature) before centrifugation (15mins, 15294 x *g*, 4°C) to separate the aqueous and hydrocarbon layers. The upper aqueous layer was transferred into a clean 1.5ml RNase free microfuge tube and 500µl isopropyl alcohol (Sigma) added. Following incubation (10mins, room temperature) samples were frozen at -80°C for a minimum of 1hour or overnight. Samples were allowed to thaw then were centrifuged, (10mins, 15294 x *g*, 4°C). Supernatants were removed and the pellets washed in 1ml ethanol; this involved a brief vortex followed by centrifugation (5mins, 5974 x *g*, 4°C) to pellet the RNA. Supernatants were removed and pellets allowed to air-dry before resuspension in 15µl RNase free water.

Samples were DNase treated using the 'DNA-free DNase treatment and removal kit' (Ambion) according to the manufacturer's instructions: Buffer and DNase were diluted 1 in 10 in the RNA (1.5µl of each added to the RNA) and incubated (30mins, 37°C). Inactivator was added at 1 in 10 dilution (1.5µl) and pulse vortexed to mix. Inactivator was removed by centrifugation

(2mins, 10621x *g*) followed by transfer of the RNA to a clean 1.5ml RNase free microfuge tube. The RNA concentration was measured using a Nano-drop 3300 fluorospectrometer.

2.6.2 cDNA synthesis

cDNA was synthesised from 125ng RNA. Samples with and without the reverse transcriptase enzyme were prepared in parallel to permit verification that expression measured was due to mRNA and not contaminating DNA. 20µl cDNA reactions were prepared comprising: 8µl 10mM dNTPs, 2µl 50mM $MgCl_2$, 2µl 10X PCR buffer, 1µl oligo dT, 1µl RNase inhibitor, 1µl MuLV reverse transcriptase (or pure water) (all from Applied Biosystems), 5µl 125ng RNA diluted in pure water. All components were mixed and cDNA synthesised by a heating program of 42°C for 1hour followed by 95°C for 5min. On completion of the program, samples were held at 4°C.

2.6.3 PCR

Laminin messenger RNAs (mRNA) for the main endothelial laminin chains including α4, α5, β1, β2 and γ1, were amplified by polymerase chain reaction using primers designed with the aid of the NCBI Primer designing tool **(Table 2.2)**. Desalted laminin primers (Invitrogen) were reconstituted in pure water to a final concentration of 200ng/µl. 25µl PCR reactions were prepared comprising: 5µl 5X GoTaq buffer (Promega), 0.5µl forward primer, 0.5µl reverse primer, 0.5µl 10mM dNTPs (Bioline), 0.5µl cDNA, 0.25µl GoTaq DNA Polymerase (Promega), 17.25µl pure water. Amplification of β-actin mRNA was used as an endogenous control and the

KSHV viral FLIP mRNA as a positive control for KSHV-infection. PCR reaction mixtures for these two controls were prepared according to the volumes used for PCR of the laminin transcripts although primer concentrations were unknown. vGPCR mRNAs were amplified using 1.0µl cDNA as opposed to 0.5µl, volumes of all other PCR-reaction components were as for the laminin PCRs. Conditions of PCR amplification were: 2minutes at 95°C, followed by between 21 and 35 PCR cycles **(Table 2.2)** involving: chain separation (1min, 95°C), primer annealing (45secs, primer-specific temperature (**Table 2.2)**) and elongation (45secs, 72°C). Reactions were held at 72°C for a final 7minutes then held at 4°C. The number of PCR cycles was dependent upon the gene of interest **(Table 2.2)** and was such that differences in abundance would be evident from the ethidium bromide gel eletctrophoresis of the PCR product as determined by titration of cDNA into the reaction mixture across a range of cycle numbers.

1% (w/v) agarose ethidium bromide gels (50ml) were prepared from electrophoresis grade agarose powder (Invitrogen) dissolved in 0.5x Tris-Borate-EDTA (TBE) buffer (0.5x TBE was prepared from a 10x TBE stock (108g tris base/litre; 55g boric acid/litre; 7.44g EDTA/litre). To prepare one gel (50ml), 0.5g agarose was dissolved in 50ml 0.5x TBE by heating in the microwave (3mins, 600W). Once the gel had cooled to hand temperature 2.5µl ethidium bromide were added and the gel poured into a cast into which a comb had been positioned. Once the gel had set, the comb was removed and the gel submerged in 0.5x TBE running buffer. 5µl 6x loading dye was added to the PCR samples and the samples loaded onto the gel. It was desirable to be able to use a similar exposure for visualisation of all transcripts; therefore the volumes of product loaded varied between transcripts **(Table 2.2)**. A 100bp molecular ladder (Bio Labs) was

run in the first lane for determination of the product sizes. The gel tank was connected to a power supply (Bio-Rad powerpac 200) and the PCR products separated at 90V for 50minutes.

The bands were visualised using a Gene Genius Bio Imaging System machine together with Genesnap (from Syngene software) and an image captured. The intensities of the product bands were measured using ImageJ software and the intensity of a control region above each band was subtracted. Results were finally normalised to that of the endogenous control gene (β-actin).

Table 2.2: Primer sequences and conditions for PCR

Target mRNA		Primer (5'-3')	Amplicon length (bp)	Annealing temp (°C)	Number of PCR cycles	Volume loaded on EtBr agarose gel (µl)
LAMA4	Forward	GCGCAGCCACCTCGGGATAC	441	65	29	10.0
LAMA4	Reverse	CCGCTGGCAGTGCACACAGT				
LAMA5	Forward	GCACCCCACGGGATCTTGCC	563	65	30	14.0
LAMA5	Reverse	GGTCGACTTGGAGCGGGCAC				
LAMB1	Forward	CGTGGAGTGCCGAGCCTGTG	336	65	27	10.0
LAMB1	Reverse	GGGCTCTGCGCCAGGATGTC				
LAMB2	Forward	GCAGGCTATACGGGGCTGCG	454	65	30	12.5
LAMB2	Reverse	CGTTGCAGGTGGGGCCTCTG				
LAMC1	Forward	GCCCGAGCTGATGCTGCCAA	563	65	28	12.5
LAMC1	Reverse	AGCTGCCCCAGCTGCTCCAA				
β-actin	Forward	CATCACCATTGGCAATGAGC		55	21	12.5
β-actin	Reverse	CGATCCACACGGAGTACTTG				
vFLIP	Forward	ATGGCCACTTACGAGGTTCT		65	29	10.0
vFLIP	Reverse	ACGTGGAGAACAGTGAGCTG				
vGPCR	Forward	CCCGTCAGGGGAGTGACAAG		62	35	14.0
vGPCR	Reverse	CCAGACCTAACACACCCCTGTC				

2.7 IMMUNOFLUORESCENCE ASSAY

2.7.1 Immunofluorescence assay for LANA-1 following inoculation of HUVEC with BCBL-1 derived KSHV

Cells were detached from the culture plate using trypsin and transferred to 15ml tubes. PBS was added to a total volume of 13ml and cells pelleted (5mins, 500 x *g*). The supernatant was decanted, cells resuspended in the residual volume and spotted onto a well of an IFA Multitest 8-well slide (MP Biomedicals). Before the suspension dried, it was observed under a light microscope to ensure that the density of seeding was appropriate and suspension was added or removed as necessary. Generally ~3µl were required. For each test, two wells were spotted to enable both LANA-1 and control staining (secondary antibody only) to be performed for each. Alongside each experiment, two wells of BCBL-1 cells were spotted to serve as a positive control for LANA-1 staining. Slides were set up in duplicate.

Once spotted, slides were left to air-dry (5-10mins, room temperature) and cells fixed by immersing the slide in ice-cold 1:1 acetone-methanol solution (5mins). Once dry, slides were stored at 4°C until staining.

Solutions required for staining were freshly prepared on the day of staining. In order that different solutions could be contained over each of the eight wells during staining and smaller volumes of antibody used, a wax grid was drawn around the eight wells on each slide using a wax pen (Dako). Cells were permeabilised by incubation in 0.2% (v/v) Triton X-100 detergent in PBS (30mins, room temperature) and non-specific antigen binding sites blocked by incubation in 3% BSA (w/v) in PBS (3%PBSA) (15mins, room temperature). Slides were blotted on tissue to

remove excess solution and 20µl of either primary antibody (mouse anti-LANA-1) **(Table 2.1)** diluted in 3%PBSA or 3%PBSA (secondary antibody only negative control) applied to each well for positive or negative staining respectively. Slides were incubated in a humidified chamber (1h, 37°C) then excess antibody washed off by swirling the slides twice in a beaker containing 0.1% BSA (w/v) in PBS (0.1%PBSA). Slides were blotted on tissue and 20µl secondary antibody (goat anti-mouse IgG conjugated to Alex Fluor 594) **(Table 2.1)** diluted in 3%PBSA were then applied to each well, both positive staining and negative control wells, and the slide incubated in the humidified chamber (60mins, 37°C). Slides were washed twice in 0.1%PBSA and the cell nuclei counterstained with 20µl DAPI (1µg/ml diluted in PBS) applied to each well (5mins, room temperature, dark). Excess stain was washed off by swirling the slides in a beaker of distilled water. Once dry, slides were mounted using Citifluor (Citifluor Ltd) and sealed with nail varnish. Slides were stored at 4°C and viewed on a Nikon Eclipse E600 flurorescence microscope using a 40x oil immersion objective lens.

2.7.2 Immunofluorescence assay for analysis of LANA-1 dots and coincident GFP expression in rKSHV.219-infected HUVEC

24hours post-inoculation, HUVEC in µ-slide IV channels (Ibidi, Thistle Scientific) were fixed with 4% (w/v) formaldehyde (15minutes, room temperature), permeabilised with 100% (v/v) methanol (10minutes, -20°C), washed with PBS and blocked with 5% (v/v) goat serum in PBS for 1hour. The blocking buffer was aspirated and cells incubated with rat anti-LANA-1 unconjugated primary antibody **(Table 2.1)** (overnight, 4°C). Cells were washed three times with

PBS and incubated with Alexa Fluor 633-conjugated goat anti-rat IgG secondary antibody **(Table 2.1)** (1-2hours, room temperature, dark). Excess antibody was removed through five washes with PBS. Bisbenzimide (2μg/ml) (Sigma) was included in one wash to stain nuclei. Channels were coated with ProLong Gold anti-fade mountant (Invitrogen, Molecular Probes) prior to visualization. Images were captured on a Zeiss LSM510 confocal microscope fitted with a water immersion, 63x objective lens and analysed using ImageJ software. This analysis involved determining whether cells expressed GFP and/or stained positively for LANA-1. The number of LANA-1 dots was also recorded for each cell.

2.7.3 Immunofluorescence assay for analysis of actin cytoskeleton organisation and focal adhesion (vinculin) distribution in KSHV infected HUVEC

HUVEC were plated at a density of $7.4x10^4$ cells/24-well in 420μl culture medium and inoculated with KSHV the following day at MOI10. Six days post inoculation, eight-chamber slides (BD Falcon) were gelatin-coated using a 1% (w/v) gelatin solution. Cells were detached from the inoculation plate using trypsin and pelleted in 1.5ml microgfuge tubes (5mins, 425 x *g*). Cells were resuspended in culture medium, 1320μl per original 24-well and 200μl aliquoted to each of six wells of an eight-chamber slide forming a sparse distribution of cells in each well. Spare wells were filled with 200μl medium to avoid loss of media from cell-containing wells by capillary action. Cells were cultured for 24hours. On day-seven post-inoculation the medium was removed, cells washed once with 200μl PBS and fixed in 300μl 4% (w/v) formaldehyde (room temperature, 15mins). Fixative was removed and cells covered with 200μl PBS. Slides were

either placed in the fridge wrapped in cling film and foil to prevent evaporation or were stained immediately.

To stain, chambers were removed from the slides using the tool provided and moisture carefully removed from the divisions using a cotton bud. The divisions were then drawn over using a wax pen (Dako). Once dry, slides were washed once in a beaker of PBS then immersed in 0.1% (v/v) triton X-100 (diluted in PBS) for exactly 4minutes. Slides were washed once in a beaker of PBS, the backs of the slides were dried with paper towel and surplus PBS removed from the tops of the slides using a cotton bud to absorb the liquid but taking care not to touch the cells. Slides were placed on a rack and 100µl 4% (w/v) BSA in PBS (4%PBSA) aliquoted to each 'well' created by the wax divisions. Cells were blocked at room temperature for 1hour. The 4%PBSA solution was removed and cells incubated (50mins, room temperature, dark) with 100µl primary antibody diluted in 4%PBSA or 4%PBSA only (unstained control). Primary antibodies used included mouse anti-vinculin and mouse IgG1 isotype control **(Table 2.1).** Staining was performed in duplicate.

Next, slides were washed in a jar of PBS and dried using cotton buds to remove surplus PBS. Cells were incubated (40mins, room temperature, dark) with 100µl secondary antibody staining solution containing: Alexa Fluor 633 goat anti-mouse IgG secondary antibody **(Table 2.1)**; Phalloidin-tetramethylrhodamine B isothiocyanate (diluted 1 in 500) (Sigma); bisbenzimide (2µg/ml) (Sigma) diluted in 4%PBSA solution. Slides were washed in a jar of PBS and then rinsed in a jar of distilled water, dried and mounted with ProLong Gold anti-fade mountant (Invitrogen, Molecular Probes). Slides were left to air dry at room temperature, in the dark, for

24hours then sealed with nail varnish and stored at -20°C until viewing on a Zeiss LSM510 confocal microscope with a water immersion 63x objective lens. Images collected were analysed using Image-Pro and ImageJ software. Conditions of capture for Rhodamine-labelled Phalloidin staining of filament actin (F-actin) were such that pixel intensity values were less than 255.

2.8 SIRNA TRANSFECTION OF HUVEC

2.8.1. Sources and preparation of siRNA.

Three siRNAs to target laminin-α4 chain mRNAs were chosen from the Sigma catalogue on the basis that they should target a region common to all laminin-α4 chain mRNA variants **(Table 2.3)**. These siRNAs (10μmol) were received lyophilised and were resuspended in 100μl RNase free water (Qiagen) to a concentration of 100μM. To distinguish between the three siRNAs they were assigned the letters A, B and C. 50μl of each one was diluted to 20μM with RNase free water, aliquoted and stored at -80°C as the working stock. The remainder (50μl) was stored at -80°C.

AllStars negative control siRNA conjugated to Alexa Fluor 647 (20μmol) (Qiagen) **(Table 2.3)** was received lyophilised and resuspended in 1ml RNase free water (Qiagen) to a concentration of 20μM. This was aliquoted and stored at -80°C as the working stock.

Table 2.3: siRNA duplexes

siRNA	Duplex sequence	Catalogue number	Company
Laminin-a4 siRNA-A	CUCAGCGGUUGGCAGGCAA[dT][dT] ASUUGCCUGCCAACCGCUGAG[dT][dT]	SASI_Hs02_00324004	Sigma
Laminin-a4 siRNA-B	GGGAGCUCAGCGGUUGGCA[dT][dT] ASUGCCAACCGCUGAGCUCCC[dT][dT]	SASI_Hs02_00324005	Sigma
Laminin-a4 siRNA-C	CUCAGCGGUUGGCAGGCAA[dT][dT] ASUUGCCUGCCAACCGCUGAG[dT][dT]	SASI_Hs02_00324014	Sigma
AllStars Negative Control siRNA AF647	-	1027295	Qiagen

2.8.2 Assay to examine the impact of laminin-α4 knockdown on the transmigration of HUVEC and their intracellular synthesis and deposition of the laminin-α4 chain.

HUVEC were plated in 46-48 wells of 24-well platesat $3.8x10^4$ cells/24-well. The next day, cells in half of the wells were inoculated with KSHV at MOI10. On day-five post-inoculation, cells were detached using trypsin. Cells from like cultures were pooled. Cells were re-plated in 24-well plates at $3.8x10^4$ cells/well in HUVEC culture medium without antibiotics such that one well of cells could be used for each repeat of an assay (transmigration, ELISA or flow cytometry). On day-six post-inoculation, cells were transfected with siRNA at 100nM. Transfection conditions for each of KSHV-inoculated and untreated cultures included: RNAse free water (2 wells for flow cytometry), AllStars negative control siRNA conjugated to Alexa Fluor 647 (2 or 3 wells for transmigration assay, 4 wells for ELISA), siRNA C to laminin-α4 (2

or 3 wells for transmigration assay, 4 wells for ELISA, 1 well for flow cytometry) and siRNA B to laminin-α4 (2 or 3 wells for transmigration assay, 4 wells for ELISA, 1 well for flow cytometry). A sufficient volume of each transfection condition was prepared to transfect all wells requiring identical treatment.

To prepare 300µl of transfection solution (amount for 1 well), 1.5µl siRNA (20µM working stock) was added to 32.5µl Optimem (Gibco, Invitrogen) and in a separate tube, 0.6µl RNAiMAX Lipofectamine (Invitrogen) was added to 5.4µl Optimem. The two were incubated at room temperature for 10minutes then combined, flicking the tube gently to mix. The mix was incubated for a further 10minutes at room temperature for complexes to form. During this time, HUVEC to be treated were washed twice with 500µl PBS. 260µl Optimem were then added to the siRNA-Lipofectamine mix and pipeted gently to give a uniform suspension. PBS was removed from the cells and transfection solution (300µl) added. The cells were then cultured for 4hours. Transfection solution was removed and the cells washed twice with 500µl HUVEC culture medium without antibiotics. The cells were cultured overnight then re-transfected, following the same protocol, on the morning of day-seven. Following removal of the transfection solution, the cells were given a brief recovery period (45mins) before removing them from the transfection plates using trypsin in order to transfer them into the transmigration assay or into a 96-well plate to verify knockdown of laminin-α4 deposition by ELISA. Cells to be processed for verification of laminin-α4 knockdown by flow cytometry were left in the transfection plate until the end of the experiment.

To conserve cells, they were pelleted (5mins, 425 x *g*) in 1.5ml microfuge tubes rather than 15ml centrifuge tubes. Cell pellets were resuspended in HUVEC culture medium without antibiotics, 200µl per original 24-well for plating into the transmigration assay or 120µl for plating into the ELISA. Culture medium was aliquoted to six additional wells on the ELISA plate for measurement of background signal. The transmigration assay was ended after 48hours and filters prepared for analysis of percent transmigration **(section 2.3.1)**. The ELISA was developed after 40hours and laminin-α4 and fibronectin deposition assessed **(section 2.4).** Each condition examined by ELISA was restricted to analysis in duplicate rather than triplicate due to limited cell numbers. Assessment of fibronectin content was included in order to control for possible differences in cell number across the multiple treatments, since it was a concern that the siRNA treatments could affect the efficiency with which cells re-plated. The efficiency of knockdown was also examined by assessment of intracellular laminin-α4 content by flow cytometry at 40hours **(section 2.2.4.1).** Since the secondary antibody available and suitable for detection of laminin-α4 in the GFP positive, rKSHV.219-infected cells was conjugated to Alexa Fluor 633, it was not possible to use the AllStars negative control siRNA (Qiagen) that was available in the lab for this assay as this was conjugated to Alexa Fluor 647. Therefore, the control transfection for flow cytometry was performed using water in place of siRNA. This was considered appropriate since by ELISA the AllStars negative control did not appear to disrupt laminin-α4 transcription and secretion.

2.9 IMMUNOFLUORESCENCE IMAGE ANALYSIS

2.9.1 Measurement of cell shape parameters

Measurements of cell shape parameters including: area, perimeter, roundness and mean intensity of phalloidin staining (related to the amount of F-actin) were made from confocal images of phalloidin-stained cells using Image-Pro software. Working with the 'Count/Size' facility, the image was thresholded for observation of intensities in the range 1-255 and the '8-connect' and 'fill holes' settings were applied in order to create a mask of the cell. The lowest area limit by which objects within the range for analysis were defined was also increased until a single object was within range (by increasing the lower limit, small spots of debris/background staining were excluded). Once the cell of interest was counted as a single object (the 'irregular AOI' tool was used to select the cell of interest when more than one was present on an image) the data for the measurements of interest, as highlighted in the 'set measurements' menu, were exported to Excel.

2.9.2 Concentric ring analysis of F-actin distribution

A macro was devised in Image-Pro by David Kelly (Wellcome Trust Centre for Cell Biology, University of Edinburgh, UK) to quantify F-actin distribution within cells in order to study the possibility that KSHV infection redistributes F-actin. The macro divided the cell into four concentric rings of equal area and reported the total intensity of staining in each **(Figure 2.7)**. The data for area and intensity were reported as cumulative values. Therefore, after exporting the results to Excel, the area and total fluorescence intensity associated with each ring was calculated

(i.e. area of ring 4 = (sum of areas of rings 1, 2, 3 and 4) – (sum of areas of rings 1, 2 and 3)).Total intensity values for each ring were plotted normalised for ring area.

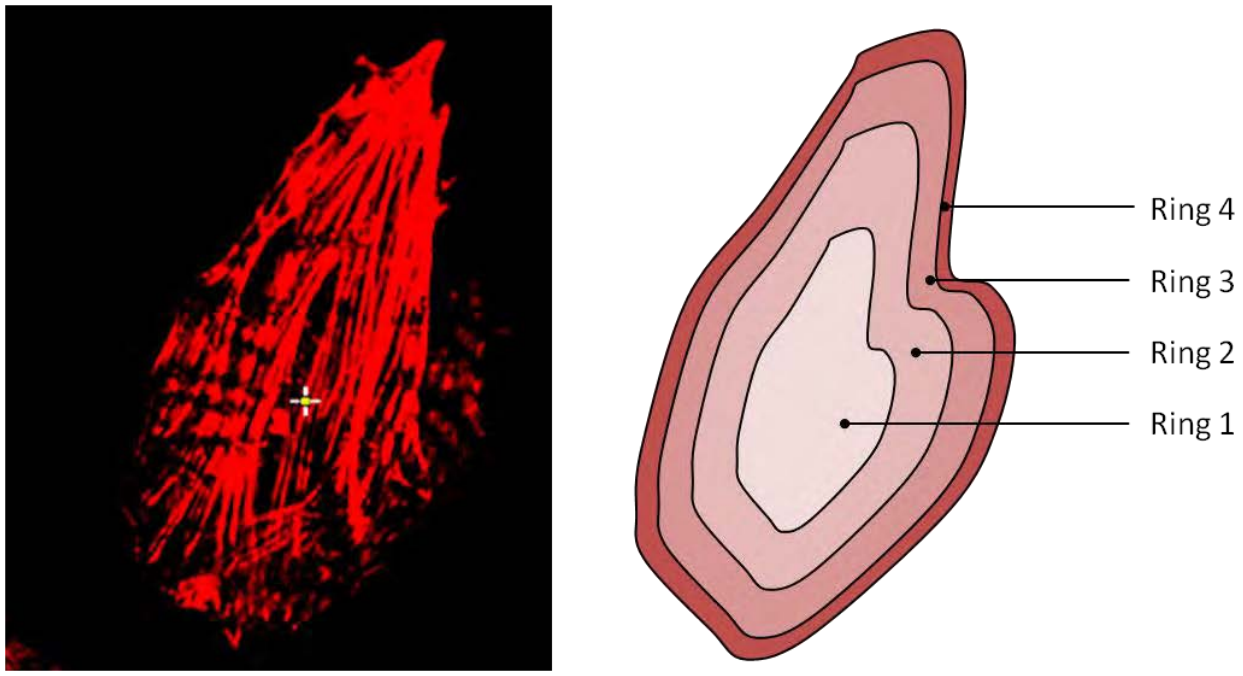

Figure 2.7: The principle underlying the macro devised in Image-Pro for concentric ring analysis of F-actin distribution.

Images of HUVEC stained with rhodamine-phalloidin were opened in Image-Pro and the macro for concentric ring analysis of F-actin distribution, that had been written in this software, was performed. Steps involved thresholding the image then selecting the cell of interest from among those on the image. Next the software divided the cell into four concentrically arranged rings of equal area (rings 1-4). The total intensity of rhodamine fluorescence in each of the four rings was determined from total intensity values reported that were the sums of the intensities in rings 1-4; 1-3; 1-2 and 1. In the same way, the area of each ring was calculated (artoon not to scale).

2.9.3 Concentric ring analysis of F-actin distribution based on intensity line profiles for rhodamine-phalloidin

A method was devised with ImageJ to quantify F-actin distribution within cells and study the possibility that KSHV infection redistributes F-actin. For greater clarity, a full description of the method is given in the figure legend **(Figure 2.8)**.

2.9.4 Analysis of focal adhesion size, number and distribution based on immunofluorescence assay for vinculin.

Images were analysed using Image-Pro. Images were opened in Image-Pro and thresholded to clear background specs that fluoresced within the range examined, as well as cytoplasmic, perinuclear vinculin not recruited to focal adhesions, and establish sizes of focal adhesion structures. The 'irregular AOI' tool was used to draw around the region containing the focal adhesions of the cell of interest (comparison with the image of Phalloidin staining of F-actin for the same cell helped ascertain cell boundaries when cells neared their neighbours). The count facility under 'Count/Size' was used to count the number of focal adhesions using a minimum size boundary of 0.3μm. Measurements of the area of each structure were also exported to Excel and the total area covered by focal adhesions was calculated **(Figure 2.9)**. From knowledge of cell area and perimeter length, focal adhesion number and total area could be normalised to parameters of cell size.

Figure 2.8: Strategy for concentric ring analysis of F-actin distribution based on intensity line profiles of rhodamine-phalloidin staining.

Images of HUVEC stained with rhodamine-phalloidin were opened in ImageJ and thresholded to establish the areas of the individual cells . The wand 'tracing tool' was used to highlight the cell of interest and the midpoint (x,y) coordinates for the cell were determined. A new copy of the image was opened and a line passing through the midpoint was drawn for the longest axis between the leading and trailing cell edges. A line through the midpoint and perpendicular to this longest axis was then drawn and the profile of the intensity of rhodamine-phalloidin staining along this short axis generated. The list of values was exported to Excel. The line drawn protruded beyond the edge of the cell. In the protruding regions intensity values were zero. To divide the line profie into five concentric rings to measure the distribution of F-actin across the cell, the total number of intensity values reported between the first positive value and the last positive value was divided by ten. This gave the number of intensity values to attribute to each segment of the profile. When the total number of intensities was not a multiple of ten, the start and end intensities associated with the segment were multiplied by the fraction that they were to contribute. For example if 9.5 values were included in each segment, the value given to segment 1 was the sum of intensities 1 to 9 + (0.5 x intensity value 10). The value given to segment 2 was (0.5 x intensity value 10) + the sum of intensities 11 to 19. To account for differences in cell dimensions, these values were normalised by dividing the total intensity by the number of intensity values per segment. The concentric rings 1 to 5 were arranged such that 1 was innermost and 5 outermost. The intensity associated with each was the average intensity (normalised for width) for the contributing segments. Ring 1 = segments 5 and 6; ring 2 = segments 4 and 7; ring 3 = segments 3 and 8; ring 4 = segments 2 and 9 and ring 5 = segments 1 and 10). Average normalised phalloidin intensity was plotted against ring number.

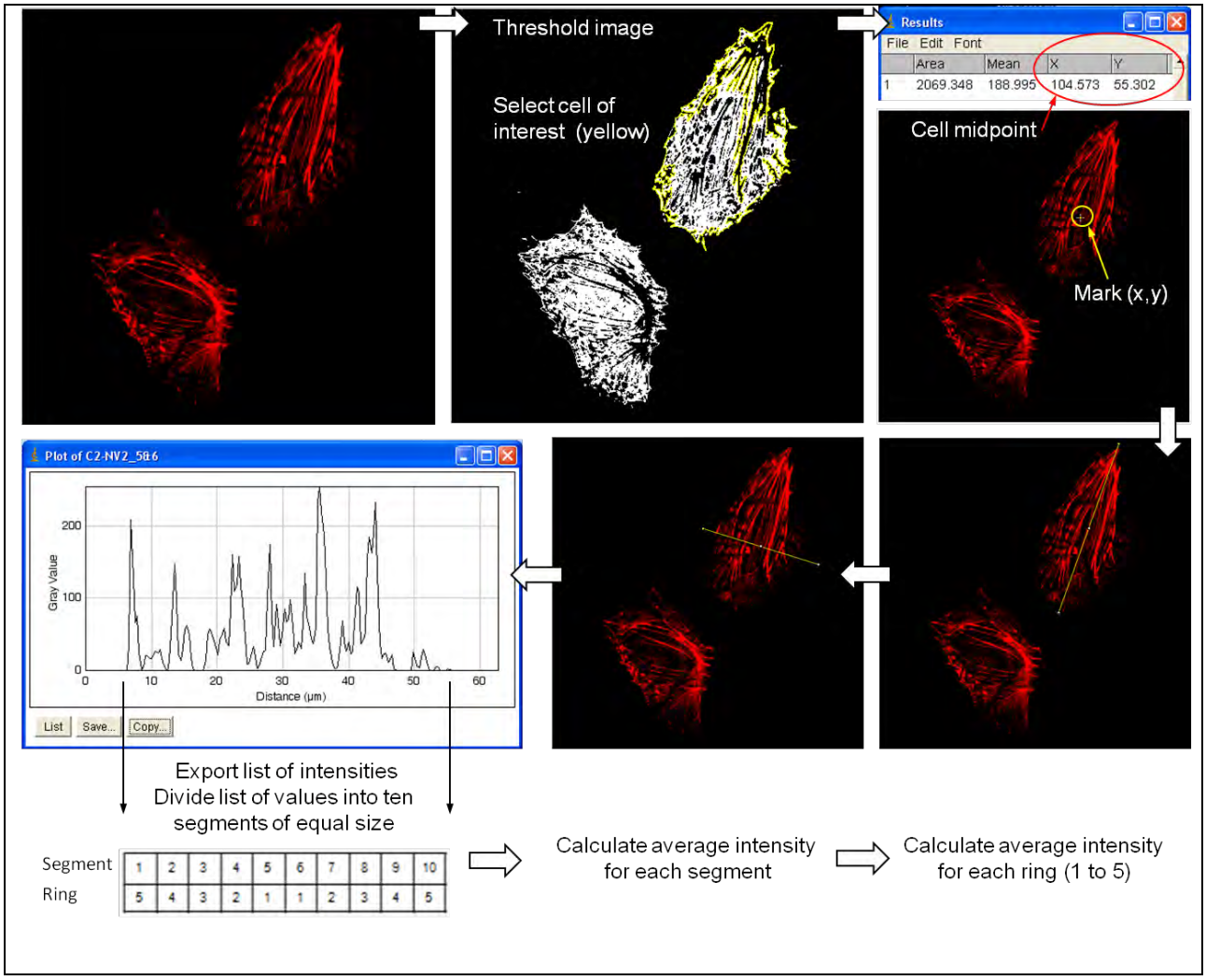
Threshold image
Select cell of interest (yellow)
Results
File Edit Font
Area Mean X Y
1 2069.348 188.995 104.573 55.302
Cell midpoint
Mark (x,y)
Plot of C2-NV2_586
Gray Value
Distance (µm)
List Save... Copy...
Export list of intensities
Divide list of values into ten segments of equal size
Segment 1 2 3 4 5 6 7 8 9 10
Ring 5 4 3 2 1 1 2 3 4 5
Calculate average intensity for each segment
Calculate average intensity for each ring (1 to 5)

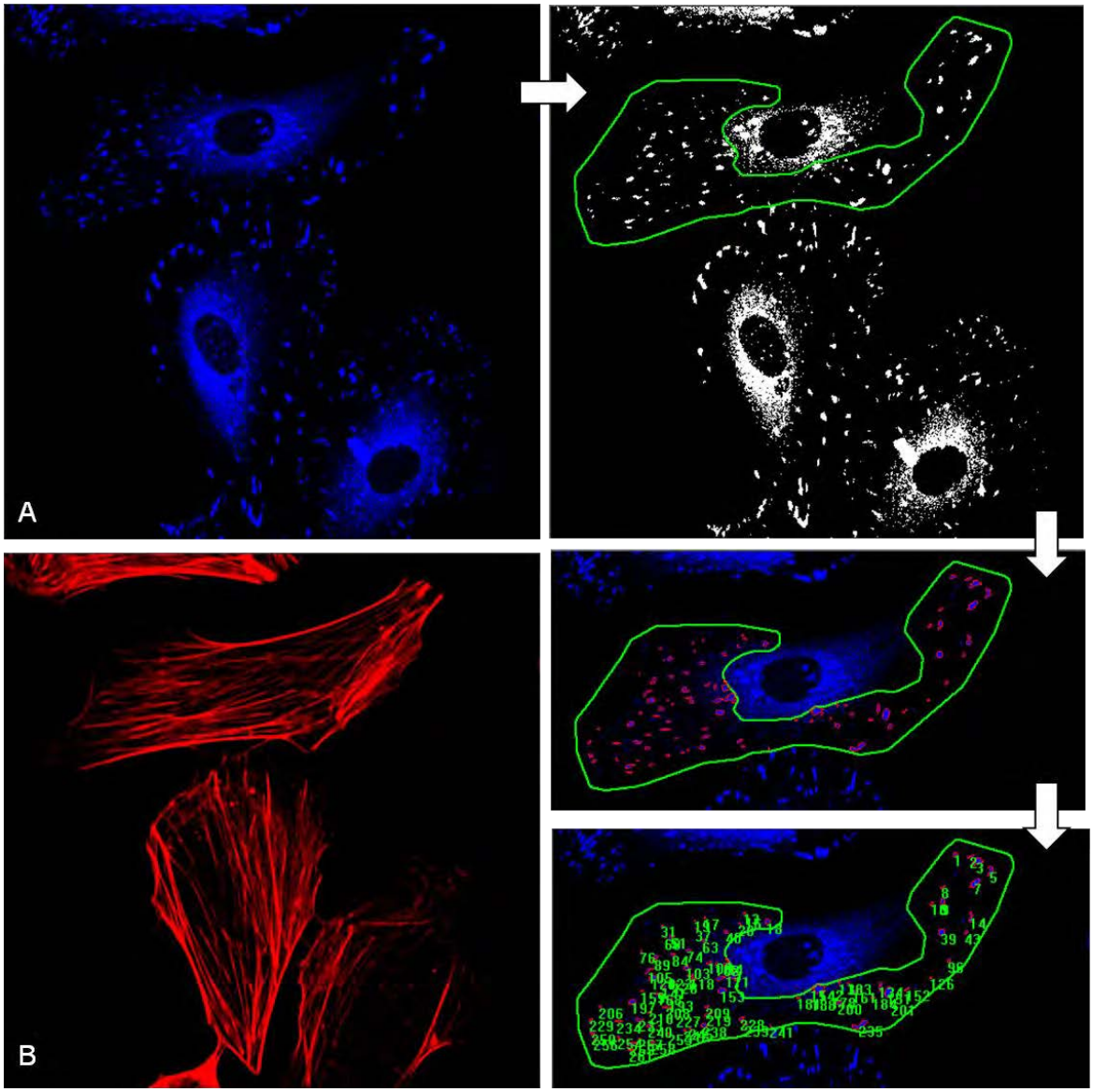

Figure 2.9: Strategy for analysis of focal adhesion size and number.

(A) Images of HUVEC stained for vinculin were opened in Image-Pro and thresholded to identify the peripheral focal adhesions distinct from background and cytoplasmic/perinulear vinculin. The focal adhesions associated with the cell of interest were isolated using the area of interest tool. Images of the cells stained with rhodamine-phalloidin to identify F-actin helped to clarify the focal adhesions associated with the cell **(B)**. The number and areas of the focal adhesion structures (>0.3μm) were determined using the 'Count/Size' facility.

2.10 ANALYSIS OF THE EFFECT OF KSHV-INOCULATION UPON CELL DENSITY OVER TIME.

HUVEC were plated in μ-slides VI channels (Ibidi, Thistle Scientific) ($5.5x10^4$ cells per $60mm^2$ channel). Following overnight incubation, monolayers were imaged then inoculated with KSHV at MOI10. At timepoints up to day-ten post-inoculation, phase contrast, GFP fluorescence and RFP fluorescsence images were taken along the length of the monolayer. The monolayer was viewed with the 4x objective lens. After imaging, monolayers were washed four times with complete medium and images retaken of the monolayer so that the number of lytic cells that had not been washed out could be subtracted from the number observed at the next timepoint and the extent of lytic reactivation between timepoints calculated.

The number of viable cells per complete image was too great to count manually. Therefore, areas of interest were positioned automatically onto the phase contrast image at six sites and the number of cells within the enclosed region counted using the 'manual tag' facility in Image-Pro. The number of cells counted was converted to a density of cells per mm^2 **(Figure 2.10)**.

The number of lytic cells was determined from RFP fluorescence pictures. The images were thresholded and an automated count of the number of objects in the image performed using a size restriction of greater than $15\mu m^2$ that would allow exclusion of background specs **(Figure 2.10)**

Ibidi μ-slides were used for this study in preference to multi-well plates because:

- Assessments of cell density over time were less sensitive to differences in the precise field of observation at each timepoint since HUVEC formed monolayers of uniform

density across the growth surface of μ-slide channels whereas in multi-well plates, cell density was higher in the centre and at the very edge of the well.

- Optical interference in multiwell plates meant that only a proportion of the growth area near to the centre of the well could be viewed whereas in μ-slide channels the full growth area was observable.
- The improved optics with μ-slides enabled the 4x objective lens to be used as opposed to the 10x or 20x lenses required for 24-well or smaller multi well plates. Using the 4x objective lens, only one image (phase contrast) or two images (RFP fluorescence) had to be captured at each timepoint in order to count sufficient cells. This was important considering the time taken to change the image capture conditions and acquire the fluorescence images for each of GFP and RFP in addition to phase contrast.

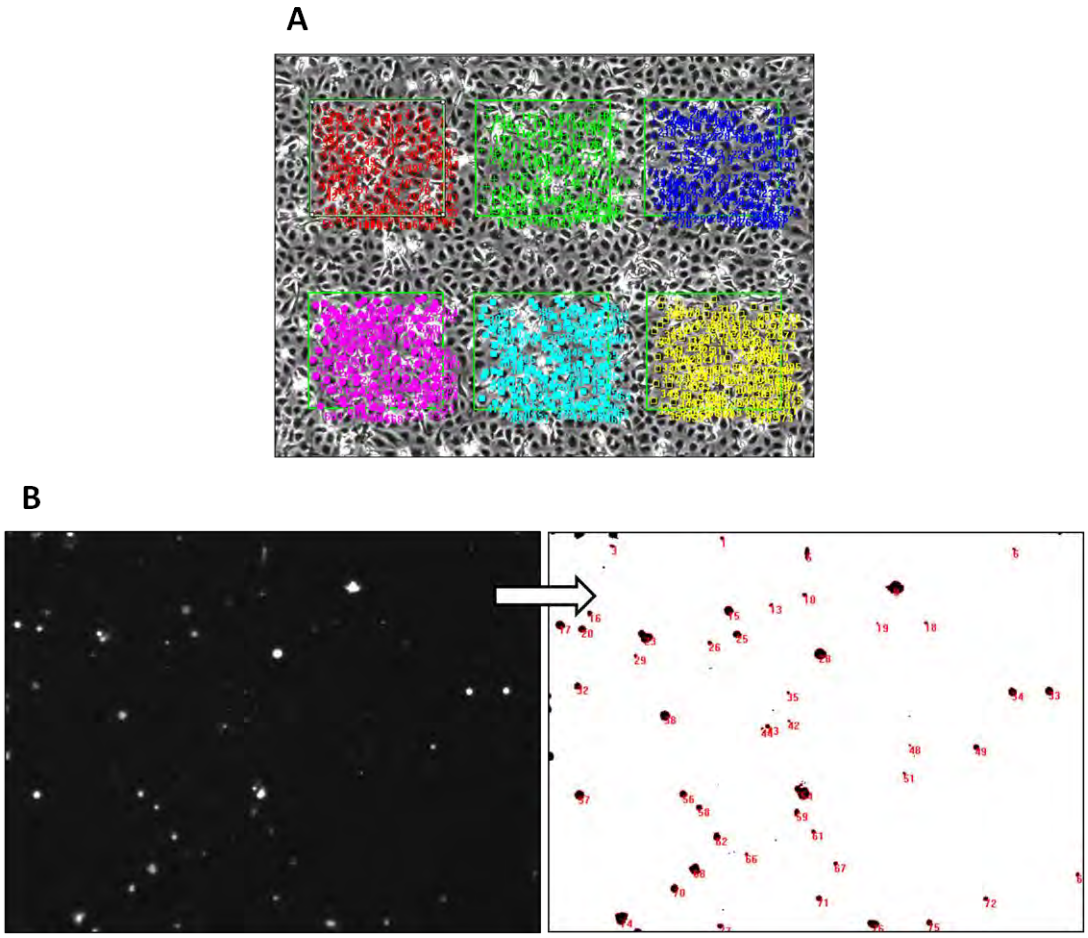

Figure 2.10: Strategy for analysis of viable and lytic cell densities.

(A) Phase contrast images of HUVEC monolayers in μ-slide VI channels were opened in Image-Pro and six areas of interest (0.07mm^2) superimposed onto the image. The number of cells within each region was counted and converted to number of cells per mm^2. **(B)** Images (0.98mm^2) of the RFP fluorescent cells generated in HUVEC monolayers due to lytic reactivation were opened in Image-Pro and thresholded. The number of RFP positive cells was counted applying a size restriction of greater than 15μm^2 to exclude objects considered too small to be cells. The number of cells counted was converted to number per mm^2.

2.11 ASSAY TO EXAMINE HORIZONTAL TRANSMISSION OF INFECTION THROUGH KSHV-INOCULATED HUVEC MONOLAYERS

To determine if KSHV was transmitted horizontally through HUVEC monolayers, rKSHV.219 inoculated cells were co-cultured with untreated cells that had been labelled with a fluorescent tracer. In this way KSHV transmission to untreated cells could be identified by their dual fluorescence for GFP and the dye tracer. The methods are described below.

Ten wells of a 24-well plate were seeded with HUVEC ($9x10^4$ cells/well) yielding a confluent monolayer overnight and three wells were inoculated with KSHV (MOI10) the next day. The remaining seven wells were left untreated. Either 2hours or three days post-inoculation, four wells of untreated HUVEC were labelled with the far-red fluorescent tracer, DDAO-SE (Invitrogen, Molecular Probes), which is a dye tracer suitable for long-term cell labelling.

Staining with DDAO-SE was done in the plate and involved: washing the monolayer twice with 1ml PBS to remove traces of serum in the culture medium, since serum proteins will quench the dye; incubating the cells in 200µl dye (5µM) solution (40mins, 37°C); removing the dye solution; washing the monolayer with 500µl culture medium; culturing in 1ml culture medium (20min); changing the medium and culturing for a further 2hours in a second 1ml volume of culture medium. Such prolonged and serial washes were to ensure full quenching of excess dye before mixing of cell populations.

HUVEC in the ten wells (three KSHV-inoculated, non-labelled; four untreated, DDAO-SE-labelled; three untreated, non-labelled) were then detached using trypsin and resuspended in 300µl culture medium per original well. 600µl of cell combinations (i-v below) were prepared

and 300µl from each aliquoted to a 48-well plate. The remainder was transferred to FACS tubes and fixed in 2% (w/v) formaldehyde for analysis by flow cytometry in parallel with the cultures after five-days of co-culture as a measurement of the starting/background percentages of each cell type (non-labelled, non-infected; non-labelled, KSHV-infected, DDAO-SE-labelled, non-infected, DDAO-SE-labelled, KSHV-infected) within each culture.

The culture plate was covered with silver foil due to the light-sensitivity of the dye and the cells cultured for five days. The culture medium was changed on day-two according to normal culturing procedures. Cells were detached from the culture plate on day-five and fixed in 2% (w/v) formaldehyde for analysis by flow cytometry using a Dako Cyan flow cytometer and analysed using Dako Summit 4.3 software.

The single population controls and co-culture of non-labelled untreated and DDAO-SE-labelled, untreated HUVEC were included to verify that the cells concluded as having been infected by transmission of KSHV-infection were unlikely to be products of dye transfer or generous positioning of the gates in the analysis. In the analysis of the flow cytometry data, the GFP positive gate was set such that for non-labelled, untreated HUVEC at the end of five days of co-culture with KSHV-inoculated HUVEC, 1% of cells were GFP positive. The DDAO-SE positive gate was set such that for DDAO-SE-labelled, untreated HUVEC at the end of five days of culture, 99% of cells were DDAO-SE positive.

Cell combinations assayed included: (i) non-labelled, untreated; (ii) DDAO-SE-labelled, untreated; (ii) non-labelled, KSHV-inoculated; (iv) non-labelled, untreated + DDAO-SE-labelled, untreated (1:1); (v) DDAO-SE labelled, untreated + non-labelled, KSHV-inoculated (1:1).

2.12 MICROSCOPES USED:

Unless otherwise stated, the microscope used for phase contrast and GFP, RFP and UV (bisbenzimide) fluorescence imaging was an Olympus 1X70 invert microcope fitted with a Lumen 200 bulb (PRIOR) and Qicam Qimaging fast 1394 camera. The imaging software was Image-Pro Version 6.2. Image-Pro Version 7 was also used for offline analysis.

2.13 STATISTICS

Graphs were created using GraphPad Prism 3.02 or Excel 2007. Error bars represent the standard error of the mean (SEM). Parametric statistical tests were performed using GraphPad Prism 3.02 following testing to confirm that the data were normally distributed using the Kolmogorov-Smirnov (KS) test. To test for differences between the means of two populations, two-tailed paired or unpaired t-tests were performed. Where data for KSHV-infected and non-infected populations had been normalised to that of the untreated control population, t-tests comparing to a value of one were used. Two way Analysis of Variance (ANOVA) was performed to test the effects of both time and virus inoculation on a variable. One way ANOVA was used to test the effect of virus treatment (untreated, non-infected and KSHV-infected) on a variable. This was followed by Bonferroni's multiple comparison post-hoc analysis to investigate which populations were significantly different. Pearson Product Moment Correlation Coefficients were calculated to test for correlation between two variables. Coefficients of variance, were calculated from the statistic: [Coefficient of variance = (standard deviation $\times 100$)/(mean $\times \sqrt{n}$)], where 'n' is the number of experiments.

2.14 SUPPLIERS OF THE REAGENTS, EQUIPMENT AND SOFTWARE USED IN THESE STUDIES

Table 2.4: Addresses for the suppliers of equipment, reagents and software used in these studies

Supplier	Address
AbD Serotec	Endeavour House, Langford Lane, Kidlington, OX5 1GE, UK
Advanced Biotechnologies	Advanced Biotechnologies Inc, 9108 Guilford Rd, Columbia MD 21046-2701, USA
Becton Dickinson (BD)	The Danby Building, Edmund Haley Road, Oxford Science Park, Oxford, OX4 4DQ, UK
Bioline	Bioline Reagents Ltd, Unit 16, The Edge Business Centre, Humber Road, London, NW2 6EW
New England BioLabs	New England BioLabs , 75-77 Knowl Piece, Wilbury Way, Hitchin, Herts, SG4 0TY
BioLegend	BioLegend UK Ltd, Munro House, Trafalgar Way, Bar Hill, Cambridge, CB23 8SQ, UK
Calbiochem	Merck Chemicals Ltd, Boulevard Industrial Park, Padge Road, Beeston, Nottingham, NG9 2JR, UK
Chemicon, Millipore	Millipore (U.K.) Limited, Suite 3 & 5, Building 6, Croxley Green Business Park, Watford, WD18 8YH
Citifluor Ltd	18 Enfield Cloisters, Fanshaw Street, London, N1 6LD, UK

Dako	Flow Cytometry Products and Specific Proteins, Alere Ltd (formerly Inverness Medical UK Ltd), Pepper Road Hazel Grove, Stockport, SK7 5BW
eBioscience	2nd Floor, Titan Court, 3 Bishop Square, Hatfield, AL10 9NA, UK
Fischer Scientific Ltd	Bishop Meadow Road, Loughborough, Leicestershire, LE11 5RG, UK
Flowjo	TreeStar Inc, 340 A Street Suite # 206, Ashland, OR 97520, USA
Image-Pro	Media Cybernetics Inc, 4340 East-West Hwy, Suite 400, Bethesda, MD, 20814-4411, USA
ImageJ	Public domain Java-based image processing program, developed at the National Institutes of Health
Immunotools	Altenoyther Strasse, 10, 26169 Friesoythe, Germany
Life Technologies Corporation †	5791 Van Allen Way, PO Box 6482, Carlsbad, 92008, California
MP Biomedicals	MP Biomedicals Europe, Parc d'Innovation, BP 50067, Rue Geiler de Kaysersberg, Illkirch Cedex 67402, France
PAA Laboratories	PAA Laboratories Ltd, Termare Close, Houndstone Business Park, Yeovil, Somerset, BA22 8YG, UK
Promega	Delta House, Southampton Science Park, Southampton, SO16 7NS, UK
PromoCell	PromoCell, GmbH, Sickingenstraße 63/65, D-69126 Heidelberg, Germany,

Qiagen	Qiagen House, Fleming Way, Crawley, West Sussex, RH10 9NQ
R&D Systems Europe Ltd	19 Barton Lane, Abingdon Science Park, Abingdon, OX14 3NB, UK
Santa Crtutz	Santa Cruz Biotechnology, Inc, 2145 Delaware Avenue, Santa Cruz, California 95060, U.S.A
	Santa Cruz Biotechnology, Inc, Bergheimer Str. 89-2, 69115 Heidelberg, Germany
Sarstedt	SelectScience Ltd, Church Farm Business Park, Corston, Bath, BA2 9AP, UK
Sigma-Aldrich (Sigma)	Fancy Road, Poole, Dorset, BH12 4QH,UK
Thermo Scientific	ABgene House, Blenheim Road, Epsom, Surrey, KT19 9AP, UK
Thistle Scientific	Thistle Scientific Ltd, DFDS House, Goldie Road, Uddingston, Glasgow, G71 6NZ, UK
Vector Laboratories Inc	3, Accent Park, Bakewell Road, Orton Southgate, Peterborough,PE2 6XS, United Kingdom

†includes: Applied Biosystems, Gibco, Invitrogen, Invitrogen Molecular Probes (MP)

CHAPTER THREE

DEVELOPMENT AND CHARACTERISATION OF AN *IN VITRO* SYSTEM TO STUDY THE FUNCTIONAL EFFECTS OF KSHV INFECTION OF PRIMARY ENDOTHELIAL CELLS

3.1 INTRODUCTION

In this chapter studies to optimise a protocol for the production of concentrated KSHV and generation of high efficiency (>50%) infection of primary endothelial cells are described. For the optimised inoculation conditions, the temporal changes in endothelial cell morphology, monolayer density and extents of latent infection and lytic reactivation are reported. Studies which determined the contribution of horizontal transmission of infection to the rise in percent infection with time post-inoculation are also described.

Endothelial cells were the cell type chosen for the studies in this thesis into KS pathogenesis. This was because spindle cells, which are the major proliferative component of KS lesions, are infected with KSHV and are endothelial in nature, suggesting that KS development involves infection of an endothelial cell. It was desirable to use primary endothelial cells, as opposed to endothelial cell lines, for their closer physiologic relevance but previous studies that infected primary endothelial cells reported low (<10%) infection efficiencies (Ciufo et al., 2001; Flore et al., 1998; Guo et al., 2003; Sharma-Walia et al., 2005) which would be inadequate for the assessment of KSHV effects on endothelial cell functions. Other groups have used instead endothelial cell lines, which are easier to obtain, maintain and infect (Lagunoff et al., 2002; Moses et al., 1999).

The aims of the initial studies in this thesis were therefore to establish a method for the production of infectious virus and inoculation of primary endothelial cells that would achieve over 50% infection. Human umbilical vein endothelial cells (HUVEC), which are macrovascular

primary cells, were the endothelial cell type chosen for these studies, since umbilical cords were available with consent from the nearby Birmingham Women's Hospital.

3.2 RESULTS

3.2.1 Infection of HUVEC with BCBL-1 derived KSHV

Infection of HUVEC with KSHV prepared from the supernatants of reactivated BCBL-1 cells by centrifugation **(Figure 3.1A)** or ultracentrifugation on a sucrose cushion **(Figure 3.1B)** was originally tested. Infection efficiencies using these virus preparations were quantified by immunofluorescence staining for the KSHV protein, LANA-1. Even at the lowest dilution tested (1:2), the virus preparations gave only ~20% infection **(Figure 3.1)** which was inadequate for functional studies. Alternative methods for KSHV production and HUVEC infection were therefore sought.

3.2.2 Production of rKSHV.219 for use in infection studies

The recombinant KSHV strain, rKSHV.219 (Vieira and O'Hearn, 2004) encodes GFP under the control of the human elongation factor 1-α promoter and RFP under the control of the lytic PAN RNA promoter. Using this virus, latently infected cells become GFP positive and lytic infection is indicated by RFP expression; thus, KSHV-infected and non-infected cells can be distinguished in KSHV-inoculated cultures without relying on antibody staining of KSHV proteins, which expedites analysis. Collaborators at the Medizinische Hochschule, Hannover, had developed a method for the production of high titre rKSHV.219. We adopted and optimised this protocol for our purposes.

Concentrated rKSHV.219, hereafter referred to as KSHV, was titrated on HEK293 cells. Dilutions of the stock virus tested ranged between 1 in 100 and 1 in 80,000. It was assumed that one infectious unit generated one infected, GFP positive cell by 48hours. Monitoring the virus titre over time revealed a decrease in infectivity with prolonged storage at 4°C **(Figure 3.2)**. Titres were therefore re-determined if the virus was not used within three weeks of production.

Next I determined whether storing aliquots of concentrated virus at -80°C would maintain their titre. The aim was to produce high titre batches of KSHV. This approach would reduce the frequency of KSHV production needed and ensure consistent infection efficiency across experiments. One week after production, storage temperature did not affect the infection efficiency but by three-to-four weeks post production, storage at -80°C reduced infection efficiency compared to storage at 4°C **(Figure 3.3)**. Virus used in the experiments in this thesis was therefore always stored at 4°C.

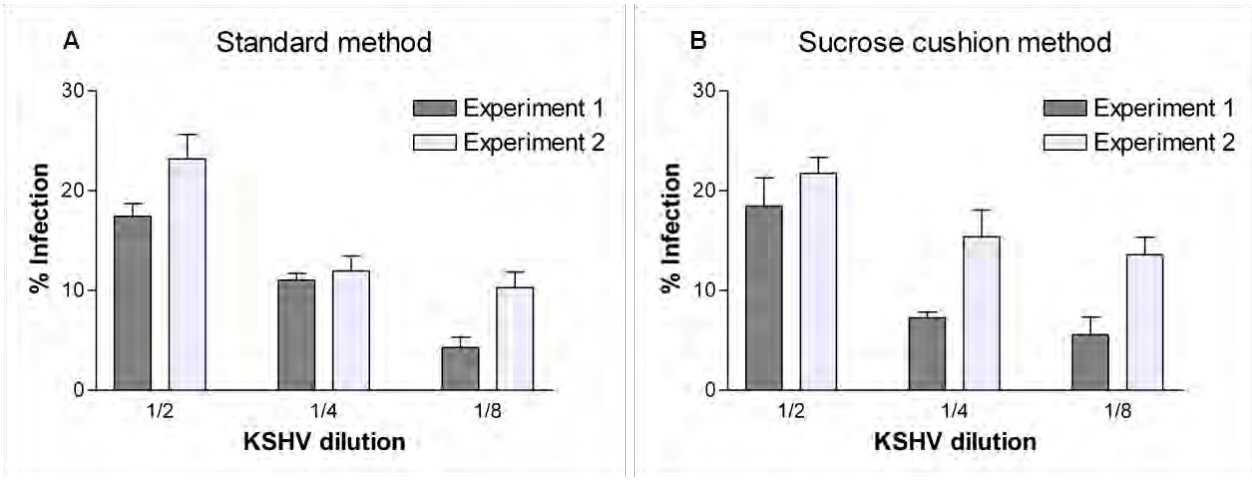

Figure 3.1: Comparison of BCBL-1 derived KSHV preparations for infection of HUVEC. KSHV from the supernatants of reactivated BCBL-1 cells was concentrated by **(A)** standard centrifugation or **(B)** ultracentrifugation on a sucrose cushion. The virus was diluted 2, 4 or 8-fold in EBM-2 medium and inoculated onto HUVEC monolayers. Four days post-inoculation the percent of infection was quantified by immunofluorescence assay, staining for the KSHV protein LANA-1. Data plotted are the mean ± SEM across several fields of view for each of two experiments.

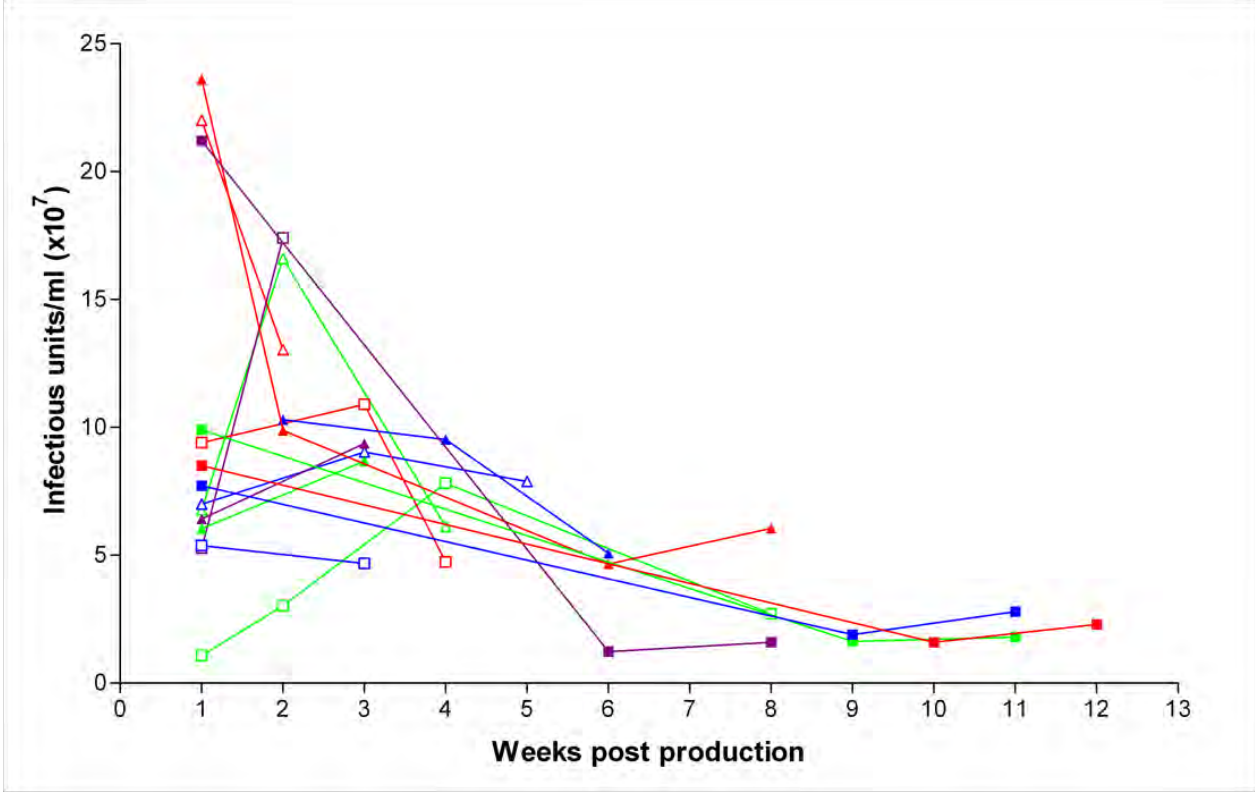

Figure 3.2: Effect of storage time upon KSHV titre.

The titres of KSHV preparations stored at 4°C were analysed at timepoints up to twelve weeks post production by titration on HEK293 cells. Each line represents a different virus preparation.

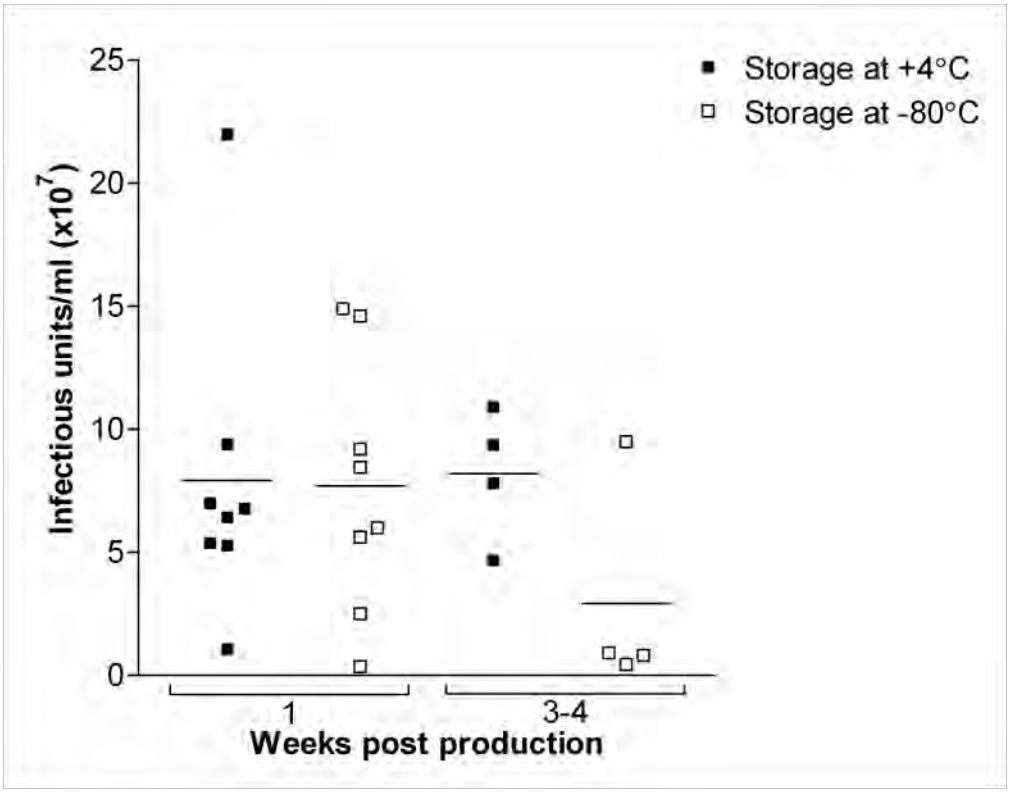

Figure 3.3: Effect of storage temperature upon KSHV titre.

KSHV preparations were aliquoted immediately following production and stored at 4°C and -80°C. Titres of these preparations were then assessed in parallel on HEK293 cells after one or three-to-four weeks storage. Week one represents the earliest titre established. Each point represents the test results for a separate preparation. The four preparations included in the 'three-to-four weeks storage category are paired with observations in the 'one-week storage' set.

3.2.3 Infection of HUVEC with rKSHV.219

KSHV was titrated on HUVEC with readout of percent infection on either day-three or day-ten post-inoculation. A multiplicity of infection of 5 (MOI5) gave saturating infection **(Figure 3.4)**. However, since the titration assay was subject to error; KSHV titres decreased with time **(Figure 3.2)**; and empirical observations had indicated variation in donor permissiveness to infection, HUVEC were inoculated with MOI10 for the assays performed in this thesis.

To optimize the infection protocol, the effects of cell density were investigated. HUVEC monolayers, ranging in density from sparse to fully confluent, were inoculated with KSHV at MOI10. One-way ANOVA suggested however, that the efficiency of KSHV infection was not significantly altered by monolayer density **(Figure 3.5)** (ANOVA $P>0.05$).

To characterise the temporal development of KSHV infection within the HUVEC monolayer, KSHV-inoculated HUVEC were observed up to day-ten post-inoculation by phase contrast and fluorescence microscopy. The prevalence of GFP expression was quantified by flow cytometry. A profound change in the morphology of infected cells from cobblestone to an elongated spindle shape was observed by day-three post-inoculation and became more exaggerated with time. Untreated control cells maintained a cobblestone shape throughout **(Figure 3.6)**. The extent of infection as determined by percentage of GFP positive cells increased with time to 80% by day-ten post-inoculation **(Figures 3.6 and 3.7A)**. Following an early lytic burst, peaking at day-two as determined by RFP expression, the extent of reactivation subsided **(Figures 3.6, 3.7B and 3.11B)**.

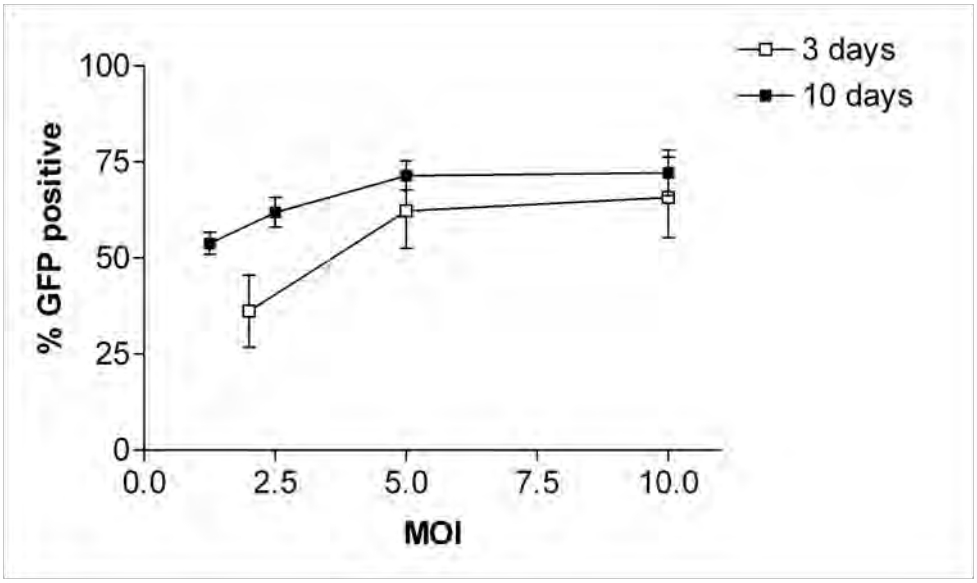

Figure 3.4: Effect of KSHV titre on infection of HUVEC.

HUVEC were inoculated with KSHV at multiplicities of infection (MOI) between 1.25 and 10 and the percent infection on eiter day-three or day-ten post-inoculation assessed by flow cytometry for GFP. Data are mean ± SEM for three experiments, except MOI10 with readout at day-ten, which was two experiments.

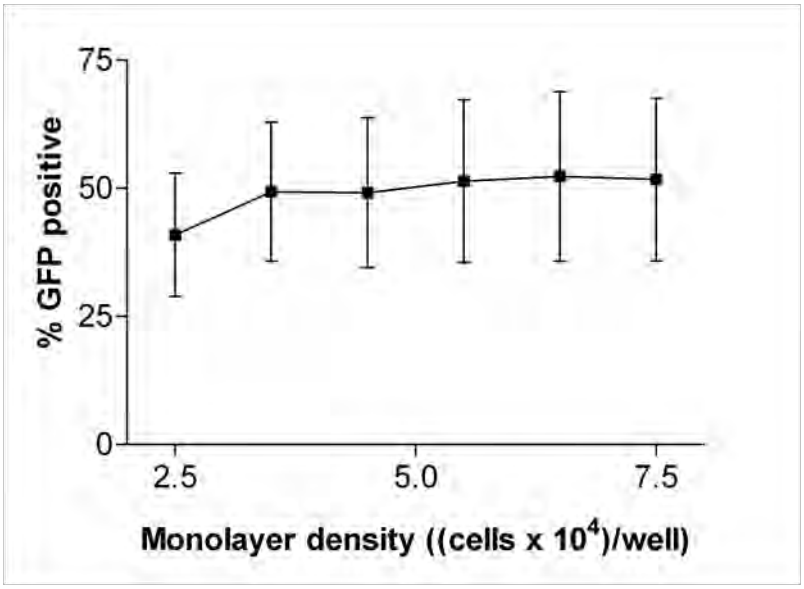

Figure 3.5: Effect of HUVEC density upon KSHV infection efficiency.

HUVEC were plated at densities between 2.5 and 7.5×10^4 cells/48-well and infected with KSHV at MOI10. Each well had a surface area of $75mm^2$. The percentages of infected cells at day-seven post-inoculation were assessed by flow cytometry for GFP. ANOVA did not show a significant effect of density ($P>0.05$). Data are mean ± SEM for three experiments.

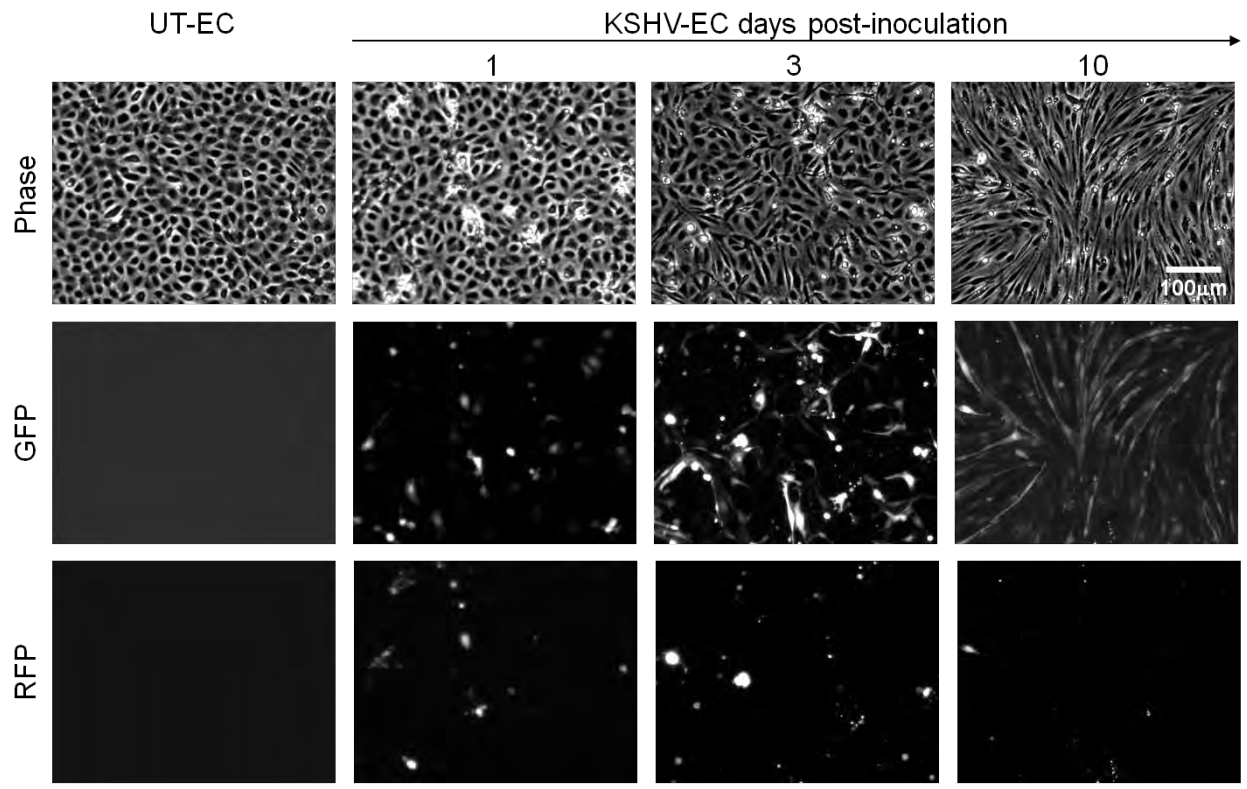

Figure 3.6: Effect of time post KSHV inoculation on cell morphology, GFP expression and RFP expression.

KSHV-infected and untreated HUVEC were cultured in μ-slides and imaged at regular intervals up to day-ten post-inoculation using a 4x objective lens. Phase contrast, GFP and RFP fluorescence images were taken for each field to show the overall monolayer, the distribution and morphology of KSHV-infected cells and the extent of ongoing lytic reactivation respectively. Changing of the culture medium during the course of culture removed most dead, lytic cells, thus RFP positive cells primarily represent those evolved since the last washing rather than the cumulative numbers generated by the infection. The panel shown is a time course for one experiment but is representative of each infection.

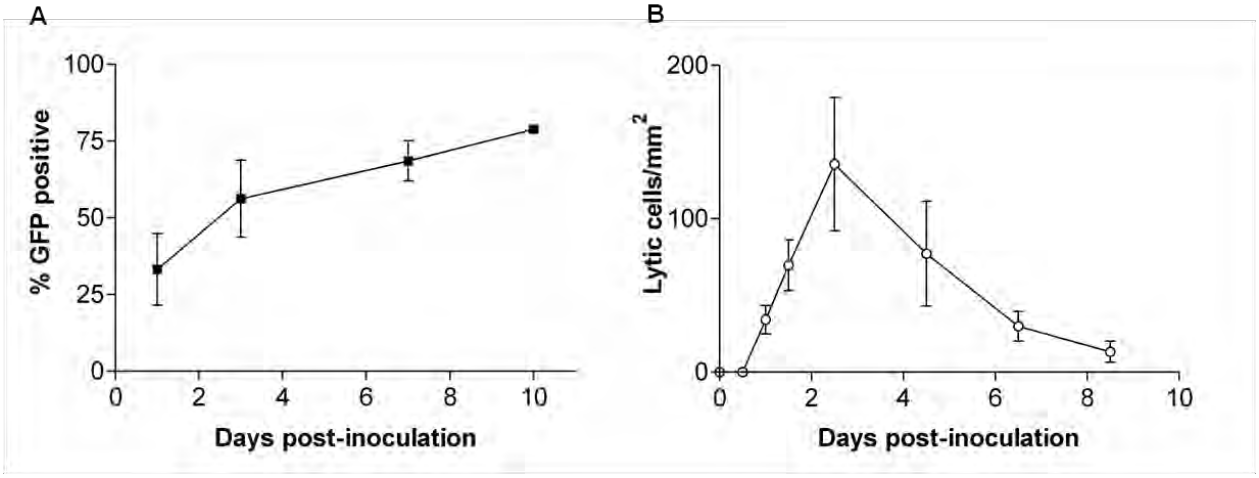

Figure 3.7: Effect of time post-inoculation on the extent of KSHV infection within HUVEC monolayers.

(A) HUVEC were infected with KSHV at MOI10 and the percentage of infected, GFP positive cells assessed by flow cytometry at timepoints up to day-ten post-inoculation. Data are mean ± SEM for four experiments. **(B)** HUVEC seeded in μ-slides were infected with KSHV at MOI10 and RFP fluorescence images of the monolayers observed using a 4x objective lens, taken at timepoints up to 8.5 days post-inoclation. The numbers of RFP positive cells were counted before and after thorough washing of the monolayer at each timepoint and the numbers of cells evolved since the previous timepoint calculated. Data are mean ± SEM for three experiments.

To determine whether the temporal increase in KSHV-infected (GFP positive) HUVEC was due to productive infection (as suggested by RFP expression peaking at day-2.5) leading to horizontal transmission of infection, untreated HUVEC labelled with DDAO-SE were mixed with non-labelled, KSHV-inoculated HUVEC from the same donor either immediately following inoculation (day-zero) or on day-three post-inoculation and co-cultured for five days. DDAO-SE positive, KSHV-infected (GFP positive) cells were quantified by flow cytometry **(Figure 3.8)**.

Consistent with an early lytic burst, the percentage transmission of infection to untreated cells decreased when co-cultures were established on day-three post-inoculation compared to day-zero **(Figure 3.9A)**. 35% of non-infected cells within KSHV-inoculated cultures acquired infection between days three and eight post-inoculation in contrast to horizontal transmission to only 3.3% of untreated cells **(Figure 3.9B)**. These data suggest that the extent of infection by day-ten was achieved by initial inoculation, and intracellular amplification of infection over time was required for quantification by GFP readout. In agreement, in our laboratory we have detected LANA-1 expression (one or more LANA-1 dots) in 38% of GFP negative cells at 24hours post-inoculation **(Figure 3.10)** (Blackbourn and Butler, unpublished data).

An alternative explanation is that KSHV-infected cells out-proliferate non-infected cells within KSHV-inoculated cultures. To investigate the effect of KSHV inoculation upon HUVEC numbers, uniform monolayers were seeded in μ-slide channels, inoculated with KSHV and the cell density counted at regular intervals up to day-ten post-inoculation **(Figure 3.11A)**. KSHV inoculation caused a progressive decrease in density after 12hours post-inoculation. The reduction was significant ($P<0.01$) compared to the starting density by 4.5 days. In contrast, untreated monolayers showed no significant decrease in density for the duration of the assay.

The window of peak lytic reactivation was between 1 and 2.5 days; thereafter lytic reactivation subsided **(Figures 3.7B and 3.11B)**. 15% of the culture died due to lytic death in the first 2.5 days. Lytic death explained the decrease in monolayer density up to 2.5 days but by 4.5 days did not completely account for the cell loss observed **(Figure 3.11B)**.

Figure 3.8: Quantification of the extent of horizontal transmission of KSHV infection through HUVEC monolayers.

DDAO-SE-labelled untreated (UT-EC) HUVEC and KSHV-inoculated (KSHV-EC) HUVEC were mixed and co-cultured for five days before analysing the percentage of DDAO-SE positive cells that were also GFP positive by flow cytometry. GFP Log v DDAO-SE Log plots are shown for a representative assay fixed at the start and end of the five-day co-culture period begun on day-three post-inoculation. In the assay, single population controls including: non-labelled UT-EC; DDAO-SE-labelled UT-EC; and non-labelled KSHV-EC single population cultures, as well as a co-culture control of non-labelled UT-EC and DDAO-SE-labelled UT-EC, were established in parallel to verify that double positive cells were not due to dye transfer or to the positioning of the quadrants for analysis. The GFP positive gate was set such that for UT-EC at the end of five days culture, 1% of cells were GFP positive. The DDAO-SE positive gate was set such that for DDAO-SE-labelled UT-EC at the end of five days of culture, 99% of cells were DDAO-SE positive. Quantification of the data is presented in Figure 3.9A.

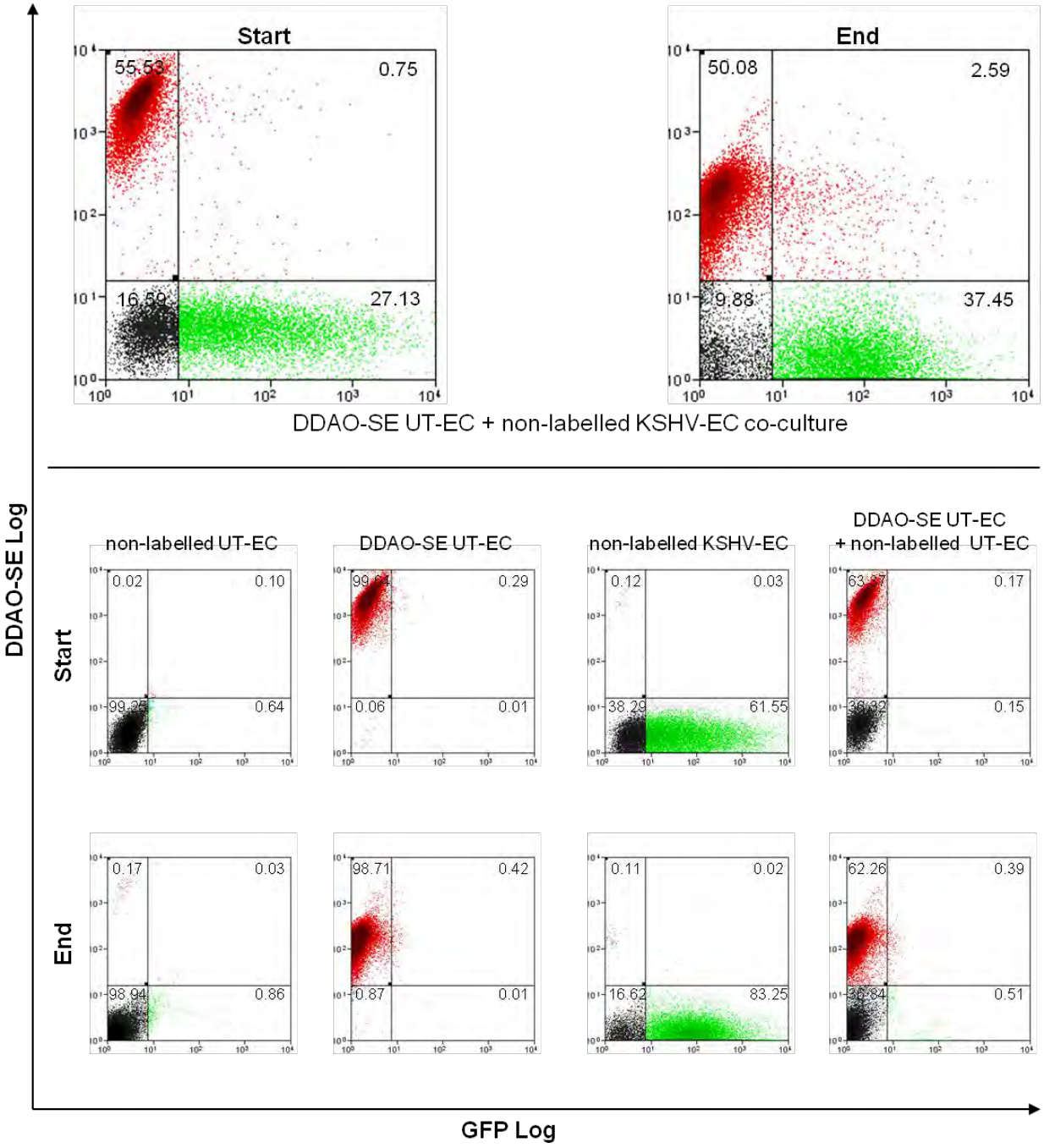
Start
End
55.53
0.75
16.59
27.13
50.08
2.59
9.88
37.45
DDAO-SE UT-EC + non-labelled KSHV-EC co-culture
DDAO-SE Log
GFP Log
Start
End
non-labelled UT-EC
DDAO-SE UT-EC
non-labelled KSHV-EC
DDAO-SE UT-EC
+ non-labelled UT-EC
0.02
0.10
99.25
0.64
0.06
0.01
38.29
61.55
0.17
0.03
98.94
0.86
98.71
0.42
0.87
0.01
0.11
0.02
16.62
83.25
62.26
0.39
0.51

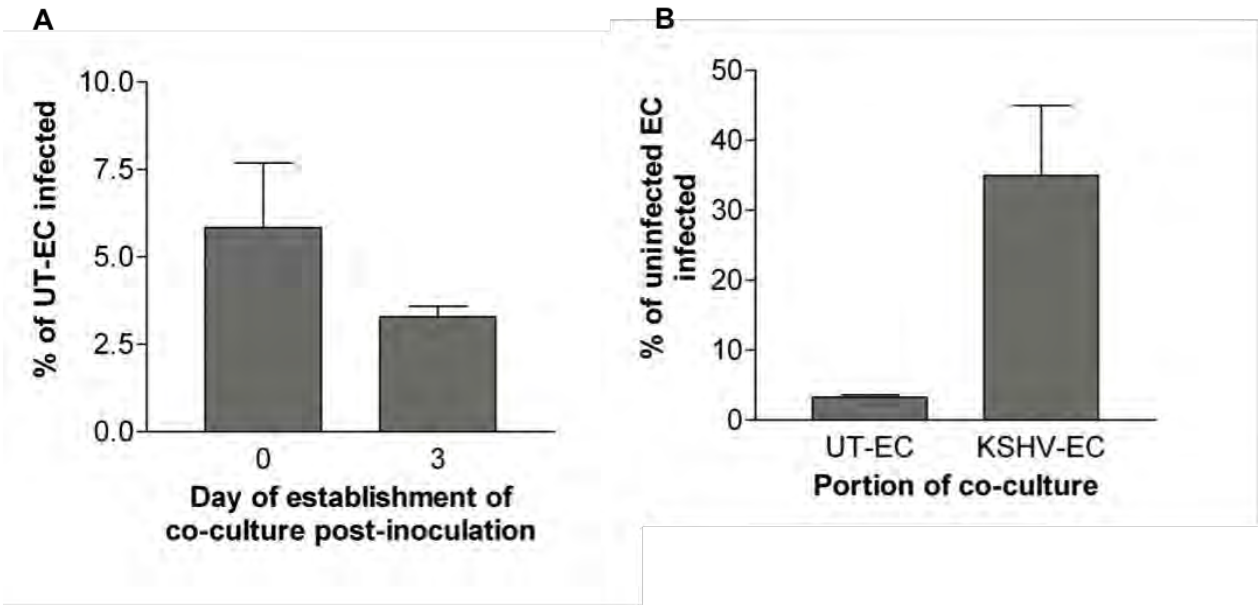

Figure 3.9: Quantification of the extent of horizontal transmission of KSHV infection through HUVEC monolayers.

(A) Co-cultures of DDAO-SE-labelled untreated (UT-EC) HUVEC and KSHV-inoculated (KSHV-EC) HUVEC were established immediately after inoculation (day-zero) and on day-three post-inoculation and cultured for five days before analysing the percentage of DDAO-SE positive cells that were also GFP positive by flow cytometry. Data are mean ± SEM for two (day-three) or three (day-zero) experiments. **(B)** The percentage transmission of infection to uninfected cells during the five days of co-culture, for cultures established on day-three post-inoculation, was calculated for sub-populations that were originally untreated (DDAO-SE positive) or KSHV-inoculated (DDAO-SE negative). Data are mean ± SEM for two experiments.

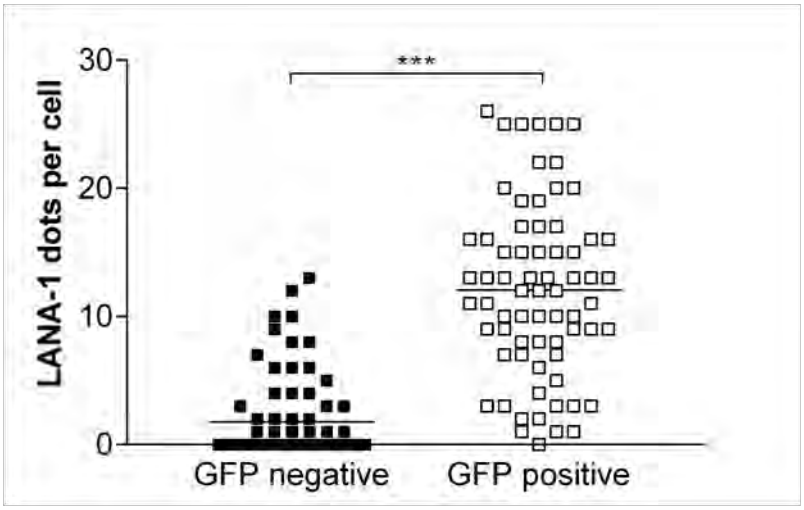

Figure 3.10: Quantification of the number of KSHV LANA-1 dots in the nuclei of GFP positive and GFP negative HUVEC from KSHV-inoculated cultures at 24hours post-inoculation.

KSHV-inoculated monolayers were fixed at 24hours post-inoculation, permeabilised with 100% methanol and stained for LANA-1. Nuclei were counterstained with bisbenzimide. Fields of the monolayer were imaged on an inverted laser scanning confocal microscope using a 63x water immersion objective lens and the number of LANA-1 dots found in each nucleus counted. The GFP status of each cell was also recored as GFP positive or negative. Individual points represent separate cells across two experiments. Horizontal lines indicate the mean number of LANA-1 dots per cell. *** = $P<0.0001$by unpaired t-test.

Figure 3.11: Effect of KSHV inoculation upon HUVEC monolayer densities.

HUVEC seeded in μ-slides were infected with KSHV at MOI10 and imaged using a 4x objective lens at timepoints up to day-ten post-inoculation. **(A)** Viable cell densities were estimated from counts of cell nuclei observed under phase contrast. ANOVA revealed a significant effect of time post-inoculation upon density of both untreated (UT-EC) ($P<0.05$) and KSHV-inoculated (KSHV-EC) ($P<0.0001$) HUVEC monolayers. Stars indicate significant differences in density compared to the starting density (day-zero) as determined by the Bonferroni's multiple comparison post-hoc test. ** = $P<0.01$; *** = $P<0.001$. **(B)** The numbers of RFP positive cells were counted before and after thorough washing of the monolayer at each timepoint and the number of lytic cells evolved since the previous timepoint calculated and plotted cumulatively. The overall effect of lytic death upon cell numbers was calculated at each of the timepoints up to 8.5 days post-inoculation by summation of the number of viable cells present and the cumulative number of and lytic cells generated. Data are mean ± SEM for three experiments.

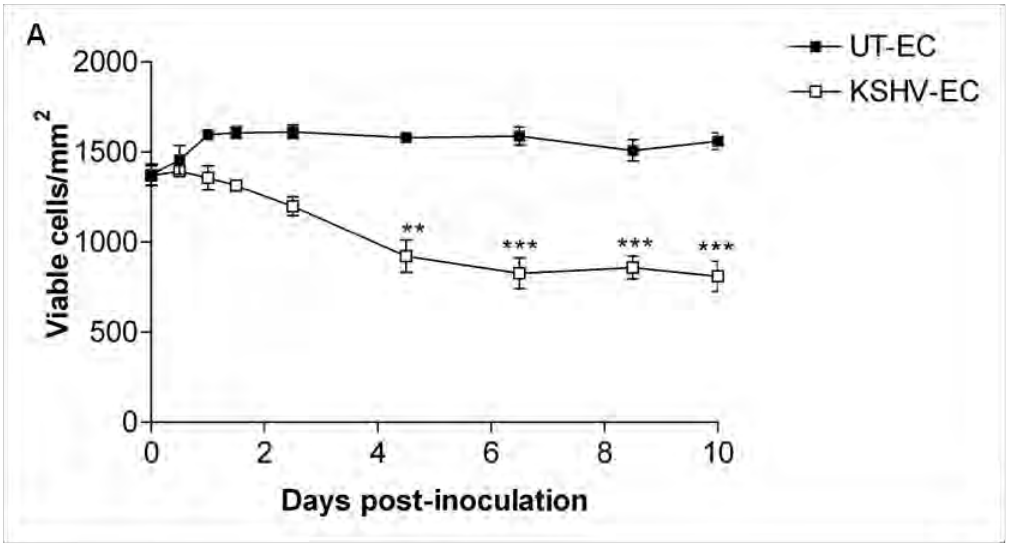
A
UT-EC
KSHV-EC
Viable cells/mm2
2000
1500
1000
500
0
0
2
4
6
8
10
Days post-inoculation
**
***
***
***

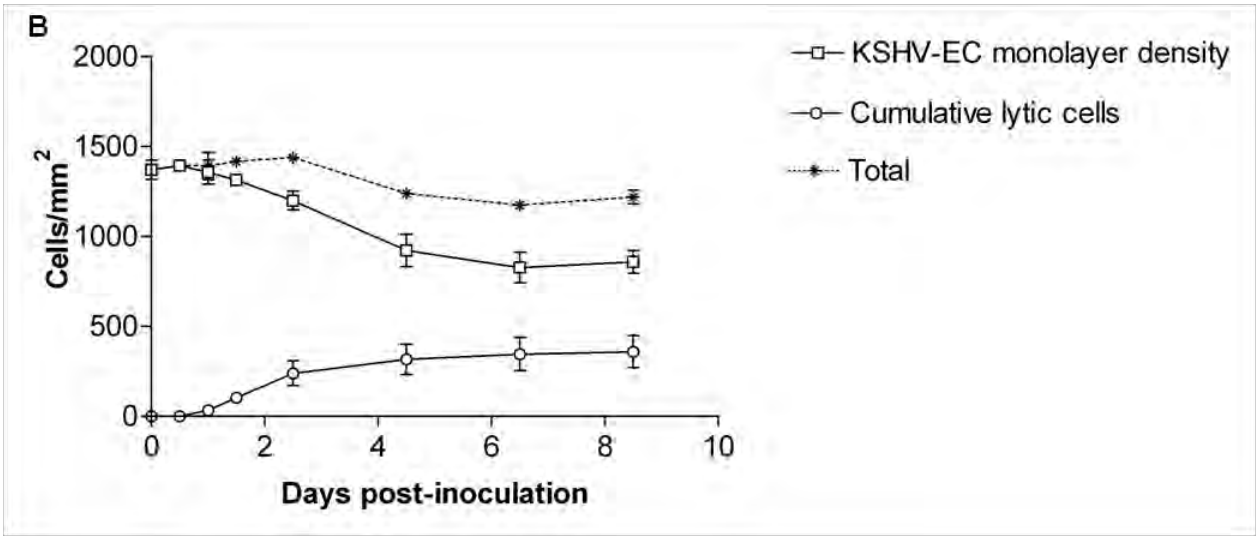
B
KSHV-EC monolayer density
Cumulative lytic cells
Total
Cells/mm2
2000
1500
1000
500
0
0
2
4
6
8
10
Days post-inoculation

3.3 DISCUSSION

This chapter described the development of a method to infect primary endothelial cells (HUVEC) with KSHV in order to create an *in vitro* system with which to study the effects of KSHV infection on endothelial cell functions.

Initial attempts to infect HUVEC with virus sourced from reactivated PEL (BCBL-1) cells yielded inadequate infection frequencies for examining the influence of virus infection on endothelial cell behaviour. Infection of up to only 20% was possible **(Figure 3.1)**. Inoculating with the recombinant KSHV strain, rKSHV.219, achieved instead a highly successful primary infection that: (1) induced a transition in cell morphology from cobblestone to spindle shape, reminiscent of the tumour cells in KS lesions **(Figure 3.6)**; (2) was predominantly latent **(Figure 3.7)** and (3) increased with time: ~80% of cells were infected by day-ten post infection **(Figure 3.7)**. Such high infection of HUVEC required a virus to cell ratio (MOI) that was five-to-ten-fold greater than that needed to infect HEK293 cells **(Figure 3.4)**. Others have similarly reported HEK293 cells to be more permissive to KSHV infection than other cell types (Foreman et al., 1997; Renne et al., 1998). In my hands, the efficiency of rKSHV.219 infection was not influenced significantly by the density of the HUVEC monolayer **(Figure 3.5)** and infection was not transforming **(Figure 3.11)**. This finding is in contrast to that of others who inoculate cultures at 60-80% confluence (Ciufo et al., 2001; Gao et al., 2003; Moses et al., 1999). For its use in this research I also determined that rKSHV.219 infectivity is best conserved by storage at 4°C compared to -80°C **(Figure 3.3)**.

The result that KSHV concentrated from PMA-induced PEL cultures gave low percent infection of HUVEC agreed with most previous studies which reported low (<10%) infection levels following inoculation of several cell types (Blackbourn et al., 2000; Gao et al., 2003; Renne et al., 1998), including primary endothelial cells (Ciufo et al., 2001; Flore et al., 1998), with PEL-derived KSHV. To my knowledge, prior to this study, the only *in vitro* models that had accomplished greater than 50% infection of endothelial cells, using KSHV harvested from reactivated PEL cultures, had involved the inoculation of microvascular endothelial cell lines. The endothelial cells were immortalised by telomerase (Lagunoff et al., 2002) or the E6 and E7 genes of Human Papilomavirus (Moses et al., 1999).

50% infection or greater was desired for experiments in this thesis but the use of similar immortalised endothelial cell systems was unfavourable because whilst immortalisation does render cells more permissive to KSHV latent infection, it also confounds observation of virus-imposed changes to cell behaviour (Lagunoff et al., 2002). For example, Lagunoff et al (2002) identified that in the generation of telomerase-immortalised microvascular endothelial (TIME) cells, the immortalisation by transduction with the hTERT retrovirus induced spindle morphology in the absence of KSHV infection and further elongation with KSHV infection was not evident. Using rKSHV.219, however, I achieved infection of HUVEC that was similar in efficiency to that seen with these immortalised cell systems. In fact the timecourse of rKSHV.219 infection of HUVEC, based on GFP percentage positivity (56% ± 12.6 at day-three rising to 80% ± 0.96 at day-ten **(Figure 3.7A))** closely mirrored the infection profile of transformed endothelial cells reported by Moses et al (1999).

To my knowledge, at the time of these studies, only one model had been reported that gave higher percent infection of primary HUVEC than our system. That model used the recombinant KSHV reactivated from BAC36 propagated in HEK293 cells (Zhou et al., 2002) and attained ~90% infection by day-two post-inoculation (Gao et al., 2003). However, in our hands BAC36 titres are too low to provide a tractable model (Chanas and Blackbourn, unpublished data). Thus we question the reproducibility of 90% de-novo infection as observed by Gao et al (2003) and the BAC36-derived virus was not considered for use in these studies. Interestingly, recently duplication of a 9kb fragment of the long unique region within the terminal repeat region of the BAC36-KSHV genome was identified that is thought to have originated during BAC cloning since it is not detectable in BCBL-1 cells (Yakushko et al., 2011). It is possible that this disruption of the terminal repeat impairs productive lytic replication and generation of infectious virus. However, by genetic engineering of the BAC36 genome to drive constitutive expression of RTA a virus that caused cytopathic effect when inoculated onto various cell lines was generated (Budt et al., 2011). This counters the hypothesis that BAC36-KSHV cannot encode the synthesis of proteins required to form infectious virions. Nonetheless, while BAC36 might serve as a tool in mutagenesis studies to examine the functions of KSHV genes in the context of the KSHV genome, the genetic duplication is a concern for studies aiming to properly model the effects of natural KSHV-infection since it alters the balance of gene expression compared to wildtype virus.

With the aid of RFP as a surrogate marker for rKSHV.219 lytic reactivation, I determined that KSHV infection of HUVEC featured an early lytic burst which subsequently declined **(Figures 3.6, 3.7B and 3.11B)**: during the two days between days 0.5 and 2.5, 15% of the culture died due to virus undergoing lytic reactivation whereas between days 6.5 and 8.5 only 1.5% of the culture

died due to reactivation of the virus **(Figure 3.11B).** Thus, in agreement with previous studies observing KSHV infection of endothelial cells (Ciufo et al., 2001; Flore et al., 1998; Gao et al., 2003; Lagunoff et al., 2002; Moses et al., 1999), chronic infection in this system was predominantly latent. Accordingly, this system provides a valid model for KSHV-infected spindle cells in *in vivo* disease, where, following primary infection, KSHV establishes latent infection in the host and productive lytic infection is found occurring spontaneously in a small proportion (2-5%) of cells (Moses et al., 1999; Orenstein et al., 1997; Staskus et al., 1997; Zhong et al., 1996).

The rise in percentage infection that we and others (Moses et al., 1999) observed over the first seven-to-ten days post-inoculation was previously hypothesised to be a consequence of either horizontal transmission of infection or the proliferation of infected cells (Moses et al., 1999). However, the data in this chapter, for the co-culture of untreated and KSHV-inoculated HUVEC, strongly suggest that horizontal transmission contributed little to the temporal rise in percentage infection during this period. This finding was especially clear when comparing the percentage transmissions of infection to non-infected and untreated cells, originating from KSHV-inoculated (DDAO-SE negative) and untreated (DDAO-SE positive) cultures respectively during the five-day period of co-culture between days three and eight post-inoculation. In contrast to 35% of non-infected cells that acquired infection after five days, transmission of infection to only 3.3% of untreated cells occurred **(Figure 3.9B)**. The observation that cell numbers within KSHV-inoculated monolayers decreased, largely due to lytic death, during the first week following inoculation, suggested that the increase in percent infection was also not attributable to a faster proliferation rate of infected compared to non-infected cells **(Figure 3.11)**.

The data summing the number of viable cells in the monolayer with the cumulative number of cells lost by lytic death suggested a 15% deficit in the number of cells accounted for at day 8.5 post-inoculation compared to day 2.5: whether the additional cells that died were predominantly KSHV-infected or non-infected could not be determined **(Figure 3.11B)**. If, in the establishment of this deficit, KSHV infection induced the death of bystander, non-infected cells whilst aiding the survival of KSHV-infected cells, percentage infection would have increased. Such an impact of KSHV infection could provide an alternative or contributory explanation for the increase in percentage infection that occurred with time. By microscopic inspection, KSHV-infected cultures often appeared to have greater resilience than untreated cells. Nonetheless, it has been demonstrated that KSHV-infection enhances, through paracrine signalling, the survival of both infected and non-infected cells in inoculated cultures (Flore et al., 1998), dissuading the hypothesis of KSHV-induced death of non-infected cells. Moreover, the idea that KSHV should enhance the survival of infected cells, whilst promoting the death of non-infected cells, is counterintuitive as a viral survival strategy since it would reduce the number of cells available as potential hosts.

In this regard, *in vivo* establishment of latency is considered inefficient and requires a low level lytic replication to render infection of uninfected cells that can replace those infected cells which lose the viral episome upon cell division (Grundhoff and Ganem, 2004). Altogether, the hypothesis that suggests a disproportionate increase occurred in the death of non-infected compared to infected cells and contributed significantly to the rise in infection with time, is not favoured. From evaluating the limitations of this assay, it is felt that errors in counting cell numbers might explain much of the deficit reported. For example, as cells became more elongate

their cell bodies became more difficult to identify and this feature most probably resulted in underestimation of the viable cell number. At the same time, the demise of lysed cells might have caused under reporting of the number of cells lost by lytic death. The latter would have become of greater influence when the times between observations were increased beyond the 2.5-day timepoint.

The number of infectious units that infect each cell is modelled by the Poisson distribution **(Figure 3.12)** (Condit, 2007).

$$P(k) = e^{-m}m^{-k}/k!$$

where: $P(k)$ is the fraction of cells infected by k infectious units and m is the MOI.

This means that although cells are inoculated with virus at a specific ratio of infectious units to cells, the number of infectious units that enters each cell is not equal. Accordingly, I propose that the increase in percentage infection, toward 80% by day-ten, occurred primarily as a consequence of variation in the number of copies of virus entering each cell at inoculation.. In cells where the initial virus load received was lower, more time was required for the amplification of the viral episomes within the cell to be adequate for the cell to be identified as infected by GFP positivity.

In our system KSHV was titrated on HEK293 as opposed to HUVEC. According to the Poisson distribution for the proportion of cells infected by k infectious units, our observation of 80% HUVEC infection at day-ten ($P(0) = 0.2$) suggests that the actual MOI used for inoculation of HUVEC did not exceed 1.6. We observed 33.2% ± 11.6% infection at 24h and 56.2% ± 12.5% at day-three. According to the Poisson distribution for MOI1.6 **(Figure 3.13)** 48% of the population

would be expected to be infected with two or more infectious units and 22% with three or more. Therefore these data suggest that intracellular amplification of the viral episome, to give a minimum of between two and three infectious units per cell, was required for visualisation of the cell as infected by GFP positivity.

According to the proposed requirement for episome amplification to render an infected phenotype, it is possible that upon infection, detectable GFP expression and full spindle transformation are delayed markers of infection. Our observation that a subset of the GFP negative population of KSHV-inoculated HUVEC cultures stains positively for the KSHV protein LANA-1 at 24hours is consistent with this hypothesis **(Figure 3.10)**. This hypothesis might also help to explain the 25-day delay between inoculation and observation of KSHV-infected cell colonies in the studies by Ciufo et al (2001).

In-cell accumulation of infection appeared to predominate in this system as the mechanism by which rKSHV.219 established an increasingly prominent infection with time in the first ten days post-inoculation. However, the fact that percentage transmission was greater for co-cultures prepared in advance of the lytic burst **(Figure 3.9A)** agrees with the premise that horizontal transmission, involving the release of new virions and re-infection within the monolayer, contributed to some extent to the temporal increase in infection. The co-culture period was limited to five days in this study, due to the decrease in DDAO-SE fluorescence that occurs with time, but if a longer period before analysis were possible, based on the principle that in-cell accumulation of infection is necessary for observation of infection by GFP read-out, a higher percentage of transmission might have been evident.

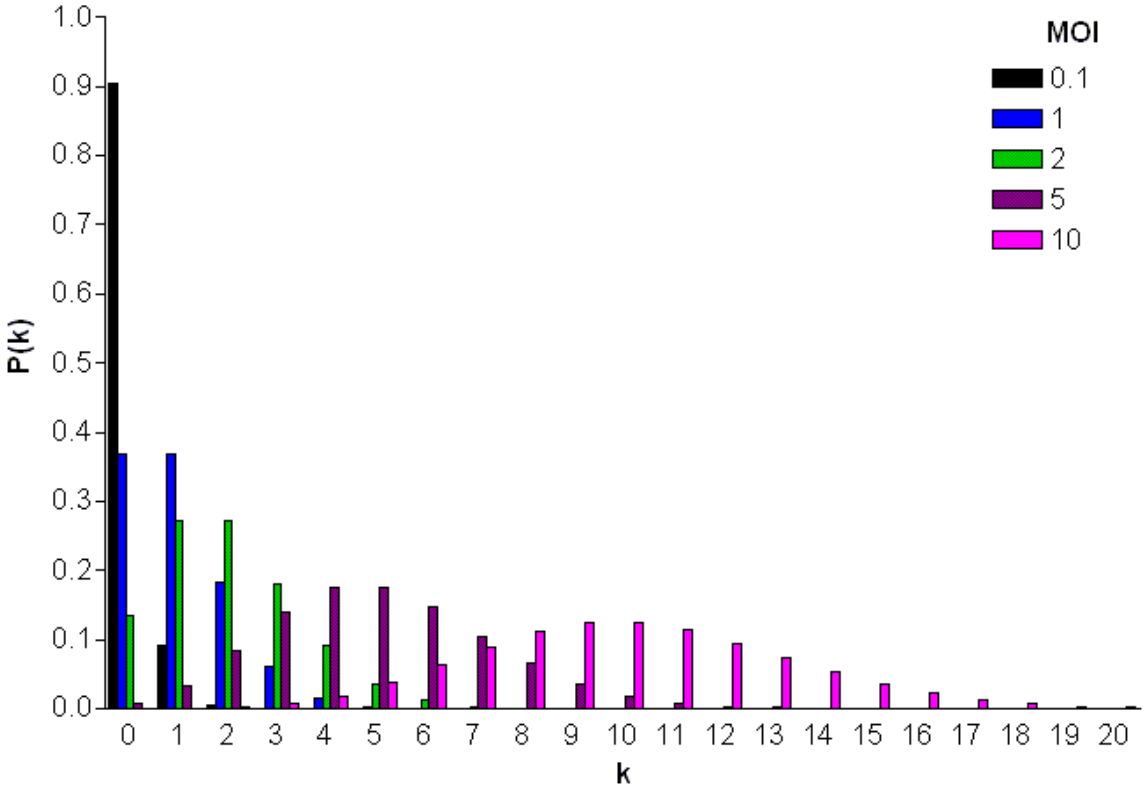

Figure 3.12: Poisson distributions for the proportion of cells in a population that are expected to be infected with k infectious units when inoculated with virus at multiplicities of infection (MOIs) between 0.1 and 10.

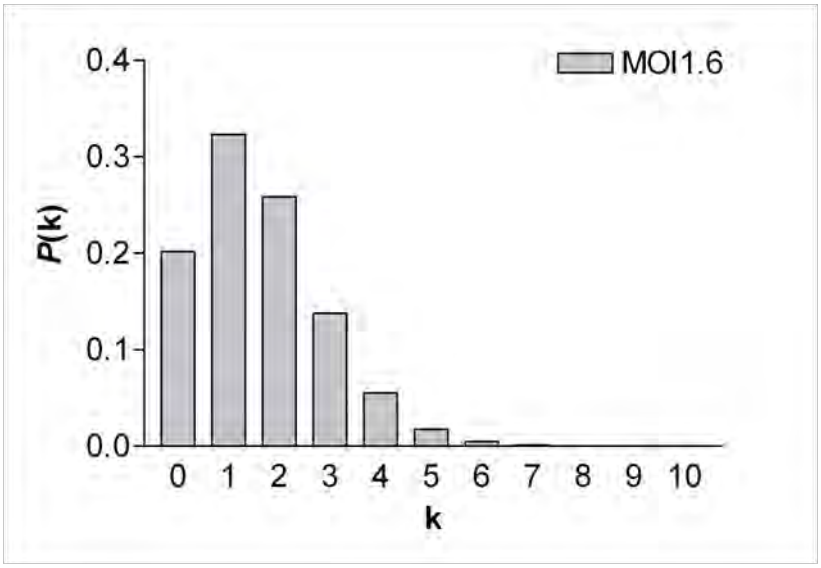

Figure 3.13: Poisson distribution for the proportion of cells in a population that are expected to be infected with k infectious units when inoculated with virus at a multiplicity of infection (MOI) of 1.6.

Serial infection transmission, albeit of low percentage without chemical induction, has been routinely described in manuscripts presenting novel systems for studying *de novo* KSHV infection, and models for KS lesion progression propose that a background of spontaneous lytic replication is critical to maintain fundamental latent infection (Grundhoff and Ganem, 2004; Zhong et al., 1996). Consistent with this concept, ganciclovir treatment, which blocks lytic but not latent KSHV infection, decreased KS risk in patients with advanced AIDS (Martin et al., 1999). Thus, the incidence of a low background of spontaneous lytic replication of rKSHV.219 during infection of HUVEC, and the potential for some horizontal transmission of infection, is further support for the validity of this *in vitro* system as one in which to study the effects of KSHV infection of endothelial cells that are relevant to disease.

In summary, this chapter described the development of a protocol that yielded up to 80% infection of primary endothelial cells with KSHV and characterised this infection up to day-ten post inoculation: the time-period over which studies conducted in this thesis will be performed. For the following reasons the *in vitro* system established here was considered highly suitable for investigating, in subsequent chapters of this thesis, the impact of KSHV infection upon endothelial cell functions within the context of KS pathogenesis: (1) KSHV infection occurred at high efficiency (up to 80%) even using primary endothelial cells; (2) Primary endothelial cells, as opposed to transformed endothelial cells, were used as the target host-cell population; hence observation of any KSHV-induced effects was not obscured by the underlying transformed state of the cell; (3) KSHV infection was latent in most cells with only a small proportion of cells entering spontaneous lytic reactivation. A predominant latent infection is reminiscent of KSHV infection in the malignant endothelial-like spindle cells of KS lesions; (4) Infected and non-infected cells could be distinguished on the basis of GFP positivity and lytic reactivation by RFP fluorescence. Alterations in phenotype and whether they were infected-cell specific or paracrine in nature could thus be readily identified without the use of antibody staining for KSHV-specific antigens.

CHAPTER FOUR

EFFECT OF KSHV INFECTION UPON ENDOTHELIAL CELL MOTILITY

4.1 INTRODUCTION

KS lesions have a large abnormal vasculature. The vessels are poorly developed, appearing as vascular spaces. The cells lining these spaces are infected with KSHV, suggesting a direct role for KSHV in the development of the aberrant angiogenesis.

Since endothelial cell migration is involved in angiogenesis it was hypothesised that KSHV infection might alter cell migration. Prior to this thesis, a restricted number of KSHV genes had been examined for their influence upon cell migration and had demonstrated opposing effects: K15M (Tsai et al., 2009) increased cell migration whilst vGPCR (Couty et al., 2009) and K5 (Mansouri et al., 2006) inhibited migration. To my knowledge, no study had explored the effect of infection by whole KSHV upon the migration of any endothelial cell lines or primary endothelial cells. Thus in this chapter, migration assays were developed and used to examine the effect of the virus upon the migration of primary endothelial cells.

Cell migration can be examined by techniques that monitor the passage of cells between seeding and destination chambers that may be arranged vertically, separated by a porous membrane, or arranged either concentrically (Dunn chamber) or side by side (Zigmond chamber), separated by a bridge. Such assays were originally developed to study the chemotactic behavior of cells by the addition of chemoattractants to the destination chamber, but their principles may be adopted to examine intrinsic cell motility. Techniques that monitor closure of a 'scratch-wound' can also provide an indication of migration rates when cells are not proliferating rapidly; analysis may be endpoint or continuous monitoring by time-lapse microscopy. The latter enables total migration distances, migration rates and direction paths to be assessed.

The assays developed in this chapter to assess the effect of KSHV infection on primary endothelial cell migration quantified endothelial cell migration in terms of: (1) transmigration (the migration of cells across a porous membrane, from an upper seeding chamber to lower destination chamber); (2) wound recovery; (3) distance, rate and/direction of movement.

4.2 RESULTS

4.2.1 Development of a transmigration assay

Membranes with 8μm-pores have been recommended for monitoring the transmigration of endothelial cells by manufacturers (Becton Dickinson Labware). The membranes are sometimes coated with extracellular matrix proteins such as collagen or fibronectin or a reconstituted tumour cell matrix termed 'Matrigel' (e.g. Dawson et al., 2008; Qin et al., 2011; Tsai et al., 2009). However, since deposited patterns of basement membrane proteins might influence migration (see Hamill et al., 2009; Sehgal et al., 2006), non-coated filters were selected for these studies.

To conserve reagents and scarce primary and infected cells, 24-well format cell culture inserts, termed in this thesis 'transwell chambers', were chosen as they have a growth area of only 30mm^2. Despite this small area, percentage transmigration could be calculated for multiple fields, thereby achieving a reliable estimate of the average transmigration rate.

Although most transmigration studies have used 8μm-pore filters (e.g. Couty et al., 2009; Dawson et al., 2008; Tsai et al., 2009), we noticed that HUVEC could also pass through 3μm-pore filters. To establish a suitable duration for the assay and to compare sensitivity of the assay with different pore sizes, migration assays with untreated HUVEC were performed using

transwell chambers with 3μm or 8μm-pore filters for durations of 24 or 48hours. Migration was markedly slower using 3μm-pore filters, and for either pore size only a small proportion of cells migrated in 24hours **(Figure 4.1)**. All subsequent assays were conducted with 8μm-pore filters and 48hour duration because under these conditions, percentage transmigration was at a level that if KSHV infection enhanced or decreased motility it could be detected.

4.2.2 The effect of KSHV infection upon endothelial cell transmigration

Since the spindle morphology of KSHV-infected HUVEC became more pronounced with time and the percentage infection of the inoculated cultures increased with time **(Chapter 3)**, I considered that alteration of cell migration by KSHV might be dependent upon the timepoint of observation post-inoculation. To address fully whether KSHV inoculation altered endothelial cell migration, the transmigration of HUVEC was examined at one, three, seven and ten days post-inoculation. By day-three and beyond, KSHV inoculation enhanced HUVEC transmigration compared with no treatment **(Figure 4.2)**. Even though the increase was not significant at day-ten post-inoculation, the trend toward enhanced transmigration with inoculation was still present. Since KSHV repeatedly enhanced transmigration at day-seven post-inoculation, subsequent migration studies were conducted at day-seven post-inoculation.

For the KSHV-inoculated cultures, it was not possible to ascertain the percentage transmigrations of KSHV-infected and non-infected cells separately by fluorescence microscopy alone. This was because the GFP fluorescence of infected cells was too faint, when observed on the fixed filters, to distinguish reliably between infected and non-infected cells.

To establish whether the enhanced transmigration of KSHV-inoculated cultures compared with untreated controls involved increased motility of both KSHV-infected and non-infected cells or one population only, cells were removed from the top and bottom surfaces of the transwell chamber filters at 48hours and the percentages of GFP positive cells in each population were assessed by flow cytometry. Percentages of GFP positive cells were consistently higher in the cultures removed from the bottom compared to the top of the filter **(Figure 4.3A)**. In parallel with this analysis, the percentage transmigrations of the KSHV-inoculated and untreated monolayers were quantified by microscopy using separate filters. Combining these data, the percentage transmigrations of KSHV-infected and non-infected cells were calculated and revealed preferential migration of infected cells. Non-infected cells maintained a rate of transmigration equivalent to that of untreated control cells **(Figure 4.3B and Appendix Table 9.1**). These data therefore suggested that enhancement of endothelial cell motility with infection was not due to the paracrine action of a secreted factor, but to effects on the infected cells themselves. To test this hypothesis further, transmigration assays for HUVEC that had not been previously treated with either KSHV or mock inoculums were performed in the presence of supernatants collected from KSHV-inoculated or untreated cultures. Consistent with the above, no effect of supernatant was observed **(Figure 4.4)**.

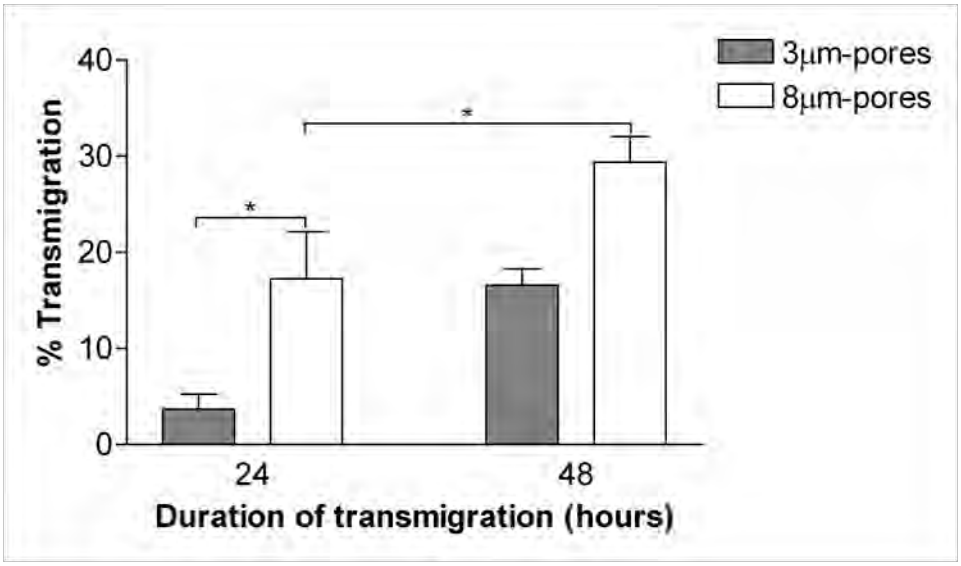

Figure 4.1: Effect of pore size and duration of assay upon the endpoint percent transmigration of HUVEC.

HUVEC were seeded into 8μm-pore or 3μm-pore transwell chambers and the percentage transmigration after 24 or 48hours quantified by microscopy. Data are mean ± SEM for two (24hours) or three (48hours) experiments. * = $P<0.05$ by t-test.

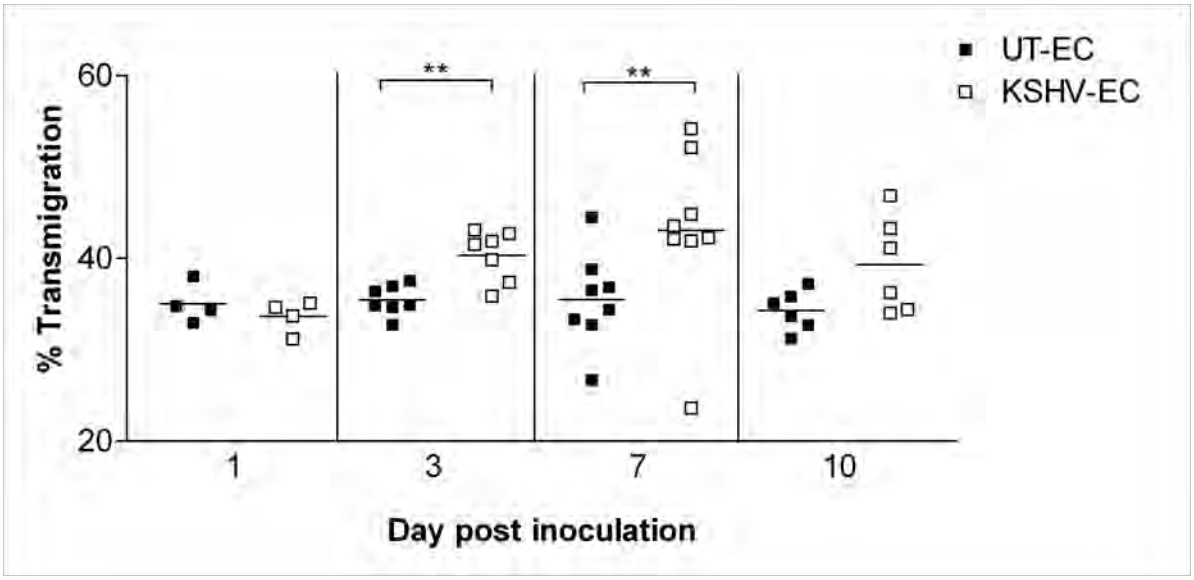

Figure 4.2: Effect of duration of KSHV infection upon the transmigration of HUVEC.

KSHV-inoculated (KSHV-EC) or untreated (UT-EC) HUVEC were seeded into 8μm-pore transwell chambers on days one, three, seven or ten post-inoculation and the percentage transmigration after 48hours quantified by microscopy. Individual points represent separate experiments. Horizontal lines indicate mean percentage transmigration. Two way ANOVA revealed a significant effect of KSHV upon transmigration ($P<0.01$); ** = $P<0.01$by paired t-test.

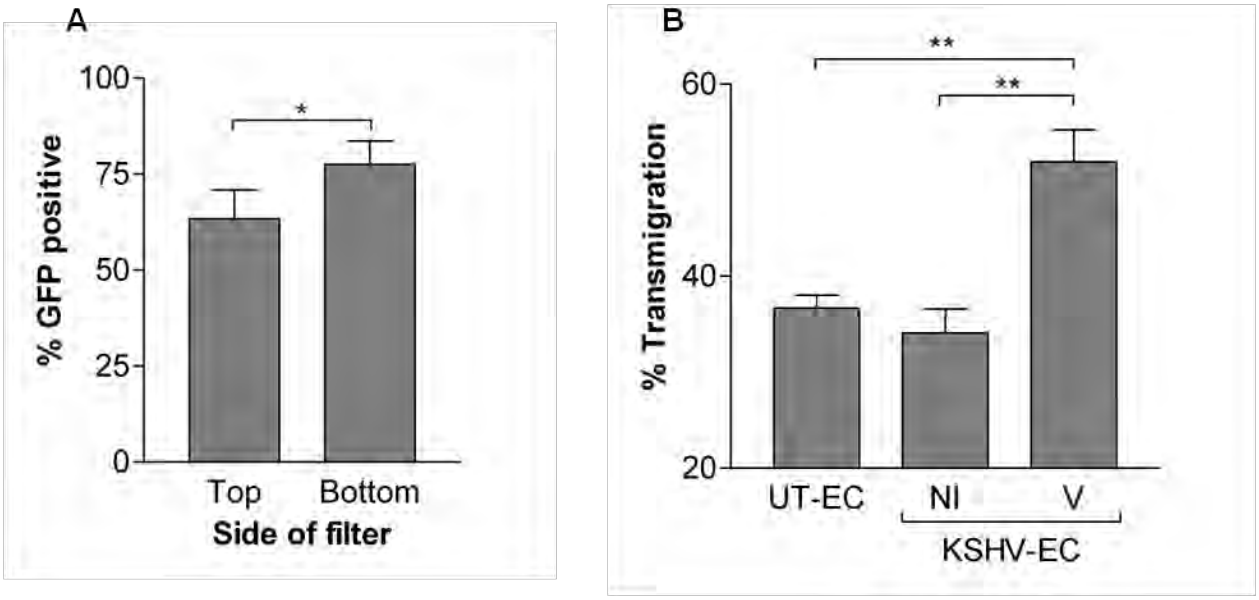

Figure 4.3: Comparison of transmigration by KSHV-infected, non-infected and untreated HUVEC.

KSHV-inoculated (KSHV-EC) or untreated (UT-EC) HUVEC were seeded into 8μm-pore transwell chambers on day-seven post-inoculation and the proportion of cells above or below the filter that were GFP positive, and the percentage transmigration were analysed after 48hours. **(A)** Percentage of GFP positive cells quantified by flow cytometry for KSHV-EC cultures removed from the top and bottom surfaces of filters. ** = $P<0.05$ by paired t-test. **(B)** Percentage transmigration of KSHV-infected (V), non-infected (NI) and UT-EC HUVEC as determined from the proportion of GFP positive cells each side of the filter and the percentage transmigration quantified by microscopy. ANOVA revealed a significant effect of KSHV upon transmigration ($P<0.01$); ** = $P<0.01$ by Bonferroni's multiple comparison test. Data are mean ± SEM for four experiments.

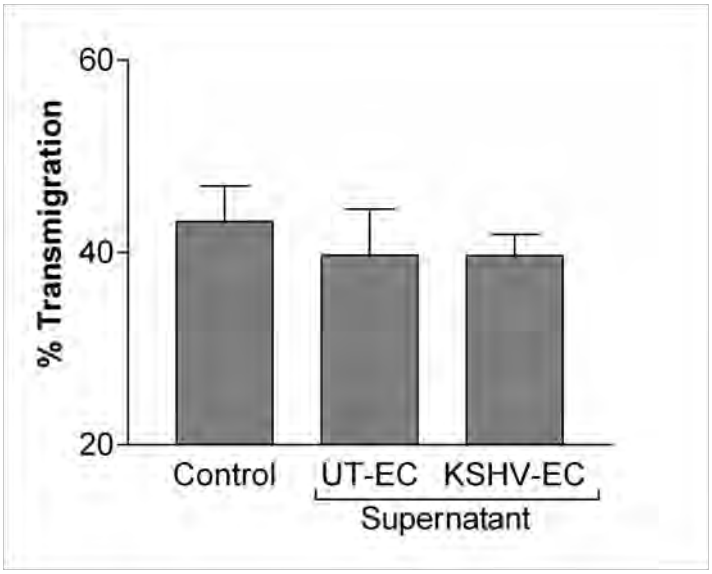

Figure 4.4: Effect of culture supernatants from KSHV-inoculated HUVEC on HUVEC transmigration.

Transmigration assays for otherwsie-untreated HUVEC were performed in the presence of fresh medium (Control) or media containing 25% 48hour culture supernatants from 24-well plate cultures of KSHV-inoculated (KSHV-EC) or untreated (UT-EC) HUVEC. 25% supernatants were used in order to recapitulate the lower concentrations of transmigration assay supernatants compared with 24-well plate supernatants. Data are mean ± SEM for three experiments.

4.2.3 Development of a wound recovery assay

To complement my observations of enhanced endothelial cell transmigration with KSHV infection, I developed a wound recovery assay. Using this system, the two-dimensional migration of cells in the absence of a barrier was studied.

Typically, wound recovery assays involve making a scratch along the centre of the monolayer using a fine tool such as a sterile 20μl pipette tip. During the migration period, cells migrate from the surrounding monolayer to recover the wound. Percentage recovery at a fixed endpoint and/or at intervals throughout the recovery phase is measured and compared across treatments.

To conserve reagents, a 24-well plate format was first tested in preference to a 12- or 6-well plate format, but at the level of magnification required to view the entire width of the wound, only one central field had adequate optical quality under phase-contrast light microscopy for quantification of the percentage wound recovery. Outside of this central field, scattering of the light by the well edge disrupted the image **(Figures 4.5A, B)**. Larger well formats were tried and 12-well or larger found suitable for observation of at least three fields along the wound, as required for reliable quantification **(Figure 4.5C)**.

Wounding may be performed one-day after seeding (e.g. Sheldon et al., 2009) but to study the effect of KSHV-inoculation upon cell migration at day-seven post-inoculation, eight days of culture from seeding were required prior to wounding. Pilot studies to test whether wound recovery assays could be performed on such 'aged' cultures highlighted a problem. Upon wounding, these monolayers peeled generating an irregular wound **(Figure 4.5D)**; the effect was also incurred four days after seeding **(Figure 4.5E)**. It was suggested that coating culture

plates with 0.1% (w/v) gelatin might reduce the risk of peeling. I found that coating the plates with 0.1% (w/v) gelatin delayed the onset of monolayer peeling (**Figures 4.5F, G**) but the monolayers still peeled when wounded eight days after seeding **(Figure 4.5H).** Therefore, an alternative method was sought.

Transferring cells to new culture surfaces on day-six post-inoculation and wounding the monolayer on day-seven would be expected to overcome the problems of peeling that establish with prolonged culture on the same surface. Of standard culture vessels, wells of 12-well plates were the smallest available that were suitable optically. However, to seed a confluent monolayer for each test condition in 12-well plates required more cells than were available for each donor. Novel silicon culture inserts produced by Ibidi were used. The inserts were placed in the centre of a multi-well plate well (for example a well of a 6-well plate) and created two parallel 22mm^2 patches of cells separated by a 500μm (+/-50μm) gap into which cells migrated during the assay. These inserts enabled wound-recovery assays to be performed using comparatively few cells (3×10^4 cells/test compared to 1.5×10^5 cells/test for a confluent well of a 12-well plate).

Figure 4.5: Developmment of a wound recovery assay to examine the effect of KSHV on HUVEC migration at day-seven post-inoculation.

HUVEC were seeded to confluence, wounded down the centre of the well using a 20μl pipette tip on the day indicated post-seeding and visualised under phase contrast using a 4x objective lens. Plates were left uncoated or were coated with 0.1% (w/v) gelatin as indicated. **(A and B)** Monolayers in uncoated 24-well plates wounded one day post-seeding. **(C)** Monolayer in uncoated 12-well plate wounded one-day post-seeding. **(D)** Monolayer in uncoated 12-well plate wounded five-days post seeding. **(E and F)** Monolayers in uncoated **(E)** or 0.1% (w/v) gelatin-coated **(F)** plates wounded three-days post-seeding. **(G)** monolayer in 0.1% (w/v) gelatin-coated 12-well plate wounded five-days post seeding. **(H)** Monolayer in 0.1% (w/v) gelatin-coated 12-well plate eight days post-seeding.

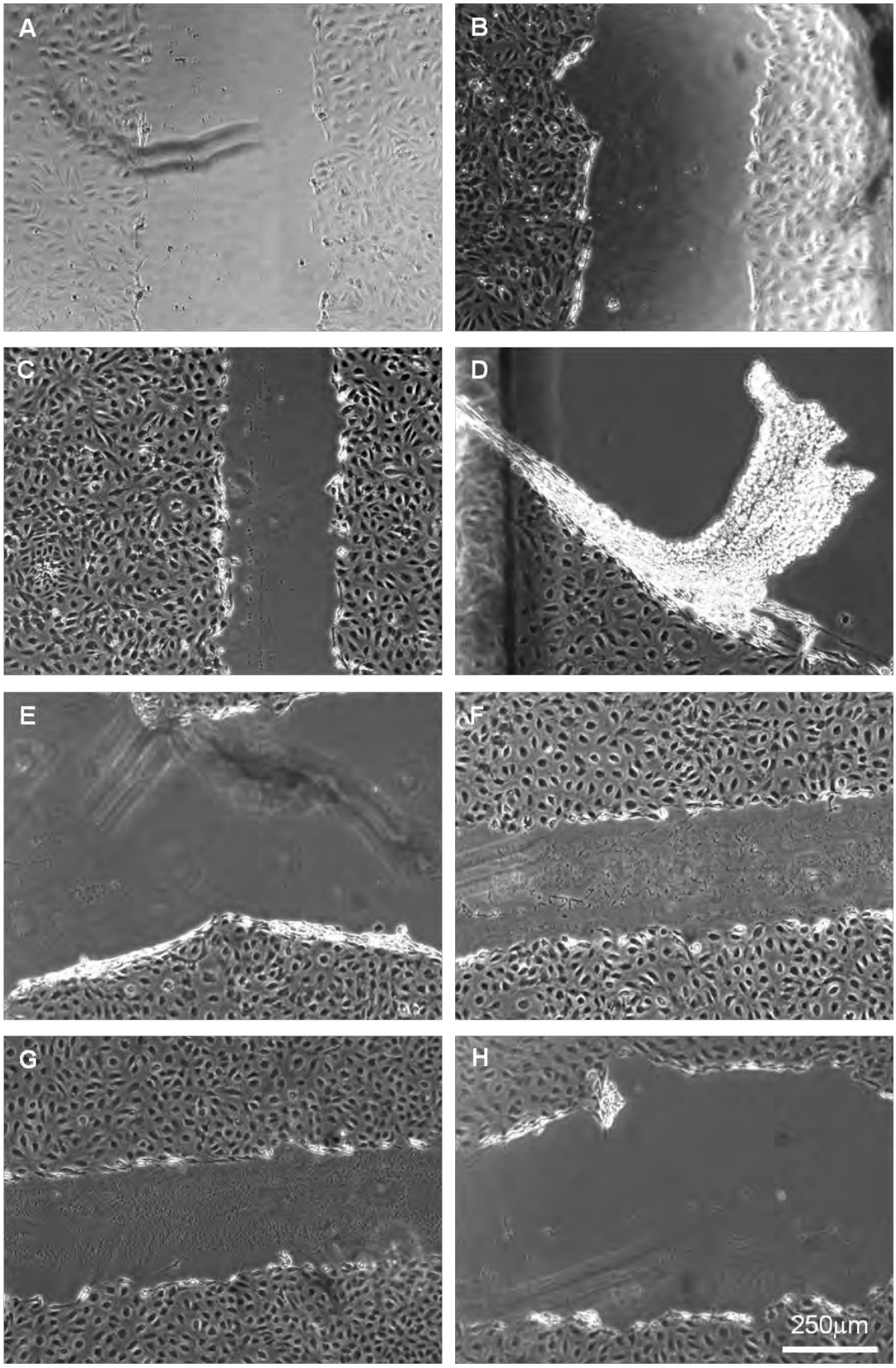
A
B
C
D
E
F
G
H
250µm

4.2.4 The effect of KSHV infection upon endothelial cell wound recovery

KSHV inoculation enhanced wound recovery at day-seven post-inoculation **(Figures 4.6A, B)**.

I considered that KSHV inoculation might modify cell-density of cultures and this might affect recovery. For instance, during wound recovery, regions of the monolayer where cells are at higher density might close more rapidly. To test whether wound recovery with KSHV inoculation was influenced by seeding density, the starting cell densities surrounding the wounds were counted from the phase contrast images and plotted against percentage recovery. Wound recovery increased with increasing cell density and across all densities was greater with KSHV inoculation (**Figure 4.7A**). For matched KSHV-inoculated and untreated cultures, density tended to be lower for the inoculated cultures but across all pairs of densities, wound recovery was still greater with KSHV inoculation **(Figure 4.7B)**. Thus, the increase in wound recovery after inoculation was not through an effect on cell density.

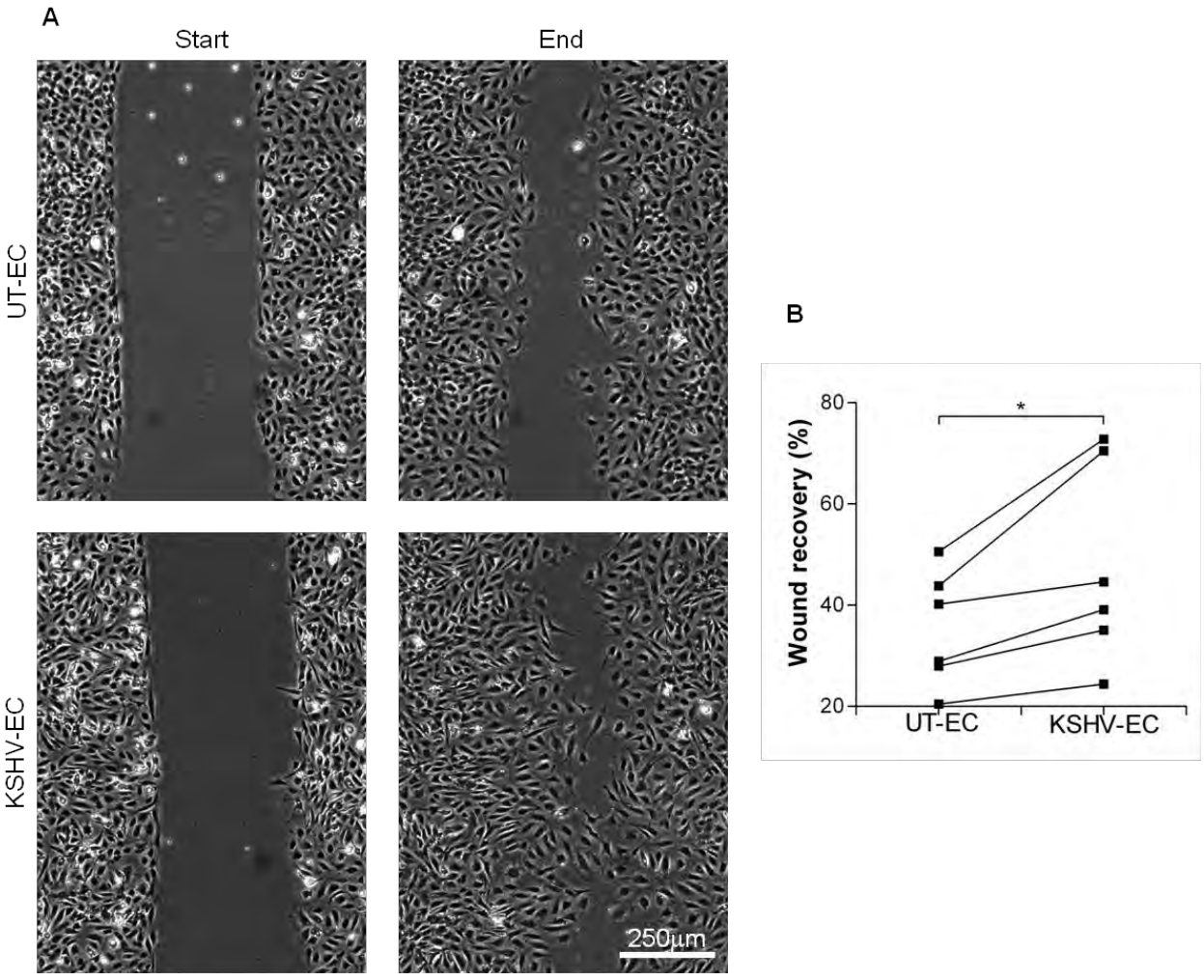

Figure 4.6: Effect of KSHV infection on HUVEC wound recovery.

KSHV-inoculated (KSHV-EC) or untreated (UT-EC) HUVEC were plated into culture inserts on day-six post-inoculation. Inserts were removed on day-seven and the percentage wound recovery in 32hours measured. **(A)** Representative start and endpoint images of UT-EC and KSHV-EC monolayers. **(B)** Average percentage wound recovery for KSHV-EC and matched UT-EC cultures. Each line represents a different experiment. * = $P<0.05$ by paired t-test.

Figure 4.7: Effect of cell density on KSHV-enhanced wound recovery.

KSHV-inoculated (KSHV-EC) or untreated (UT-EC) HUVEC were plated into culture inserts on day-six post-inoculation. Inserts were removed on day-seven. The starting density surrounding the wound was calculated and the percentage wound recovery in 32hours measured. **(A)** Percentage wound recovery in relation to starting density for untreated (UT-EC) and KSHV-inoculated (KSHV-EC) HUVEC monolayers. Individual points represent separate wound sites analysed across 6 experiments. The Pearson Product Moment Correlation Coefficients for the relationship between density and wound recovery were: UT-EC: $r = -0.1239$, $P>0.05$ and KSHV-EC: $r = 0.3430$, $P>0.05$. **(B)** Data for the experiments in Figure 4.6B plotted to show the average cell density and percentage wound recovery of the UT-EC and KSHV-EC cultures in each of the six paired experiments.

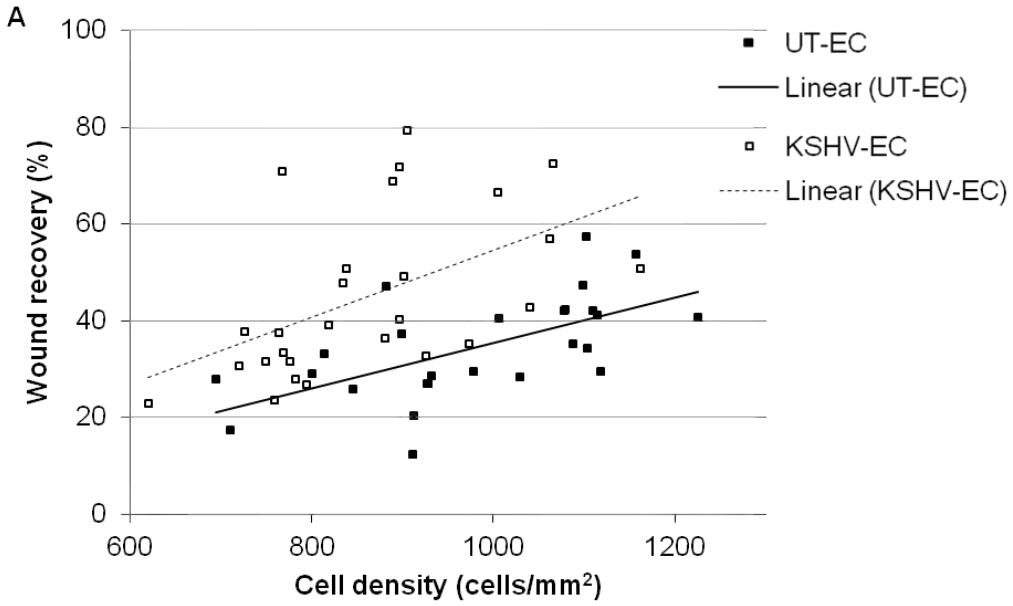
A
100
80
60
40
20
0
Wound recovery (%)
600
800
1000
1200
Cell density (cells/mm2)
UT-EC
Linear (UT-EC)
KSHV-EC
Linear (KSHV-EC)

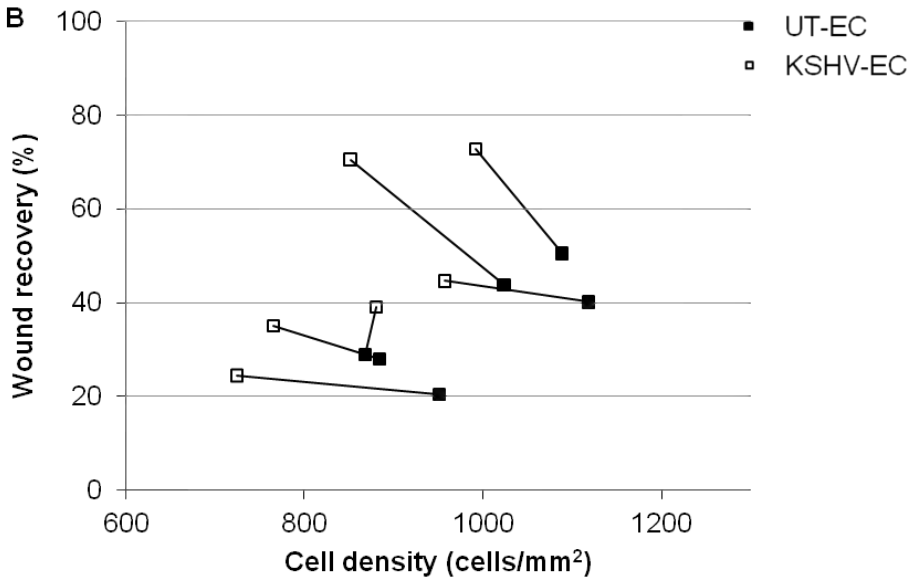
B
100
80
60
40
20
0
Wound recovery (%)
600
800
1000
1200
Cell density (cells/mm2)
UT-EC
KSHV-EC

Enhanced proliferation rates rather than, or in addition to enhanced migration might in principle contribute to increased rates of wound recovery. The lack of transformation toward an enhanced proliferative potential for KSHV-inoculated monolayers **(Figure 3.11)** makes this an unlikely explanation for faster wound recovery by inoculated monolayers**.** Nevertheless, I calculated ratios of endpoint cell numbers to initial numbers per field of view, and found them to be the same for untreated and KSHV-inoculated monolayers **(Figure 4.8)**. Thus, proliferation was not enhanced under KSHV-inoculation compared to no treatment and could not explain the increased wound recovery with inoculation.

The transmigration studies indicated that KSHV-infected cells migrated preferentially to non-infected cells **(Figure 4.3)**. To address whether this followed in wound recovery, 15-minute interval time-lapse recordings of KSHV-inoculated monolayers were made over 8hours during wound closure. The cells tracked were selected at random from within a 120μm band surrounding the wound: GFP fluorescence images overlayed onto the phase contrast image at the start of the recording enabled the KSHV-infected cells to be distinguished from the non-infected cells. The centroid coordinates of the cell nuclei were recorded every 2hours and the total distance migrated computed. No difference was found between the total distances migrated by infected and non-infected cells **(Figure 4.9)**. The total distance of migration might remain constant but the directionality of migration be altered by infection. As a measurement of the directionality of migration, persistence, the ratio of final displacement to total distance migrated was calculated. This parameter was not altered by infection either. Thus these data suggest that the cellular mechanisms which underlay enhanced transmigration and enhanced wound recovery were different.

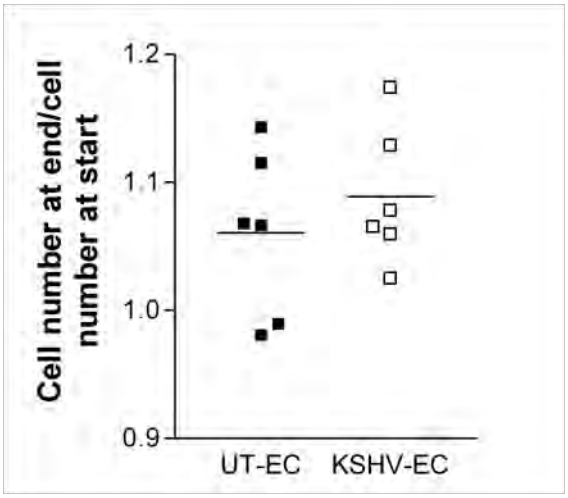

Figure 4.8: Effect of KSHV inoculation on start and endpoint cell numbers in fields analysed in the wound recovery assay.

The number of cells per field of view was counted at the start and end of the wound recovery assay and expressed as a ratio. Individual points represent separate experiments. Horizontal lines indicate the mean.

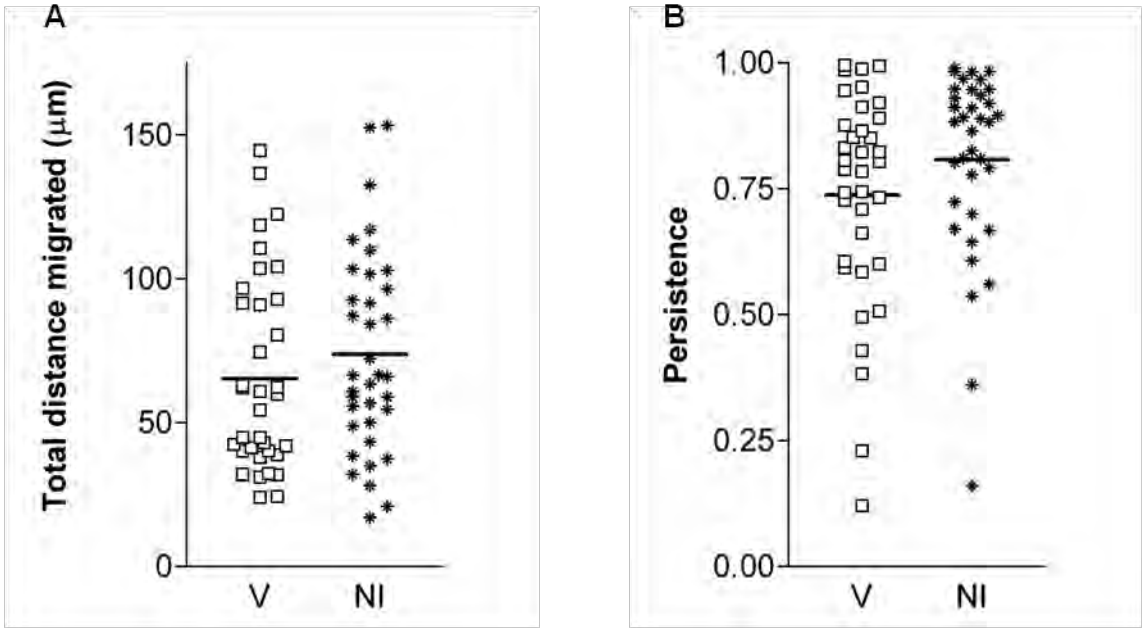

Figure 4.9: Comparison of the distances migrated by infected and non-infected cells at the edges of wounded monolayers.

Wound recovery of KSHV-inoculated monolayers was observed under 6x magnification at 15-minute intervals over 8hours. **(A)** The positions of the cells at 2hour intervals were tracked and the total distances migrated by KSHV-infected (V) and non-infected (NI) HUVEC computed. V and NI were distinguished on the basis of GFP positivity. **(B)** The persistence of migration for V and NI was calculated as the ratio of final displacement (compared to the starting position) to total distance migrated in 8hours. Individual points represent separate cells tracked from three experiments. Horizontal lines are the mean.

4.2.5 The effect of KSHV infection upon the motility of isolated endothelial cells

I questioned whether KSHV infection would increase the intrinsic motility of endothelial cells when sparsely distributed rather than in a monolayer. To examine the effect of the virus on individual cells, untreated and KSHV-inoculated cultures were seeded at low density and 10-minute interval time-lapse recordings made over 2.5hours. Overlay of GFP fluorescence images enabled infected cells and non-infected cells to be distinguished.

Analysis of migration distances showed that total migration distances calculated by this protocol were affected by the time interval between the images analysed **(Figure 4.10)**. This is a well-known phenomenon (arising because cells frequently change their direction of movement) and was the same irrespective of whether the cells were untreated, KSHV-infected or non-infected. Regardless of interval, the analyses showed that KSHV-infection did not affect the total distance migrated by isolated HUVEC over 2.5hours **(Figure 4.10).** Whilst the shortest interval (10minutes) gave the greatest distance, there was a greater relative error in these measurements because individually they were very short (only ~2μm). 30-minute intervals between images were felt appropriate in order to identify an element of the non-directional migration occurring whilst minimizing the magnitude of the error and were chosen for subsequent studies.

To examine the effect of KSHV upon migration direction and persistence, plots were constructed using the coordinates of the cells' positions at 30-minute intervals relative to their positions at the start and persistence (ratio of final displacement to total distance migrated) was calculated. No striking differences in the migration pathways **(Figure 4.11)** or persistence **(Figure 4.12)** of cells were noticed according to their infection status.

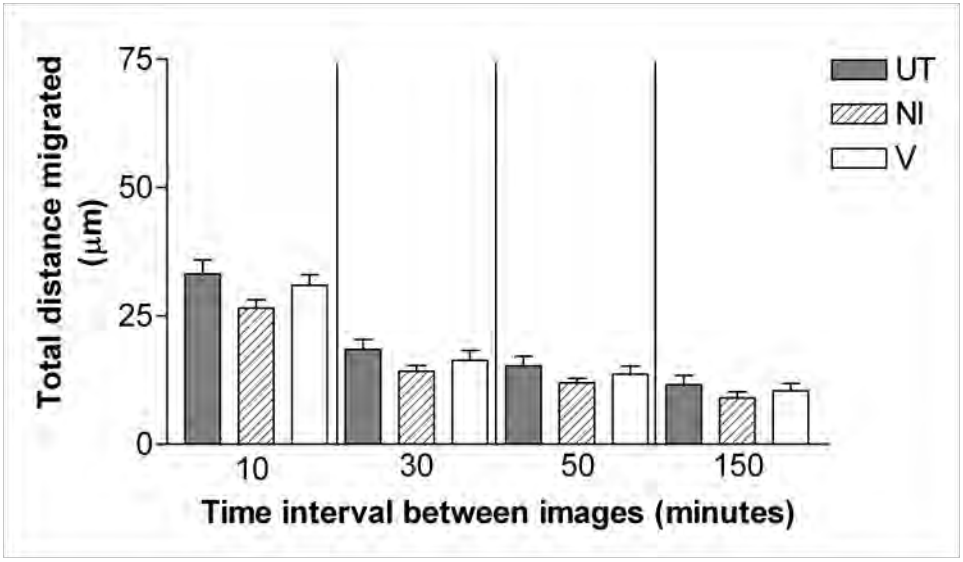

Figure 4.10: Effect of KSHV infection on the distances migrated by sparsely distributed HUVEC.

Untreated (UT-EC) or KSHV-inoculated (KSHV-EC) HUVEC were removed from 24-well inoculation plates on day-six post inoculation and seeded sparsely in 12-well plates. On day-seven post-inoculation, cells were viewed under phase contrast using a 10x objective lens and images recorded every 10minutes for 2.5hours. The total distances migrated by untreated (UT), non-infected (NI) and KSHV-infected (V) HUVEC were calculated when the times intervals between the images included in the analysis were 10, 30, 50 and 150minutes. V and NI HUVEC were distinguished on the basis of GFP positivity. Data are mean ± SEM for 18-21cells from from across three experiments.

Figure 4.11: Effect of KSHV infection on the migration pathways of sparsely distributed HUVEC.

Plots illustrating the migration pathways of untreated (UT), non-infected (NI) and KSHV-infected (V) HUVEC were constructed by plotting (x,y) coordinates of the cell centroids at 30minute intervals relative to their start position. The total period of observation was 150minutes. Each coloured line represents the migration pathway for a different cell. Cells shown are from one experiment included in Figures 4.10 and 4.12 but are representative of the behaviours of cells from all three experiments.

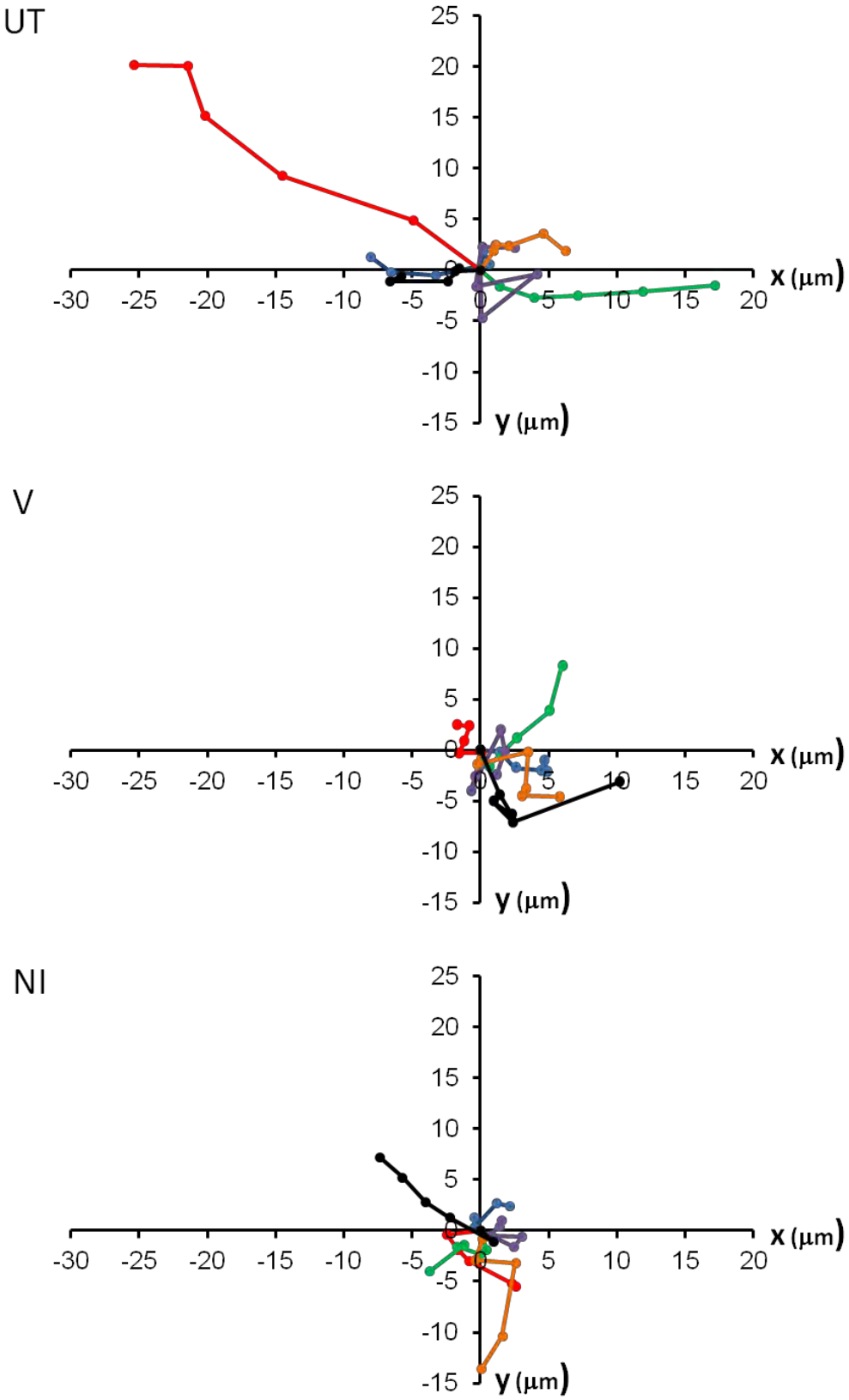
UT
V
NI
x (µm)
y (µm)
25
20
15
10
5
0
-5
-10
-15
-30
-25
-20
-15
-10
-5
0
5
10
15
20

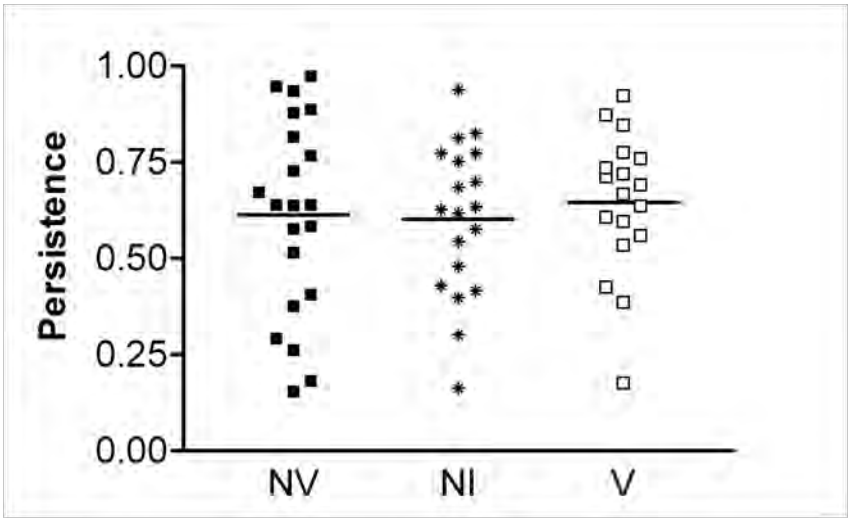

Figure 4.12: Effect of KSHV on the persistence of migration of sparsely distributed HUVEC.

Persistence of migration for untreated (UT), non-infected (NI) and KSHV-infected (V) HUVEC was calculated as the ratio of final displacement (compared to the starting position) to total distance migrated in 150minutes. The time interval between observations was 30minutes. Individual points represent separate cells tracked from three experiments. Horizontal lines are the mean persistence. Cells included were those for which total migration distance data are presented in Figure 4.10.

4.3 DISCUSSION

The migration of endothelial cells is required for the formation of new vascular structures during angiogenesis. Extensive aberrant angiogenesis is a hallmark of KS lesions. Previous studies had identified both positive and negative effects of isolated KSHV genes upon cell migration but the impact of infection by the whole virus on cell migration was not known. Here I have shown for the first time that KSHV infection of primary HUVEC increases the migration of cells from confluent monolayers across a porous barrier (transmigration) **(Figures 4.2 and 4.3)** or into an adjacent space (wound recovery) **(Figure 4.6).** Interestingly, tracking individual infected cells at the edge of a 'wound' or when sparsely seeded did not reveal an increase in migration speed **(Figures 4.9. and 4.10).**

In the study of transmigration, KSHV enhanced transmigration at day-three post-inoculation and beyond **(Figure 4.2)**, the virus conferring increased transmigration potential specifically to the infected cells **(Figure 4.3)**. By 48hours, the endpoint percentage transmigration of non-infected cells was equal to that of untreated controls, suggesting that KSHV infection does not influence the migration of non-infected cells through a paracrine mechanism, and that if KSHV-enhanced transmigration is coordinated by a secreted factor, it only acts on infected cells. Whilst KSHV infection is known to induce the release of promigratory factors such as VEGFA, bFGF and angiopoietins (Akula et al., 2005; Haddad et al., 2008; Masood et al., 2002; Montaner et al., 2004; Naranatt et al., 2004; Sadagopan et al., 2009; Sivakumar et al., 2008; Vart et al., 2007; Wang et al., 2004a; Xie et al., 2005; Ye et al., 2007), the absence of an increase in the transmigration of untreated HUVEC in the presence of supernatants from KSHV-inoculated cultures **(Figure 4.4)** supported the conclusion that increased transmigration was an intrinsic

property of infected cells. In contrast, faster rates of two-dimensional migration for inoculated compared to untreated cultures appeared to be an integral property of the inoculated monolayer, rather than specific to KSHV-infected cells **(Figures 4.6 and 4.9)**. KSHV-infected and non-infected cells did not present different migration rates or persistence of migration when followed under time-lapse during wound recovery **(Figure 4.9)**. Thus, the mechanisms that underlie the enhancement of migration with KSHV inoculation may in fact be different in the transmigration and wound recovery models. It is possible to speculate that the distinction in behaviour between the two models (preferential transmigration of infected cells but equal migration rates of infected and non-infected cells during wound recovery) is due to the different physical properties of the two systems such as the requirement for cells to negotiate the porous barrier of the transwell chamber filters during the transmigration assay. Perhaps the morphological transformation of infected cells, becoming longer but thinner, underlies their improved propensity to traverse the pores.

In the wound recovery system, the absence of a discriminating barrier might make paracrine, chemokinetic signaling influential. For example, KSHV-induces VEGFA (Sivakumar et al., 2008) and VEGFA signaling through VEGFR2 promotes focal adhesion turnover and endothelial cell migration (Lamalice et al., 2007). Alternatively, or in addition, provision for maintenance of cell-cell contacts during wound recovery might facilitate sheet-like rather than independent movement of cells enabling KSHV-infected cells to influence the migration rates of bystander, non-infected cells. Such communication might be important in the formation of the aberrant vascular structures of KS lesions where non-spindle endothelial cells do not harbour KSHV infection (Dupin et al., 1999).

Whilst KSHV genes were traditionally classified as lytic or latent, based upon expression profiles in PEL cells, in HUVEC this distinction is less clear (Ye et al., 2007) with many lytic transcripts, including K5, still detectable up to day-ten post-inoculation in our system (Butler and Blackbourn, unpublished data). K15 has similarly been reported by others to be expressed during both latent and lytic phases (Chen et al., 2009). Therefore there may be a role for KSHV 'lytic' proteins such as K5 and K15 (Tsai et al., 2009) in KSHV-induced enhanced migration despite the latent phenotype of the culture at day-seven in terms of RFP expression **(Section 3.2.3).** Although depletion of CD31 by KSHV-K5 overexpression reduced wound-recovery (Mansouri et al., 2006), it may be that under conditions of modest expression as with whole virus infection, in contrast to ectopic overexpression, KSHV-K5 supports an increase in wound-recovery by reducing the strength of cell-cell contacts, thereby rendering both infected and non-infected cells in the same monolayer with greater freedom to migrate compared to untreated controls.

The increase in cell migration with whole virus infection, as demonstrated here, suggests that the overall balance of KSHV gene functions, in predominantly latent cultures, promotes motility. This is in contrast to HHV6 infection of lymphatic and vascular endothelial cells, which, in a mechanism attributed to the HHV6 latency-associated U94/REP protein, inhibited migration and angiogenic properties of both types of endothelial cell: Evidence for this inhibition included the impaired ability of HHV6-infected cells to close scratch wounds and to form capillary-like tubes in basal membrane extracts (Caruso et al., 2009). Similar to the enhanced transmigration with KSHV infection, however, HCMV infection increased the transmigration of arterial smooth muscle cells in a mechanism involving MCP-1 activation of the viral chemokine receptor US28. The enhanced transmigration was specific to infected cells, since whilst MCP-1 is generated by

non-infected smooth muscle cells it was only through the expression of the viral receptor that cells gained transmigration potential (Streblow et al., 1999). An analogous mechanism might underlie enhancement of HUVEC transmigration with KSHV infection in these studies.

Aside from these studies on HHV6 and HCMV, there is a paucity of literature on the effects of infection by other herpesviruses and DNA-tumour viruses upon cell migration, with most studies addressing the effects of single viral proteins on cell migration. Phylogenetically, KSHV is closely related to the ubiquitous gammaherpesvirus EBV which is associated with infectious mononucleosis and cancers including Hodgkin's lymphoma, Burkitt's lymphoma and nasopharyngeal carcinoma (NPC). These diseases are characterized by different latency programs of the virus in which some or all of the latency genes are expressed. For relevance to the metastatic nature of late stage NPC, in particular, the latency genes latent membrane protein (LMP)1, LMP2A, LMP2B and EBV nuclear antigen-1 (EBNA1) have been studied for their effects on cell motility and migration and all shown to increase cell motility. Interestingly, there are structural and sequence similarities between the K15 protein of KSHV and LMP1 and LMP2A (Tsai et al., 2009).

LMP1, formerly denoted the major transforming protein of EBV, appears to enhance cell motility through multiple mechanisms including induction of the transcription factor Ets1 (Kim et al., 2000), upregulation of Decoy receptor 3 via NFκB and PI3K signaling (Ho et al., 2009), and activation of the ERK-MAPK pathway (Dawson et al., 2008). Whether KSHV proteins target similar pathways remains to be determined. Interestingly, LMP1-transformed Madin-Darby canine kidney (MDCK) cells (Kim et al., 2000) and SV40-immortalised nasopharyngeal epithelial (NP69) cells (Lo et al., 2003) migrated away from the monolayer edge into the

wounded area in contrast to control cells, which maintained smooth monolayer fronts during wound closure. Similar behaviour was not apparent with KSHV-infection at day-seven post-inoculation in these studies, where instead, infected cells moved with the rest of the monolayer and since infected and non-infected cells migrated at the same rate, polarization of infected cells toward the wound front was also not evident. Analogous to KSHV infection, however, LMP1 overexpression induced spindle morphology to the cells (Kim et al., 2000). Thus, cytoskeletal changes upon spindling might have significance to the property of enhanced motility. Indeed, loss of cell-to-cell contacts and remodeling of the actin cytoskeleton into filopodia and stress fibres, involving PI3K dependent activation of the small GTPases Rho and Cdc42, was reported upon LMP1 overexpression (Dawson et al., 2003).

Analogous to KSHV infection in these assays, studies looking at the roles of the EBV integral membrane proteins LMP2A and LMP2B suggested LMP2 increases the transmigratory and in-plane migration of cells (Allen et al., 2005; Pegtel et al., 2005). The promigratory effects of the LMP2 isoforms were linked to an improved ability of the cells to spread and establish focal adhesions rather than to form an initial attachment to the underlying extracellular matrix. This involved tyrosine kinase phosphorylation of FAK and structural proteins at focal adhesions (Allen et al., 2005; Lu et al., 2006). In contrast to LMP1, the activation of Protein Kinase C (PKC), ERK-MAPK or PI3K pathways was not evident for LMP2. Presumably therefore, in the context of whole virus infection, the signaling cascades most responsible for regulation of motility would be those activated by the viral proteins with predominant function.

EBNA1 expressed in all EBV-associated malignancies is described as functionally analogous to the KSHV protein LANA1. Both are latent origin binding proteins that act to ensure the

maintenance and segregation of the viral episome in infected cells. EBNA1 has also been shown to enhance cell migration through interaction with the suppressor of metastasis and cell migration, Nm23-H1. This interaction relocates Nm23-H1 from the cytosol to the nucleus, thereby relieving its inhibitory effect upon cell migration (Murakami et al., 2005). Targeting of Nm23-H1 appears to be a strategy harnessed by other viral proteins to promote cell migration as illustrated by EBNA3C and the E7 oncoprotein of Human Papillomavirus (Choudhuri et al., 2006; Mileo et al., 2006). A recent study looking at the effect of KSHV infection upon Nm23-H1 identified that whilst KSHV infection upregulated Nm23-H1 expression, LANA1 induced its translocation to the nucleus thereby promoting an invasive phenotype (Qin et al., 2011).

Overall, the fact that other herpesviruses encode genes with migration-promoting effects provides further support for the data presented here showing that KSHV inoculation increases cell migration, since it suggests that to increase host-cell migration might be of benefit to herpesviruses and is thus conserved as a viral survival strategy. Moreover, KSHV might use similar mechanisms and/or homologuos proteins to other herpesviruses to confer enhanced migration.

In summary, assays to monitor endothelial cell migration were developed in this chapter and KSHV infection shown to increase the motility of primary endothelial cells, both in transmigration and in-plane migration assays. The assays were designed around the use of commercially available devices that would enable the number of cells required to be minimized and therefore also the amount of high titre virus: this was necessary since the supplies of both were limited.

The most detailed analysis of the effect of KSHV upon endothelial cell transmigration was provided by parallel microscopic counting and GFP flow cytometry assays, which enabled the percentage transmigration of untreated, KSHV-infected or non-infected HUVEC to be determined separately. However, the limitations over cell availability would not permit both analyses routinely. It was not desirable to expand HUVEC across multiple passages since we observe this to alter HUVEC functions in our assays.

In considering the best method to use for further studies, I first considered the percentage transmigration by microscopy or the difference between percentage infection of cultures on the top and bottom surfaces of the transwell chamber filters. The coefficients of variation for the two methods were 25.4% and 26.6% respectively suggesting that they were comparable in terms of their power to assess the impact of KSHV on migration. Analysis of transmigration by microscopic analysis was chosen as the preferred method since each repeat assay required one instead of two transwell chamber filters, therefore enabling more duplicate assessments to be made, improving precision. The coefficient of variation associated with the wound recovery method was 31.8%; thus this method was less precise. Subsequently, it was decided that the underlying mechanisms for KSHV-enhanced cell migration would be addressed using the transmigration method with quantification by microscopy.

Possible mechanisms underlying KSHV-enhancement of endothelial cell migration, such as alterations to: composition of the sub-endothelial matrix of basement membrane proteins; surface integrin expression profile; actin cytoskeleton and focal adhesion distribution; secretion of promigratory chemokines and growth factors and expression of their receptors; activation of the p38 MAPK pathway are addressed in the following three chapters.

CHAPTER FIVE

EFFECT OF KSHV INFECTION UPON ENDOTHELIAL CELL DEPOSITION OF BASEMENT MEMBRANE PROTEINS AND SURFACE EXPRESSION OF INTEGRIN RECEPTORS

5.1 INTRODUCTION

In vitro endothelial cells deposit matrix proteins which form a basement membrane during prolonged culture (Butler et al., 2005). They attach to this matrix via integrin heterodimers and this binding activates integrin outside-in signaling cascades that promote, among other responses, changes to the actin cytoskeleton, potentially altering cell motility. The basement membrane may also serve as a reservoir for growth factors and chemokines enhancing their presentation to cellular receptors and affecting endothelial cell behaviour, including migration.

In this chapter, in view of the possible regulatory influence of the basement membrane upon multiple facets of endothelial cell behaviour, including migration, an indirect ELISA method was used to analyse the composition of sub-endothelial matrix and to assess the impact of KSHV-infection upon deposition of these proteins. Studies were performed to interrogate the molecular basis for the alterations in proteins deposited upon KSHV infection. Subsequently, a role for detected changes in matrix proteins in KSHV-enhanced endothelial cell migration was tested. An effect of the virus upon integrin surface expression was also examined, and changes detected tested for involvement in KSHV-enhanced migration.

5.2 RESULTS

5.2.1 Establishment of a suitable cell removal method for subsequent analysis of the sub-endothelial matrix by ELISA.

To study the composition of sub-endothelial matrix by ELISA the overlying cell monolayer needed to be removed. Detergent lysis buffer or incubation with EDTA were two methods previously used in our laboratory to expose the sub-endothelial matrix (Butler, 2005; Butler et al., 2005). I compared these methods for their influence upon the levels of matrix-proteins detectable in subsequent ELISAs. ELISAs to analyse the main protein constituents of vascular basement membrane (collagen IV, fibronectin and laminin) were performed on four-day cultures since previous studies showed that in four days, basement membrane proteins deposited by HUVEC monolayers were detectable by ELISA (Butler et al., 2005). Endothelial cells were seeded directly on plastic, as was the case in migration assays. The method for HUVEC removal did not alter the detection of any of the matrix proteins screened, suggesting that possible release of intracellular matrix-protein stores upon cell lysis did not confound the assay and that EDTA, a gentler treatment that removes cells intact, did clear the monolayer thoroughly **(Figure 5.1)**. Lysis buffer was chosen as the treatment for removing cells in all subsequent assays since it was the shorter method.

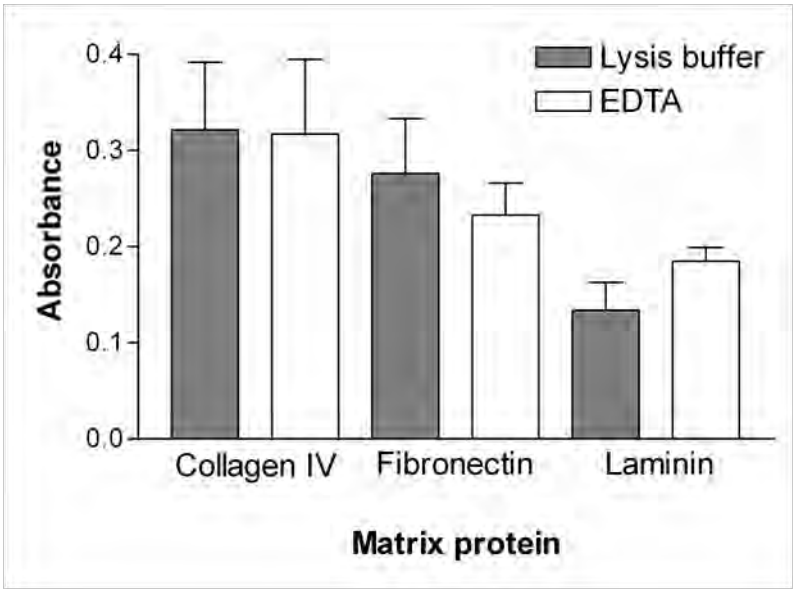

Figure 5.1: Comparisons of cell removal methods to expose the sub-endothelial matrix for analysis by ELISA.

HUVEC were plated into 96-well plates, cultured for four-days and stripped from the deposited matrix using detergent lysis buffer (PBS containing 0.5% (v/v) Triton X-100, 20mM NH_4OH) or 4hour incubation in 0.02% (w/v) EDTA at 37°C. The composition of the sub-endothelial matrix was analysed by ELISA with absorbance readout at 490nm. Data are mean ± SEM for three experiments.

5.2.2 The effect of KSHV infection on the production and secretion of basement membrane components by endothelial cells

The effect of KSHV inoculation on the deposition of basement membrane proteins by endothelial cells was first analysed four days following inoculation. Cells were seeded to confluence and inoculated as soon as they had settled and adhered to the plate (~4hours) (no significant deposition of matrix proteins was anticipated in 4hours). Relative to no treatment, KSHV inoculation did not alter the amount of collagen IV or fibronectin deposited but reduced the amount of laminin by two-thirds. Using UV-irradiated KSHV, this reduction was not observed, indicating that it was a specific response to KSHV infection **(Figure 5.2)**.

In Chapter 3 I observed a decrease in cell density with KSHV inoculation. Here, there was reduction seen in laminin but not collagen-IV or fibronectin. Therefore, I decided to test whether cell number and protein deposition were similarly related for all three proteins. Untreated HUVEC were seeded at densities between $0.3x10^4$cells/well and $3x10^4$cells/well and the collagen IV, fibronectin and laminin composition of the four-day sub-endothelial matrix assayed by ELISA for each cell density. In parallel the number of cells per field of view was counted by fluorescence microscopy looking at bisbenzimide-stained cell nuclei. Plots of absorbance against density suggested that a positive relationship existed between cell density and matrix protein deposition for all three proteins tested **(Figure 5.3)**. The Pearson Product Moment Correlation Coefficients were statistically significant for each protein (Collagen IV: $r = 0.8465$, $P<0.01$; Fibronectin: $r = 0.6558$, $P<0.05$; Laminin: $r = 0.9791$, $P<0.0001$) further supporting this hypothesis. In parallel with this study, KSHV-inoculated HUVEC, seeded at $3x10^4$cells/well prior to inoculation, were assayed for matrix deposition and cell density. The absorbance values

for collagen IV and fibronectin deposited by inoculated cultures were comparable to those for untreated HUVEC at the same cell density but for laminin were lower with KSHV inoculation **(Figure 5.3B)**. Thus the observed reduction in laminin deposition by inoculated cultures was not an artifact of differences in cell density.

Having identified an effect on protein deposition during the four days immediately after KSHV inoculation, I tested whether this change extended to later timepoints, relevant to the modulation of endothelial cell migration seen at day-seven. To investigate this, untreated and KSHV-inoculated HUVEC were cultured until day-seven post-inoculation before seeding for ELISA. Four-day basement membranes generated between days seven and eleven also showed a reduction in laminin deposition with inoculation whilst amounts of collagen IV and fibronectin were not altered **(Figure 5.4)**, implying that a reduction in deposition of laminin was maintained for a long period after inoculation.

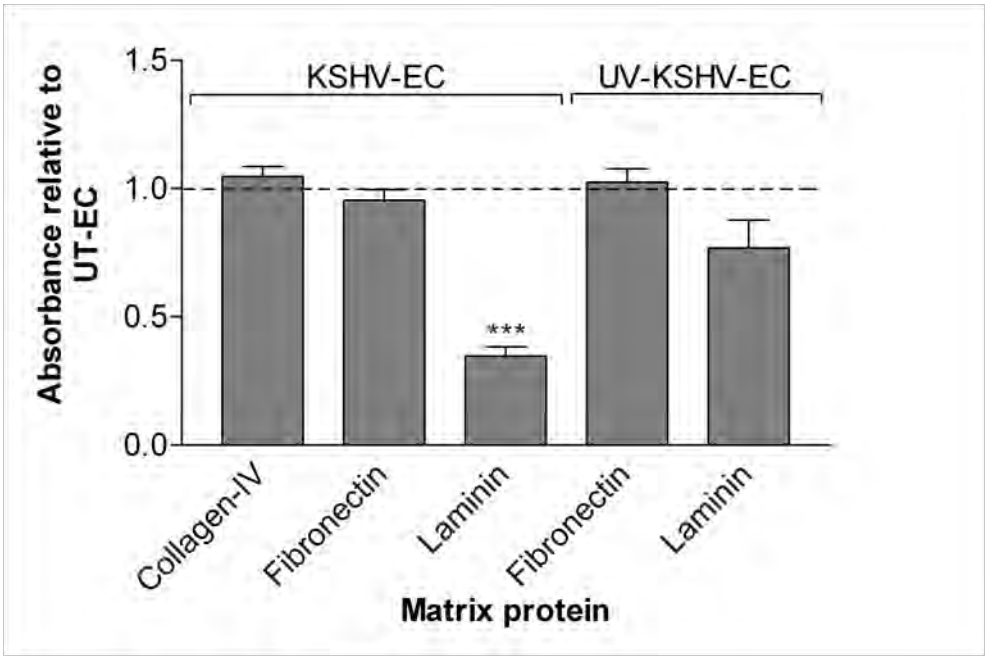

Figure 5.2: Effect of KSHV inoculation on the protein content of sub-endothelial matrix.
HUVEC were plated in 96-well plates and inoculated with KSHV (KSHV-EC), UV-irradiated KSHV (UV-KSHV-EC) or were left untreated (UT-EC). Cells were stripped from the sub-endothelial matrix on day-four post-inoculation using detergent lysis buffer. The matrix composition was analysed by ELISA with absorbance readout at 490nm for each protein. Absorbance values for KSHV-EC and UV-KSHV-EC cultures are reported relative to values for UT-EC. Data are mean ± SEM for three to eight experiments. *** = $P<0.0001$ compared to value of 1 by t-test.

Figure 5.3: Relationship between cell density and matrix protein deposition.

Untreated HUVEC (UT-EC) were plated in 96-well plates at densities between 0.3×10^4cells/well and 3×10^4cells/well. Each well had a growth area of $32mm^2$. Cells were stripped on day-four post- seeding using detergent lysis and the amounts of **(A)** collagen IV, **(B)** fibronectin and **(C)** laminin present in the sub-endothelial matrix analysed by ELISA with absorbance readout at 490nm. In parallel, cells at each density were fixed and nuclear stained using bisbenzimide (2μg/ml). Absorbance was plotted against cell density for each protein (filled squares). Trend lines were fitted by linear regression. In parallel, HUVEC were plated in 96-well plates at 3×10^4cells/well and inoculated with KSHV (KSHV-EC) immediately following adherence. The four-day sub-endothelial matrix was analysed by ELISA and cell density determined. Data points for absorbance and cell density of KSHV-EC are plotted superimposed on the scatter plots for UT-EC for reference but do not contribute to calculation of the trend lines for UT-EC. Data are the pooled results of two experiments.

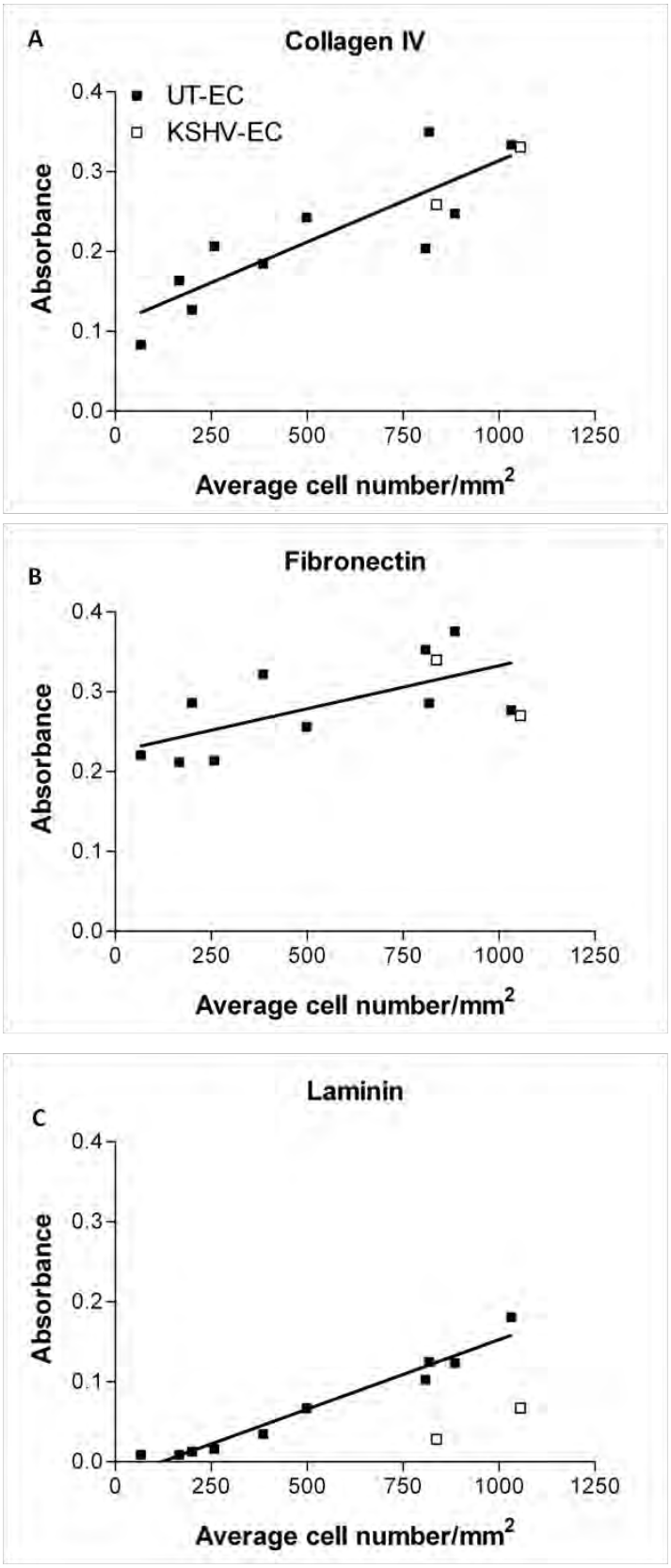
A
Collagen IV
UT-EC
KSHV-EC
Absorbance
0.0
0.1
0.2
0.3
0.4
0
250
500
750
1000
1250
Average cell number/mm2
B
Fibronectin
Absorbance
Average cell number/mm2
C
Laminin
Absorbance
Average cell number/mm2

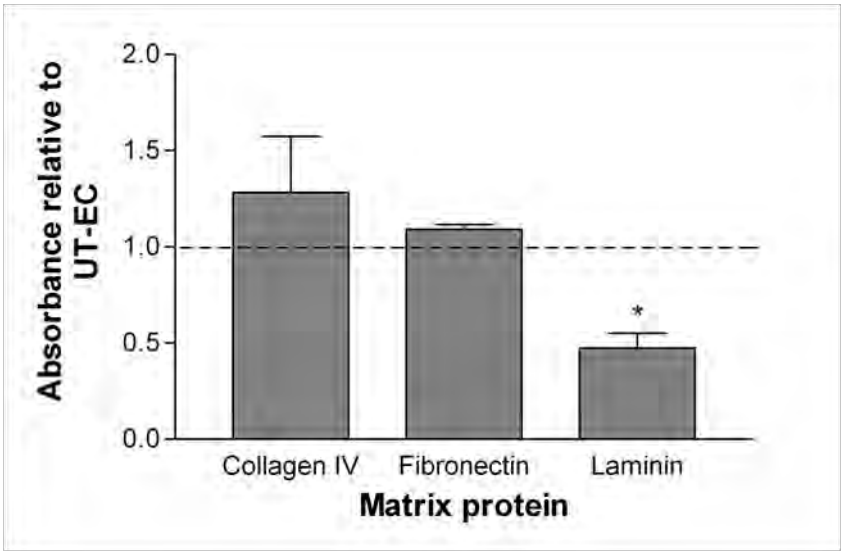

Figure 5.4: Effect of long-term KSHV inoculation on the protein content of sub-endothelial matrix.

KSHV-inoculated (KSHV-EC) and untreated (UT-EC) HUVEC cultures were transferred to wells of a 96-well plate on day-seven post-inoculation. Cells were cultured for four days then stripped from the sub-endothelial matrix using detergent lysis. The matrix composition was analysed by ELISA with absorbance readout at 490nm for each protein. Absorbance is reported for KSHV-EC basement membrane protein deposition relative to UT-EC. Data are mean ± SEM for three experiments. * = $P<0.05$ compared to value of 1 by t-test.

To assess the possibility that a secreted factor was responsible for the decrease in laminin, sub-endothelial matrix generated by four-day untreated HUVEC cultures was incubated in the presence of supernatants taken from untreated or KSHV-inoculated cultures. Since culture media were routinely changed every two days, 0-2 and 2-4 day post-inoculation culture supernatants were tested separately. Neither supernatant reduced the laminin or collagen IV content **(Figures 5.5A, B)**.

Whilst the above suggested that a secreted factor was not responsible for KSHV-induced reductions in laminin, it was considered that the responsible factor(s) might have been at insufficient concentration in the culture supernatant or that a membrane-bound protease might be responsible. To further investigate the role of proteases, broad spectrum MMP and serine protease inhibitors, Galardin and Aprotinin respectively, and an MMP2/MMP9 selective inhibitor, were included in the culture media of untreated and KSHV-inoculated cultures throughout the deposition phase. None of these treatments impaired the reduction in laminin that occurred with KSHV inoculation **(Figure 5.6)** supporting the conclusion that secreted or membrane-presented enzymes did not reduce laminin deposition.

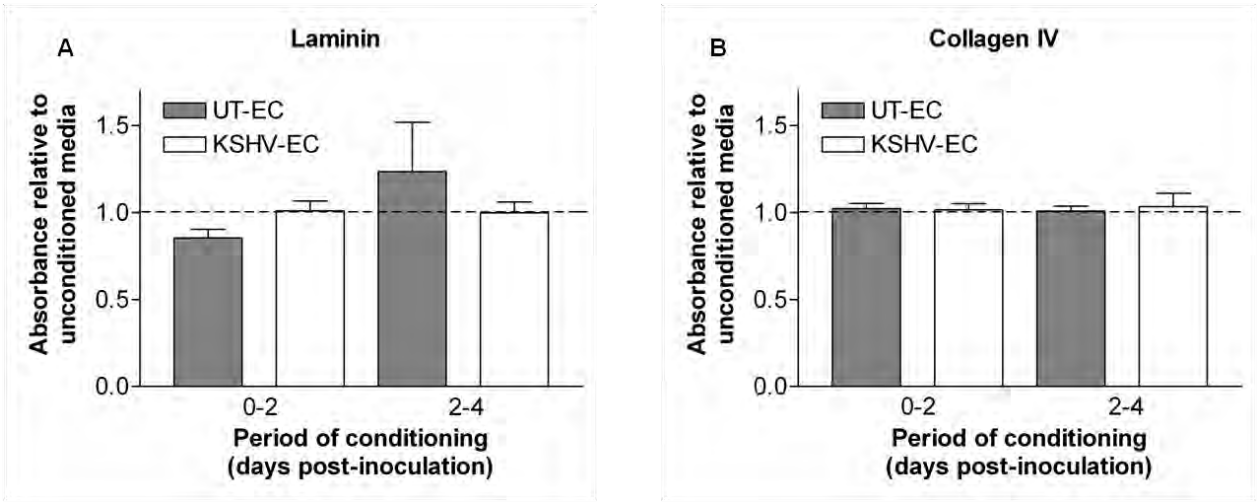

Figure 5.5: Effects of culture supernatants from KSHV-inoculated cultures on the composition of previously deposited sub-endothelial matrix.

Four-day sub-endothelial matrices deposited by untreated HUVEC were exposed for two days to two-day supernatants (days 0-2 or 2-4 post-inoculation) collected from KSHV-inoculated (KSHV-EC) or untreated (UT-EC) HUVEC, before analysis of **(A)** laminin or **(B)** collagen IV content by ELISA. Absorbance at 490nm is reported for matrices exposed to culture supernatants relative to that for matrices treated with unconditioned medium. Data are mean ± SEM for two experiments.

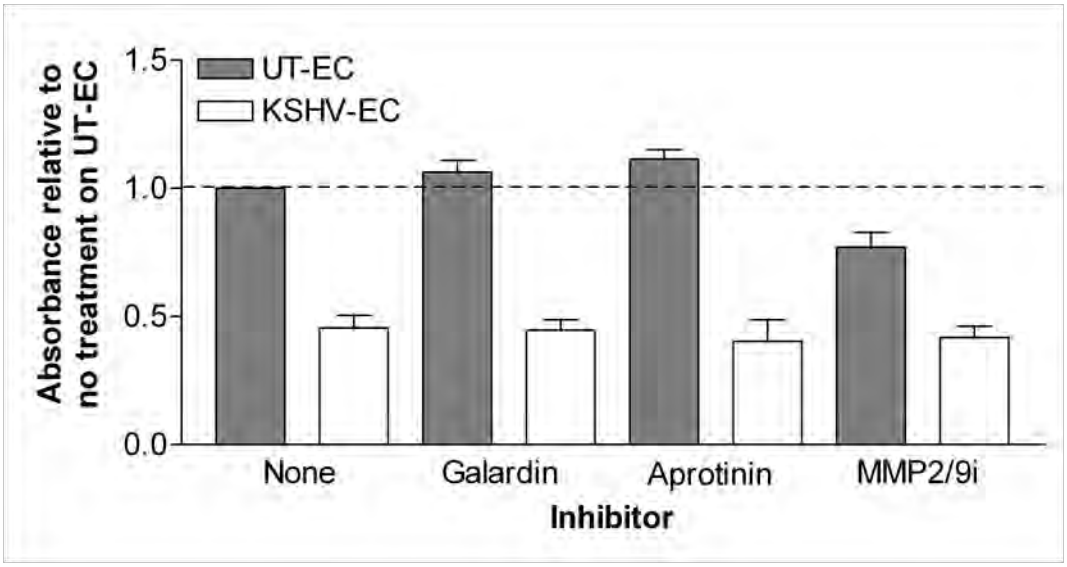

Figure 5.6: Effects of inhibitors of matrix-metalloproteinases or serine proteases on KSHV-induced suppression of laminin deposition in the sub-endothelial matrix.

HUVEC were plated in 96 well plates and inoculated with KSHV immediately following adherence (KSHV-EC) or were left untreated (UT-EC). Cells were cultured during the four-day matrix deposition period of the ELISA assay for laminin in the presence or absence of the broad-spectrum matrix-metalloproteinase (MMP) inhibitor Galardin (10μM), the serine protease inhibitor Aprotinin (50mg/ml) or a selective inhibitor of MMP2/MMP9 (MMP2/9i) (50μM). Endpoint absorbance at 490nm is reported relative to that for the UT-EC matrix treated with fresh medium. Data are mean ± SEM for three experiments.

Since protease activity did not appear responsible for the reduction in laminin, it was hypothesized that KSHV infection might impair the production or secretion of the laminin constituent chains. Flow cytometry for intracellular laminin was used to examine this since a block in secretion would be reflected by intracellular accumulation and therefore an increase in intracellular staining, whilst either a decrease in production, or the targeted degradation of intracellular stores, would cause a decrease in staining. However, neither KSHV-infected nor non-infected cells showed an altered intracellular laminin content compared to untreated HUVEC by flow cytometry **(Figure 5.7)**.

It is possible however, that intracellular stores were maintained at a constant level if production and secretion were both reduced. For this to occur, regulation would be evident at the level of transcription or translation.

To determine whether laminin transcription was affected by the virus, semi-quantitative reverse transcription polymerase chain reaction (RT-PCR) primers were designed to amplify transcripts of each of the α, β and γ laminin chains present in the main endothelial laminins (laminins 411, 511, 421 and 521). β-actin as an endogenous control and KSHV-ORF71/vFLIP as an infection control were amplified in parallel using primers already available. Titration of template cDNA confirmed that differences in the amount of template present could be resolved by this method when the number of amplification cycles was optimal as illustrated for β-actin **(Figure 5.8)**. The number of cycles for each pair of primers was such that the band generated on the ethidium bromide gel did not saturate the image, permitting densitometry of the banding pattern. For example, for β-actin, using 0.5μl cDNA per reaction, the optimum cycle number was

between 20 and 25 cycles. I settled for 21 cycles for β-actin. Overall, no change in the transcript level was detected for any of the laminin chains studied **(Figure 5.9)**.

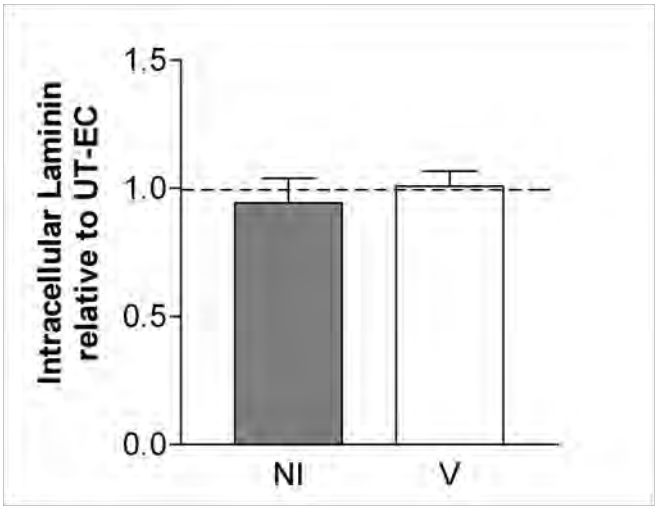

Figure 5.7: Effect of KSHV inoculation on intracellular levels of laminin.
Intracellular levels of laminin were assessed by flow cytometry for KSHV-infected (V) (GFP positive), non-infected (NI) (GFP negative) and untreated (UT-EC) HUVEC. The median fluorescence of staining is expressed for the V and NI cell populations relative to the level for UT-EC. Data are mean ± SEM for four experiments.

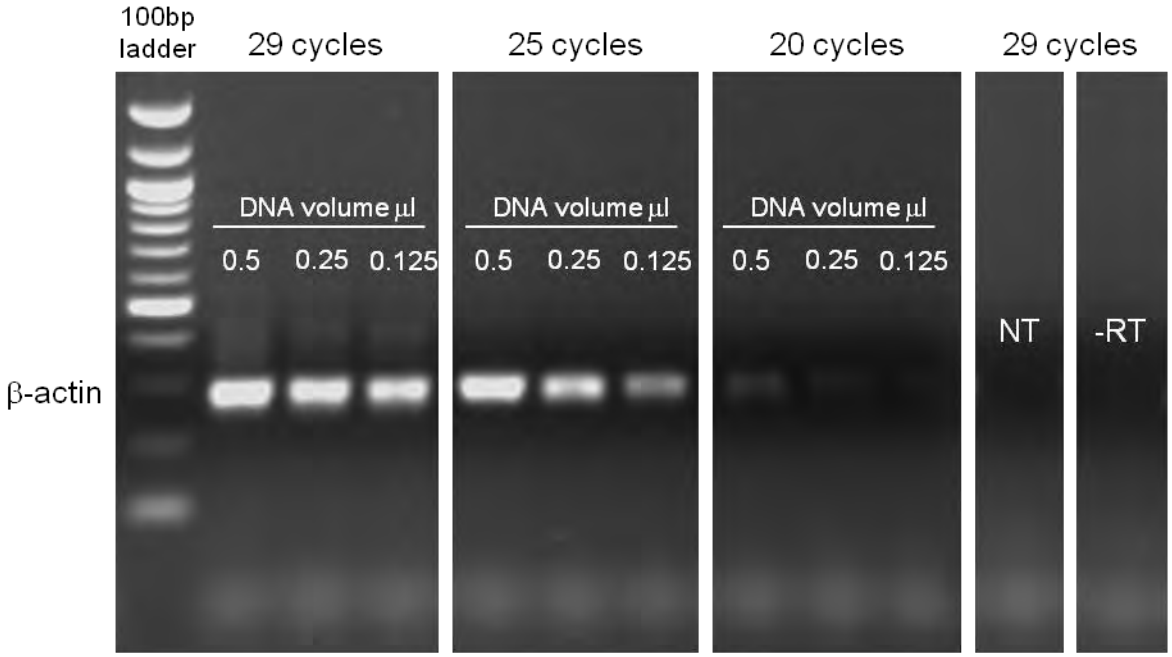

Figure 5.8: Effect of the number of PCR amplification cycles upon the resolution of a cDNA titration when analysed by ethidium bromide gel electropheresis.

A two-fold dilution series of cDNA template was prepared and added to the PCR reaction mixture such that 0.5, 0.25 and 0.125µl cDNA volumes were included per 25µl reaction. Samples were amplified for 20, 25 or 29 PCR cycles. No products were detected for the no template (NT) and no reverse transcriptase (-RT) cDNA controls with 29 cycles of amplification. This confirmed the specificity of the PCR for mRNA and/or absence of DNA contamination in the preparation.

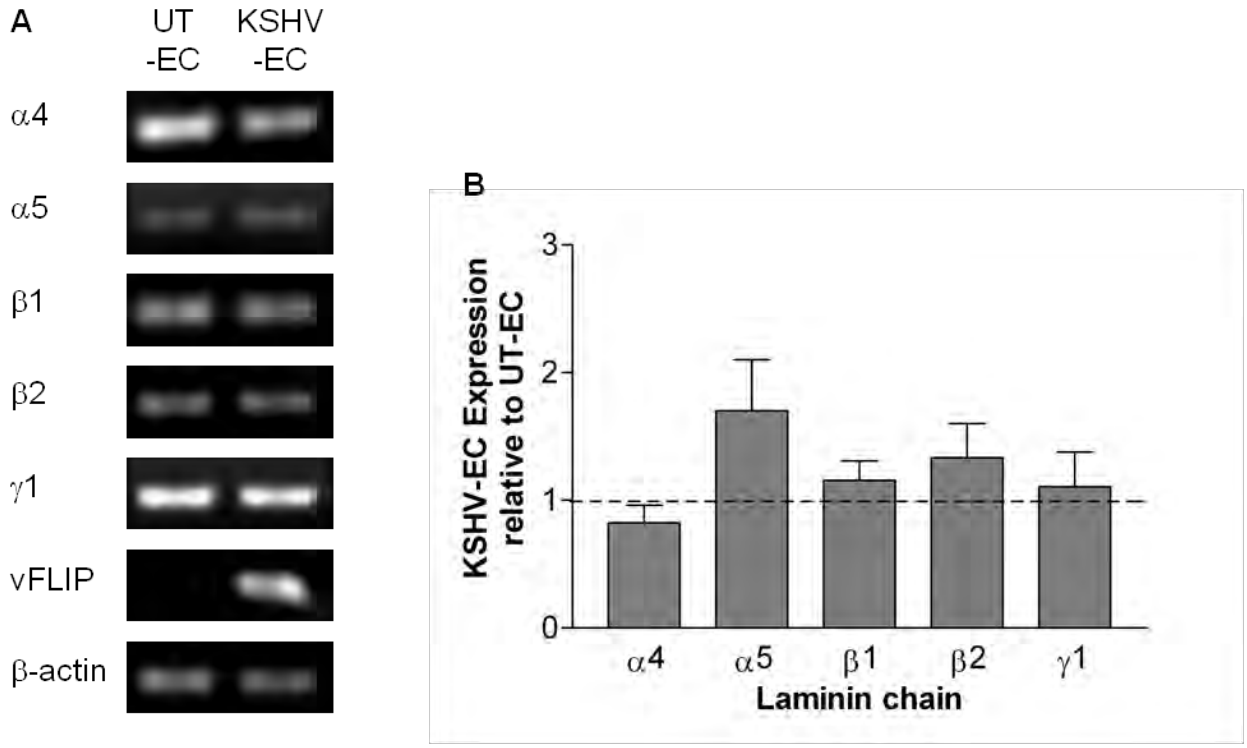

Figure 5.9: Effect of KSHV inoculation on transcript levels of endothelial laminin subunits.

Total RNA was isolated from untreated (UT-EC) and KSHV-inoculated (KSHV-EC) cultures on day-four post-inoculation and mRNAs for the laminin chains that constitute laminins 411, 511, 421 and 521 (α4, α5, β1, β2 and γ1 chains) amplified by PCR. β-actin and KSHV-ORF71/vFLIP mRNAs were amplified by PCR in parallel as endogenous and infection controls respectively. **(A)** Ethidium-bromide gel electrophoresis photographs for one HUVEC donor, representative of three. No template and without reverse transcriptase controls gave no detectable bands by ethidium bromide gel electrophoresis (not shown). **(B)** Densitometry of ethidium-briomide gel electrophoresis photographs. Normalisation is to β-actin. Expression is reported for KSHV-EC relative to UT-EC. Data are mean ± SEM for three experiments.

The laminin antibody used for ELISA was a monoclonal antibody generally assumed to give a measurement of total laminin. It was raised against the P1 pepsin-resistant fragment of human placental laminin but the precise location and conformation of the epitope recognised is not known. To investigate further the reduction in laminin, referred to as laminin-P1 in the remainder of this thesis, chain-specific antibodies against the main endothelial laminin alpha chains, laminin-α4 and laminin-α5, were used. In contrast to laminin-P1, ELISA for laminin-α4 identified a three-fold increase in the laminin-α4 chain with KSHV-inoculation. The response was much reduced using UV-irradiated KSHV **(Figure 5.10A)**. In addition, flow cytometry for intracellular laminin-α4 showed a small but statistically significant increase in intracellular laminin-α4 in KSHV-infected HUVEC **(Figure 5.11)**. KSHV infection also appeared to increase laminin-α5 deposition **(Figure 5.10B)** although the absorbance values for laminin-α5 were very low.

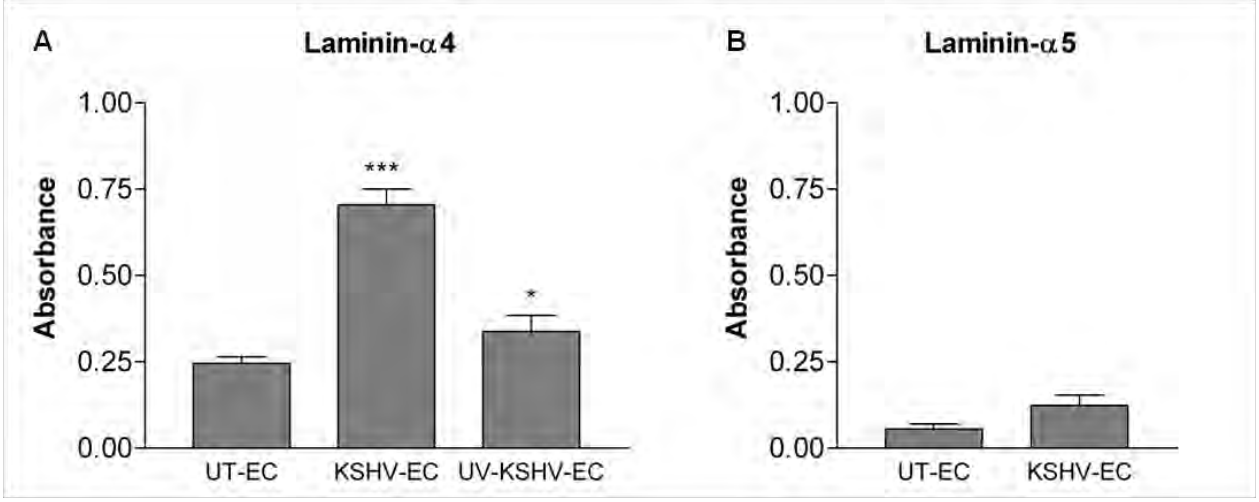

Figure 5.10: Effect of KSHV inoculation on the laminin-alpha chain content of sub-endothelial matrix.

HUVEC were plated in 96-well plates and once adhered were inoculated with KSHV (KSHV-EC), UV-irradiated KSHV (UV-KSHV-EC) or were left untreated (UT-EC). Cells were stripped from the sub-endothelial matrix on day-four post-inoculation using detergent lysis and **(A)** laminin-α4 chain or **(B)** laminin-α5 chain contents of the matrix analysed by ELISA using chain specific antibodies. Absorbance at 490nm is reported. Data are mean ± SEM for four-to-six experiments (A) or two experiments (B). * = $P<0.05$; *** = $P<0.0001$ by paired t-tests comparing to UT-EC.

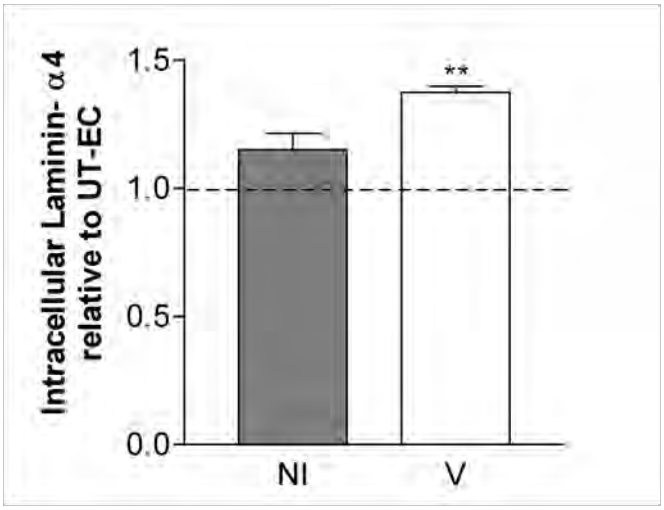

Figure 5.11: Effect of KSHV inoculation on intracellular levels of the laminin-α4 chain. Intracellular levels of the laminin-α4 chain were assessed by flow cytometry for KSHV-infected (V) (GFP positive), non-infected (NI) (GFP negative) and untreated (UT-EC) HUVEC. The median fluorescence of staining is expressed for the V and NI cell populations relative to the level for UT-EC. Data are mean ± SEM for three experiments. ** = $P<0.01$ compared to value of 1 by t-test.

5.2.3 The effect of deposited matrices on endothelial cell migration

I hypothesised that the changes to sub-endothelial matrix laminins might underlie the enhanced motility of cells within KSHV-inoculated cultures. To test this, wound recovery assays were carried out on matrices deposited by KSHV-inoculated and untreated cultures. The wound recovery method was chosen since, based on previous studies (Butler et al., 2005) a basement membrane could be generated on plates then stripped and used as a substrate for newly deposited HUVEC.

Untreated or KSHV-inoculated HUVEC cultures were seeded in wound recovery culture inserts for 24hours to deposit matrix proteins. The HUVEC were removed by cell lysis and fresh, untreated HUVEC seeded on to the matrix for six hours, before inserts were removed and wound recovery analysed. A short seeding period was used to minimise deposition of basement membrane by the untreated endothelial cells. Recovery was tested in parallel on uncoated plastic for comparison. There was a trend toward increased recovery on deposited matrices compared to uncoated plastic, with recovery consistently greater on matrix from KSHV-inoculated cultures than on plastic. However, there was no significant difference between recovery on the KSHV-inoculated and untreated cell matrices (**Figure 5.12**).

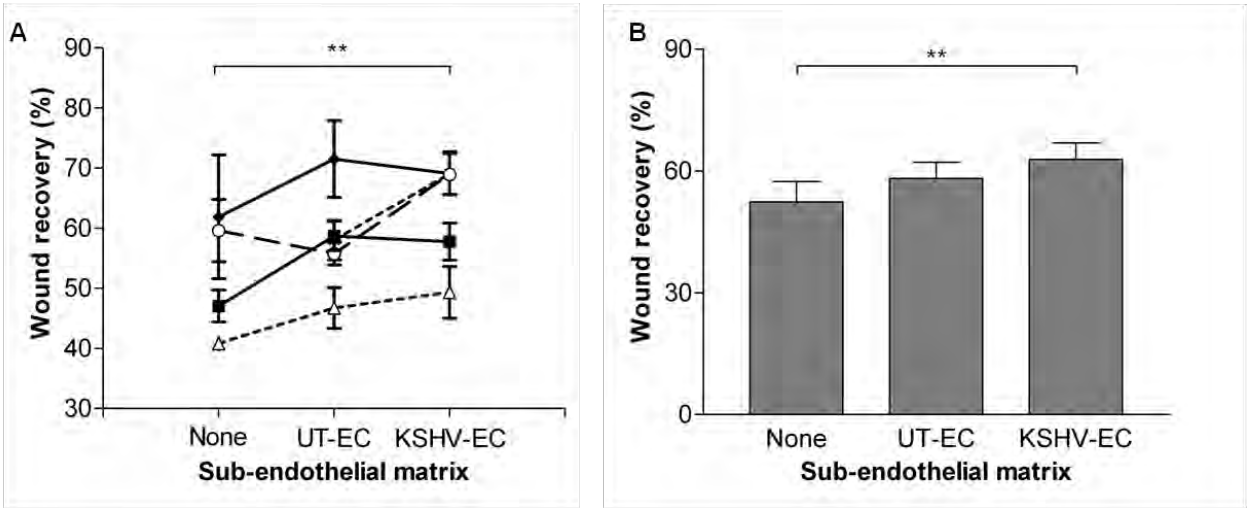

Figure 5.12: Effects of matrix proteins, deposited by KSHV-inoculated (KSHV-EC) or untreated (UT-EC) HUVEC cultures, upon HUVEC migration.

KSHV-inoculated (KSHV-EC) and untreated (UT-EC) HUVEC were seeded in wound recovery culture inserts on day-six post-inoculation, allowed to deposit matrix proteins for 24hours then stripped using detergent lysis. Untreated HUVEC were plated on the matrices and wound recovery in 18hours was measured for each surface. Results were also compared to migration on uncoated plastic-ware (None). These control inserts received culture media during the deposition phase and received lysis buffer and washings in parallel with matrix-protein coated inserts prior to seeding of cells for migration analysis. **(A)** Each line represents the matched results for a different experiment. Error bars represent the SEM for duplicate or triplicate wounds in an experiment. **(B)** Data in A illustrating the mean and ±SEM for the four (None) or five (UT-EC and KSHV-EC) experiments. ** = $P<0.01$ by paired t-test.

5.2.4 The effect of reducing laminin-α4 chain expression on endothelial cell migration

To study further the involvement of KSHV-induced modulation of the basement membrane on migration, in particular the substantial (three-fold) upregulation of laminin-α4, the effect of knocking down laminin-α4 using siRNA on transmigration was tested. The transmigration assay was chosen for its greater resolution, given no requirement for pre-deposition of a matrix.

Three siRNA duplexes to laminin-α4 were purchased (A, B and C) and tested in preliminary experiments at 5nM and 50nM concentrations. 48hours following transfection, cells were stained for intracellular laminin-α4 expression and analysed by flow cytometry. siRNA duplexes A and C decreased intracellular laminin-α4 48hours post-transfection but duplex B did not (**Figure 5.13**). Since duplex C gave the greatest knockdown it was chosen for optimisation in subsequent preliminary experiments. Duplex B was also pursued as a possible control for the study.

The duration of transmigration assays was 48hours **(Chapter 4, section 4.2.1)** and the assays began immediately upon seeding cells into the transwell chamber; thus knockdown of laminin-α4 had to be established prior to transferring cells to the transwell chambers and had to be sustained throughout the 48hour transmigration period. To satisfy these requirements, untreated and KSHV-inoculated HUVEC were transfected twice (double transfection) in subsequent experiments. The first transfection was on the day prior to seeding the cells into the transmigration assay and was performed in order to reduce laminin-α4 in cells before they entered the functional stage of the assay. The second was immediately before seeding the cells

into the transmigration assay and was performed in order to maintain laminin-α4 knockdown for the full 48hours.

Using this protocol, transfection with duplex C gave approximately 70% reduction in intracellular laminin-α4, combination of duplex A with duplex C gave no further reduction, and duplex B did not give significant reduction (**Figure 5.14A**). ELISA on two-day sub-endothelial matrices, for cells plated immediately following the second transfection confirmed that a reduction in laminin-α4 deposition was achieved with duplex C (**Figure 5.14B**). Using duplexes C and A together did not improve the efficiency of knockdown judged by deposited laminin. Therefore it was decided to use duplex C alone in the transmigration assays. Duplex B and a non-specific control siRNA were also used in order to verify that any effects of knockdown were specific.

Using the optimal conditions for knockdown of laminin-α4, transmigration assays were performed. Flow cytometry and ELISA confirmed knockdown of laminin-α4 for untreated, KSHV-infected and non-infected cells treated with duplex C (**Figures 5.15A, B**). However, although the deposition of laminin-α4 by siRNA-treated-KSHV-inoculated cultures was reduced to a level close to that produced by untreated control HUVEC using duplex C siRNA, their transmigration rates were not reduced (**Figure 5.15C**).

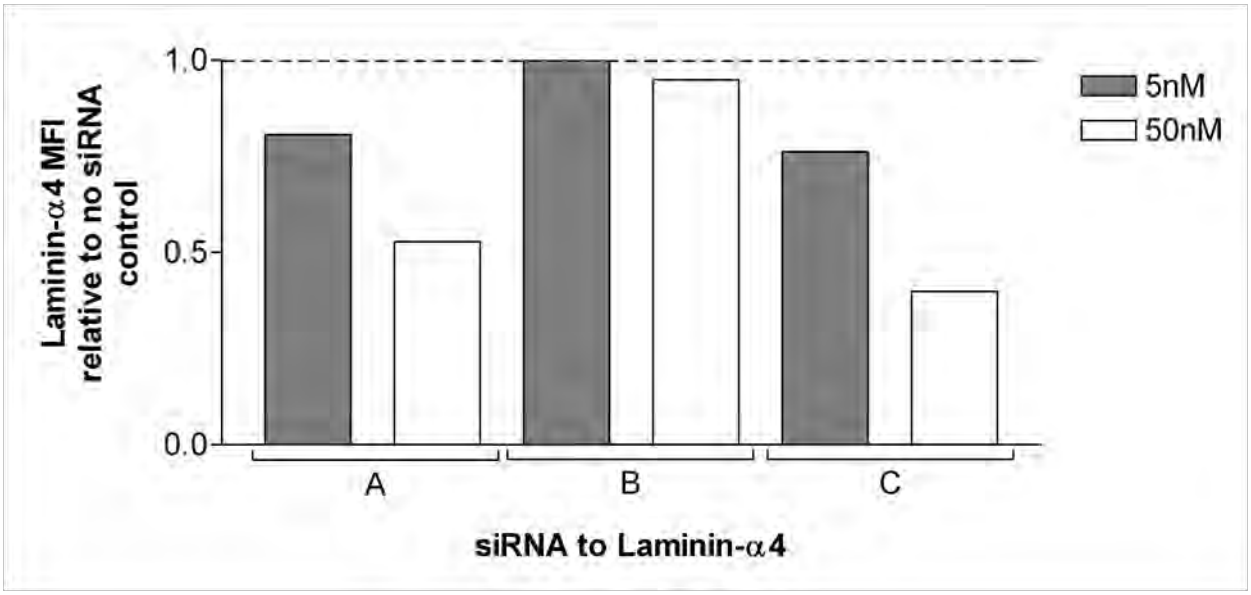

Figure 5.13: Comparison of the efficiency of siRNA duplexes in knockdown of the laminin-α4 chain in HUVEC.

HUVEC were transfected with three different 'off the shelf' siRNA duplexes (A, B and C) using RNAiMAX lipofectamine reagent as the carrier. Duplexes were at final concentrations of 5 or 50nM. Intracellular levels of laminin-α4 were measured by flow cytometry 48hours post-transfection. The median fluorescence intensity (MFI) of staining is reported relative to the value for control cells treated with lipofectamine alone. Results are from a single experiment.

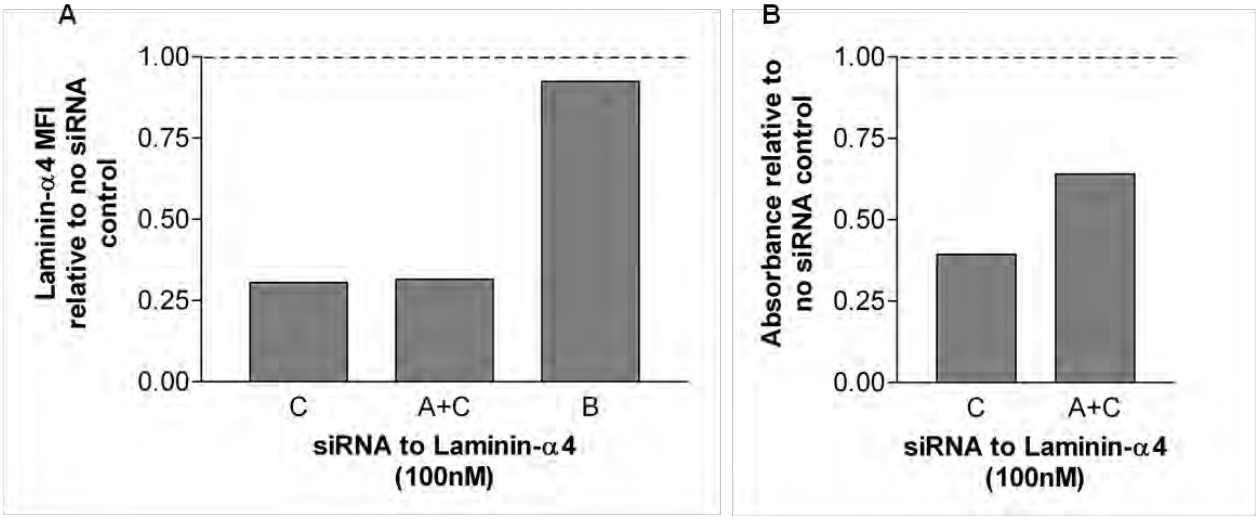

Figure 5.14: Comparison of the efficacy of siRNA duplexes used singly and in combination in knockdown of the laminin-α4 chain in HUVEC.

HUVEC were transfected with 100nM siRNA duplexes (A, B or A+C (1:1)), or lipofectamine only (no siRNA). After 24hours cells were retransfected with the same siRNAs at 100nM concentration and either transferred to 96-well plate format for ELISA or kept in culture for a further 48hours before analyzing **(A)** intracellular laminin-α4 chain levels by flow cytometry (relative to no siRNA) and **(B)** laminin-α4 chain deposition by ELISA (relative to no siRNA). In B, to account for possible differences in cell number across treatments, parallel samples were analysed for fibronectin, and absorbance due to laminin was normalised to the absorbance due to fibronectin. Data are from a single experiment.

Figure 5.15: Effects of laminin-α4 chain siRNA on laminin-α4 content and deposition, and on transmigration for KSHV-inoculated (KSHV-EC) and untreated (UT-EC) HUVEC.
HUVEC were transfected with lipofectamine only (no siRNA), or 100nM final concentration of either negative control siRNA (Control), or duplex B or duplex C on day six-post inoculation and were retransfected on day-seven. Cells were then either left in culture; transferred to wells of a 96-well plate; or transferred to 24-well format 8μm pore transwell chamber filters for analysis after 48hours of: **(A)** intracellular laminin-α4 chain content**; (B)** laminin-α4 chain deposition or **(C)** transmigration. Data are mean ± SEM for three experiments (A and C) or two or three experiments (B). * = $P<0.05$, ** = $P<0.01$ by paired t-test. In B, to account for possible differences in cell number across treatments, parallel samples were analysed for fibronectin, and absorbance due to laminin was normalised to the absorbance due to fibronectin.

A

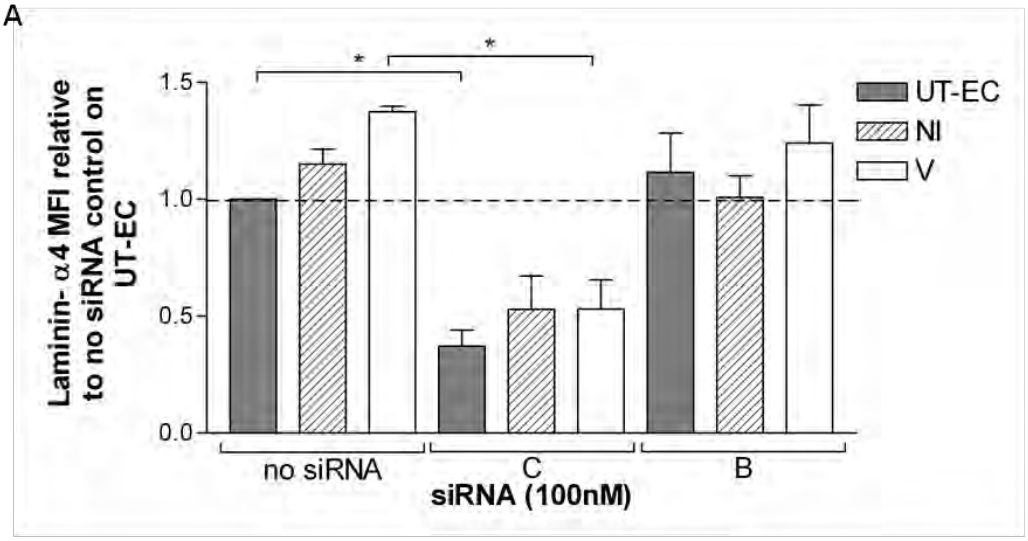
Laminin- α4 MFI relative to no siRNA control on UT-EC
1.5
1.0
0.5
0.0
*
*
UT-EC
NI
V
no siRNA
C
B
siRNA (100nM)

B

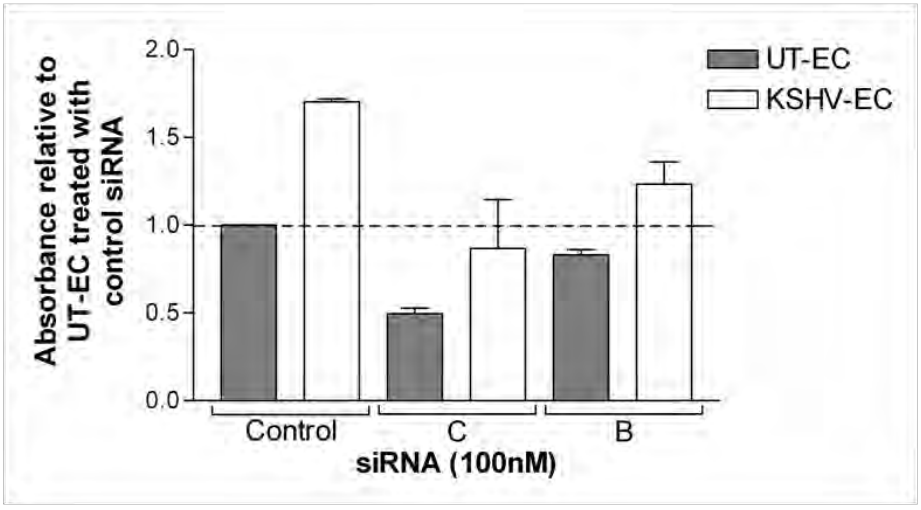
Absorbance relative to UT-EC treated with control siRNA
2.0
1.5
1.0
0.5
0.0
UT-EC
KSHV-EC
Control
C
B
siRNA (100nM)

C

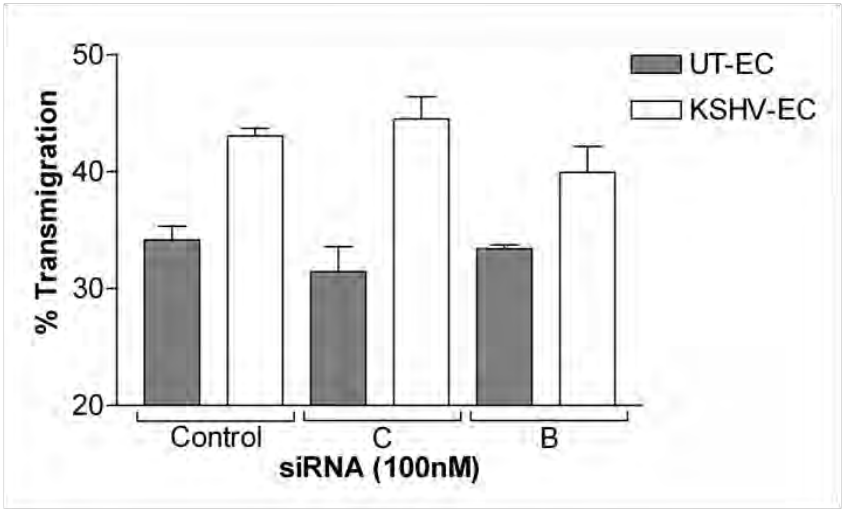
% Transmigration
50
40
30
20
UT-EC
KSHV-EC
Control
C
B
siRNA (100nM)

5.2.5 The effect of KSHV infection on the expression of endothelial cell surface integrins

Transmembrane integrin heterodimers provide the functional connections between the extracellular matrix and the cell cytoskeleton and their binding regulates cell migration. Accordingly, I examined whether KSHV inoculation altered expression of surface integrins. KSHV-inoculated and untreated HUVEC were surface-stained using a panel of antibodies against integrin subunits (β1, β3, α2, α6) or heterodimers (αvβ3, α3β1) and the intensity of staining was analysed by flow cytometry **(Figures 5.16 and 5.17)**. The greatest change observed was an approximate doubling in integrin α6 on KSHV-infected cells. There were smaller increases (~25%) in integrins α3β1 and αvβ3 on the non-infected cells, but not infected cells. KSHV inoculation did not alter expression of integrins β1, β3 or α2 on KSHV-infected or non-infected HUVEC compared to untreated controls **(Figure 5.17)**.

I postulated that increased integrin α6 expression might contribute to preferential transmigration of KSHV-infected cells. To test this hypothesis, transmigration assays were performed in the presence of a function-blocking antibody against integrin α6. The antibody did not affect the transmigration of either untreated or KSHV-inoculated cultures although the difference between them was lost **(Figure 5.18)**.

.

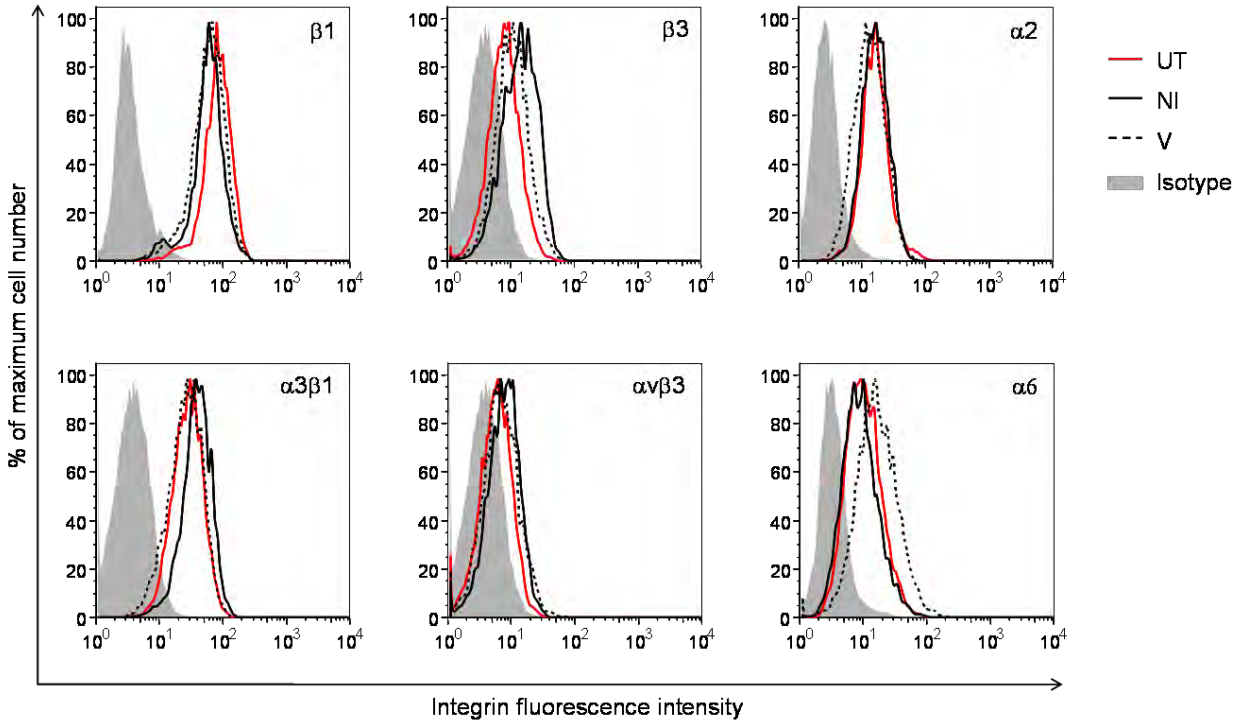

Figure 5.16: The effect of KSHV inoculation upon the HUVEC surface-integrin expression profile.

KSHV-inoculated (KSHV-EC) and untreated (UT) HUVEC cultures were stained on day-seven post-inoculation for their surface expression of the integrin subunits/heterodimers: β1, β3, α2, α3β1, αvβ3 and α6. KSHV-infected (V) cells were distinguished from non-infected (NI) cells within KSHV-EC monolayers on the basis of GFP positivity. Representative histograms for integrin staining of UT, V and NI.

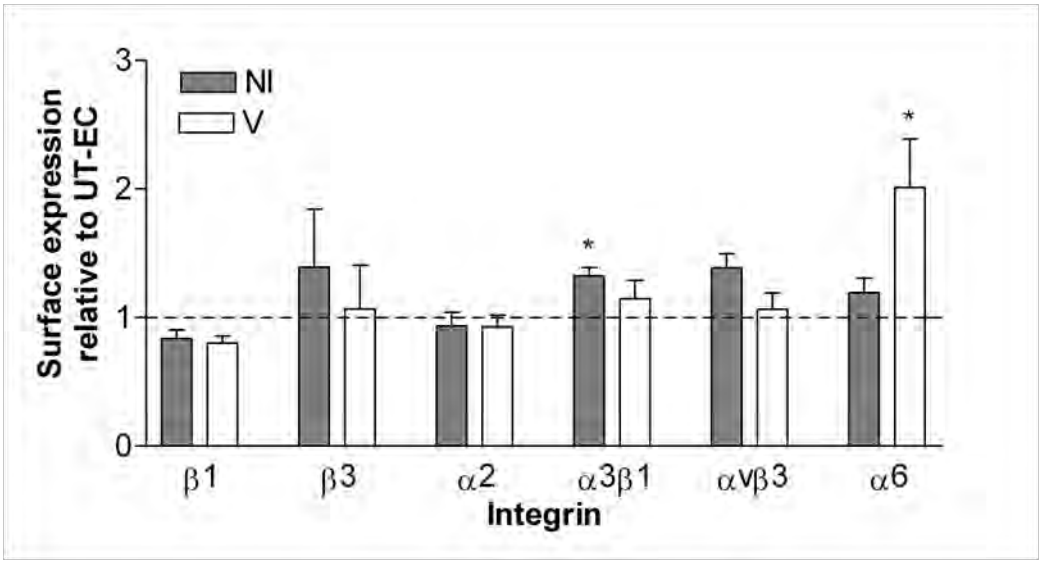

Figure 5.17: The effect of KSHV inoculation upon the HUVEC surface-integrin expression profile.

KSHV-inoculated (KSHV-EC) and untreated (UT) HUVEC cultures were stained on day-seven post-inoculation for their surface expression of the integrin subunits/heterodimers: β1, β3, α2, α3β1, αvβ3 and α6. KSHV-infected (V) cells were distinguished from non-infected (NI) cells within KSHV-EC monolayers on the basis of GFP positivity. Integrin expression on V and NI was measured in terms of median fluorescent intensity and expressed relative to expression on UT. Data are mean ± SEM for three-to-six experiments. * = $P<0.05$ compared to value of 1 by *t*-test.

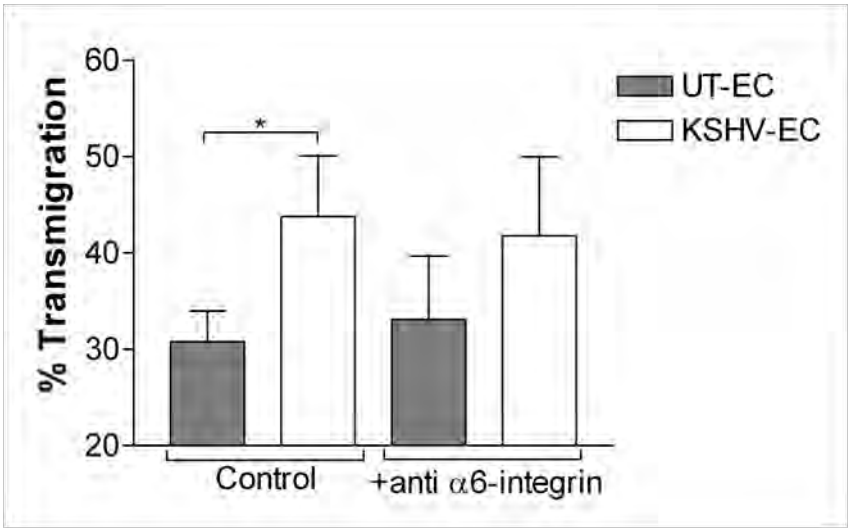

Figure 5.18: Effect of blocking integrin α6 on KSHV-enhanced transmigration of HUVEC. KSHV-inoculated (KSHV-EC) and untreated (UT-EC) HUVEC were plated into 8μm pore transwell culture inserts on day-seven post-inoculation and the percentage transmigration after 48hours examined by microscopy for cells in the presence or absence of a function-blocking antibody against integrin α6 (10μg/ml). Data are mean +/- SEM for three experiments.

5.3 DISCUSSION

In vivo, a thin sheet-like network of protein fibres, termed the basement membrane, interfaces the endothelium and underlying extracellular matrix and has critical regulatory effects upon the functions of the endothelium, including cell migration (Hamill et al., 2009; Kruegel and Miosge, 2010). In this chapter the effect of KSHV infection upon the composition of the vascular sub-endothelial matrix generated *in vitro* was studied by ELISA and subsequently the matrix was tested for its role in the enhancement of cell migration with KSHV infection. Alterations to the cell surface profile of integrin receptors of basement membrane proteins were also examined and tested for involvement in KSHV-increased cell migration. Clear changes in deposition of laminin-P1, and laminin-α4 and upregulation of α6 integrin surface expression were found with KSHV infection but none of these changes was demonstrated to underlie KSHV-enhanced cell migration.

The predominant proteins of the endothelial basement membrane include collagen IV, fibronectin and laminins. Whilst KSHV inoculation modulated the laminin composition, reducing laminin-P1 and increasing amounts of the laminin-α4 chain it did not alter the abundance of either collagen IV or fibronectin **(Figure 5.2)**. Inoculating with UV-inactivated KSHV, laminin-P1 was not altered and the upregulation of laminin-α4 deposition was much reduced **(Figures 5.2 and 5.10)**, confirming that KSHV infection and gene expression underlie these responses. The effects were evident for four-day matrices deposited between days zero and four post-inoculation **(Figure 5.2)** and also for two or four-day matrices started on day-seven **(Figures 5.15 and 5.4)**. Thus, the changes incurred to the sub-endothelial matrix with KSHV inoculation were chronic

rather than acute. The underlying cause for the alterations in laminin with infection remains unclear but these studies ruled out several mechanistic possibilities.

With KSHV inoculation, there was no evidence for changes in mRNA levels of any of the main endothelial laminin chains which could explain reduced trimer formation and thus reduced laminin-P1 deposition **(Figure 5.9)**. Intracellular laminin-P1 was constant across untreated, non-infected and KSHV-infected cells **(Figure 5.7)**; therefore, KSHV inoculation did not appear to suppress laminin-P1 deposition by inhibiting either its translation or secretion. However, if cells have tight control over their intracellular laminin levels, then it is possible that even under conditions of impaired secretion, intracellular laminin-P1 content was maintained. This might be achieved by the upregulation of proteasomal activity or suppression of laminin translation.

The observation that the transcription of one or more laminin chain mRNAs was not altered by KSHV inoculation was unexpected since Hong et al (2004) previously reported downregulation of laminin gene expression following KSHV infection. Titration of cDNA followed by PCR with readout of relative transcript abundance by ethidium bromide electrophoresis indicated that a three-fold difference in expression, as observed for laminin-α4 deposition by ELISA, should have been detectable by the semi-quantitative PCR method if enhanced transcription was responsible for the increase in laminin-α4 with infection; thus it is unlikely that the discrepancy between the two studies was due to insufficient sensitivity of the semi-quantitative PCR approach used in the present study.

Proteolytic degradation of deposited protein by the action of secreted proteases was an alternative hypothesis for the decrease in laminin-P1. However, exposure of normal sub-endothelial matrices to supernatants from KSHV-inoculated cultures failed to mimic the effects of KSHV inoculation **(Figure 5.5)** and adding protease inhibitors against enzymes known to act on laminins, including MMPs and serine proteases such as plasmin (reviewed by Tzu and Marinkovich, 2008) did not prevent the reduction in laminin-P1 with infection **(Figure 5.6)**. This result was surprising since the expression of a number of MMPs has been reported in KS tumour cells and KSHV infection is known to upregulate the transcriptional expression, synthesis and activity of matrix degrading proteases including: MMP1, MMP2 and MMP9 (Meade-Tollin et al., 1999; Qian et al., 2007; Wang et al., 2004b). Nonetheless, increased MMP activity would be expected to have decreased the collagen-IV and fibronectin content too (Visse and Nagase, 2003; Zeng et al., 1999) but this was not observed, suggesting that the actual mechanism by which KSHV altered sub-endothelial laminins was more selective toward laminin.

In contrast to observations for laminin-P1, the intracellular expression of laminin-α4 was increased in KSHV-infected compared to untreated cells. There was also a trend toward upregulation in non-infected cells **(Figure 5.11)**. Therefore, expression of the laminin-α4 chain may have been enhanced at the level of translation by KSHV infection. The rise in laminin-α5 deposition, also identified with KSHV infection **(Figure 5.10)**, suggested that KSHV may have altered the expression of multiple laminin chains. It might also have been interesting to examine the changes in deposition of the β and γ endothelial laminin chains individually in order to confirm whether the effect was specific to α chains but a panel of antibodies to single laminin chains was not available for the study.

Models for laminin heterotrimer formation and deposition describe trimerisation of the α, β and γ chains to precede secretion. However, when recombinant α, β and γ chains of mammalian laminin 111 were expressed singly and in all combinations, only the α chain was detected secreted into the supernatant, both as intact protein and protein cleaved in the coiled coil domain, when expressed alone. This was in contrast to the β and γ chains which remained intracellularly localised irrespective of whether they were expressed singly or together: ββ and βγ dimers formed but heterotrimerisation with the α chain was necessary for secretion. Thus for the deposition of laminins, the α chain appears to drive secretion but it might also be secreted independently (Yurchenco et al., 1997). Increased laminin-α4 chain secretion might therefore explain the opposite results obtained in the present study by ELISA using anti-laminin-P1 and anti-laminin-α4 antibodies.

Integrin α6 is a laminin-α4 binding integrin. Possibly the upregulation of integrin α6 on the surface of KSHV-infected HUVEC **(Figure 5.17)** reflected a feedback mechanism induced by the increased ligand availability. The upregulation of integrin α6 was a specific response of KSHV-infected cells and was therefore hypothesized to have a role in KSHV-enhanced transmigration but while the difference in transmigration of untreated and KSHV-inoculated cultures was not significant in the presence of a function blocking antibody to integrin α6, the reduction in enhanced transmigration was slight **(Figure 5.18)**. Thus, upregulation of integrin α6 might contribute to the mechanism that underlies KSHV-enhanced transmigration but is unlikely to be the principle factor responsible for this behavior. The assessment of the percentage of GFP positive cells on either side of the transwell chamber filter at the 48hour timepoint in the presence

and absence of an integrin α6 blocking antibody would provide further verification of the extent of involvement of this integrin in enhanced endothelial cell migration.

The absence of a convincing role for integrin α6 in this study might have reflected the cooperative actions of several laminin-binding integrins. In this regard one study identified that the addition of blocking antibodies to either integrin α3 or integrin α6 had minimal effect upon the adhesion of endothelial cells to the $G^{919-1207}$ domain of recombinant laminin-α4 (the region of laminin–α4 to which integrin-attachment had been attributed), whereas adding the antibodies in combination reduced adhesion by over 54% (Gonzalez et al., 2002). The use of multiple integrin receptors for binding laminin has also been reported by others (Lotz et al., 1990; Rabinovitz et al., 1995). Consistent with KSHV as the aetiologic agent for malignancies, elevated integrin α6 expression is reported for other lesions. This is in contrast to a number of other integrins that are downregulated; for example integrins α3, α4, α5, α7 and αv are reduced in prostate cancer (Goel et al., 2008).

Although upregulation of integrin α6 was not demonstrated to affect motility in the assays reported in this thesis, studies in the context of other cancers have implicated increased integrin α6 expression in the induction of a migratory and invasive phenotype important for angiogenesis and metastasis. There are suggestions that cleavage of integrin α6 by urokinase-type plasminogen activator may be important for promoting invasion and migration (Pawar et al., 2007) and disease progression (King et al., 2008). In addition, remodeling of the basement membrane—packing the basement membrane beneath the cell and removing it from adjacent areas—might be involved. Such promigratory roles for integrin α6 were however observed for cells grown on exogenous

laminin-rich substrates (Primo et al., 2010; Rabinovitz et al., 1995); accordingly these reports cannot be directly compared with the uncoated transwell system used in this thesis and it is possible that on laminin-rich substrates, the migration of KSHV-infected cells would also be regulated compared to untreated HUVEC in an integrin α6 dependent manner.

A promigratory function for integrin α6 is not however supported by all reports. For example one study concluded that integrin α3β1 is the predominant mediator of keratinocyte migration whereas integrin α6β4 functions to provide anchorage (Nguyen et al., 2000). In carcinogenesis, it is suggested that a major role of integrin α6 is the promotion of cell survival through activation of the PI3K-Protein kinase B (PKB) pathway leading to the induction of VEGF (Chung et al., 2002). VEGF might in fact feedback positively to upregulate integrin α6 since studies on HUVEC have shown that VEGFA and FGF-2 stimulate HUVEC expression of integrin α6 (Primo et al., 2010). In view of the latter, it is possible that induction of VEGF by KSHV infection, a previously reported response (Sivakumar et al., 2008), supported the increase in integrin α6 expression by infected cells. However, non-infected HUVEC also express receptors for VEGF. Therefore, it is predicted that an alternative stimulus, cell intrinsic or extrinsic, to which KSHV-infected cells selectively respond, upregulating integrin α6, underlies the upregulation of integrin α6 induced by KSHV infection of HUVEC.

Although the studies in this chapter did not provide a link between an upregulated integrin and enhanced migration, other integrins not screened might be altered upon KSHV infection and function in this capacity. For example, HCMV infection of endothelial cells led to upregulation of the epithelial-associated integrin αvβ6 (Tabata et al., 2008).

It is important to note here that after the research reported in this thesis was completed DiMaio et al (2011) published that latent KSHV infection of endothelial cells increased integrin β3 expression at both the mRNA and total protein levels and led to a modest increase in integrin αvβ3 surface expression. Since the effect of KSHV on integrin mRNA transcript levels was not examined in this thesis; it is not possible to compare directly the results of the two studies. Moreover, the rise in β3 protein on KSHV infected endothelial cells, reported by DiMaio et al (2011), was at the level of total protein rather than surface protein as examined in this chapter. Although DiMaio et al (2011) showed by flow cytometry an increase in surface αvβ3 on TIME cells, it was only a modest enhancement in comparison to the increase in total integrin β3 expression. Therefore, considering that the inter-experiment variability would be expected to be greater with primary HUVEC compared to the TIME cell line, when using different HUVEC donors for each experiment, it is perhaps not surprising that no overall effect of KSHV infection on integrin αvβ3 was found in the present study. However, it is also possible that different endothelial cell types respond differently and that time of observation post-infection is influential. Indeed DiMaio et al (2011) looked at 48hours post-inoculation of microvascular endothelial cells whereas the work on integrin expression in this thesis was at day-seven post-inoculation of macrovascular endothelial cells.

In their study DiMaio et al (2011) also reported enhanced FAK and Src activity in infected cells and suggested that RGD peptide-binding integrins, such as αvβ3, were necessary for the adhesion of infected cells to RGD peptide-containing proteins (fibronectin and vitronectin) and also for the formation of capillary-like structures by infected cells. For the same behaviours by untreated cells they were more dispensible. Since αvβ3 was only modestly increased on infected

cells (DiMaio et al., 2011) the activity of an integrin rather than its surface expression level might be more indicative of its role in a cell behavior such as motility, thus it would be informative to perform transmigration assays in the presence of function blocking antibodies or siRNA to a panel of integrins before ruling out their role in the phenotype of KSHV-enhanced HUVEC motility on the basis of no change in surface expression.

The alterations in laminin composition of the sub-endothelial matrix observed in this chapter invited the hypothesis that KSHV-enhanced migration is facilitated by the changes to the laminin profile. Despite the heterotrimeric structure of all laminin molecules, different patterns of laminin deposition are found in extracellular matrices generated by cultured cells (Hamill et al., 2009). It is proposed that the different organizations *in vitro*—meshworks, fibrils, rosette, punctuate or linear arrays, strings and plaques—relate to different stages in matrix formation and or differences in function, including support of migration of adhering cells. For example, laminin-322 of non-migrating human keratinocytes has a rosette pattern whereas that of migrating keratinocytes is assembled into trails (Sehgal et al., 2006). Whether such distinctions in pattern underlie differences in motility, or whether they are manifestations of differences in migratory behavior is not known (Hamill et al., 2009), but in support of regulation of migration by basement membrane pattern, matrix generated by wildtype cells was able to recover a normal migratory phenotype to abnormally migrating integrin β4-deficent cells (Sehgal et al., 2006). Disappointingly, in these studies, sub-endothelial matrix deposited by KSHV-inoculated HUVEC was unable to confer enhanced migratory behaviour to untreated HUVEC, suggesting that if matrix composition and/or organization facilitate enhanced motility, the process of depositing the altered matrix is also important.

In view of the three-fold upregulation in laminin-α4 deposition with KSHV infection, laminin-α4 was hypothesized to be a laminin chain of major importance in the mediation of KSHV-induced basement membrane protein effects on endothelial cell behaviors, which might include migration. According to the 'three arm hypothesis' for the polymerization of laminin herterotrimers, laminin-α4-containing laminins are incapable of self or co-polymerisation (Cheng et al., 1997). Hence, it is plausible that the enrichment of laminin-α4-containing laminins in KSHV-infected sub-endothelial matrix renders a matrix with a looser structure which in turn influences motility.

It was considered that if the actual process of depositing an altered matrix governs, at least in part, the propensity of cells to migrate, then reducing laminin-α4 production might prevent enhanced endothelial cell migration. However, using siRNA to knockdown laminin-α4 mRNA and reduce deposition of the laminin-α4 chain to a level similar to or lower than that detected in matrices generated by untreated HUVEC failed to inhibit KSHV-enhanced transmigration **(Figure 5.15)**. Although these data imply that laminin-α4 is not a principal determinant of the migration phenotype with infection, the compensatory effects of other laminin chains also upregulated by KSHV-infection, such as laminin-α5, or induced by laminin-α4 depletion, might have contributed to the maintenance of a normal response when laminin-α4 was depleted. Moreover, although laminin-α4 abundance was reduced using siRNA, the pattern of deposited laminin might not have been restored to that laid down by HUVEC not treated with virus, thereby facilitating maintenance of enhanced transmigration if the patterning of basement membrane proteins was a significant regulator of cell migration.

As stated above, KSHV infection also affected laminin-P1. Had cell numbers permitted, it would have been interesting to examine by ELISA whether reducing laminin-α4 also restored laminin-P1 levels as this would have provided greater insight into whether increased laminin-α4 deposition was a key determinant of KSHV-induced changes to basement membrane laminins and indicate whether the matrix laid down by inoculated cultures treated with siRNA against laminin-α4 had been brought closer in composition to that of untreated cultures. Nonetheless, even if homeostatic amounts of laminins were re-established with laminin-α4 knockdown, the patterns of assembly by inoculated cultures might have remained abnormal and affected cell migration rates.

Whilst these studies failed to demonstrate an effect of KSHV-induced modulation of basement membrane laminins upon migration rates, a number of caveats are linked to the methods used. In the wound recovery assay performed to examine the migration of untreated HUVEC on matrix deposited by untreated and KSHV-inoculated cultures (**Figure 5.12**), the matrix was stripped using detergent lysis. Although it was possible to quantify basement membrane protein constituents following lysis treatment, the impact of the detergent upon the organization of the matrix is not known. Potentially it was unwittingly disrupted and consequently the influence of the matrix was not properly tested.

A second issue was that by using culture inserts to generate the HUVEC monolayers in these assays, the sub-endothelial matrix substrate was only laid down beneath the migrating monolayer and did not coat the plastic in the region of the wound. Consequently, whilst cells within the monolayer migrated over basement membrane, cells at the wound front passed onto plastic.

Consequently, in the region of the recovering wound, untreated and KSHV-inoculated assays became essentially equivalent and whilst this assay was designed to recapitulate the original wound recovery system—where cells in the monolayer could migrate over matrix deposited between plating and the start of wound recovery but the intervening space was not coated—it was perhaps not the most discriminating of assays to address whether deposited matrix can influence migration rates.

The role of sub-endothelial matrix in underlying KSHV-enhanced two-dimensional migration might have been better resolved had it been possible to coat the intervening space with matrix. For this, multi-well plates might have been used as the culture surfaces but the culture inserts for wound recovery would not stick to the wet surface after stripping the endothelium. If coated surfaces were allowed to dry before placing the inserts into position, they would form a seal but dehydration and denaturation of the substrate with this approach was a concern as was the effect on the integrity of the matrix of pulling the insert from the plate at the start of the assay. Moreover, the low power magnification (using a 4x objective lens) meant that 12-well plates or larger would have been required with this approach in order to provide suitable optics but they were not feasible as using them too many cells were needed to generate a confluent monolayer **(section 4.2.3)**. Traditional scratch assays were therefore not an option either and were also not favoured due to the need to scratch the monolayer which might have perturbed the matrix integrity in the region of the scratch. Altogether it is felt that interrogation of a role for sub-endothelial matrix composition and structure was limited in the present studies by technical constraints.

In summary, the effect of KSHV infection upon the composition of the sub-endothelial matrix of basement membrane proteins was examined in this chapter. The virus had a profound impact on the laminin component but had no effect on the abundance of either collagen IV or fibronectin. Laminin-P1 was reduced but there was three-fold upregulation of the laminin-α4 chain. In consort, increases in the surface expressions of laminin-α4 binding integrins were identified. Most notable was a selective rise in integrin α6 on KSHV-infected cells. Roles for these changes to the sub-endothelial matrix or integrin α6 expression in KSHV-enhanced HUVEC migration were not found using the techniques available but this does not rule out their contribution to the mechanism. With regard to the sub-endothelial matrix, homeostasis of the laminin component, both its content and pattern, was unlikely to have been attained with knockdown of the laminin-α4 chain alone, and thus a structure supportive of enhanced cell migration was maintained, possibly involving compensatory upregulation of other laminin-α chains. Such dramatic changes to the basement membrane composition are unlikely to be without functional influence in KSHV-related malignancies and are worthy of further investigation. For example, modulation of basement membrane might lead to the formation of vessels with a primitive architecture and support inflammatory cell recruitment contributing to the generation of the inflammatory component that is a hallmark of KS lesions.

CHAPTER SIX

EFFECT OF KSHV INFECTION UPON THE ENDOTHELIAL CELL ACTIN CYTOSKELETON AND FOCAL ADHESIONS

6.1 INTRODUCTION

Cell migration occurs in response to chemotactic, haptotactic and mechanotactic stimuli and is mediated by cyclical changes to the polymerization state and organization of the actin cytoskeleton. Cells attach to their underlying substrate via transmembrane integrin receptors and complexes of proteins called focal adhesions assemble at the intracellular tails of these integrins to link the extracellular matrix to the intracellular actin cytoskeleton. The number, size and distribution of focal adhesions might also influence migration rates. Since increased transmigration and rates of wound recovery had been identified with KSHV inoculation, an effect of the virus on the organization of the actin cytoskeleton and on focal adhesions was investigated in this chapter using confocal microscopy.

6.2 RESULTS

In these studies, fluorophore-conjugated phalloidin and anti-vinculin antibody were used to stain F-actin and vinculin respectively in order to observe the effect of KSHV infection upon the organization of the actin cytoskeleton and the size, number and distribution of focal adhesions **(Figure 6.1)**. Phalloidin is a bicyclic heptapeptide that binds more tightly to F-actin than to monomeric actin; hence it prevents actin depolymerisation, maintaining the filament structure. Vinculin is one of the intracellular proteins recruited into focal adhesions to aid stabilization of the protein complex. Absence of staining with isotype control indicated the staining was not due to non-specific binding of the fragment crystallisable (Fc) portion of the antibody **(Figure 6.1)**. Analysis was on day-seven post-inoculation because an effect of the virus upon motility had been clearly demonstrated at that timepoint **(Chapter 4)**.

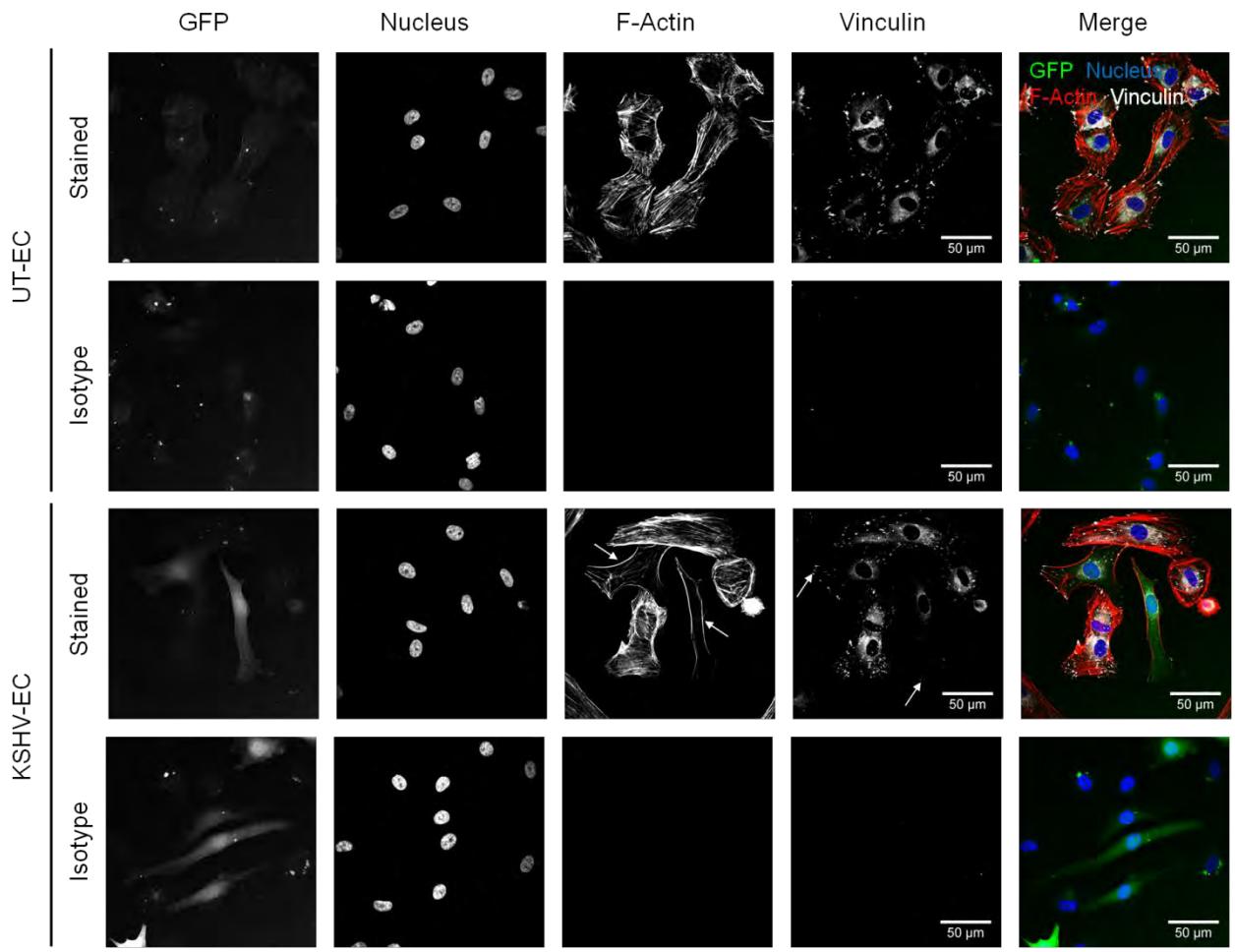

Figure 6.1 Effect of KSHV infection on the organization of F-actin and the distribution of focal adhesions in HUVEC.

KSHV-inoculated (KSHV-EC) or untreated (UT-EC) HUVEC were seeded sub-confluent into 8-well chamber slides on day-six post-inoculation. On day-seven, cells were fixed, permeabilised with 0.1% (v/v) Triton-X-100 and stained for F-actin and vinculin or isotype control. Nuclei were stained with bisbenzimide. Cells were imaged on an inverted laser scanning confocal microscope using a 63x water immersion objective lens. KSHV-infected cells were identified by their positivity for GFP expression. Arrows indicate redistribution of F-actin to the edge of KSHV-infected cells (F-actin panel) and localization of vinculin to the tips of spindle-shaped infected cells (vinculin panel). Images are representative of over 30 cells of each type from across three experiments. Scale bars are 50µm.

6.2.1 The effect of KSHV infection on the size and shape of HUVEC

The sizes and shapes of the cells (including total cell area, perimeter and roundness) were first determined to enable measurements of the staining of F-actin and vinculin to be normalised according to parameters of cell size or shape. The images of phalloidin-stained F-actin were thresholded to establish the outline of the cell shape from which measurements of the total cell area and perimeter were made and roundness was calculated. KSHV infection did not alter the cell area **(Figures 6.2A and B)** but the change in morphology with infection from cuboid to spindle-shaped resulted in a significant increase in the length of the cell perimeter **(Figures 6.2C and D)**. Roundness, a statistic that is inversely related to circularity, also increased with KSHV infection, consistent with the elongated shape of infected cells **(Figures 6.2E and F)**.

6.2.2 The effect of KSHV infection on the organisation of F-actin in HUVEC

KSHV-infection appeared to induce redistribution of F-actin to the edge of the cell. This pattern was in contrast to the maintenance of a seemingly uniform distribution of F-actin across the cell in untreated HUVEC **(Figures 6.1 and 6.3)**. Image analysis software was therefore used to quantify the extent of this distribution difference on a population basis.

The effect of KSHV infection on the total amount of F-actin within HUVEC was first assessed. The mean phalloidin intensity of staining did not change with infection **(Figures 6.4A and B)**. Consistent with the above observation that KSHV infection did not change the total area of a cell, the total phalloidin staining per cell was also not altered **(Figures 6.4C and D)**. Therefore, KSHV infection did not change the extent of actin polymerisation in HUVEC.

To investigate whether KSHV directed localization of F-actin to the edge of the cell, as postulated from the appearance of phalloidin stained cells **(Figures 6.1 and 6.3)**, I designed a method for image analysis which involved dividing each cell into concentric rings of equal area proportional to the size of the cell, and measuring the total intensity of phalloidin staining in each ring. A novel macro which divided the cells into four concentric rings was written in Image-Pro by David Kelly (Wellcome Trust Centre for Cell Biology, University of Edinburgh, UK) especially to handle this analysis. Consistent with conclusions based upon qualitative observations **(Figures 6.1 and 6.3)**, ring number had an effect upon the intensity of phalloidin staining in KSHV-infected cells: intensity was significantly greater in the outermost ring (ring 4) compared to the middle two rings (rings 2 and 3). No effect of ring number was found for untreated cells **(Figure 6.5)**.

The extent of reorganization of the actin cytoskeleton with KSHV-infection might have been under reported by use of the macro to analyse the images. Reasons include: (1) the macro was unable to process a subset of the KSHV-infected cells that had very pronounced spindle morphology and apparently marked redistribution of actin to the cell edge; (2) the macro divided the cell into only four concentric rings which were generally wider than the band of strongest staining at the edge of the cell. The adjacent regions of lower intensity within the same ring would therefore have reduced the difference between the intensities of neighbouring rings; (3) actin filaments mostly align along the longest axis through the cell and end at the leading and trailing edges; hence staining at the leading and trailing edges appeared less bright and might have reduced the effect of the prominent staining along the other sides of the cell.

I devised a second complementary method of image analysis for assessment of the effect of KSHV-infection upon F-actin distribution which aimed to overcome the above mentioned limitations of the macro-aided concentric ring approach. This second method compared the phalloidin intensity profiles of untreated and KSHV-infected cells along the axis which passed through the midpoint of the cell perpendicular to the longest axis between the leading and trailing edges **(Figure 6.6A)**. The intensity profiles generated were separated into ten sections that gave five concentric rings **(Figure 6.6B)** and the average total intensity for each ring, normalized for ring width, was plotted **(Figure 6.6C)**. An effect of ring number on phalloidin staining was evident by this method of analysis for both KSHV-infected and untreated cells. However, post-hoc tests indicated that while untreated cells showed a difference between only the innermost and outermost rings, there was a stepwise increase in intensity of staining across all five rings in KSHV-infected cells **(Figure 6.6C).**

Figure 6.2: Effect of KSHV infection on the size and shape of HUVEC.

Images of KSHV-infected (V) and untreated (UT) HUVEC stained for F-actin were thresholded to create a mask for each cell. The image analysis software, Image-Pro, was used to measure the total area of each cell **(A and B)** and its perimeter **(C and D)** and to calculate its roundness according to the equation: $(\text{Perimeter})^2/(4\pi\text{Area})$ **(E and F)**. (A, C and E) Each square represents the measurement of the area, perimeter or roundness for a single cell. Data are the pooled results of three experiments. Horizontal lines indicate the mean measurement for each parameter. * = $P<0.05$ by unpaired t-test. (B, D and F) are the data in A, C and E separated according to experiment. Each line connects the mean measurements for the UT and V cells in a single experiment. Means were calculated from data on eight or more cells. * = $P<0.05$ by paired t-test.

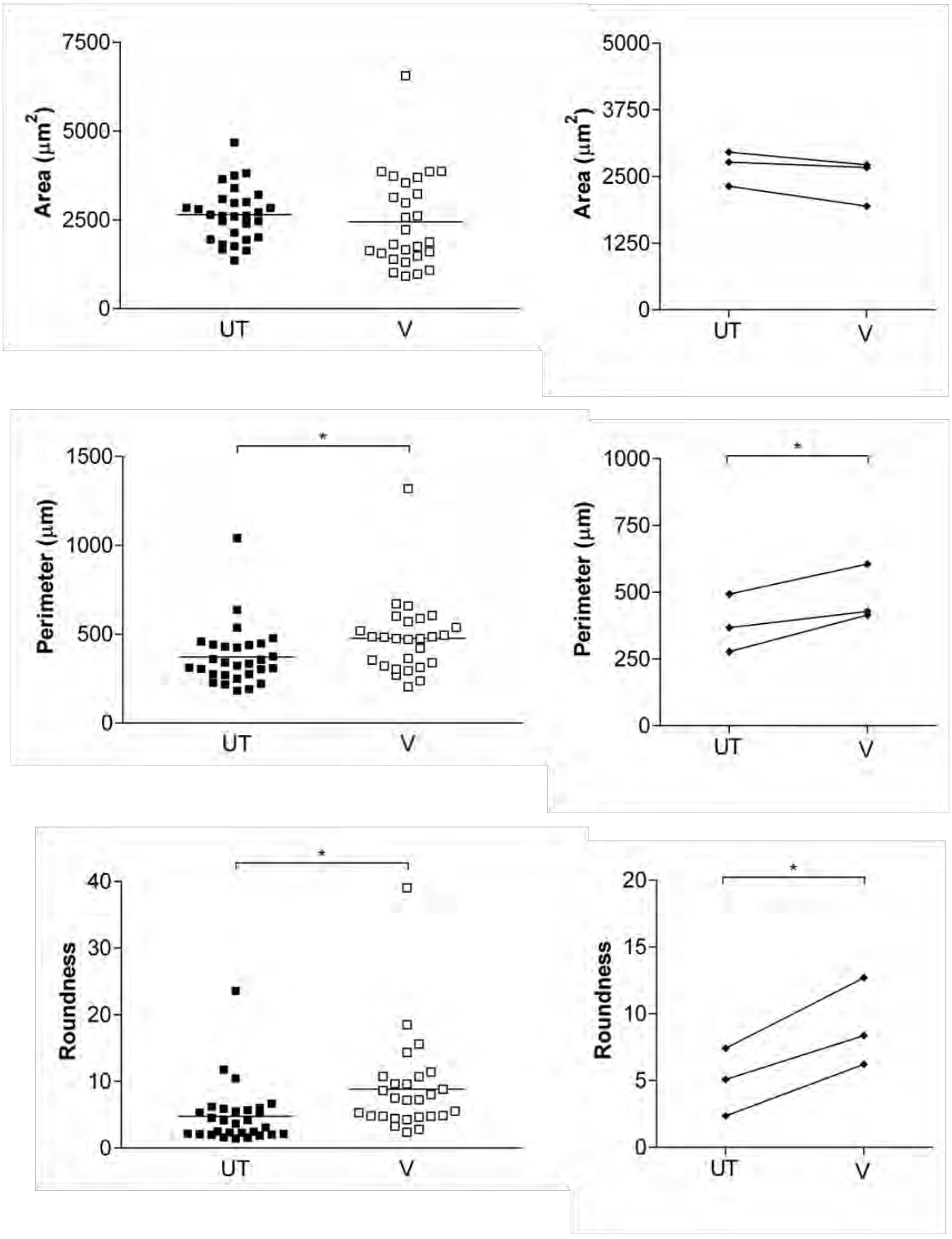
Area (μm²)
7500
5000
2500
0
UT
V
Area (μm²)
5000
3750
2500
1250
0
UT
V
Perimeter (μm)
1500
1000
500
0
*
UT
V
Perimeter (μm)
1000
750
500
250
0
*
UT
V
Roundness
40
30
20
10
0
*
UT
V
Roundness
20
15
10
5
0
*
UT
V

Figure 6.3: Effect of KSHV infection on the organisation of F-actin in HUVEC.
KSHV-inoculated (KSHV-EC) or untreated (UT-EC) HUVEC were seeded sub-confluent into 8-well chamber slides on day-six post-inoculation. On day-seven, cells were fixed, permeabilised with 0.1% (v/v) Triton-X-100 and stained for vinculin (not shown) and F-actin. Nuclei were stained with bisbenzimide (not shown). Cells were imaged on an inverted laser scanning confocal microscope using a 63x water immersion objective. KSHV-infected cells were identified by their expression of GFP. The UT-EC and KSHV-infected cells in the panel are examples of UT-EC and KSHV-infected cells from each of three experiments and are representative of over 30 cells of each type from across these experiments. Images of GFP expression and phalloidin staining of KSHV-EC are shown individually and as a merge for clarification of the infected cells. Only F-actin images are shown for UT-EC since all cells were negative for GFP expression as illustrated in Figure 6.1.

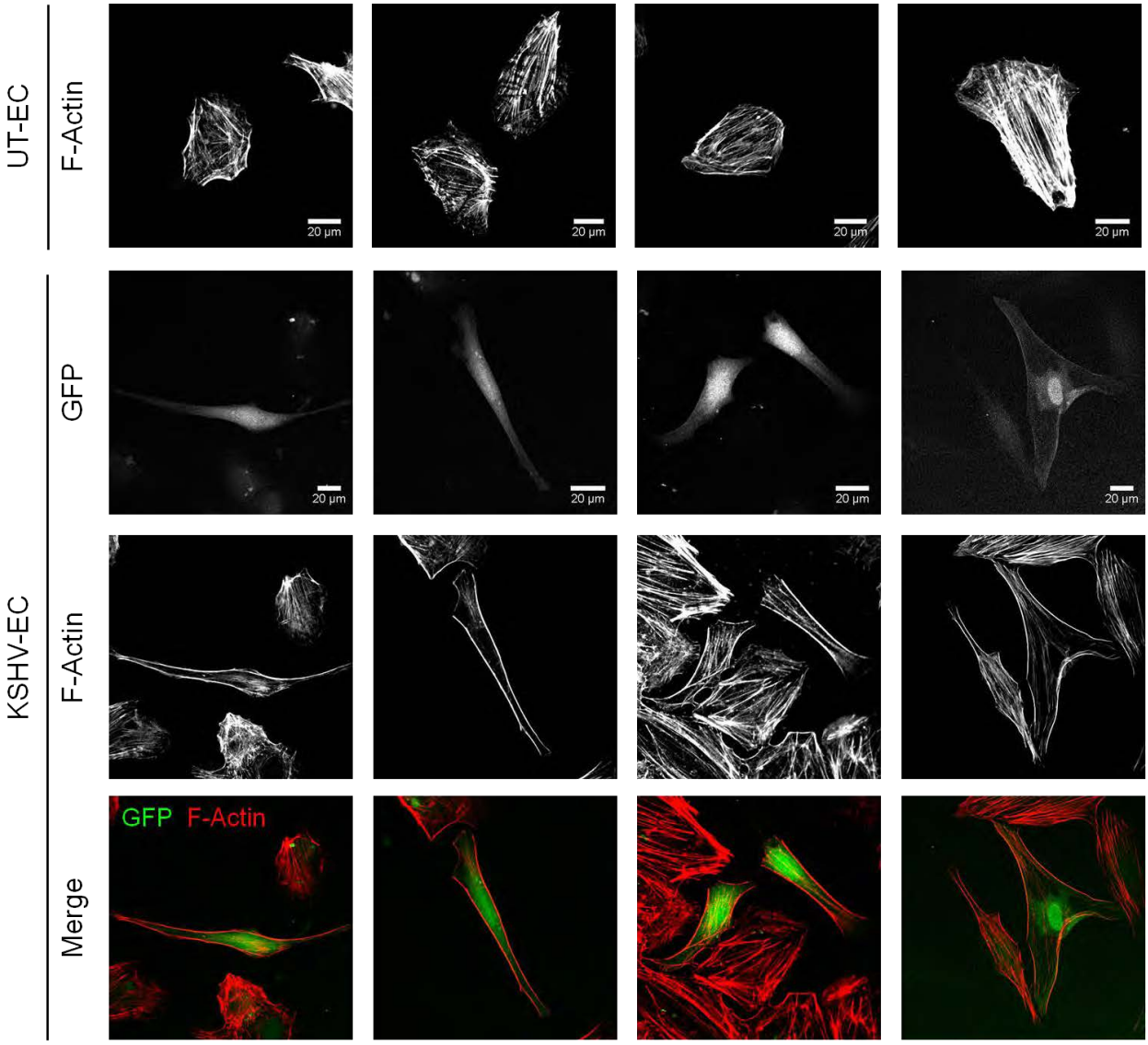
UT-EC
F-Actin
KSHV-EC
GFP
F-Actin
Merge
GFP F-Actin
20 µm

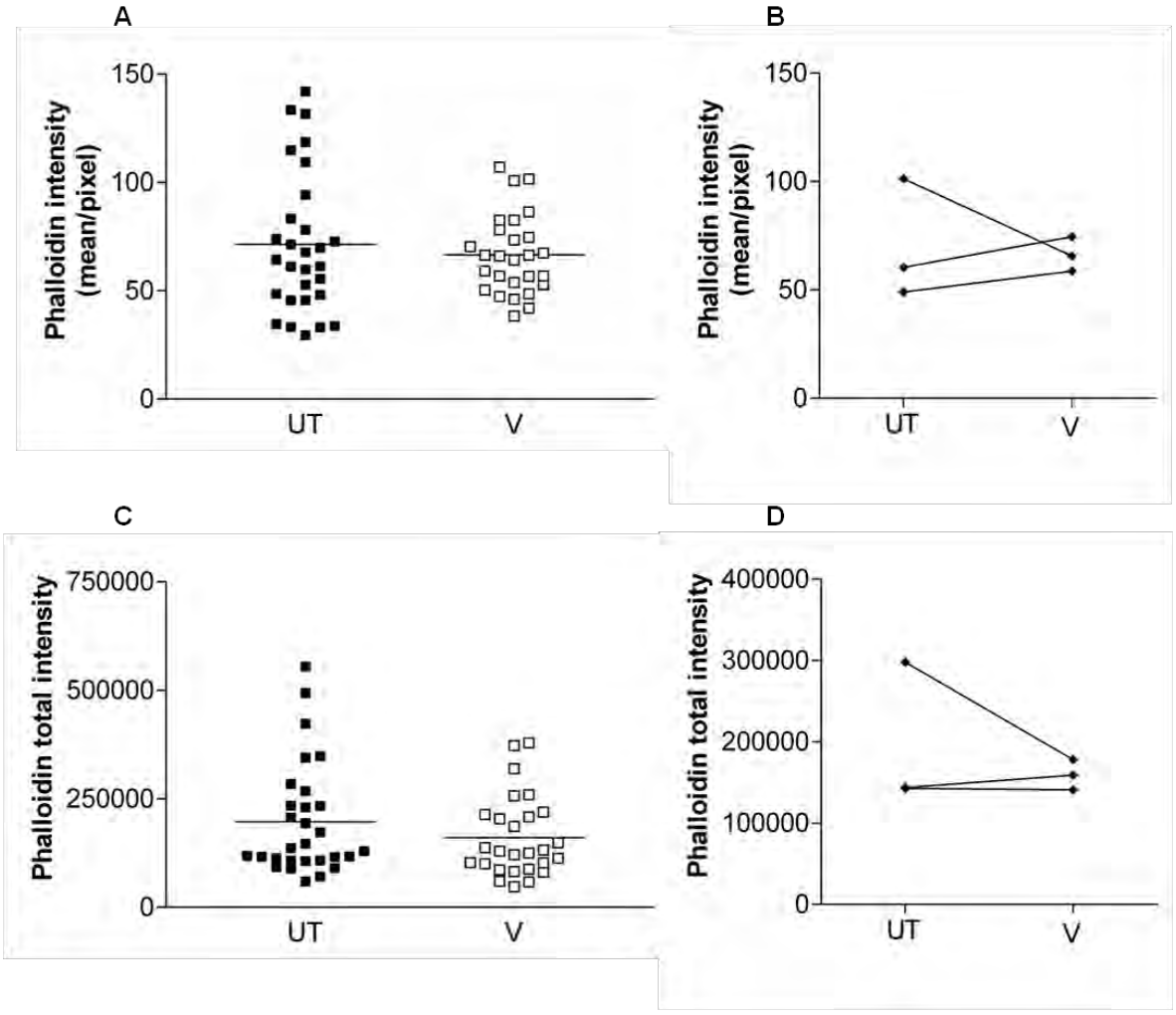

Figure 6.4: Effect of KSHV infection on the amount of F-actin in HUVEC.

Images of KSHV-infected (V) and untreated (UT) HUVEC stained for F-actin were thresholded to create a mask for each cell. The image analysis software, Image-Pro was used to measure the mean intensity of phalloidin staining for each cell (A and B) and the total cell area. The total intensity of staining was calculated as the product of the mean intensity multiplied by cell area (C and D). (A and C) Each square represents the measurement of mean phalloidin intensity for a single cell. Data are the pooled results of three experiments. Horizontal lines indicate the mean measurement for each parameter. (B and D) The data in A and C separated according to experiment. Each line connects the mean measurements for each of UT and V in a single experiment. Means were calculated for data on eight or more cells.

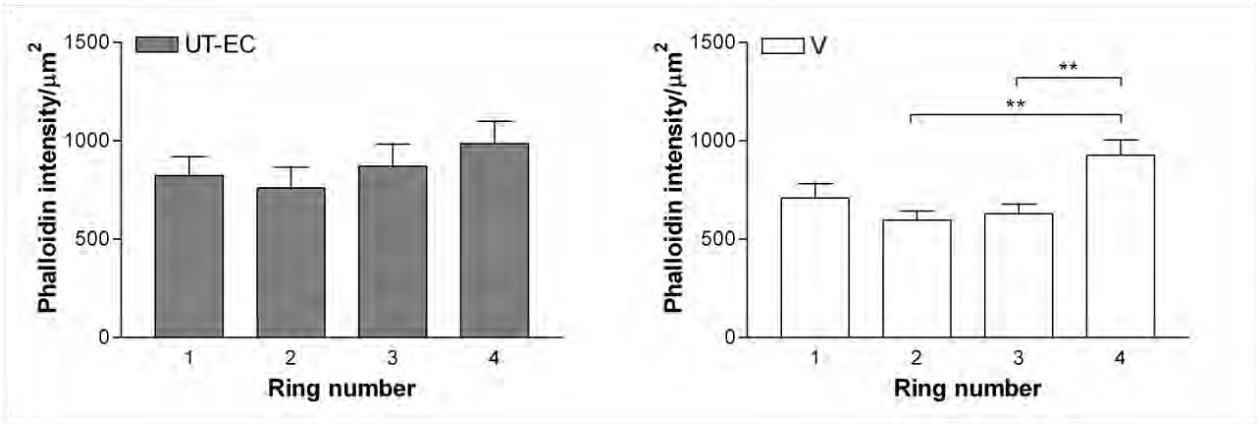

Figure 6.5: Concentric ring analysis of the effect of KSHV infection on the distribution of F-actin in HUVEC.

Images of KSHV-infected (V) and untreated (UT-EC) HUVEC stained for F-actin were analysed by a macro designed in Image-Pro which divided the cell into four concentric rings of equal area and reported the total intensity of phallodin staining of F-actin in each ring and the area of each ring. Intesnsity per unit area was calculated and is plotted against the ring number. Data are the pooled results of analysis on 30 UT-EC and 27 V HUVEC from across three experiments. Bars represent mean phalloidin intensity/μm^2 ± SEM. ANOVA revealed a significant effect of ring number upon intensity of staining for V ($P<0.05$). ** = $P<0.01$ by Bonferroni's Multiple Comparisons Test.

Figure 6.6: Line profile analysis of the effect of KSHV infection on the distribution of F-actin in HUVEC.

Images of KSHV-infected (V) and untreated (UT-EC) HUVEC stained for F-actin were analysed using ImageJ software. **(A)** The (x,y) midpoint of the cell of interest was determined and a line drawn through the midpoint at 90° to the longest axis between the leading and trailing edges of the cell. **(B)** The phalloidin intensity profile was generated for the axis marked in 'A' and was divided into ten sections to give 5 concentric rings of intensity indicated 1 to 5. **(C)** The intensities in each of the ten sections were summed and the average in each of the five concentric regions determined and plotted against ring number. Data are the pooled results of analysis on 18 UT-EC and 18 V HUVEC across three experiments, six cells from each experiment. Bars represent mean phalloidin intensity of staining ± SEM. ANOVA revealed a significant effect of ring number upon intensity of staining for both UT-EC ($P<0.05$) and V ($P<0.0001$) HUVEC. * = $P<0.05$, ** = $P<0.01$; *** = $P<0.001$ by Bonferroni's Multiple Comparissons Test.

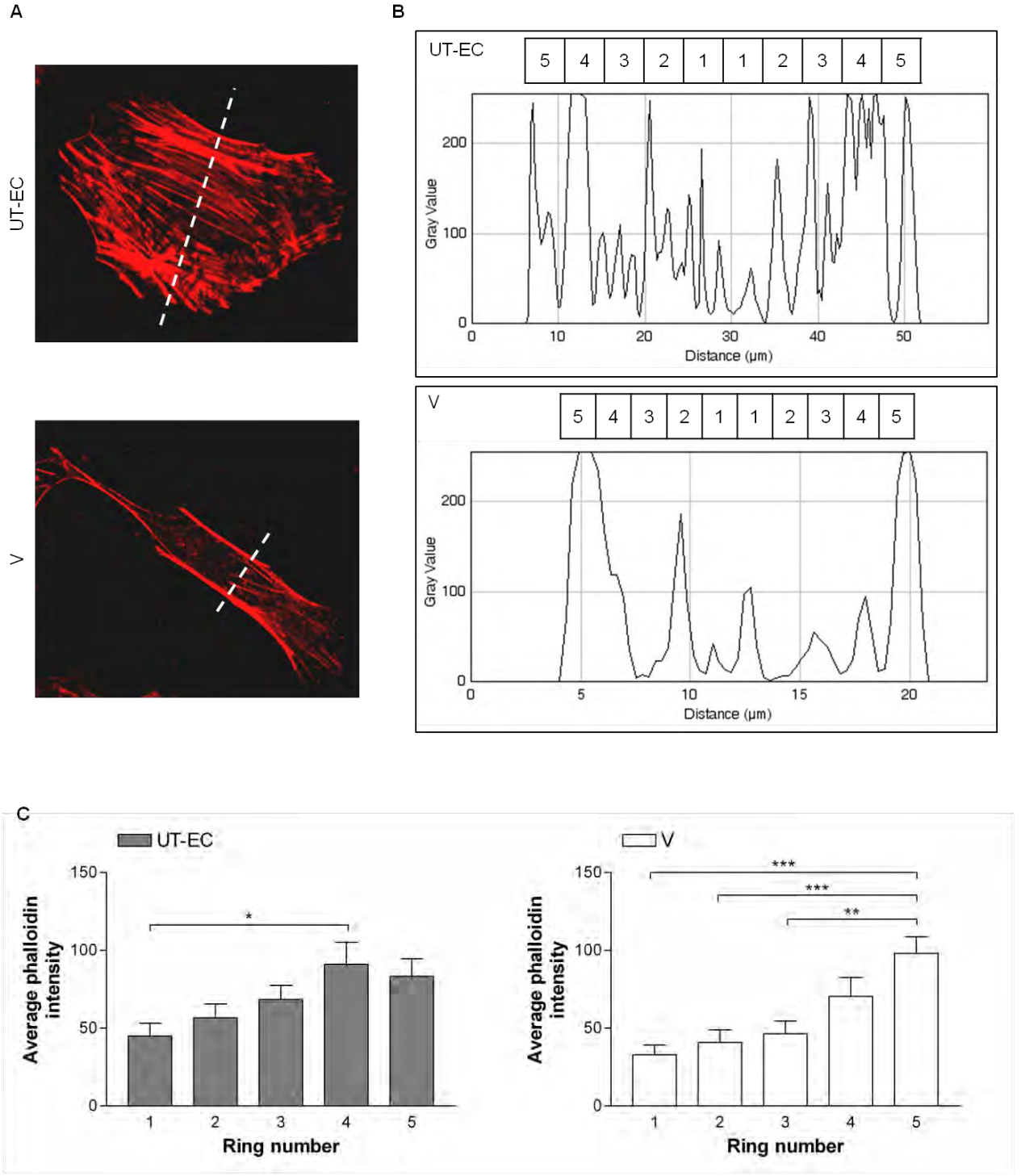
A
UT-EC
V
B
UT-EC
5 4 3 2 1 1 2 3 4 5
Gray Value
Distance (µm)
V
5 4 3 2 1 1 2 3 4 5
Gray Value
Distance (µm)
C
UT-EC
V
Average phalloidin intensity
Ring number
*
***
***
**

6.2.3 The effect of KSHV-infection on the distribution of focal adhesions in HUVEC

Anti-vinculin staining generated a punctate staining pattern at the perimeter of the cell in both untreated and KSHV-infected cells. However, while the focal adhesions appeared uniformly distributed about the perimeters of untreated cells, they were localized at the tips of KSHV-infected, spindle-shaped cells **(Figures 6.1 and 6.7)**. Localisation of the vinculin spots at the ends of actin filaments in both infected and untreated cells, consistent with vinculin as a focal adhesion protein, is more clearly demonstrated in **(Figure 6.8)**. Hereafter, in this chapter, vinculin spots are referred to as focal adhesions. Prominent vinculin staining was also identified in the cytosol and was considered to be free vinculin not recruited into focal adhesions **(Figures 6.1 and 6.7)**.

To quantify the apparent decrease in the number and size of focal adhesions per cell with KSHV infection **(Figures 6.1 and 6.7)**, images of vinculin staining were thresholded using Image-Pro software and the region containing the peripheral focal adhesions selected. The software reported the total number of focal adhesions per cell and the size of each one. KSHV-infection reduced the number of focal adhesions per cell and the total area covered by focal adhesion complexes **(Figure 6.9A to D)**. Normalising according to cell perimeter length, shown above to be increased with KSHV-infection **(Figure 6.2C and D)**, the reduction in number of focal adhesions with KSHV infection was highly significant **(Figure 6.9E)**.

Figure 6.7: Effect of KSHV infection on the size, number and distribution of focal adhesions in HUVEC.

KSHV-inoculated (KSHV-EC) or untreated (UT-EC) HUVEC were seeded sub-confluent into 8-well chamber slides on day-six post-inoculation. On day-seven, cells were fixed, permeabilised with 0.1% (v/v) Triton-X-100 and stained for vinculin and F-actin (not shown). Nuclei were stained with bisbenzimide (not shown). Cells were imaged on an inverted laser scanning confocal microscope using a 63x water immersion objective. KSHV-infected cells were identified by their expression of GFP. The UT-EC and KSHV-infected cells in the panel are examples of UT-EC and KSHV-infected cells from each of three experiments and are representative of over 30 cells of each type from across these experiments. Images of GFP expression and vinculin staining of KSHV-EC are shown individually and as a merge for clarification of the infected cells. Only vinculin images are shown for UT-EC since all cells were negative for GFP expression as illustrated in Figure 6.1.

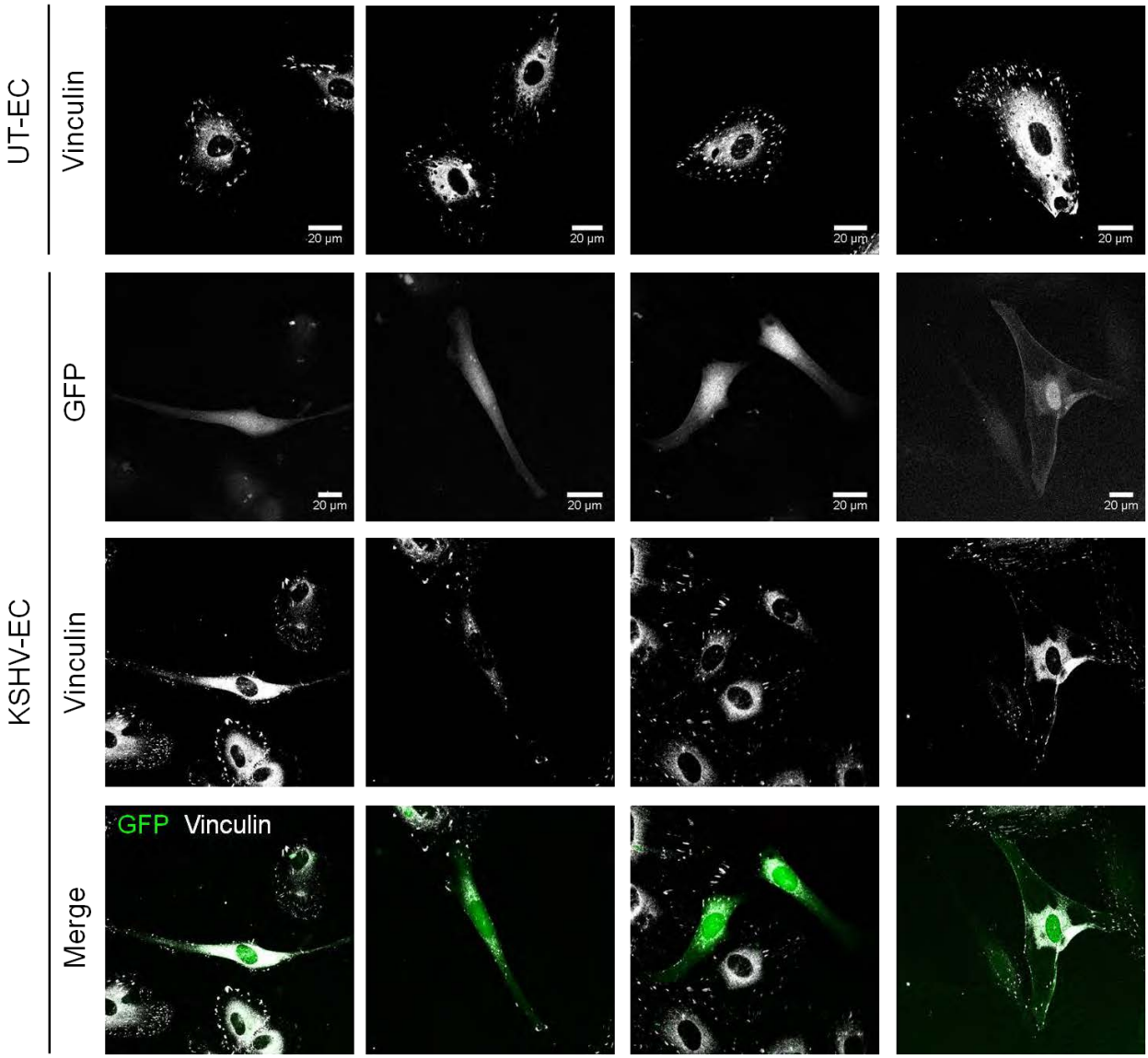
UT-EC
Vinculin
KSHV-EC
GFP
Vinculin
Merge
GFP Vinculin
20 µm

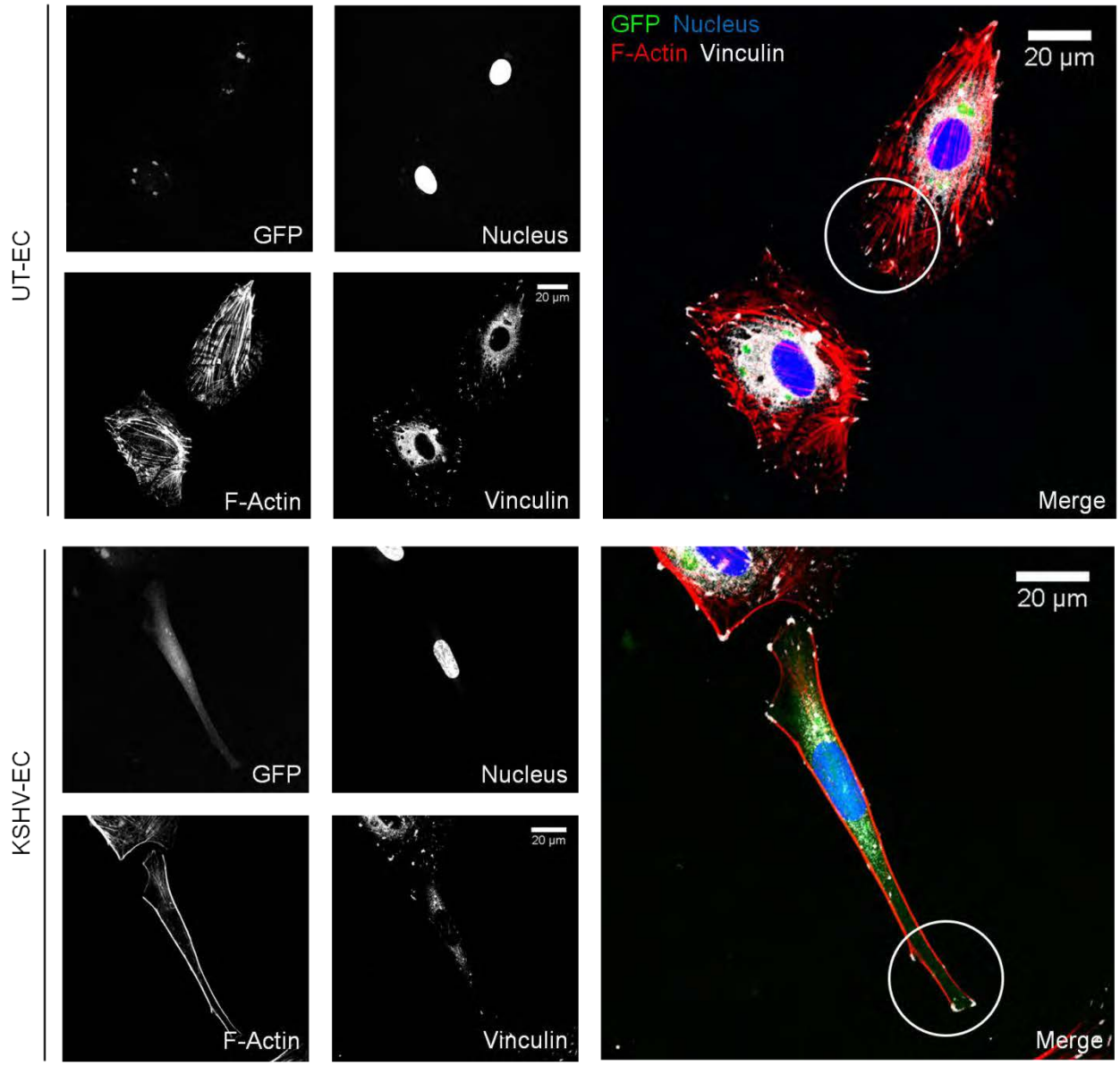

Figure 6.8: Patterns of phalloidin and anti-vinculin staining in HUVEC.

KSHV-inoculated (KSHV-EC) or untreated (UT-EC) HUVEC were seeded sub-confluent into 8-well chamber slides on day-six post-inoculation. On day-seven, cells were fixed, permeabilised with 0.1% (v/v) Triton-X-100 and stained for F-actin and vinculin. Nuclei were stained with bisbenzimide. KSHV-infected cells were identified by their positivity for GFP expression. Circles on the merge panel highlight localisation of vinculin at the tips of actin filaments. Images are representative of over 30 cells of each type from across three experiments.

Figure 6.9: Effect of KSHV infection on the number and size of focal adhesions in HUVEC. Images of KSHV-infected (V) and untreated (UT-EC) HUVEC stained for vinculin were analysed using Image-Pro software. Images were thresholded to identify the focal adhesions and the peripheral region of the cell containing focal adhesions was selected apart from the central region of non-complexed vinculin. The number of focal adhesions per cell was counted **(A and B)** and the area of each focal adhesion reported. By the summation of these areas, the total area of focal adhesion coverage per cell was calculated **(C and D)**. From images of the same cells stained for F-actin, the lengths of the cells' perimeters were measured (Figure 6.3) and used for normalization of focal adhesion number per cell **(E and F).** (A, C and E) each square represents the result of the parameter for a single cell. Data are the pooled results of three experiments. Horizontal lines indicate the mean. * = $P<0.05$; *** = $P<0.0001$ by unpaired t-test. (B, D and F) are the data in A, C and F separated according to experiment. Each line connects the mean measurements for each of UT and V in a single experiment. Means were calculated for data on eight or more cells. * = $P<0.05$ by paired t-test.

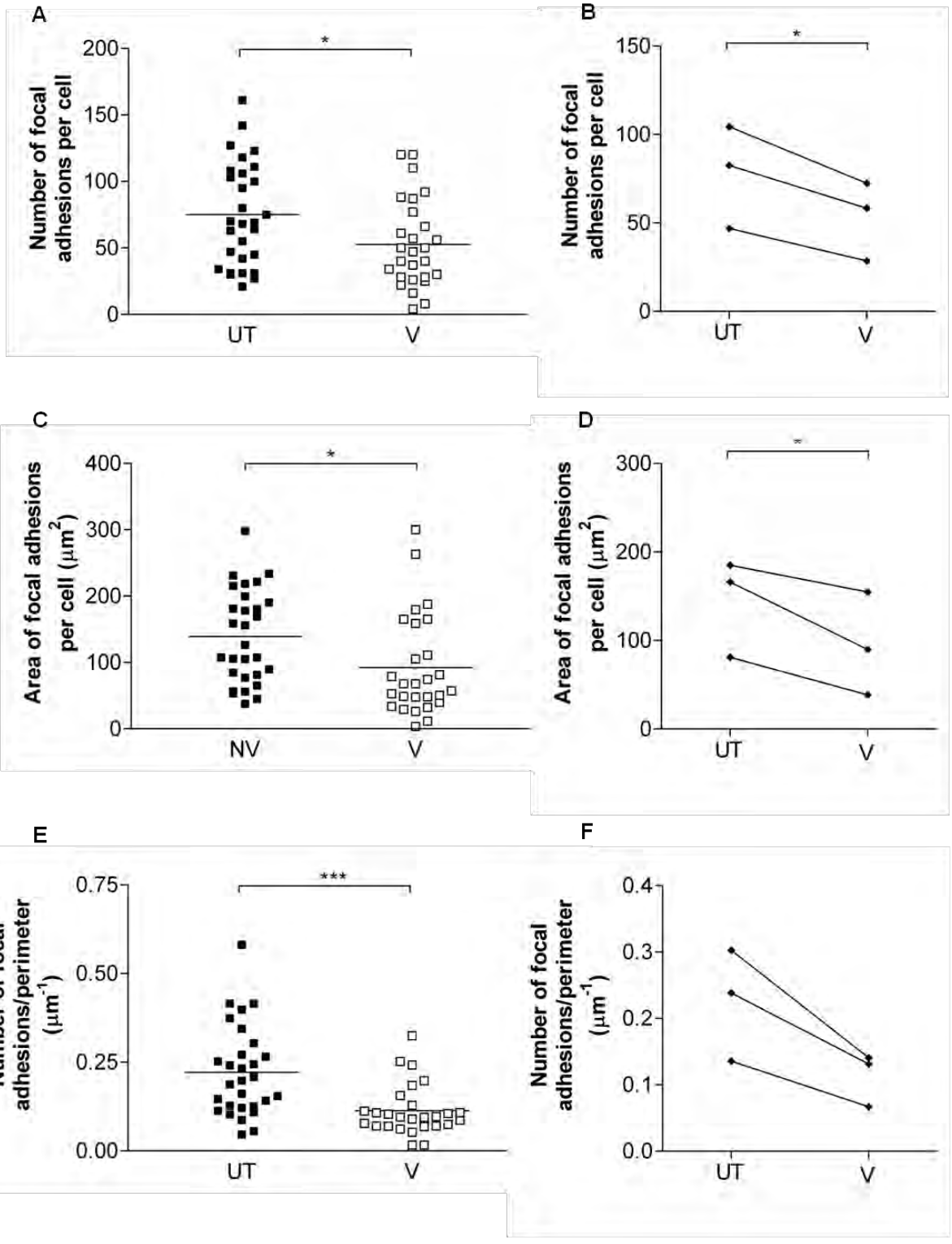
A
Number of focal adhesions per cell
200
150
100
50
0
*
UT
V
B
Number of focal adhesions per cell
150
100
50
0
*
UT
V
C
Area of focal adhesions per cell (μm²)
400
300
200
100
0
*
NV
V
D
Area of focal adhesions per cell (μm²)
300
200
100
0
*
UT
V
E
Number of focal adhesions/perimeter (μm⁻¹)
0.75
0.50
0.25
0.00
***
UT
V
F
Number of focal adhesions/perimeter (μm⁻¹)
0.4
0.3
0.2
0.1
0.0
UT
V

6.3 DISCUSSION

Cell migration involves cycles of assembly and disassembly of the actin cytoskeleton and of focal adhesion complexes. Since infection of HUVEC by KSHV increased cell migration **(Chapter 4)**, the effect of KSHV on the organization of the actin cytoskeleton and the distribution, size and number of focal adhesion complexes in HUVEC was investigated in this chapter by confocal microscopy **(Figure 6.1)**. Using novel strategies to quantify the amount of filament actin at increasing distance from the centre of the cell, this study provides the first quantitative evidence that KSHV infection of HUVEC induces partitioning of actin filaments from a mesh-like array covering the cytosol into bundles of actin filaments concentrated at the cell periphery and aligned parallel to the longest axis of the cell **(Figures 6.3, 6.5 and 6.6)**. Focal adhesions were observed to localize to the tips of infected cells. Furthermore, infection caused a reduction in the number and size of focal adhesions presented by KSHV-infected cells compared with untreated HUVEC **(Figures 6.7 and 6.9)**.

To my knowledge, prior to the work in this thesis, no study had characterised the changes in F-actin abundance and organization occurring with long term KSHV infection of primary endothelial cells. The latest timepoint of observation reported was day-three post-infection (Grossmann et al., 2006). In that study, arrangement of F-actin into parallel bundles was noted in infected cells coinciding with the elongation of cell shape. However, the authors did not comment on whether these structures partitioned to the cell cortex, analogous to the observations described in this chapter, and the images that they presented were of insufficient magnification for such a phenotype to be distinguished by the reader.

Before this study, the major focus on KSHV-induced rearrangement of the actin cytoskeleton in endothelial cells had been in the context of virus particle entry to the cell and subsequent traffic to the nucleus. Thus observations of an effect of KSHV on F-actin organization had been made during the period immediately following infection (0.5minutes to four hours). Although the precise molecular mechanism for the endocytic entry of KSHV into endothelial cells continues to be debated—both clathrin-mediated endocytosis (Greene and Gao, 2009) and macropinocytosis (Raghu et al., 2009) have been suggested—actin polymerization appears to be important for efficient infection of endothelial cells. For example, treatment of human dermal microvascular endothelial cells with the actin depolymerising agent, cytochalasin D, inhibited expression of the KSHV genes ORF50 and ORF73 by 58% and 66% respectively (Raghu et al., 2009) and treatment of HUVEC with inhibitors to disrupt actin dynamics (cytochalasin D, Latrunculin and Jasplakinolide) significantly reduced the number of virus particles docked at each nucleus (Greene and Gao, 2009).

In further support of actin involvement in the KSHV infection process, temporal changes in F-actin structures were additionally described immediately after infection. Raghu et al (2009) and Greene and Gao (2009) both reported dissolution of cortical actin structures and the induction of stress fibres followed by formation of filopodia and lamellipodia protrusions between five and 15minutes after infection of HUVEC and dermal microvascular endothelial cells. Naranatt et al (2003) identified a similar pattern of change to the F-actin cytoskeleton of fibroblasts following KSHV infection: within five minutes there was rapid actin polymerization and cell-wide assembly of stress fibres. This was followed by the appearance of filopodia by 15minutes and membrane ruffling by 30minutes. In contrast, untreated cells had a smooth surface, lacking

protrusions, and actin was peripheral and organized into cortical bundles (Naranatt et al., 2003). Subsequent work by the same group showed that signaling induced upon productive engagement of the KSHV envelope protein, gB, with the host-cell integrin entry receptor, $\alpha 3\beta 1$, activated the host cell kinase cascade FAK-Src-PI3K-RhoGTPases and cytoskeleton rearrangements (Sharma-Walia et al., 2004).

In my studies at day-seven post-inoculation filopodia and lamellipodia were not evident on the surface of infected cells, and identification of prominent peripheral actin structures was in contrast to the dissolution of cortical actin filaments by 15minutes post infection (Greene and Gao, 2009; Raghu et al., 2009). Taking these observations together, it appears that as latent infection establishes and the cell becomes spindle shaped, remodeling of the actin cytoskeleton continues. The recent report by DiMaio et al (2011), published after the work in this thesis was completed, examined qualitatively the actin cytoskeleton of KSHV-infected primary dermal microvascular endothelial cells 48hours post-infection and suggested that the peripheral organization of actin in latently infected cells is attained even by 48hours.

In agreement with the actin distributions reported for untreated and KSHV-infected cells in this thesis, expression of the KSHV K5 protein in dermal microvascular endothelial cells immortalized with human papillomavirus E6 and E7 proteins caused reorganization of F-actin from an array of cable-like filaments aligned perpendicular to the membrane and distributed throughout the cytosol to localization along the cell periphery (Mansouri et al., 2008). This effect of K5 was suggested to be a consequence of its transmembrane unbiquitin ligase activity in targeting the destruction of the VE-cadherin-catenin complex to which F-actin is linked. We have detected K5 transcripts in KSHV-infected HUVEC by RT-PCR (data not shown); thus K5 might

have contributed to the establishment of the phenotype of peripheral actin structures which I observed. Alternatively, in studies by Grossmann et al (2006), overexpression of single KSHV latency genes in endothelial cells suggested a cell-autonomous role for vFLIP in the generation of the spindle phenotype of KSHV-infected LEC and BEC in which parallel arrays of actin fibres were observed. Our infected cultures also expressed vFLIP **(Figure 5.9)**. Therefore, vFLIP activity might underlie reorganization of the actin cytoskeleton into the parallel cortical bundles at day-seven.

To my knowledge the present study was the first to examine quantitatively the impact of KSHV infection upon the distribution, number and size of focal adhesions in primary endothelial cells. The reorganization of F-actin into bundles that extended the length of the cell and partitioned to the cell edge and the localization of focal adhesions to the tips of spindle cells were thought to be interdependent phenotypes. The reduction in the number of focal adhesions was likewise consistent with filament bundling, since the maintenance of total F-actin but generation of thick bundles would require fewer sites of contact between the ECM and intracellular actin filaments **(Figure 6.4)**

The decrease in the size of focal adhesions in infected cells also agreed with the increased rates of infected cell migration reported in this thesis **(Chapter 4)**, since focal adhesions mature and increase in size when cells make firm adhesions to substrate, while intermediate strengths of attachment to substrate have been linked to increased locomotion. For example, measurements of: percentage of motile cells; migration speed and persistence of migration, determined for human smooth muscle cells, were maximal at intermediate strengths of attachment to the substrates fibronectin and collagen IV (DiMilla et al., 1993). The decrease in vinculin recruitment

to focal adhesions with KSHV-infection and a concomitant increase in cell migration is supported by previous studies that have examined the relationship between vinculin availability and motility: increasing endogenous vinculin levels by 20% in BALB/c 3T3 cells inhibited closure of wounded monolayers (Rodriguez Fernandez et al., 1992) while transfection of BALB/c 3T3 cells with vinculin antisence cDNA, reducing vinculin expression to 10-30% of controls, increased two-fold the numbers of cells entering scratch wounds and the lengths of phagokinetic tracts produced by individual cells migrating on colloidal gold-coated coverslips (Rodriguez Fernandez et al., 1993).

There was no apparent reduction in total vinculin expression with KSHV infection in the present study **(Figure 6.7)**; thus the decrease in focal adhesion size with KSHV infection might be due to either a decrease in the recruitment of vinculin to focal adhesions or increased rates of focal adhesion turnover. The assembly and growth of focal adhesions is driven by mechanical force generated by actomyosin contractility (Bershadsky et al., 2003). While a decrease in myosin-II driven tension would cause disassembly of focal adhesions, reduced recruitment of vinculin to forming complexes might also arise as a consequence of the downregulation of upstream components that associate with vinculin and bring it into focal adhesions. Infection of human foetal foreskin fibroblasts with HCMV suppressed the expression of focal adhesion-associated proteins including Hic-5, paxillin and α-actinin (Stanton et al., 2007). Paxillin binds to integrins and recruits vinculin (Mitra et al., 2005); thus if KSHV infection also downregulated paxillin it might explain the reduction in appearance of focal adhesion size identified on the basis of vinculin expression.

The mechanisms underlying focal adhesion turnover are incompletely described. Both proteolysis and clathrin mediated endocytosis of integrins have been presented as possible mechanisms. For proteolysis, activity of the intracellular calcium-dependent protease calpain appears to be critical (Franco et al., 2004). Cleavage of talin and FAK promotes turnover (Chan et al., 2010; Franco et al., 2004) but the calpain cleavage products of paxillin serve to negatively regulate turnover and thus cell migration (Cortesio et al., 2011). To determine whether increased turnover rates explain the incidence of smaller sized focal adhesions in infected cells an effect of KSHV infection upon focal adhesion turnover could be examined by Total Internal Reflection Fluorescence microscopy. Since vinculin is a major but not essential component of focal adhesions (Coll et al., 1995), the expression profiles of other focal adhesion-associated proteins might also be examined to verify that the conclusion that infection reduces focal adhesion size, as made in the present study on the basis of vinculin expression, is not peculiar to vinculin.

In summary, the effects of KSHV infection on the actin cytoskeleton and focal adhesions were examined in this chapter. This work at day-seven post-infection provides the first insight that KSHV infection continues to modulate the organization of the actin cytoskeleton and focal adhesions of endothelial cells beyond the first three days of infection. Taken together with the body of literature describing cytoskeletal changes during the early stages of infection, these data suggest that modulation of the cytoskeleton and its associated proteins has multiple functions during the virus lifecycle which might include the facilitation of virus entry and traffic to the nucleus of endothelial cells but also increased motility of the infected cell.

CHAPTER SEVEN

EFFECTS OF KSHV-INDUCED CHEMOKINES AND GROWTH FACTORS ON ENHANCED MIGRATION OF KSHV-INFECTED ENDOTHELIAL CELLS

7.1 INTRODUCTION

The preferential transmigration of KSHV-infected cells **(Figure 4.3)** suggested that KSHV infection enhanced migration through a cell intrinsic mechanism or via the release of a secreted factor that acted specifically upon infected cells. For instance, if KSHV infection caused secretion of an agent, and upregulation of its receptor that was lacking in non-infected cells, then a response only in infected cells might be seen.

Angiogenic and inflammatory factors including VEGFA, VEGFC, bFGF, Ang-2, IL-6, IL-8, ephrin B2 and Growth regulated oncogene- alpha (Gro-α) have been detected within KS lesions (Ye et al., 2007). Moreover, *in vitro* studies provide evidence that KSHV infection of endothelial cells induces generation of an angiogenic, inflammatory milieu. For example, infection of human dermal microvascular endothelial cells with KSHV induced sustained upregulation of VEGFA and VEGFC gene and protein expression (Carroll et al., 2004; Sivakumar et al., 2008) and infection of HUVEC and dermal microvascular endothelial cells caused sustained Ang-2 expression in a mechanism involving ERK/JNK/p38 MAPK activation of activator protein-1 (AP-1) and Ets1 transcription factors (Ye et al., 2007). Others have reported that KSHV infection or ectopic expression of the KSHV gene, vGPCR, activated the transcription factors AP-1 and NFkB leading to the upregulation of angiogenic cytokines, chemokines, growth factors and MMPSs (Montaner et al., 2004; Xie et al., 2005).

Of these factors, pro-migratory effects of VEGFA, VEGFC and bFGF have been demonstrated on endothelial cells (for example: Fortier et al., 1999; Lee and Kay, 2006; Marchio et al., 1999; Olsson et al., 2006) and IL-8, a chemoattractant for neutrophils, has also been shown

to influence the migration of microvascular endothelial cells (Heidemann et al., 2003; Salcedo et al., 2000; Schraufstatter et al., 2003); the extent of chemotaxis correlating with the level of receptor expression by these cells (Salcedo et al., 2000). Therefore, in this chapter, the release of chosen factors, and/or expression of their receptors or downstream signaling proteins was investigated for the contribution of signaling pathways elicited by these ligand-receptor interactions to KSHV-enhanced endothelial cell transmigration. Justification for the choice of each factor examined and the study performed is given before its results in the following commentary.

7.2 RESULTS

7.2.1 The impact of KSHV inoculation on the secretion of IL-6, IL-8 and IP-10 by HUVEC

A luminex screen of the chemokines within KSHV-inoculated cell supernatants identified strong upregulation of IL-6 and IP-10 and modest upregulation of IL-8 with inoculation **(Figure 7.1)**

IL-6 was not considered a likely mediator of increased transmigration of KSHV-infected cells and was therefore not considered further in these studies since previous work in our laboratory had demonstrated a profound paracrine effect of IL-6 upon endothelial cell function: IL-6 in KSHV-inoculated supernatants suppressed neutrophil transmigration across inflamed endothelium (Butler et al., 2011). IL-8 was not involved in the mechanism (Butler et al., 2011); therefore, a possible contribution of IL-8 to KSHV-enhanced transmigration was examined.

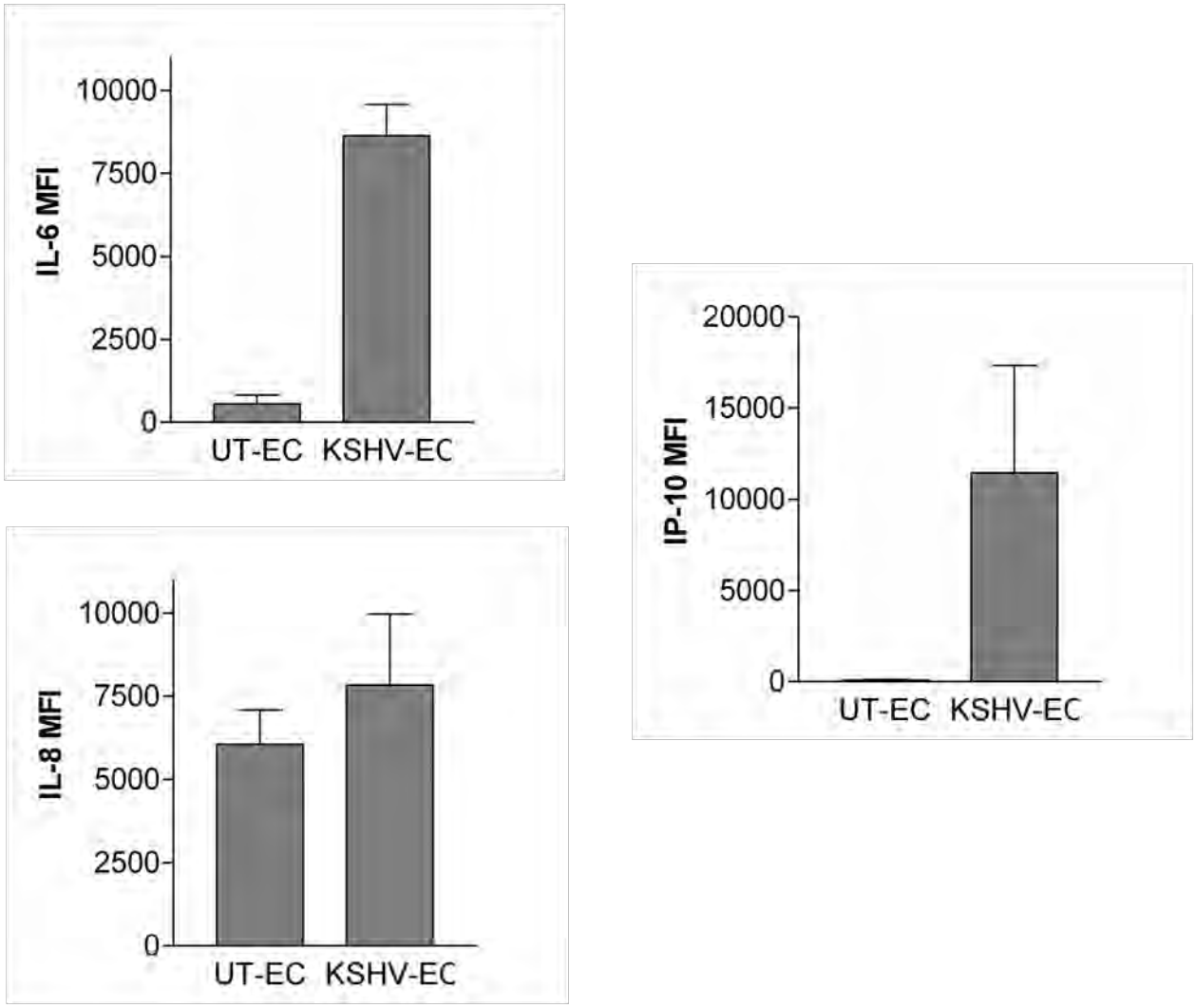

Figure 7.1: Effect of KSHV inoculation on the secretion of IL-6, IL-8 and IP-10 by HUVEC. 2-day, 24-well culture supernatants from untreated (UT-EC) and KSHV-inoculated (KSHV-EC) HUVEC cultures were collected between days three and seven post-inoculation and analysed by Luminex for the presence of IL-6, IL-8 and IP-10. Median fluorescence intensity values are reported. To concentrate secreted factors for this study, monolayers ($9x10^4$cells/well) were covered with 200µl culture medium as opposed to the usual culture volume of 420µl. Data are the mean ± SEM for two experiments.

7.2.1.1 Investigating a role for IL-8 in the enhanced transmigration of KSHV-infected HUVEC

Whilst microvascular endothelial cells express high levels of the IL-8 receptors CXCR1 and CXCR2 (Heidemann et al., 2003; Salcedo et al., 2000; Schraufstatter et al., 2003), most studies indicate that IL-8 receptor expression by endothelial cells is tissue specific with minimal expression detected on macrovascular HUVEC; accordingly, HUVEC demonstrate little migratory response to IL-8 (Li et al., 2003; Petzelbauer et al., 1995; Salcedo et al., 2000).

In previous studies a high level of CXCR1 on KS cells had been identified by immunohistochemistry whereas expression on early passage HUVEC was low. The same trend was observed by RT-PCR for both CXCR1 and CXCR2. Similarly, spindle shaped cells in KS biopsies stained positively for CXCR1 but the receptor was not detected in normal skin biopsies for the same donor (Masood et al., 2001). On the basis of these observations I hypothesised that KSHV infection might induce upregulation of one or both of these receptors on HUVEC and render infected cells sensitive to IL-8. However, flow cytometry staining for CXCR1 and CXCR2 revealed that neither CXCR1 nor CXCR2 was upregulated on HUVEC in response to KSHV infection **(Figure 7.2)** dissuading the feasibility of this hypothesis. Positive staining for CXCR1 and CXCR2 on freshly isolated neutrophils provided a positive control for the assay.

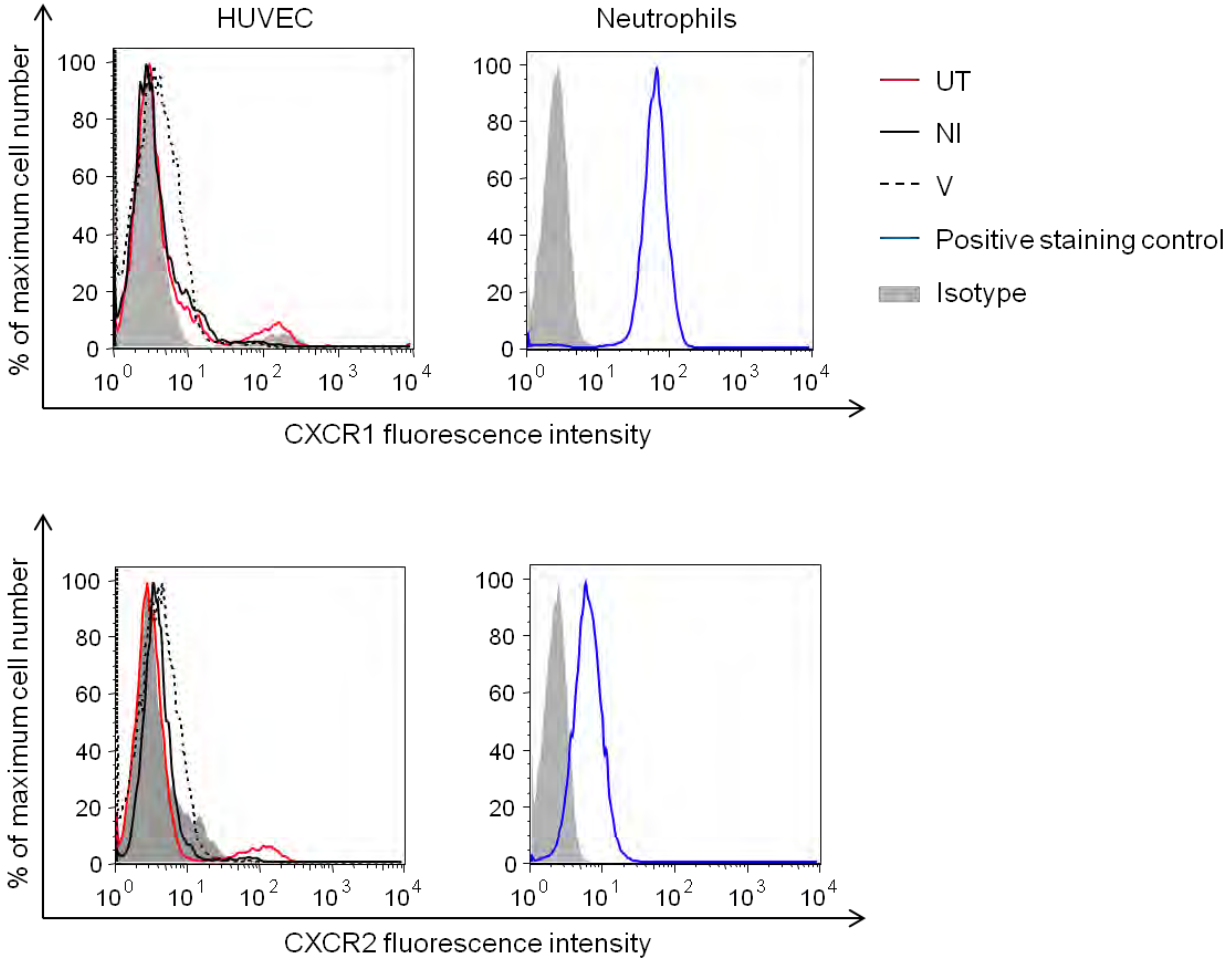

Figure 7.2: Effect of KSHV infection on cell surface expressions of CXCR1 and CXCR2. KSHV-inoculated (KSHV-EC) and untreated (UT-EC) HUVEC were stained on day-seven post-inoculation for their surface expression of the IL-8 receptors CXCR1 and CXCR2 and analysed by flow cytometry. KSHV-infected (V) cells were distinguished from non-infected (NI) cells within KSHV-EC monolayers on the basis of GFP positivity. Histograms for CXCR1 and CXCR2 staining of UT-EC (UT), V and NI populations are representative of three experiments. Staining of CXCR1 and CXCR2 on freshly isolated human neutrophils was a positive control for the assay.

7.2.1.2 Investigating a role for IP-10 in the enhanced transmigration of KSHV-infected HUVEC

IP-10 is generally considered an angiostatic molecule (Boshoff et al., 1997). However, it has been shown to act as an inverse agonist upon the KSHV protein vGPCR (Geras-Raaka et al., 1998; Rosenkilde et al., 1999) and to relieve the inhibitory effect of vGPCR overexpression upon lung endothelial cell migration, leading instead to enhanced transmigration (Couty et al., 2009).

Although vGPCR is typically considered a lytic cycle protein and cultures of KSHV-inoculated HUVEC present minimal lytic infection at day-seven post-inoculation, in our laboratory we had detected vGPCR transcripts in KSHV-inoculated HUVEC up to day-ten post-inoculation **(Figure 7.3)**. Therefore, the distinction between lytic and latent gene expression profiles might be small in a HUVEC host and lytic cycle proteins such as vGPCR might have a role in the mechanism of KSHV-enhanced transmigration. Others have similarly reported longterm expression of lytic genes following KSHV infection of HUVEC (Ye et al., 2007).

In view of the above reports, I hypothesized that the IP-10 secreted by KSHV-inoculated cultures could act through vGPCR to selectively modulate the transmigration potential of KSHV-infected cells. To test this hypothesis, a function blocking antibody against IP-10 was added to the culture medium throughout the 48hr transmigration period. Blocking IP-10 did not reduce the transmigration of KSHV-inoculated HUVEC cultures compared to no treatment control, although in the presence of anti-IP-10, the significant difference in transmigration between inoculated and untreated cultures was lost. Overall, these data suggest that the large upregulation in IP-10 alone did not coordinate the preferential transmigration of KSHV-infected cells **(Figure 7.4)**.

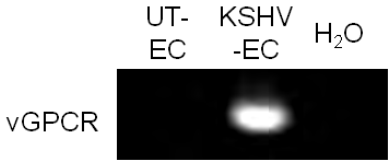

Figure 7.3: PCR for KSHV-vGPCR.

Total RNA was isolated from untreated (UT-EC) and KSHV-inoculated (KSHV-EC) HUVEC cultures and mRNA for KSHV-vGPCR amplified by PCR. Ethidium-bromide gel electrophoresis photograph for one HUVEC donor representative of three examined between days four and ten post-inoclation. β-actin endogenous control bands for the donor represented are shown in Figure 5.9A

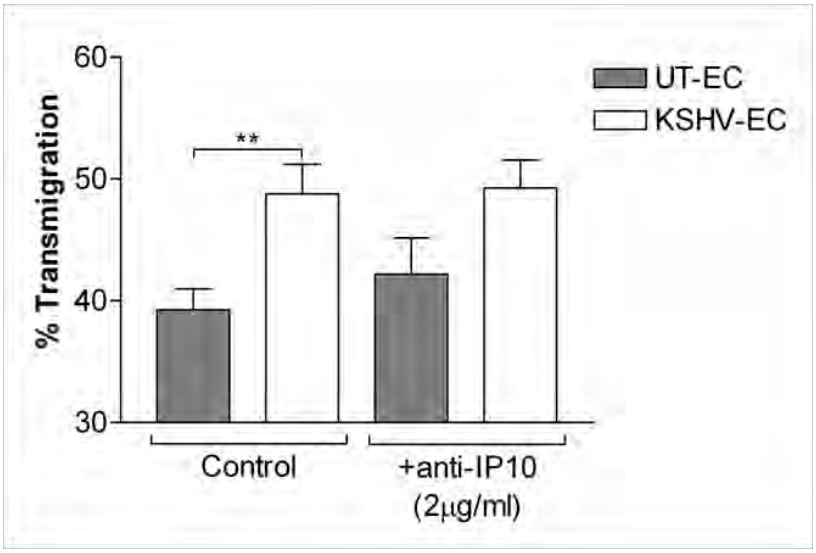

Figure 7.4: Effect of blocking IP-10 activity upon KSHV-enhanced transmigration of HUVEC.

KSHV-inoculated (KSHV-EC) and untreated (UT-EC) HUVEC were plated into 8μm-pore transwell culture inserts on day-seven post-inoculation and the percentage transmigration after 48hours examined by microscopy for cells in the presence of monoclonal mouse anti-human IP-10 function blocking antibody (2μg/ml) or no treatment control. Data are mean ± SEM for four experiments. ** = $P<0.01$ by paired t-test.

7.2.2 The impact of KSHV infection on the pro-angiogenic VEGFC/VEGFR3 axis

Besides increasing the secretion of VEGF ligands, KSHV infection has been shown to induce the transcription (Carroll et al., 2004; Hong et al., 2004) and translation of the VEGFC specific receptor, VEGFR3 (Carroll et al., 2004) in microvascular endothelial cells. The possibility of an autocrine action of VEGFC was proposed by the authors. Accordingly, I hypothesized that KSHV-infected endothelial cell migration might be specifically induced through the autocrine action of VEGFC upon VEGFR3 upregulated on infected HUVEC. I began to investigate this by examining the relative surface expression of VEGFR3 on untreated, non-infected and KSHV-infected HUVEC by flow cytometry seven days post-inoculation. The specificity and efficiency of the VEGFR3 staining protocol was verified by the positive staining of VEGFR3 on untreated LEC but no increase in VEGFR3 was observed on KSHV-infected HUVEC **(Figure 7.5)**. The absence of increased VEGFR3 expression on KSHV-infected HUVEC precluded the hypothesis of an autocrine loop for VEGFC in promoting the transmigration of KSHV-infected cells. Further studies to quantify VEGFC levels in supernatants were therefore not pursued.

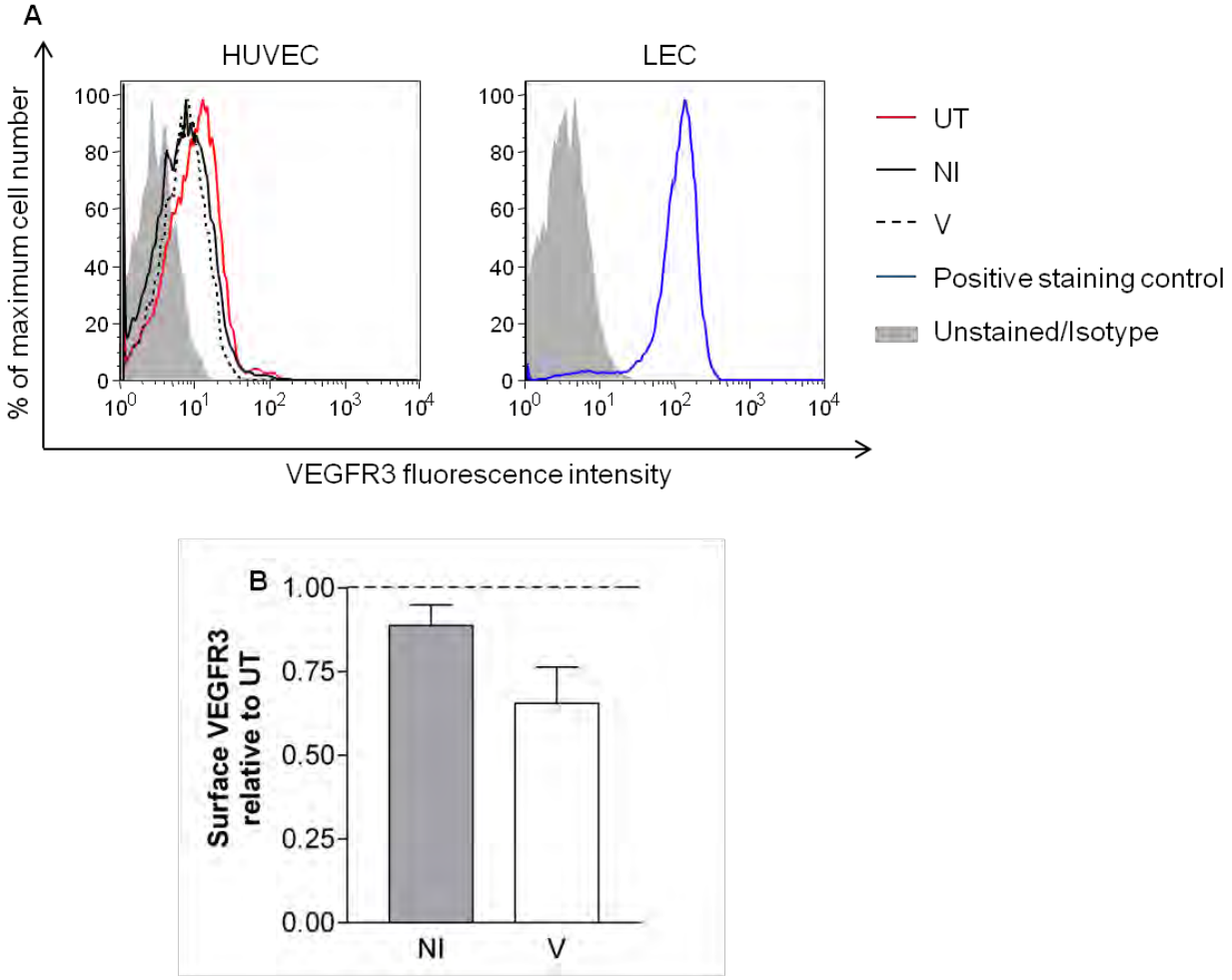

Figure 7.5: Effect of KSHV inoculation of HUVEC on cell surface expression of VEGFR3. KSHV-inoculated (KSHV-EC) and untreated (UT-EC) HUVEC cultures were stained on day-seven post inoculation for their surface expression of the VEGFC receptor, VEGFR3 and analysed by flow cytometry. KSHV-infected (V) cells were distinguished from non-infected (NI) cells within KSHV-EC monolayers on the basis of GFP positivity. **(A)** Representative histograms for VEGFR3 staining of UT-EC (UT), V and NI populations and lymphatic endothelial cells (LEC) (positive control). **(B)** VEGFR3 expression was measured in terms of median fluorescent intensity (MFI) and expressed for V and NI relative to expression on UT. Data are mean ± SEM for three experiments.

7.2.3The impact of KSHV infection on p38 MAPK activity

The p38 MAPK pathway is activated as part of the cellular response to stress stimuli such as cytokines, UV irradiation, heat shock, and osmotic shock wherein it coordinates processes of cell differentiation and apoptosis. Studies into the molecular basis of endothelial and smooth muscle cell migration in response to growth factors (VEGF and bFGF) and inflammatory cytokines have identified that activation of p38 MAPK, in particular the p38α and p38β isoforms, is also involved in coordinating cell migration in response to these factors (Denes et al., 2002; Hedges et al., 1999; Rousseau et al., 1997; Tanaka et al., 1999), Furthermore, p38 MAPK activation has been observed in response to KSHV infection of endothelial cells including HUVEC (Xie et al., 2005), human microvascular endothelial cells and human foreskin fibroblasts (Sadagopan et al., 2007)), and the use of p38 inhibitors found to suppress KSHV-induced-ANG-2 release by HUVEC (Ye et al., 2007) and vGPCR induced transcription and secretion of VEGF (Sodhi et al., 2000).

Considering these associations of the p38 MAPK pathway with cell migration, and also KSHV infection, I postulated that activation of p38 MAPK might underlie the increase in HUVEC transmigration with KSHV infection. To test this, transmigration assays were performed in the presence and absence of 10μM SB 203580, a pyridinyl imidazole derivative widely used as a specific inhibitor of the p38α and p38β isoforms. In the literature SB 203580 was used at concentrations in the range 1 to 25μM (Rousseau et al., 2000; Rousseau et al., 1997). In agreement, in our laboratory we had previously found that 10μM SB 203580 effectively inhibited sheer-induced suppression of neutrophil recruitment from flow under conditions of TNFα

stimulation (Luu and Nash, unpublished data). Therefore 10μM SB 203580 was used in these assays.

Contrary to my hypothesis, an increase in migration was observed in the presence of SB 203580 for both KSHV-inoculated and untreated HUVEC cultures relative to their no inhibitor control populations. However, the percentage increase in transmigration with inhibitor was only 11% for KSHV-inoculated cultures compared to 50% for untreated controls and the difference in transmigration in the presence of inhibitor was rendered not statistically different for KSHV-inoculated compared to untreated cultures **(Figure 7.6)**. To investigate whether in contrast to growth factor promoted migration, enhanced migration of infected cells involved suppression of p38 MAPK activity, levels of baseline phospho-p38 MAPK were analysed by flow cytometry. A prominent increase in phospho-p38 MAPK with 10-minute TNF (100U) stimulation verified that the staining protocol was robust **(Figure 7.7)** but no effect of KSHV-infection on baseline phospho-p38 MAPK was detected at day-seven post-inoculation suggesting that neither upregulation nor downregulation of p38 MAPK activity explained the enhancement in transmigration with KSHV infection.

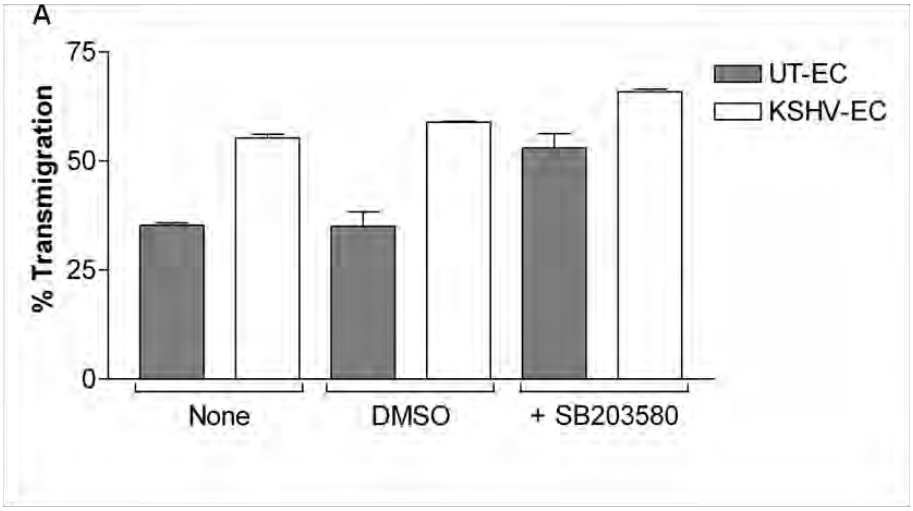

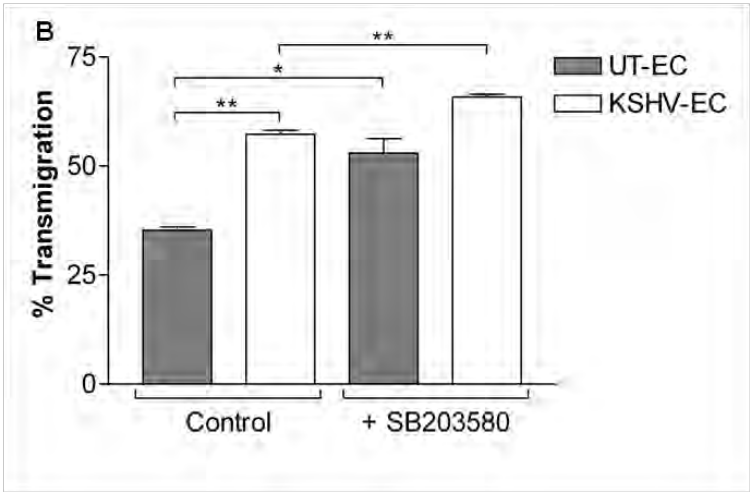

Figure 7.6: Effect of inhibition of p38 MAPK activity on KSHV enhanced transmigration of HUVEC.

(A) KSHV-inoculated (KSHV-EC) and untreated (UT-EC) HUVEC were plated into 8μm-pore transwell culture inserts on day-seven post-inoculation and the percentage transmigration after 48hours examined by microscopy for cells in the presence of the p38 MAPK inhibitor, SB203580 (10μM), or DMSO or no treatment control. Data are mean ± SEM for two-four experiments. **(B)** No effect of DMSO was apparent (panel A). Therefore, for robust statistical analysis of the effect of p38 MAPK inhibition, DMSO and no treatment control data in A were combined. Data are mean ± SEM for three or four experiments. * = $P<0.05$; ** = $P<0.01$ by paired t-test.

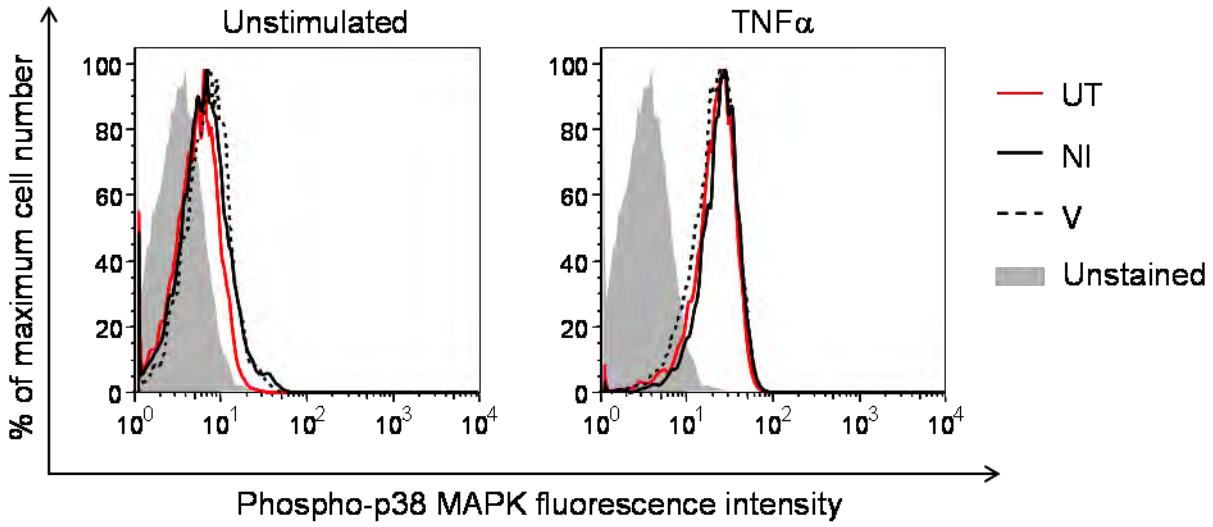

Figure 7.7: Effect of KSHV-infection on baseline p38 MAPK activity.

KSHV-inoculated (KSHV-EC) and untreated (UT-EC) HUVEC cultures were stained on day-seven post-inoculation for levels of phospho-p38 MAPK and analysed by flow cytometry. KSHV-infected (V) cells were distinguished from non-infected (NI) cells within KSHV-EC monolayers on the basis of GFP positivity. Staining of HUVEC stimulated with 100U TNFα for 10minutes served as a positive control for the assay. Histograms for phospho-p38MAPK staining of UT-EC (UT), V and NI populations are representative of three experiments.

7.3 DISCUSSION

Chemokines and certain growth factors in the extracellular milieu affect the motility of cells that express their cognate receptors. In this chapter, the hypothesis that the enhanced transmigration of KSHV-infected compared to non-infected or untreated HUVEC might be explained by infection-induced expression or upregulation of receptors to chemokines or growth factors secreted by inoculated cultures was tested.

KSHV-inoculation increased secretion of both IL-8 and IP-10 which signal via the G-protein coupled C-X-C chemokine receptors CXCR1 and CXCR2 and CXCR3 respectively **(Figure 7.1)**. Neither CXCR1 nor CXCR2 was detected on the surface of KSHV-infected, non-infected or untreated HUVEC **(Figure 7.2)**; thus a role for IL-8 in promoting migration of KSHV-infected cells was not supported by this study. Blocking the activity of IP-10 during transmigration also did not appear to reduce KSHV-enhanced transmigration **(Figure 7.4)**. Expression of the VEGFC receptor, VEGFR3, was examined but in contrast to its strong expression by lymphatic endothelium it was detected at very low level on the surfaces of KSHV-infected, non-infected and untreated HUVEC, and was not upregulated with KSHV-infection **(Figure 7.5)**; thus dissuading a role for VEGFC, a factor suggested to be upregulated upon KSHV infection of endothelial cells (Sivakumar et al., 2008), in promoting the enhanced transmigration of KSHV-infected HUVEC in this system.

P38 MAPK activity was also considered for its role in cell migration as a transducer of growth factor signaling and the upregulation of pro-angiogenic and promigratory factor expression. Interestingly an increase in transmigration rate was observed for both untreated and

KSHV-infected HUVEC in the presence of p38 MAPK inhibitor and the difference in percentage transmigration between untreated and KSHV-inoculated cultures found to be no longer significant **(Figure 7.6)**. While this might suggest that p38 MAPK activity was suppressive of transmigration and KSHV at day-seven post-infection was inhibitory to p38 MAPK activation, p38 MAPK activation was not evident for any category of cell when levels of phospho-p38 MAPK were examined **(Figure 7.7)**. Taken together, these data suggest that p38 MAPK was also not a key mediator in the mechanism of KSHV-enhanced transmigration at day-seven post-inoculation. The increased migration response in the presence of p38 inhibition might have arisen as a feedback effect to counteract the inhibition of a cellular pathway that when activated under certain conditions supports increased cell migration.

The increase in IL-8 in the supernatants of KSHV-inoculated HUVEC was consistent with previous reports that KSHV infection or transfection with KSHV-vGPCR increases secretion of IL-8 by endothelial cells. IL-8 has angiogenic properties (Schraufstatter et al., 2003); thus it is likely that during KS pathogenesis, the increased release of IL-8 by KSHV-infected spindle cells contributes to the aberrant angiogenesis that is a hallmark of the lesions. However, it remains unclear how IL-8 induces this response.

Microvascular endothelial cells are reported to express one or both of the IL-8 receptors and to demonstrate responses to IL-8 in proportion with their level of receptor expression (Salcedo et al., 2000) but it continues to be debated whether macrovascular endothelial cells, for which HUVEC provide a model, can bind and respond to IL-8: Li et al (2003) observed constitutive but low levels of IL-8 receptor on HUVEC, whereas Petzelbaur et al (1995) could not detect any IL-8 binding to HUVEC nor any receptor expression. *In vivo* CXCR1 was not expressed in normal

skin biopsies but the spindle shaped cells in KS biopsies stained positively for CXCR1 (Masood et al., 2001). Hence the data in this thesis provide further support that primary HUVEC do not express the classical receptors for IL-8 and are therefore unlikely to be directly responsive to IL-8. The absence of staining for either of the IL-8 receptors on infected HUVEC implies that KSHV infection does not impart direct responsiveness to IL-8. Further studies are needed to establish CXCR1 as a routine marker of KS spindle cells but if future studies validate it as a marker, the data in the present study suggest that KSHV-infected HUVEC may not fully recapitulate the properties of KS spindle cells *in vivo*.

Absence of VEGFR3 upregulation on KSHV-infected HUVEC appears to be another example of discrepancy between the expression profile of spindle cells in KS lesions and that of KSHV-infected HUVEC and was a surprising observation given that KSHV infection of BEC has been identified to cause modulation of the BEC phenotype toward that of lymphatic endothelium (Carroll et al., 2004; Hong et al., 2004; Wang et al., 2004a) including induction of VEGFR3 gene expression. However, the vascular bed from which BEC are isolated might be an important determinant in the response to infection.

Commercially available microvascular endothelial cells used in the work by Hong et al and Wang et al were mixed populations of blood and lymphatic endothelial cells (Hong et al., 2004; Wang et al., 2004a). While changes in the lymphatic component might have predominated in the gene expression data, microvascular blood and lymphatic cells might represent endothelial cell lineages with greater phenotype plasticity compared with HUVEC, rendering them more susceptible to a switch in phenotype under the influence of KSHV. Supportive of this hypothesis, characterisation of human dermal microvascular endothelial cells showed that most but not all of

VEGFR-3-expressing cells and a few VEGFR-3 negative cells stain for the lymphatic endothelial cell marker LYVE-1 (Makinen et al., 2001). Nonetheless, in their commentary Hong et al did report the induction of lymphatic lineage-specific genes after KSHV infection of HUVEC and the concurrent downregulation of several blood vascular-specific genes (Hong et al., 2004). Therefore, the source of KSHV, and conditions of infection and subsequent culture might be responsible for differences between studies. Notably, the recombinant KSHV used in the present study was derived from the JSC-1 cell line whereas Wang et al (2004a) and Carroll et al (2004) used BCBL-1 derived KSHV.

Although VEGFR3 was not upregulated on the surface of infected HUVEC in the present study and was therefore not a favoured candidate for KSHV-induced enhanced transmigration, it is possible that infection induced activation of the receptor (expressed at low levels) thereby facilitating enhanced transmigration potential of KSHV-infected cells within inoculated cultures in the presence of cognate ligand. In this scenario, VEGFR3 might act in consort with VEGFR2 since the motogenic stimulatory effect of VEGFC on cells of an immortalised KS cell line was reduced when a mutant form of VEGFC unable to bind to VEGFR2 was used (Marchio et al., 1999).

In KS pathogenesis, active VEGFR3 might also cooperate with VEGFR2 to promote the proliferation of KS cells since stimulation with a mutant form of VEGFC unable to bind to and activate VEGFR2 prevented KS cell proliferation (Marchio et al., 1999). Similar to the debate over VEGFR3 however, while studies using microvascular endothelial cells and microvascular blood-endothelial cells (Sivakumar et al., 2008) observed upregulation of VEGFC following KSHV infection and some have reported increased levels in lesions (Skobe et al., 1999; Ye et al.,

2007), others suggest down regulation of VEGFC expression following the infection of BEC (Hong et al., 2004) and no substantial over expression in Kaposi's sarcoma (Wang et al., 2004a). Thus it remains questionable as to whether VEGFC and VEGFR3 are present at sufficient level and appropriately activated in this system for VEGFC action on VEGFR3 to have a role in enhanced transmigration.

IP-10 is known to be an inverse agonist of KSHV-vGPCR (Geras-Raaka et al., 1998; Rosenkilde et al., 1999) and IP-10 mRNA has been detected in frozen sections of non-AIDS KS skin biopsies (Uccini et al., 2003) but to my knowledge there are no reports of induction of IP-10 secretion by KSHV-infected primary endothelial cells *in vitro*. Thus the present study provides the first indication of a feedback loop involving IP-10 in KSHV-infected endothelial cell cultures.

Physiologically, IP-10 has angiostatic properties (Boshoff et al., 1997; Strieter et al., 1995) while constitutive signaling of vGPCR is proangiogenic (Ma et al., 2010); hence the inhibitory action of IP-10 at vGPCR might be expected to protect against angiogenesis in KS. Conversely however, Couty et al (2009) demonstrated that IP-10 acting as a chemokine induced the transmigration of vGPCR expressing MLEC thereby relieving an apparent suppressive effect of KSHV-vGPCR on endothelial cell transmigration. When IP-10 was added to both sides of the transwell assay, a trend toward increased transmigration of KSHV-vGPCR was also evident, implying IP-10 might stimulate chemokinesis of vGPCR expressing cells. The data in this thesis blocking IP-10 activity does not however substantiate a role for IP-10 in KSHV-enhanced transmigration.

In the present study, although vGPCR mRNA was detected at day-seven for inoculated cultures, reagents were not available to assess the percentage of vGPCR positive cells in the cultures. Since virus gene expression follows temporal changes—vGPCR is a 'lytic' gene and lytic infection is low at day-seven—it is possible that the vGPCR mRNA signal was due to a small number of vGPCR expressing cells. Therefore, it may be that blocking IP-10 did act in our system to suppress the motility of vGPCR expressing cells but the number of cells was too few to have a significant and noticeable impact on transmigration rate at the population level. Clearly, therefore another factor was more important on the population level. In KS lesions, rather than affecting spindle cell migration, it is possible that IP-10 release is instructive in the recruitment of effector T-lymphocytes underlying the inflammatory phenotype of the lesions (Loetscher et al., 1996).

Previous reports of a role for p38 MAPK activation in cell migration have implicated the p38 MAPK pathway in mediating growth factor, chemokine and proinflammatory cytokine induced cell migration. For example each of PDGF, IL-1β and TGFβ-induced transmigration of tracheal smooth muscle myocytes involved p38 MAPK activation (Hedges et al., 1999), and endothelial cell growth factor promotion of bovine aortic endothelial cell migration in a scratch wound assay was p38 MAPK dependent (Denes et al., 2002). Couty et al (2009) also found phosphorylation of p38 MAPK occurred in vGPCR expressing MLEC concomitant with IP-10 treatment. They hypothesized that p38 MAPK activation might underlie IP-10-induced chemotaxis of vGPCR expressing MLEC.

Given these associations of p38 MAPK with growth factor and chemokine induced cell migration, the lack of observation of p38 MAPK activation in the present study following KSHV inoculation agrees with the additional findings in this chapter that growth factors and chemokines (e.g. VEGFC, IL-8 and IP-10) are unlikely mediators of KSHV-induced migration. Moreover, while Xie et al (2005) observed upregulation of AP-1 activity within 30minutes following KSHV infection and attributed this to p38 MAPK activation though studies using inhibitors and dominant negatives, Sadagopan et al (2007) reported p38 MAPK activation to subside beyond 48hours. Thus the fact that baseline p38 MAPK was not elevated at day-seven is in agreement with p38 MAPK activity as an early response to infection but not in underlying the functional phenotypes of cells harbouring established latent KSHV-infection as used in the present study.

In summary, secreted growth factors and chemokines, upregulated upon KSHV infection of endothelial cells, were investigated in this chapter for their roles in the enhanced migration of KSHV-infected primary endothelial cells. The absence of expression and upregulation of their receptors on the surfaces of KSHV-infected cells suggested that none of those tested was responsible (IL-8 via CXCR1 or CXCR2; VEGFC via VEGFR3). IP-10, an inverse agonist for vGPCR was also not involved and p38 MAPK activation was not evident. In view of the enhanced transmigration of KSHV-infected cells however, differential expression and or activation of key molecules involved in cell migration is expected between infected and uninfected cells. Candidates may be receptors or components of intracellular signaling pathways that regulate for example the plasticity of the cytoskeleton and assembly/disassembly of focal adhesions.

CHAPTER EIGHT

GENERAL DISCUSSION

8.1 SUMMARY OF FINDINGS IN RELATION TO PREVIOUS STUDIES

An extensive aberrant vasculature is a hallmark of KS, a multifocal malignancy caused by KSHV. In view of the role that cell migration plays in tumour angiogenesis, the underlying aims of this thesis were to determine, using *in vitro* methods, the impacts of KSHV infection on the migration of primary endothelial cells per se and on properties of endothelial cells that might contribute to the regulation of their motility.

Prior to this thesis, few studies had examined the effects of infection by the whole KSHV virus on the behaviours of primary endothelial cells. Instead, investigations had concentrated on characterising the functions of individual KSHV genes through approaches such as ectopic gene expression. This was presumably due, at least in part, to the paucity of endothelial cells to be infected by the virus *in vitro*. Hence for the functional studies described in this thesis, it was necessary to first establish a robust method for infection of primary endothelial cells with KSHV. Primary HUVEC were the endothelial cell of choice for this work.

KSHV concentrated from supernatants of PMA and sodium butyrate-reactivated PEL cells afforded less than 20% infection of primary HUVEC **(Figure 3.1)**. In contrast, a recombinant variant of the virus (rKSHV.219) that was propagated in the primate Vero cell line and reactivated using ectopic supply of the lytic switch protein RTA together with sodium butyrate could be concentrated to high titre and used to infect primary HUVEC with greater than 50% efficiency **(Figures 3.4 and 3.7A)**. To my knowledge, the opening studies in this thesis provide the first rigorous characterisation of the properties of HUVEC cultures infected with this recombinant virus strain over a prolonged period (up to ten days). This work provides new

information to the field that could aid the design and interpretation of functional studies in the future.

Consistent with the spindle shape of KSHV-infected cells in KS lesions, KSHV infection induced a change in cell shape from cobblestone to spindloid that became more pronounced with time post-infection **(Figure 3.6)**. Percent infection of inoculated cultures increased over time to 80% latent infection by day-ten **(Figure 3.7A)**. In contrast, following a lytic burst over the first 2.5 days, during which an average of 15% of the culture died, the numbers of infected cells in which the virus entered lytic replication decreased with time: between days 6.5 and 8.5 only 1.5% of cells died due to lytic death **(Figures 3.7B and 3.11B)**. Therefore, in the long-term, KSHV-infected cultures were predominantly latently infected consistent with the nature of KSHV infection in KS lesions. As suggested for *in vivo* disease, the low background of spontaneous lytic replication may have contributed to the maintenance of infection of inoculated cultures (Gantt and Casper, 2011; Grundhoff and Ganem, 2004).

The temporal rise in percent infection of primary HUVEC fitted with observations by others in cell lines (Moses et al., 1999). It had previously been hypothesised that such increases in percent infection over time were due to the proliferation of infected cells or horizontal spread of infection through the culture (Moses et al., 1999). However, the data presented in this thesis provide important insight that neither of these factors is the predominant cause for the time-dependent rise in infection within cultures of primary HUVEC.

Firstly, rather than an increase in cell numbers within inoculated cultures, monolayer density decreased and to an extent that was largely explained by the lytic death **(Figure 3.11)**.

There was no rise in cell numbers after the initial lytic burst to suggest enhanced proliferation rates of infected cells. Thus the virus was not found to be transforming of primary HUVEC and the effects of contact inhibition of cell division appeared to be maintained even within KSHV-infected monolayers. This recapitulates the behaviour of spindle cells isolated from KS lesions (Lagunoff et al., 2002). However, Ciufo et al (2011) showed that colonies of infected cells, which established in inoculated monolayers of primary dermal microvascular endothelial cells could be isolated and expanded to generate cultures in which all cells were infected and spindloid; thus it would be interesting to isolate infected cells from inoculated monolayers and compare the expansion of these cultures to that of parallel untreated control cells.

Secondly, when cultures of KSHV-inoculated and untreated HUVEC were mixed, transmission of infection occurred to only 3.3% of untreated cells in contrast to 35% of non-infected cells during a five-day period between days three and eight post-inoculation **(Figures 3.8 and 3.9B)**. Although a background of spontaneous lytic replication might support maintenance of infected cultures—which otherwise lose the KSHV episome over serial passages if there is no selection or re-infection (Grundhoff and Ganem, 2004)—and is in agreement with suggestions that ongoing lytic replication and infection of new cells is needed for tumour development, we postulate that a high (70-80%) infection occurs upon initial inoculation but there is a delay in appearance of infection in some cells compared to others due to heterogeneity in the number of viral particles entering cells upon inoculation: In cells where the initial loading is lower, more time is required before replication of the viral episome and subsequent gene expression reaches adequate levels for the viral and reporter genes to be expressed to levels that provide evidence of infection.

Having established a method for high level KSHV infection of primary endothelial cells, it was used to prepare populations of inoculated HUVEC, which inevitably included infected and non-infected cells, for functional studies.

In set ups that allowed observation of cell migration in the context of confluent monolayers (transmigration and wound recovery assays), KSHV infection increased HUVEC migration **(Figures 4.2, 4.3, 4.8 and 4.9)**. In contrast, the virus did not alter the distance migrated or persistence of migration of isolated cells **(Figures 4.12, 4.13 and 4.14)**. With the aid of GFP fluorescence to distinguish infected and non-infected cells, it was evident that enhanced transmigration over a 48hour period was the result of preferential transmigration of infected cells: non-infected cells in inoculated cultures maintained a level of transmigration equivalent to that of untreated controls **(Figure 4.3)**. Interestingly, in the wound recovery setting such differential behaviour between infected and non-infected HUVEC was not apparent: infected and non-infected HUVEC presented equivalent migration rates and pathways **(Figure 4.11)**. The reason for this discrepancy is not clear but might be attributed to differences in the physical constraints (presence or absence of a porous barrier) between the two systems.

Cell migration occurs in response to a stimulus that may be soluble, immobilised or mechanical force. Subsequent to detection of the stimulus by the cell via activation of its cognate receptors, the cell establishes points of contact with its underlying substrate and coordinates changes in the organisation of its actin cytoskeleton to facilitate the generation of traction forces through the cell that support its forward movement (Lamalice et al., 2007). Thus chemotactic/chemokinetic factors, molecules of underlying substratum (basement membrane proteins), integrins and other proteins of focal adhesion complexes and cytoskeleton organisation

might all contribute to the overall migration rates of cells. In this thesis the effect of the virus on major candidates selected from each one of these categories was examined in an effort to identify the key determinants of cell migration that are regulated by the virus.

At the level of possible chemokinetic factors the virus was found to increase IL-8, and IP-10 secretion by HUVEC **(Figure 7.1)**. Since transmigration of non-infected cells was less than that of infected **(Figure 4.3)** and supernatants from KSHV-inoculated cultures did not support an increase in the transmigration rates of previously untreated cells **(Figure 4.4)**, it was clear that if a soluble factor was responsible for enhanced transmigration it would have to act only on infected cells through their selective upregulation or activation of cognate receptors. Neither of the IL-8 receptors, CXCR1 or CXCR2, was induced by the virus, dissuading a migration stimulating role for IL-8 **(Figure 7.2)**.

KSHV-infection had been associated with the production of VEGFC (Carroll et al., 2004; Sivakumar et al., 2008) and the presence of VEGFR3 (Carroll et al., 2004; Hong et al., 2004) expression but no upregulation of VEGFR3 was found following KSHV infection of HUVEC dissuading the likelihood that action of VEGFC, possibly evolved into culture supernatants by KSHV infected cells was responsible **(Figure 7.5)**. Constitutive vGPCR activity had been suggested to have anti-migratory effects and IP-10, acting as an inverse agonist, shown to enhance migration (Couty et al., 2009) but use of a neutralising antibody to block the action of IP-10 secreted in this system in the presence of KSHV infection did not appear to reduce the virus-induced enhanced transmigration **(Figure 7.4)**.

Growth factors signal through p38MAPK pathways to regulate migration but induction of p38MAPK activation was not evident with KSHV infection **(Figure 7.7)** further supporting that selective control of cell motility was unlikely to be through the signalling of secreted growth factors.

Studies in this thesis to address the impact of KSHV upon the deposition of endothelial basement membrane proteins (examples of insoluble, haptotactic stimuli) highlighted that the virus modulates basement membrane laminins. Overall the proteins of the sub-endothelial matrix examined in the study included the three major constituents of endothelial basement membranes: collagen IV, fibronectin and laminins. No change in deposition of either collagen IV or fibronectin was found with KSHV infection while Laminin-P1 (laminin detected by an antibody raised against the P1 Pepsin-resistant fragment of human placental laminin, but for which the precise conformation of the epitope recognised was not known) decreased three fold **(Figures 5.2 and 5.4)** and laminin-α4 chain increased three-fold **(Figure 5.10A)**.

Follow-up studies in this thesis were unable to elucidate the reasons for these changes in laminin deposition induced by KSHV infection. Although KSHV infection had been noted to increase MMP production (Meade-Tollin et al., 1999; Qian et al., 2007; Wang et al., 2004b), the decrease in laminin-P1 following KSHV inoculation was not prevented by culture in the presence of MMPs or serine proteases **(Figure 5.6)**. In addition, exposure of untreated endothelium to supernatants from inoculated cultures failed to induce a reduction in deposition of laminin-P1 by these cultures; thus dissuading the hypothesis that a factor secreted by KSHV-infected cultures has laminin degrading activity **(Figure 5.5)**. At the mRNA level, the virus was not seen to alter expression of any one of the main endothelial laminin chains (α1, α2, β1, β2 or γ1) **(Figure 5.9)**

but intracellular protein levels of laminin-α4 were increased in KSHV-infected cells, suggesting translational regulation by the virus **(Figure 5.11)**. While laminin β and γ chains require dimerisation and subsequent incorporation of the α subunit in order to be secreted, α chains may be secreted independently (Yurchenco et al., 1997). Such enhanced α-chain secretion may explain the rise in laminin-α4 within the sub-endothelial matrix of inoculated cultures.

The impact of these changes in laminins upon HUVEC migration was investigated in this thesis but using siRNA to deplete endogenous laminin-α4 chain did not reduce transmigration rates **(Figure 5.15C)**, neither was the closure of wounds of untreated HUVEC enhanced on matrix deposited by KSHV-infected cultures **(Figure 5.12)**. Nonetheless, compensatory changes in deposition of other laminin chains might have been induced in the presence of laminin-α4 knockdown. Furthermore, simply reducing laminin-α4 levels may not have restored a normal matrix organisation and the assembly process rather than the organisation of matrix fibres could be an important determinant of migration.

Consistent with the changes in laminins deposited, KSHV infection was observed to upregulate surface expression of the laminin-binding, α6-integrin **(Figure 5.17)**. While blocking the function of this integrin during transmigration assays did not prevent KSHV-enhanced transmigration **(Figure 5.18)** the observation of changes to the laminin network and its receptors provides a strong indication that the laminin-integrin axis may play fundamental roles in the pathobiology of KS.

In addition to effects on the basement membrane proteins, KSHV infection targeted the actin cytoskeleton. Previously an effect of the virus on the actin cytoskeleton had been noticed in

the context of initial infection, mediating virus entry and traffic to the nucleus (Greene and Gao, 2009; Raghu et al., 2009). To my knowledge, the work in this thesis provides the first evidence that the virus continues to manipulate the actin cytoskeleton of endothelial cells over an extended period (up to seven days post-inoculation). Redistribution of the actin filaments from a network across the whole cytosol into stress fibres that partitioned toward the cell cortex was identified with infection **(Figures 6.3, 6.5 and 6.6)**. Since the actin cytoskeleton is known to have a key role in facilitating cell movement through generation of traction forces, it is likely that such dramatic remodelling of the cytoskeleton by the virus contributed to the altered migration rates.

Coincident with actin filament bundling and the extension of these fibres along the length of the cell, virus infection led to the presence of vinculin-stained focal adhesion structures at the tips of the cell rather than around the entire cell perimeter **(Figure 6.8)**. Moreover, the puncti formed were significantly smaller and fewer in number with KSHV infection **(Figure 6.9)**. These changes in focal adhesions are hypothesised to be key contributors to changes in motility. A reduction in focal contact size could for example reflect weaker adhesive forces and/or increased rates of turnover; such properties could facilitate an increase in migration rates providing that sufficient traction on the cell surface is still achieved.

8.2 PERSPECTIVES AND FURTHER WORK

Overall, the studies contained in this thesis indicate that KSHV infection can promote the migration of endothelial cells at least from the context of an endothelial monolayer and it is tempting to speculate that the increased transmigratory, penetrative behaviour of KSHV-infected cells is indicative of tip cell characteristics. Since there was no known chemoattractant gradient in the transmigration assay it raises the question of whether KSHV infection might even confer a

constitutive tip cell phenotype. The enhanced rates of wound recovery also indicated a potential for endothelial monolayers to move more rapidly when infected cells are present and this could also support new vessel formation.

During the process of angiogenesis, endothelial cells migrate into the tissue stroma. The studies reported in this thesis examined the effect of KSHV on HUVEC motility in the absence of tissue matrix; thus to verify enhanced motility as an inducer of angiogenesis, further studies could examine the effect of the virus on the formation of 'tube-like' structures when the cells are either plated on Matrigel or when spheroids of cells are embedded into a collagen matrix: the latter would permit observation of 3D angiogenesis *in vitro*. KSHV-infected HUVEC might also be introduced into mice to test whether they will promote angiogenesis *in vivo*. However, since the data in this study suggested that KSHV-infection of HUVEC is not transforming, it is uncertain whether tumours derived from KSHV-infected HUVEC would arise in the mouse.

The studies reported examined properties of endothelial cells through which KSHV might act to confer enhanced migratory potential to infected cells. The selection of secreted chemokines and surface receptors examined was restricted by the availability of reagents, thus within each class of molecule, other family members not examined might be responsible. For example infection might have induced the surface expression of integrins that are not typically expressed on endothelial cells as reported with HCMV infection of endothelial cells (Tabata et al., 2008). Alternatively a receptor's expression level might not alter but its activation be enhanced. Observing activating post translational modifications such as phosphorylation status could thus be informative as to the importance of a given receptor (e.g. growth factor receptors and integrins).

Besides endothelial expressed genes, KSHV genes that direct the response could be examined. K15M has been linked to enhanced migration (Tsai et al., 2009) hence is an attractive candidate. Moreover, the suggestions that KSHV- vGPCR (Couty et al., 2009) and K5 (Mansouri et al., 2006) are inhibitory to migration are based upon single studies, thus it would be informative to verify through methods such as siRNA knockdown their roles in this system also. Indeed in view of the pro-angiogenic effect of vGPCR it is counterintuitive that it should have anti-migratory effects and K5 was shown to induce changes to the actin cytoskeleton similar to those reported in this study. The latency protein vFLIP has also been noted for its effects on the actin cytoskeleton thus might be considered too (Grossmann et al., 2006).

The striking changes in laminin deposition with KSHV-infection warrant further investigation. The fact that laminin-P1 decreased whereas laminin-α4 increased raises the question as to what effect the virus had upon laminin β and γ chains. It would be interesting to examine by ELISA the effect of KSHV-infection on deposition of each of the endothelial laminin-β and γ chains (β1, β2, γ1). This would help to establish whether or not the increase in laminin α4 is due to increased α-chain secretion. Such an imbalance in chain deposition would likely have significant influence upon the properties of the matrix given that the β and γ chains each contain domains that mediate the interaction of laminin with other macromolecules of the extracellular matrix such as proteoglycans, netrin 4, and nidogen (Hamill et al., 2009).

Although studies in this thesis did not demonstrate a role for the altered sub-endothelial matrix in the phenotype of KSHV-enhanced migration, KSHV infection might have upregulated deposition of other laminin α chains, either constitutively or in response to laminin-α4

knockdown, that compensated for laminin-α4 when its levels were reduced toward those of untreated endothelium. To help provide insight into whether a 'normal' basement membrane was generated by the intervention of laminin-α4 knockdown, the laminin-P1 and laminin-α5 levels could be evaluated in consort with laminin-α4 knockdown. Electron microscopy imaging might also provide qualitative evidence to indicate whether the matrix architecture is recovered by simply reducing laminin-α4 expression.

It is important to note that the regulation of laminin-α4 by KSHV was not at the genetic level. It is likely that other proteins were regulated through a similar posttranslational mechanism to laminin-α4 and could be mediators of the enhanced migration. Thus ascertaining the mechanism underlying increased laminin-α4 deposition might help to identify key regulators of KSHV-induced endothelial cell migration. Mass spectrometry with Stable Isotype Labelling with Amino acids in Cell culture (SILAC) to compare the protein complements of KSHV-infected and untreated cells would be useful. Similar assessment of deposited sub-endothelial matrices would also be advantageous for gaining a fuller understanding of the changes arising in this extracellular substance and may help to identify further endothelial proteins that might be harnessed by the virus for enhancing migratory/angiogenic effects. Candidates could then be tested functionally. Phosphoproteome arrays could also help establish proteins whose activation states are regulated.

Using such global protein and phosphoprotein screens would also be expected to aid understanding of the changes in focal adhesion size and number that were observed in this thesis by immunofluorescence staining for vinculin. For example, if the reduction in focal adhesion size was due to reduced vinculin recruitment into focal adhesions, downregulation of proteins

involved in vinculin recruitment might be identified or increased activity of proteins associated with focal adhesion turnover might be evident. Verification of any candidate proteins identified in this way could be made using the method of immunofluorescence staining as described in this thesis for vinculin. Even without large arrays, an indication of whether the decreases in focal adhesion size and number were due to the choice of vinculin as the marker for focal adhesions would be possible from staining cells with a panel of antibodies against other proteins routinely observed at focal adhesions such as: talin, paxillin and FAK.

The vessels observed in KS lesions are described as 'leaky' suggesting that the endothelium might have greater porosity following KSHV infection. Possibly the degradation of junctional proteins catalysed by KSHV genes, such as K5, has roles in this. The alterations to the basement membrane might also make it more porous and contribute to this property of leakiness. Porosity differences could be compared for KSHV-inoculated and untreated cultures using optical fluorometric methods.

Another impact of the altered basement membrane that would be interesting to pursue is its effect upon leukocyte recruitment to tissue since KS lesions are characterised by a large inflammatory infiltrate. Consistent with the concept that basement membrane might influence this process, we recently demonstrated that the maturation of 'normal' sub-endothelial matrix hindered neutrophil migration across cytokine stimulated endothelium (Burton et al., 2011). While the work by Burton et al (2011) did not demonstrate an effect of matrix maturation upon the extravasation of lymphocytes or monocytes, other investigators have shown that laminin-α4 deficiency impairs the recruitment of all major leukocyte subsets in response to inflammatory stimuli: a role for laminin-α4 in aiding leukocyte penetration of the vessel wall was proposed

(Kenne et al., 2010; Sixt et al., 2001; Wondimu et al., 2004). Hence the increase in laminin-α4 with KSHV infection might support increased leukocyte extravasation.

To date the precursor of the KS spindle cell has not been fully defined. Both LEC and BEC are infected by KSHV and infection appears to cause a shift in the phenotype of each cell type toward that of the other (Hansen et al., 2010; Hong et al., 2004; Wang et al., 2004a). While the present study supports a pro-angiogenic impact of KSHV on endothelial cells consistent with the angiogenic nature of KS, from observations that the gene signatures of neoplastic cells of KS closely resemble those of LEC, and LEC support a higher number of KSHV genomes than BEC, Wang et al (2004) suggested that a lymphatic origin be favoured over blood vascular. Therefore, it would be interesting to examine whether KSHV infection modulates the migration and migration-influential factors of primary LEC as well as of HUVEC.

An expansion of the KS-like spindle cell population isolated from peripheral blood has been found in KS patients compared to controls and KSHV infection detected in these cells (Sirianni et al., 1997). These cells cultured from circulation express endothelial and macrophage markers (Browning et al., 1994; Sirianni et al., 1997). By their localisation into tissues they might contribute to the multifocal appearance of KS; however their specific origin continues to remain unknown. Endothelial progenitor cells, which originate in the bone marrow, are one candidate. Over recent years, methods to reliably isolate and culture endothelial progenitor cells from whole blood have been established and it would be interesting to observe the impact of KSHV infection on this class of endothelial cell too.

8.3 PHYSIOLOGICAL AND THERAPEUTIC RELEVANCE OF THIS STUDY

This study has provided evidence that infection of endothelial cells by KSHV causes chronic alterations in multiple facets of endothelial cell biology, impacting properties such as basement membrane protein deposition, integrin profiles, chemokine secretion, wound recovery migration and transmigratory, 'penetrative' migration. Although the precise intracellular mechanisms by which the virus yields these effects are not known, it is likely that together they contribute to the development of KS lesions *in vivo*.

The homology between KSHV and other herpesviruses, suggests the effects of KSHV on endothelial cells described in this study might be recapitulated in other cell types infected by other herpesviruses and contribute to the development of the diseases with which they are associated. Other cancer causing viruses including members of the polyomavirus, hepadnavirus, and papillomavirus families (Morris et al., 2008) might also utilise similar mechanisms.

To my knowledge, changes in matrix protein deposition and matrix architecture have not been widely examined in the context of virus induced cancers. The alterations in the laminin and integrin profiles with KSHV infection of primary endothelial cells provide strong support that the ECM secreted by tumour-associated cells, such as endothelial cells, governs lesion formation. This influence of the ECM may be via effects on the adhesion and migration, proliferation and survival of both the secreting cell and the other cell types present in the lesions (fibroblasts, endothelial cells, immune cells, proliferating cells).

Clinical trials to establish the most appropriate regimens for the treatment of KS are ongoing. Strategies include the use of chemotherapeutic agents, radiotherapy, Highly Active

Anti-Retroviral Therapy (HAART) and herpesvirus DNA synthesis inhibitors (Gantt and Casper, 2011; Sarwar et al., 2007; Uldrick and Whitby, 2011). Both monotherapy and combination therapy approaches have been tried. HAART and herpesvirus DNA synthesis inhibitors have also been tested prophylactically with some indication of benefit. In fact inhibitors of herpesvirus DNA synthesis, when given as a monotherapy, appear more effective for preventative medicine than as an active therapy (Gantt and Casper, 2011).

HAART, a combination of nucleoside reverse transcriptase inhibitors with a non-nucleoside reverse transcriptase inhibitor or protease inhibitor, was first introduced based on the association of HIV-infection with increased risk of KS (AIDS-KS). Immune reconstitution is central to the clinical benefit of HAART; however, there is some indication that the protease inhibitors might target KS development in a mechanism independent of effects on HIV replication and restoration of the immune system, thereby having a therapeutic effect even in a non-HIV setting (Gantt and Casper, 2011).

The use of HAART has greatly reduced incidence of AIDS-KS in developed countries when given either alone to treat early stage AIDS-KS or in combination with chemotherapeutic agents to treat advanced AIDS-KS (Sarwar et al., 2007). Such positive results with HAART in western countries mean that the current clinical burden of KS is primarily in the developing world, where HAART is not only too expensive but non-HIV-associated endemic-KS is prevalent. Sadly, due to this divide between resource wealthy and resource poor countries, in terms of the pressure placed by KS on healthcare resources, the development of new drugs to treat KS has received minimal investment by pharmaceutical industries. Since current KSHV-targeting drugs/strategies available are often ineffective, novel therapies are needed in order to

successfully treat or prevent non-AIDS-KS, which is a cause of high morbidity and mortality in parts of Africa. Treatments which target KSHV and/or its mechanism of induced tumourigenesis may be of benefit, possibly also affording reduced side effects compared to traditional chemotherapeutic approaches. The design of such drugs requires greater understanding of the mechanisms underlying KS pathogenesis.

While the present study has not identified a viral or host cell gene that might be targeted therapeutically, it has described functional effects of KSHV infection on endothelial cell biology (migration, laminins, actin cytoskeleton, focal adhesions, chemokines), which may be targeted or for which the viral genes responsible might now be pursued. If future studies show other viruses to be inducers of similar responses, such novel therapies might have application in the treatment of a range of diseases besides KS.

CHAPTER NINE

APPENDIX

		% Transmigration by microscopy		Number of KSHV-EC/100cells		% GFP positive cells by flow cytometry		Number of GFP+ve/100 cells		Number of GFP-ve/100 cells		% Transmigration by microscopy and flow cytometry combined	
	Expt	**UT-EC**	**KSHV-EC**	**Top**	**Bottom**	**Top**	**Bottom**	**Top**	**Bottom**	**Top**	**Bottom**	**V**	**NI**
48 hr	**A**	36.54	44.83	55.17	44.83	46.94	62.49	25.90	28.02	29.27	16.82	51.97	36.49
	B	36.86	52.11	47.89	52.11	60.80	84.80	29.12	44.19	18.77	7.92	60.28	29.67
	C	33.34	41.91	58.09	41.91	82.96	89.80	48.18	37.64	9.90	4.28	43.86	30.16
	D	39.96	47.78	52.22	47.78	62.97	73.06	32.88	34.91	19.34	12.87	51.50	39.97

Table 9.1: Determination of the percentage transmigration of KSHV-infected (V) and non-infected (NI) HUVEC by calculation from the results of parallel 48hour transmigration assays with microscopic and flow cytometry readout.

KSHV-inoculated (KSHV-EC) and untreated (UT-EC) HUVEC were seeded into 8μm-pore transwell chambers on day-seven post-inoculation and the percentage transmigration after 48hours examined by microscopy. The number of KSHV-EC in every 100 cells that were on each side of the filter was calculated. The percentage of GFP positive cells in KSHV-EC cultures removed from the top and bottom surfaces of parallel 8μm-pore transwell chamber filters at 48hours was quantified by flow cytometry. By multiplying together the number of KSHV-EC/100 cells (as determined by microscopy) and the proportion that were GFP positive or negative, the numbers of GFP positive (KSHV-infected (V)) and GFP negative (non-infected (NI)) cells on each side of the filter were calculated and the percentage transmigration determined for each of V and NI.

REFERENCES

Abbott, N.J., Patabendige, A.A., Dolman, D.E., Yusof, S.R., and Begley, D.J. (2010). Structure and function of the blood-brain barrier. Neurobiol Dis *37*, 13-25.

Achen, M.G., and Stacker, S.A. (2008). Molecular control of lymphatic metastasis. Ann N Y Acad Sci *1131*, 225-234.

Adams, R.H., and Alitalo, K. (2007). Molecular regulation of angiogenesis and lymphangiogenesis. Nat Rev Mol Cell Biol *8*, 464-478.

Ahmed, S.R., McGettrick, H.M., Yates, C.M., Buckley, C.D., Ratcliffe, M.J., Nash, G.B., and Rainger, G.E. (2011). Prostaglandin D2 regulates CD4+ memory T cell trafficking across blood vascular endothelium and primes these cells for clearance across lymphatic endothelium. J Immunol *187*, 1432-1439.

Aird, W.C. (2007). Phenotypic heterogeneity of the endothelium: II. Representative vascular beds. Circ Res *100*, 174-190.

Akula, S.M., Ford, P.W., Whitman, A.G., Hamden, K.E., Bryan, B.A., Cook, P.P., and McCubrey, J.A. (2005). B-Raf-dependent expression of vascular endothelial growth factor-A in Kaposi sarcoma-associated herpesvirus-infected human B cells. Blood *105*, 4516-4522.

Akula, S.M., Naranatt, P.P., Walia, N.S., Wang, F.Z., Fegley, B., and Chandran, B. (2003). Kaposi's sarcoma-associated herpesvirus (human herpesvirus 8) infection of human fibroblast cells occurs through endocytosis. J Virol *77*, 7978-7990.

Akula, S.M., Pramod, N.P., Wang, F.Z., and Chandran, B. (2001a). Human herpesvirus 8 envelope-associated glycoprotein B interacts with heparan sulfate-like moieties. Virology *284*, 235-249.

Akula, S.M., Pramod, N.P., Wang, F.Z., and Chandran, B. (2002). Integrin alpha3beta1 (CD 49c/29) is a cellular receptor for Kaposi's sarcoma-associated herpesvirus (KSHV/HHV-8) entry into the target cells. Cell *108*, 407-419.

Akula, S.M., Wang, F.Z., Vieira, J., and Chandran, B. (2001b). Human herpesvirus 8 interaction with target cells involves heparan sulfate. Virology *282*, 245-255.

Alberts, B., Johnson, A., Lewis, J., Raff, M., Roberts, K., and Walter, P. (2002). Molecular Biology of The Cell, Fourth edn (New York, Garland Science).

Albrecht, I., and Christofori, G. (2011). Molecular mechanisms of lymphangiogenesis in development and cancer. Int J Dev Biol *55*, 483-494.

Alexander, L., Denekamp, L., Knapp, A., Auerbach, M.R., Damania, B., and Desrosiers, R.C. (2000). The primary sequence of rhesus monkey rhadinovirus isolate 26-95: sequence similarities to Kaposi's sarcoma-associated herpesvirus and rhesus monkey rhadinovirus isolate 17577. J Virol *74*, 3388-3398.

Alitalo, K. (2011). The lymphatic vasculature in disease. Nat Med *17*, 1371-1380.

Allen, M.D., Young, L.S., and Dawson, C.W. (2005). The Epstein-Barr virus-encoded LMP2A and LMP2B proteins promote epithelial cell spreading and motility. J Virol *79*, 1789-1802.

Ambroziak, J.A., Blackbourn, D.J., Herndier, B.G., Glogau, R.G., Gullett, J.H., McDonald, A.R., Lennette, E.T., and Levy, J.A. (1995). Herpes-like sequences in HIV-infected and uninfected Kaposi's sarcoma patients. Science *268*, 582-583.

Anthis, N.J., and Campbell, I.D. (2011). The tail of integrin activation. Trends Biochem Sci *36*, 191-198.

Antman, K., and Chang, Y. (2000). Kaposi's sarcoma. N Engl J Med *342*, 1027-1038.

Ascoli, V., Senis, G., Zucchetto, A., Valerio, L., Facchinelli, L., Budroni, M., Dal Maso, L., and Coluzzi, M. (2009). Distribution of 'promoter' sandflies associated with incidence of classic Kaposi's sarcoma. Med Vet Entomol *23*, 217-225.

Assoian, R.K., and Schwartz, M.A. (2001). Coordinate signaling by integrins and receptor tyrosine kinases in the regulation of G1 phase cell-cycle progression. Curr Opin Genet Dev *11*, 48-53.

Bechtel, J., Grundhoff, A., and Ganem, D. (2005a). RNAs in the virion of Kaposi's sarcoma-associated herpesvirus. J Virol *79*, 10138-10146.

Bechtel, J.T., Winant, R.C., and Ganem, D. (2005b). Host and viral proteins in the virion of Kaposi's sarcoma-associated herpesvirus. J Virol *79*, 4952-4964.

Bedi, G.C., Westra, W.H., Farzadegan, H., Pitha, P.M., and Sidransky, D. (1995). Microsatellite instability in primary neoplasms from HIV + patients. Nat Med *1*, 65-68.

Bergers, G., and Benjamin, L.E. (2003). Tumorigenesis and the angiogenic switch. Nat Rev Cancer *3*, 401-410.

Bershadsky, A.D., Balaban, N.Q., and Geiger, B. (2003). Adhesion-dependent cell mechanosensitivity. Annu Rev Cell Dev Biol *19*, 677-695.

Bhatt, A., Kaverina, I., Otey, C., and Huttenlocher, A. (2002). Regulation of focal complex composition and disassembly by the calcium-dependent protease calpain. J Cell Sci *115*, 3415-3425.

Blackbourn, D.J., Ambroziak, J., Lennette, E., Adams, M., Ramachandran, B., and Levy, J.A. (1997). Infectious human herpesvirus 8 in a healthy North American blood donor. Lancet *349*, 609-611.

Blackbourn, D.J., Lennette, E., Klencke, B., Moses, A., Chandran, B., Weinstein, M., Glogau, R.G., Witte, M.H., Way, D.L., Kutzkey, T.*, et al.* (2000). The restricted cellular host range of human herpesvirus 8. AIDS *14*, 1123-1133.

Blackbourn, D.J., Lennette, E.T., Ambroziak, J., Mourich, D.V., and Levy, J.A. (1998). Human herpesvirus 8 detection in nasal secretions and saliva. J Infect Dis *177*, 213-216.

Borowsky, M.L., and Hynes, R.O. (1998). Layilin, a novel talin-binding transmembrane protein homologous with C-type lectins, is localized in membrane ruffles. J Cell Biol *143*, 429-442.

Boshoff, C., Endo, Y., Collins, P.D., Takeuchi, Y., Reeves, J.D., Schweickart, V.L., Siani, M.A., Sasaki, T., Williams, T.J., Gray, P.W.*, et al.* (1997). Angiogenic and HIV-inhibitory functions of KSHV-encoded chemokines. Science *278*, 290-294.

Boshoff, C., Schulz, T.F., Kennedy, M.M., Graham, A.K., Fisher, C., Thomas, A., McGee, J.O., Weiss, R.A., and O'Leary, J.J. (1995a). Kaposi's sarcoma-associated herpesvirus infects endothelial and spindle cells. Nat Med *1*, 1274-1278.

Boshoff, C., and Weiss, R.A. (1997). Aetiology of Kaposi's sarcoma: current understanding and implications for therapy. Molecular Medicine Today *3*, 488-494.

Boshoff, C., Whitby, D., Hatziioannou, T., Fisher, C., van der Walt, J., Hatzakis, A., Weiss, R., and Schulz, T. (1995b). Kaposi's-sarcoma-associated herpesvirus in HIV-negative Kaposi's sarcoma. Lancet *345*, 1043-1044.

Bouvard, V., Baan, R., Straif, K., Grosse, Y., Secretan, B., Ghissassi, F.E., Benbrahim-Tallaa, L., Guha, N., Freeman, C., Galichet, L.*, et al.* (2009). A review of human carcinogens--Part B: biological agents. The Lancet Oncology *10*, 321-322.

Brown, E.E., Fallin, M.D., Goedert, J.J., Chen, R., Whitby, D., Foster, C.B., Lauria, C., Alberg, A.J., Messina, A., Montella, M.*, et al.* (2005). A common genetic variant in FCGR3A-V158F and risk of Kaposi sarcoma herpesvirus infection and classic Kaposi sarcoma. Cancer Epidemiol Biomarkers Prev *14*, 633-637.

Browning, P.J., Sechler, J.M., Kaplan, M., Washington, R.H., Gendelman, R., Yarchoan, R., Ensoli, B., and Gallo, R.C. (1994). Identification and culture of Kaposi's sarcoma-like spindle cells from the peripheral blood of human immunodeficiency virus-1-infected individuals and normal controls. Blood *84*, 2711-2720.

Budt, M., Hristozova, T., Hille, G., Berger, K., and Brune, W. (2011). Construction of a Lytically Replicating Kaposi's Sarcoma-Associated Herpesvirus. J Virol *85*, 10415-10420.

Burridge, K. (2005). Foot in mouth: do focal adhesions disassemble by endocytosis? Nat Cell Biol *7*, 545-547.

Burton, V.J., Butler, L.M., McGettrick, H.M., Stone, P.C., Jeffery, H.C., Savage, C.O., Rainger, G.E., and Nash, G.B. (2011). Delay of migrating leukocytes by the basement membrane deposited by endothelial cells in long-term culture. Exp Cell Res *317*, 276-292.

Butler, L.M. (2005). Effect of prolonged culture of endothelial cells and deposition of basement membrane on neutrophil recruitment. PhD Thesis. In The Department of Cardiovascular Research (Birmingham, University of Birmingham).

Butler, L.M., Jeffery, H.C., Wheat, R.L., Rae, P.C., Townsend, K., Alkharsah, K.R., Schulz, T.F., Nash, G.B., and Blackbourn, D.J. (2011). Kaposi's sarcoma-associated herpesvirus infection of endothelial cells inhibits neutrophil recruitment through an interleukin-6-dependent mechanism: a new paradigm for viral immune evasion. J Virol *85*, 7321-7332.

Butler, L.M., Rainger, G.E., Rahman, M., and Nash, G.B. (2005). Prolonged culture of endothelial cells and deposition of basement membrane modify the recruitment of neutrophils. Exp Cell Res *310*, 22-32.

Cannon, M.J., Dollard, S.C., Black, J.B., Edlin, B.R., Hannah, C., Hogan, S.E., Patel, M.M., Jaffe, H.W., Offermann, M.K., Spira, T.J.*, et al.* (2003). Risk factors for Kaposi's sarcoma in men seropositive for both human herpesvirus 8 and human immunodeficiency virus. AIDS *17*, 215-222.

Carlsen, H.S., Haraldsen, G., Brandtzaeg, P., and Baekkevold, E.S. (2005). Disparate lymphoid chemokine expression in mice and men: no evidence of CCL21 synthesis by human high endothelial venules. Blood *106*, 444-446.

Carmeliet, P., and Collen, D. (2000). Molecular basis of angiogenesis. Role of VEGF and VE-cadherin. Ann N Y Acad Sci *902*, 249-262; discussion 262-244.

Carmeliet, P., and Jain, R.K. (2011). Molecular mechanisms and clinical applications of angiogenesis. Nature *473*, 298-307.

Carroll, P.A., Brazeau, E., and Lagunoff, M. (2004). Kaposi's sarcoma-associated herpesvirus infection of blood endothelial cells induces lymphatic differentiation. Virology *328*, 7-18.

Caruso, A., Caselli, E., Fiorentini, S., Rotola, A., Prandini, A., Garrafa, E., Saba, E., Alessandri, G., Cassai, E., and Di Luca, D. (2009). U94 of human herpesvirus 6 inhibits in vitro angiogenesis and lymphangiogenesis. Proc Natl Acad Sci U S A *106*, 20446-20451.

Chan, K.T., Bennin, D.A., and Huttenlocher, A. (2010). Regulation of adhesion dynamics by calpain-mediated proteolysis of focal adhesion kinase (FAK). J Biol Chem *285*, 11418-11426.

Chang, Y., Cesarman, E., Pessin, M.S., Lee, F., Culpepper, J., Knowles, D.M., and Moore, P.S. (1994). Identification of herpesvirus-like DNA sequences in AIDS-associated Kaposi's sarcoma. Science *266*, 1865-1869.

Chapman, H.A., and Wei, Y. (2001). Protease crosstalk with integrins: the urokinase receptor paradigm. Thromb Haemost *86*, 124-129.

Chen, J., Ye, F., Xie, J., Kuhne, K., and Gao, S.J. (2009). Genome-wide identification of binding sites for Kaposi's sarcoma-associated herpesvirus lytic switch protein, RTA. Virology *386*, 290-302.

Cheng, Y.S., Champliaud, M.F., Burgeson, R.E., Marinkovich, M.P., and Yurchenco, P.D. (1997). Self-assembly of laminin isoforms. J Biol Chem *272*, 31525-31532.

Cherepanova, O.A., Kalmykova, N.V., Koronkina, I.V., Are, A.F., Gorelik Iu, V., and Pinaev, G.P. (2002). [Differences in the character of interaction of normal and transformed human keratinocytes with laminin isoforms]. Tsitologiia *44*, 151-158.

Choudhuri, T., Verma, S.C., Lan, K., and Robertson, E.S. (2006). Expression of alpha V integrin is modulated by Epstein-Barr virus nuclear antigen 3C and the metastasis suppressor Nm23-H1 through interaction with the GATA-1 and Sp1 transcription factors. Virology *351*, 58-72.

Chung, J., Bachelder, R.E., Lipscomb, E.A., Shaw, L.M., and Mercurio, A.M. (2002). Integrin (alpha 6 beta 4) regulation of eIF-4E activity and VEGF translation: a survival mechanism for carcinoma cells. J Cell Biol *158*, 165-174.

Cines, D.B., Pollak, E.S., Buck, C.A., Loscalzo, J., Zimmerman, G.A., McEver, R.P., Pober, J.S., Wick, T.M., Konkle, B.A., Schwartz, B.S., *et al.* (1998). Endothelial cells in physiology and in the pathophysiology of vascular disorders. Blood *91*, 3527-3561.

Ciufo, D.M., Cannon, J.S., Poole, L.J., Wu, F.Y., Murray, P., Ambinder, R.F., and Hayward, G.S. (2001). Spindle Cell Conversion by Kaposi's Sarcoma-Associated Herpesvirus: Formation of Colonies and Plaques with Mixed Lytic and Latent Gene Expression in Infected Primary Dermal Microvascular Endothelial Cell Cultures. J Virol *75*, 5614-5626.

Coll, J.L., Ben-Ze'ev, A., Ezzell, R.M., Rodriguez Fernandez, J.L., Baribault, H., Oshima, R.G., and Adamson, E.D. (1995). Targeted disruption of vinculin genes in F9 and embryonic stem cells changes cell morphology, adhesion, and locomotion. Proc Natl Acad Sci U S A *92*, 9161-9165.

Colman, R., and Blackbourn, D.J. (2008). Risk factors in the development of Kaposi's sarcoma. AIDS *22*, 1629-1632.

Coluzzi, M., Manno, D., Guzzinati, S., Tognazzo, S., Zambon, P., Arca, B., Costantini, C., and Ascoli, V. (2002). The bloodsucking arthropod bite as possible cofactor in the transmission of human herpesvirus-8 infection and in the expression of Kaposi's sarcoma disease. Parassitologia *44*, 123-129.

Condit, R. (2007). Principles of virology. In Fields Virology Vol I, D.M. Knipe, and P.M. Howley, eds. (Philadelphia, USA, Lippincott Williams & Wilkins, a Wolters Kluwer Business).

Conway, E.M., Collen, D., and Carmeliet, P. (2001). Molecular mechanisms of blood vessel growth. Cardiovasc Res *49*, 507-521.

Cook-Mozaffari, P., Newton, R., Beral, V., and Burkitt, D.P. (1998). The geographical distribution of Kaposi's sarcoma and of lymphomas in Africa before the AIDS epidemic. Br J Cancer *78*, 1521-1528.

Corey, L., Brodie, S., Huang, M.L., Koelle, D.M., and Wald, A. (2002). HHV-8 infection: a model for reactivation and transmission. Rev Med Virol *12*, 47-63.

Cortesio, C.L., Boateng, L.R., Piazza, T.M., Bennin, D.A., and Huttenlocher, A. (2011). Calpain-mediated proteolysis of paxillin negatively regulates focal adhesion dynamics and cell migration. J Biol Chem *286*, 9998-10006.

Cottoni, F., Masala, M.V., Budroni, M., Rosella, M., Satta, R., Locatelli, F., Montesu, M.A., and De Marco, R. (1997). The role of occupation and a past history of malaria in the etiology of classic Kaposi's sarcoma: a case-control study in north-east Sardinia. Br J Cancer *76*, 1518-1520.

Cottoni, F., Masala, M.V., Pattaro, C., Pirodda, C., Montesu, M.A., Satta, R., Cerimele, D., and de Marco, R. (2006). Classic Kaposi sarcoma in northern Sardinia: a prospective epidemiologic overview (1977-2003) correlated with malaria prevalence (1934). J Am Acad Dermatol *55*, 990-995.

Couty, J.P., Lupu-Meiri, M., Oron, Y., and Gershengorn, M.C. (2009). Kaposi's sarcoma-associated herpesvirus-G protein-coupled receptor-expressing endothelial cells exhibit reduced migration and stimulated chemotaxis by chemokine inverse agonists. J Pharmacol Exp Ther *329*, 1142-1147.

Davis, G.E., and Senger, D.R. (2005). Endothelial extracellular matrix: biosynthesis, remodeling, and functions during vascular morphogenesis and neovessel stabilization. Circ Res *97*, 1093-1107.

Davison, A.J., Eberle, R., Ehlers, B., Hayward, G.S., McGeoch, D.J., Minson, A.C., Pellett, P.E., Roizman, B., Studdert, M.J., and Thiry, E. (2009). The order Herpesvirales. Arch Virol *154*, 171-177.

Dawson, C.W., Laverick, L., Morris, M.A., Tramoutanis, G., and Young, L.S. (2008). Epstein-Barr virus-encoded LMP1 regulates epithelial cell motility and invasion via the ERK-MAPK pathway. J Virol *82*, 3654-3664.

Dawson, C.W., Tramountanis, G., Eliopoulos, A.G., and Young, L.S. (2003). Epstein-Barr virus latent membrane protein 1 (LMP1) activates the phosphatidylinositol 3-kinase/Akt pathway to promote cell survival and induce actin filament remodeling. J Biol Chem *278*, 3694-3704.

Deakin, N.O., and Turner, C.E. (2008). Paxillin comes of age. J Cell Sci *121*, 2435-2444.

Dedicoat, M., Newton, R., Alkharsah, K.R., Sheldon, J., Szabados, I., Ndlovu, B., Page, T., Casabonne, D., Gilks, C.F., Cassol, S.A., *et al.* (2004). Mother-to-child transmission of human herpesvirus-8 in South Africa. J Infect Dis *190*, 1068-1075.

Dejana, E., Languino, L.R., Polentarutti, N., Balconi, G., Ryckewaert, J.J., Larrieu, M.J., Donati, M.B., Mantovani, A., and Marguerie, G. (1985). Interaction between fibrinogen and cultured endothelial cells. Induction of migration and specific binding. J Clin Invest *75*, 11-18.

Denes, L., Jednakovits, A., Hargitai, J., Penzes, Z., Balla, A., Talosi, L., Krajcsi, P., and Csermely, P. (2002). Pharmacologically activated migration of aortic endothelial cells is mediated through p38 SAPK. Br J Pharmacol *136*, 597-603.

Dezube, B.J., Zambela, M., Sage, D.R., Wang, J.F., and Fingeroth, J.D. (2002). Characterization of Kaposi sarcoma-associated herpesvirus/human herpesvirus-8 infection of human vascular endothelial cells: early events. Blood *100*, 888-896.

Dictor, M., Ferno, M., and Baldetorp, B. (1991). Flow cytometric DNA content in Kaposi's sarcoma by histologic stage. Comparison with angiosarcoma. Anal Quant Cytol Histol *13*, 201-208.

DiMaio, T.A., Gutierrez, K.D., and Lagunoff, M. (2011). Latent KSHV infection of endothelial cells induces integrin beta3 to activate angiogenic phenotypes. PLoS Pathog *7*, e1002424.

DiMilla, P.A., Stone, J.A., Quinn, J.A., Albelda, S.M., and Lauffenburger, D.A. (1993). Maximal migration of human smooth muscle cells on fibronectin and type IV collagen occurs at an intermediate attachment strength. J Cell Biol *122*, 729-737.

Dorak, M.T., Yee, L.J., Tang, J., Shao, W., Lobashevsky, E.S., Jacobson, L.P., and Kaslow, R.A. (2005). HLA-B, -DRB1/3/4/5, and -DQB1 gene polymorphisms in human immunodeficiency virus-related Kaposi's sarcoma. J Med Virol *76*, 302-310.

Dukers, N.H., and Rezza, G. (2003). Human herpesvirus 8 epidemiology: what we do and do not know. AIDS *17*, 1717-1730.

Dupin, N., Fisher, C., Kellam, P., Ariad, S., Tulliez, M., Franck, N., van Marck, E., Salmon, D., Gorin, I., Escande, J.P., *et al.* (1999). Distribution of human herpesvirus-8 latently infected cells in Kaposi's sarcoma, multicentric Castleman's disease, and primary effusion lymphoma. Proc Natl Acad Sci U S A *96*, 4546-4551.

Dupin, N., Grandadam, M., Calvez, V., Gorin, I., Aubin, J.T., Havard, S., Lamy, F., Leibowitch, M., Huraux, J.M., Escande, J.P., *et al.* (1995). Herpesvirus-like DNA sequences in patients with Mediterranean Kaposi's sarcoma. Lancet *345*, 761-762.

Echtermeyer, F., Baciu, P.C., Saoncella, S., Ge, Y., and Goetinck, P.F. (1999). Syndecan-4 core protein is sufficient for the assembly of focal adhesions and actin stress fibers. J Cell Sci *112 (Pt 20)*, 3433-3441.

Elbaum, M., Chausovsky, A., Levy, E.T., Shtutman, M., and Bershadsky, A.D. (1999). Microtubule involvement in regulating cell contractility and adhesion-dependent signalling: a possible mechanism for polarization of cell motility. Biochem Soc Symp *65*, 147-172.

Ensoli, B., Sgadari, C., Barillari, G., Sirianni, M.C., Sturzl, M., and Monini, P. (2001). Biology of Kaposi's sarcoma. Eur J Cancer *37*, 1251-1269.

Escalon, M.P., and Hagemeister, F.B. (2006). AIDS-Related Malignancies. In: Kantarjianm HM, Wolff RA and Koller CA. The MD Anderson Manual of Medical Oncology, (McGraw-Hill).

Ezratty, E.J., Partridge, M.A., and Gundersen, G.G. (2005). Microtubule-induced focal adhesion disassembly is mediated by dynamin and focal adhesion kinase. Nat Cell Biol *7*, 581-590.

Flore, O., Rafii, S., Ely, S., O'Leary, J.J., Hyjek, E.M., and Cesarman, E. (1998). Transformation of primary human endothelial cells by Kaposi's sarcoma-associated herpesvirus. Nature *394*, 588-592.

Foreman, K.E., Friborg, J., Jr., Kong, W.P., Woffendin, C., Polverini, P.J., Nickoloff, B.J., and Nabel, G.J. (1997). Propagation of a human herpesvirus from AIDS-associated Kaposi's sarcoma. N Engl J Med *336*, 163-171.

Forster, R., Davalos-Misslitz, A.C., and Rot, A. (2008). CCR7 and its ligands: balancing immunity and tolerance. Nat Rev Immunol *8*, 362-371.

Fortier, A.H., Nelson, B.J., Grella, D.K., and Holaday, J.W. (1999). Antiangiogenic activity of prostate-specific antigen. J Natl Cancer Inst *91*, 1635-1640.

Foster, C.B., Lehrnbecher, T., Samuels, S., Stein, S., Mol, F., Metcalf, J.A., Wyvill, K., Steinberg, S.M., Kovacs, J., Blauvelt, A.*, et al.* (2000). An IL6 promoter polymorphism is associated with a lifetime risk of development of Kaposi sarcoma in men infected with human immunodeficiency virus. Blood *96*, 2562-2567.

Frame, M.C., Patel, H., Serrels, B., Lietha, D., and Eck, M.J. (2010). The FERM domain: organizing the structure and function of FAK. Nat Rev Mol Cell Biol *11*, 802-814.

Franco, S.J., Rodgers, M.A., Perrin, B.J., Han, J., Bennin, D.A., Critchley, D.R., and Huttenlocher, A. (2004). Calpain-mediated proteolysis of talin regulates adhesion dynamics. Nat Cell Biol *6*, 977-983.

Ganem, D. (2007). Kaposi's Sarcoma-Associated Herpesvirus. In Fields Virology Vol II, D.M. Knipe, and P.M. Howley, eds. (Philadelphia, USA, Lippincott Williams & Wilkins, a Wolters Kluwer Business).

Gantt, S., and Casper, C. (2011). Human herpesvirus 8-associated neoplasms: the roles of viral replication and antiviral treatment. Curr Opin Infect Dis *24*, 295-301.

Gao, S.J., Deng, J.H., and Zhou, F.C. (2003). Productive lytic replication of a recombinant Kaposi's sarcoma-associated herpesvirus in efficient primary infection of primary human endothelial cells. J Virol *77*, 9738-9749.

Gardel, M.L., Schneider, I.C., Aratyn-Schaus, Y., and Waterman, C.M. (2010). Mechanical integration of actin and adhesion dynamics in cell migration. Annu Rev Cell Dev Biol *26*, 315-333.

Garlanda, C., and Dejana, E. (1997). Heterogeneity of endothelial cells. Specific markers. Arterioscler Thromb Vasc Biol *17*, 1193-1202.

Garrigues, H.J., Rubinchikova, Y.E., Dipersio, C.M., and Rose, T.M. (2008). Integrin alphaVbeta3 Binds to the RGD motif of glycoprotein B of Kaposi's sarcoma-associated herpesvirus and functions as an RGD-dependent entry receptor. J Virol *82*, 1570-1580.

Gaya, A., Esteve, A., Casabona, J., McCarthy, J.J., Martorell, J., Schulz, T.F., and Whitby, D. (2004). Amino acid residue at position 13 in HLA-DR beta chain plays a critical role in the development of Kaposi's sarcoma in AIDS patients. AIDS *18*, 199-204.

Geddes, M., Franceschi, S., Balzi, D., Arniani, S., Gafa, L., and Zanetti, R. (1995). Birthplace and classic Kaposi's sarcoma in Italy. Associazione Italiana Registri Tumori. J Natl Cancer Inst *87*, 1015-1017.

Geiger, B., Bershadsky, A., Pankov, R., and Yamada, K.M. (2001). Transmembrane crosstalk between the extracellular matrix--cytoskeleton crosstalk. Nat Rev Mol Cell Biol *2*, 793-805.

Geras-Raaka, E., Varma, A., Ho, H., Clark-Lewis, I., and Gershengorn, M.C. (1998). Human interferon-gamma-inducible protein 10 (IP-10) inhibits constitutive signaling of Kaposi's sarcoma-associated herpesvirus G protein-coupled receptor. J Exp Med *188*, 405-408.

Gerhardt, H., and Betsholtz, C. (2003). Endothelial-pericyte interactions in angiogenesis. Cell Tissue Res *314*, 15-23.

Girard, J.P., and Springer, T.A. (1995). High endothelial venules (HEVs): specialized endothelium for lymphocyte migration. Immunol Today *16*, 449-457.

Goel, H.L., Li, J., Kogan, S., and Languino, L.R. (2008). Integrins in prostate cancer progression. Endocr Relat Cancer *15*, 657-664.

Goldfinger, L.E., Stack, M.S., and Jones, J.C. (1998). Processing of laminin-5 and its functional consequences: role of plasmin and tissue-type plasminogen activator. J Cell Biol *141*, 255-265.

Gonzalez, A.M., Gonzales, M., Herron, G.S., Nagavarapu, U., Hopkinson, S.B., Tsuruta, D., and Jones, J.C. (2002). Complex interactions between the laminin alpha 4 subunit and integrins regulate endothelial cell behavior in vitro and angiogenesis in vivo. Proc Natl Acad Sci U S A *99*, 16075-16080.

Gratzinger, D., Canosa, S., Engelhardt, B., and Madri, J.A. (2003). Platelet endothelial cell adhesion molecule-1 modulates endothelial cell motility through the small G-protein Rho. FASEB J *17*, 1458-1469.

Greene, W., and Gao, S.J. (2009). Actin dynamics regulate multiple endosomal steps during Kaposi's sarcoma-associated herpesvirus entry and trafficking in endothelial cells. PLoS Pathog *5*, e1000512.

Grossmann, C., Podgrabinska, S., Skobe, M., and Ganem, D. (2006). Activation of NF-kappaB by the latent vFLIP gene of Kaposi's sarcoma-associated herpesvirus is required for the spindle shape of virus-infected endothelial cells and contributes to their proinflammatory phenotype. J Virol *80*, 7179-7185.

Grundhoff, A., and Ganem, D. (2004). Inefficient establishment of KSHV latency suggests an additional role for continued lytic replication in Kaposi sarcoma pathogenesis. J Clin Invest *113*, 124-136.

Guo, H.G., Sadowska, M., Reid, W., Tschachler, E., Hayward, G., and Reitz, M. (2003). Kaposi's sarcoma-like tumors in a human herpesvirus 8 ORF74 transgenic mouse. J Virol *77*, 2631-2639.

Haddad, L., El Hajj, H., Abou-Merhi, R., Kfoury, Y., Mahieux, R., El-Sabban, M., and Bazarbachi, A. (2008). KSHV-transformed primary effusion lymphoma cells induce a VEGF-dependent angiogenesis and establish functional gap junctions with endothelial cells. Leukemia *22*, 826-834.

Hamill, K.J., Kligys, K., Hopkinson, S.B., and Jones, J.C. (2009). Laminin deposition in the extracellular matrix: a complex picture emerges. J Cell Sci *122*, 4409-4417.

Hansen, A., Henderson, S., Lagos, D., Nikitenko, L., Coulter, E., Roberts, S., Gratrix, F., Plaisance, K., Renne, R., Bower, M.*, et al.* (2010). KSHV-encoded miRNAs target MAF to induce endothelial cell reprogramming. Genes Dev *24*, 195-205.

Hedges, J.C., Dechert, M.A., Yamboliev, I.A., Martin, J.L., Hickey, E., Weber, L.A., and Gerthoffer, W.T. (1999). A role for p38(MAPK)/HSP27 pathway in smooth muscle cell migration. J Biol Chem *274*, 24211-24219.

Heidemann, J., Ogawa, H., Dwinell, M.B., Rafiee, P., Maaser, C., Gockel, H.R., Otterson, M.F., Ota, D.M., Lugering, N., Domschke, W.*, et al.* (2003). Angiogenic effects of interleukin 8 (CXCL8) in human intestinal microvascular endothelial cells are mediated by CXCR2. J Biol Chem *278*, 8508-8515.

Herbst, T.J., McCarthy, J.B., Tsilibary, E.C., and Furcht, L.T. (1988). Differential effects of laminin, intact type IV collagen, and specific domains of type IV collagen on endothelial cell adhesion and migration. J Cell Biol *106*, 1365-1373.

Hillen, F., and Griffioen, A.W. (2007). Tumour vascularization: sprouting angiogenesis and beyond. Cancer Metastasis Rev *26*, 489-502.

Hintermann, E., Yang, N., O'Sullivan, D., Higgins, J.M., and Quaranta, V. (2005). Integrin alpha6beta4-erbB2 complex inhibits haptotaxis by up-regulating E-cadherin cell-cell junctions in keratinocytes. J Biol Chem *280*, 8004-8015.

Ho, C.H., Chen, C.L., Li, W.Y., and Chen, C.J. (2009). Decoy receptor 3, upregulated by Epstein-Barr virus latent membrane protein 1, enhances nasopharyngeal carcinoma cell migration and invasion. Carcinogenesis *30*, 1443-1451.

Hong, Y.K., Foreman, K., Shin, J.W., Hirakawa, S., Curry, C.L., Sage, D.R., Libermann, T., Dezube, B.J., Fingeroth, J.D., and Detmar, M. (2004). Lymphatic reprogramming of blood vascular endothelium by Kaposi sarcoma-associated herpesvirus. Nat Genet *36*, 683-685.

Horenstein, M.G., Moontasri, N.J., and Cesarman, E. (2008). The pathobiology of Kaposi's sarcoma: advances since the onset of the AIDS epidemic. J Cutan Pathol *35 Suppl 2*, 40-44.

Humphries, M.J. (2000). Integrin structure. Biochem Soc Trans *28*, 311-339.

Hynes, R.O. (1992). Integrins: versatility, modulation, and signaling in cell adhesion. Cell *69*, 11-25.

Hynes, R.O. (2002). Integrins: bidirectional, allosteric signaling machines. Cell *110*, 673-687.

Ilic, D., Furuta, Y., Kanazawa, S., Takeda, N., Sobue, K., Nakatsuji, N., Nomura, S., Fujimoto, J., Okada, M., and Yamamoto, T. (1995). Reduced cell motility and enhanced focal adhesion contact formation in cells from FAK-deficient mice. Nature *377*, 539-544.

Inoue, N., Winter, J., Lal, R.B., Offermann, M.K., and Koyano, S. (2003). Characterization of entry mechanisms of human herpesvirus 8 by using an Rta-dependent reporter cell line. J Virol *77*, 8147-8152.

Jackson, S.P. (2011). Arterial thrombosis--insidious, unpredictable and deadly. Nat Med *17*, 1423-1436.

Jensen, K.K., Manfra, D.J., Grisotto, M.G., Martin, A.P., Vassileva, G., Kelley, K., Schwartz, T.W., and Lira, S.A. (2005). The Human Herpes Virus 8-Encoded Chemokine Receptor Is Required for Angioproliferation in a Murine Model of Kaposi's Sarcoma. J Immunol *174*, 3686-3694.

Kaleeba, J.A., and Berger, E.A. (2006a). Broad target cell selectivity of Kaposi's sarcoma-associated herpesvirus glycoprotein-mediated cell fusion and virion entry. Virology *354*, 7-14.

Kaleeba, J.A., and Berger, E.A. (2006b). Kaposi's sarcoma-associated herpesvirus fusion-entry receptor: cystine transporter xCT. Science *311*, 1921-1924.

Kalmykova, N.V., Cherepanova, O.A., Gorelik Iu, V., Voronkina, I.V., Blinova, M.I., and Pinaev, G.P. (2002). [Various effects of laminin-1 and laminin-2/4 on adhesion and migration of cultured human keratinocytes]. Tsitologiia *44*, 792-798.

Karnezis, T., Shayan, R., Caesar, C., Roufail, S., Harris, N.C., Ardipradja, K., Zhang, Y.F., Williams, S.P., Farnsworth, R.H., Chai, M.G., *et al.* (2012). VEGF-D promotes tumor metastasis by regulating prostaglandins produced by the collecting lymphatic endothelium. Cancer Cell *21*, 181-195.

Kedes, D.H., Operskalski, E., Busch, M., Kohn, R., Flood, J., and Ganem, D. (1996). The seroepidemiology of human herpesvirus 8 (Kaposi's sarcoma-associated herpesvirus): distribution of infection in KS risk groups and evidence for sexual transmission. Nat Med *2*, 918-924.

Kempf, W., Adams, V., Wey, N., Moos, R., Schmid, M., Avitabile, E., and Campadelli-Fiume, G. (1997). CD68+ cells of monocyte/macrophage lineage in the environment of AIDS-associated and classic-sporadic Kaposi sarcoma are singly or doubly infected with human herpesviruses 7 and 6B. Proc Natl Acad Sci U S A *94*, 7600-7605.

Kenne, E., Soehnlein, O., Genove, G., Rotzius, P., Eriksson, E.E., and Lindbom, L. (2010). Immune cell recruitment to inflammatory loci is impaired in mice deficient in basement membrane protein laminin alpha4. J Leukoc Biol *88*, 523-528.

Khoshnoodi, J., Cartailler, J.P., Alvares, K., Veis, A., and Hudson, B.G. (2006). Molecular recognition in the assembly of collagens: terminal noncollagenous domains are key recognition modules in the formation of triple helical protomers. J Biol Chem *281*, 38117-38121.

Khoshnoodi, J., Pedchenko, V., and Hudson, B.G. (2008). Mammalian collagen IV. Microsc Res Tech *71*, 357-370.

Kim, K.R., Yoshizaki, T., Miyamori, H., Hasegawa, K., Horikawa, T., Furukawa, M., Harada, S., Seiki, M., and Sato, H. (2000). Transformation of Madin-Darby canine kidney (MDCK) epithelial cells by Epstein-Barr virus latent membrane protein 1 (LMP1) induces expression of Ets1 and invasive growth. Oncogene *19*, 1764-1771.

King, T.E., Pawar, S.C., Majuta, L., Sroka, I.C., Wynn, D., Demetriou, M.C., Nagle, R.B., Porreca, F., and Cress, A.E. (2008). The role of alpha 6 integrin in prostate cancer migration and bone pain in a novel xenograft model. PLoS One *3*, e3535.

Koelle, D.M., Huang, M.L., Chandran, B., Vieira, J., Piepkorn, M., and Corey, L. (1997). Frequent detection of Kaposi's sarcoma-associated herpesvirus (human herpesvirus 8) DNA in saliva of human immunodeficiency virus-infected men: clinical and immunologic correlates. J Infect Dis *176*, 94-102.

Koshikawa, N., Minegishi, T., Sharabi, A., Quaranta, V., and Seiki, M. (2005). Membrane-type matrix metalloproteinase-1 (MT1-MMP) is a processing enzyme for human laminin gamma 2 chain. J Biol Chem *280*, 88-93.

Kruegel, J., and Miosge, N. (2010). Basement membrane components are key players in specialized extracellular matrices. Cell Mol Life Sci *67*, 2879-2895.

Lagunoff, M., Bechtel, J., Venetsanakos, E., Roy, A.M., Abbey, N., Herndier, B., McMahon, M., and Ganem, D. (2002). De novo infection and serial transmission of Kaposi's sarcoma-associated herpesvirus in cultured endothelial cells. J Virol *76*, 2440-2448.

Lamalice, L., Le Boeuf, F., and Huot, J. (2007). Endothelial cell migration during angiogenesis. Circ Res *100*, 782-794.

Lee, J.G., and Kay, E.P. (2006). FGF-2-induced wound healing in corneal endothelial cells requires Cdc42 activation and Rho inactivation through the phosphatidylinositol 3-kinase pathway. Invest Ophthalmol Vis Sci *47*, 1376-1386.

Lehrnbecher, T.L., Foster, C.B., Zhu, S., Venzon, D., Steinberg, S.M., Wyvill, K., Metcalf, J.A., Cohen, S.S., Kovacs, J., Yarchoan, R.*, et al.* (2000). Variant genotypes of FcgammaRIIIA influence the development of Kaposi's sarcoma in HIV-infected men. Blood *95*, 2386-2390.

Leitinger, B., and Hohenester, E. (2007). Mammalian collagen receptors. Matrix Biol *26*, 146-155.

Li, A., Dubey, S., Varney, M.L., Dave, B.J., and Singh, R.K. (2003). IL-8 directly enhanced endothelial cell survival, proliferation, and matrix metalloproteinases production and regulated angiogenesis. J Immunol *170*, 3369-3376.

Lin, C.J., Katongole-Mbidde, E., Byekwaso, T., Orem, J., Rabkin, C.S., and Mbulaiteye, S.M. (2008). Intestinal parasites in Kaposi sarcoma patients in Uganda: indication of shared risk factors or etiologic association. Am J Trop Med Hyg *78*, 409-412.

Lo, A.K., Liu, Y., Wang, X.H., Huang, D.P., Yuen, P.W., Wong, Y.C., and Tsao, G.S. (2003). Alterations of biologic properties and gene expression in nasopharyngeal epithelial cells by the Epstein-Barr virus-encoded latent membrane protein 1. Lab Invest *83*, 697-709.

Loetscher, M., Gerber, B., Loetscher, P., Jones, S.A., Piali, L., Clark-Lewis, I., Baggiolini, M., and Moser, B. (1996). Chemokine receptor specific for IP10 and mig: structure, function, and expression in activated T-lymphocytes. J Exp Med *184*, 963-969.

Lotz, M.M., Korzelius, C.A., and Mercurio, A.M. (1990). Human colon carcinoma cells use multiple receptors to adhere to laminin: involvement of alpha 6 beta 4 and alpha 2 beta 1 integrins. Cell Regul *1*, 249-257.

Lu, J., Lin, W.H., Chen, S.Y., Longnecker, R., Tsai, S.C., Chen, C.L., and Tsai, C.H. (2006). Syk tyrosine kinase mediates Epstein-Barr virus latent membrane protein 2A-induced cell migration in epithelial cells. J Biol Chem *281*, 8806-8814.

Ma, T., Jham, B.C., Hu, J., Friedman, E.R., Basile, J.R., Molinolo, A., Sodhi, A., and Montaner, S. (2010). Viral G protein-coupled receptor up-regulates Angiopoietin-like 4 promoting angiogenesis and vascular permeability in Kaposi's sarcoma. Proc Natl Acad Sci U S A *107*, 14363-14368.

Makinen, T., Veikkola, T., Mustjoki, S., Karpanen, T., Catimel, B., Nice, E.C., Wise, L., Mercer, A., Kowalski, H., Kerjaschki, D., *et al.* (2001). Isolated lymphatic endothelial cells transduce growth, survival and migratory signals via the VEGF-C/D receptor VEGFR-3. EMBO J *20*, 4762-4773.

Mansouri, M., Douglas, J., Rose, P.P., Gouveia, K., Thomas, G., Means, R.E., Moses, A.V., and Fruh, K. (2006). Kaposi sarcoma herpesvirus K5 removes CD31/PECAM from endothelial cells. Blood *108*, 1932-1940.

Mansouri, M., Rose, P.P., Moses, A.V., and Fruh, K. (2008). Remodeling of endothelial adherens junctions by Kaposi's sarcoma-associated herpesvirus. J Virol *82*, 9615-9628.

Marchio, S., Primo, L., Pagano, M., Palestro, G., Albini, A., Veikkola, T., Cascone, I., Alitalo, K., and Bussolino, F. (1999). Vascular endothelial growth factor-C stimulates the migration and proliferation of Kaposi's sarcoma cells. J Biol Chem *274*, 27617-27622.

Martin, D.F., Kuppermann, B.D., Wolitz, R.A., Palestine, A.G., Li, H., and Robinson, C.A. (1999). Oral ganciclovir for patients with cytomegalovirus retinitis treated with a ganciclovir implant. Roche Ganciclovir Study Group. N Engl J Med *340*, 1063-1070.

Masala, M.V., Carcassi, C., Cottoni, F., Mulargia, M., Contu, L., and Cerimele, D. (2005). Classic Kaposi's sarcoma in Sardinia: HLA positive and negative associations. Int J Dermatol *44*, 743-745.

Masood, R., Cai, J., Tulpule, A., Zheng, T., Hamilton, A., Sharma, S., Espina, B.M., Smith, D.L., and Gill, P.S. (2001). Interleukin 8 is an autocrine growth factor and a surrogate marker for Kaposi's sarcoma. Clin Cancer Res *7*, 2693-2702.

Masood, R., Cesarman, E., Smith, D.L., Gill, P.S., and Flore, O. (2002). Human herpesvirus-8-transformed endothelial cells have functionally activated vascular endothelial growth factor/vascular endothelial growth factor receptor. Am J Pathol *160*, 23-29.

Mbulaiteye, S.M., Biggar, R.J., Pfeiffer, R.M., Bakaki, P.M., Gamache, C., Owor, A.M., Katongole-Mbidde, E., Ndugwa, C.M., Goedert, J.J., Whitby, D., *et al.* (2005). Water, socioeconomic factors, and human herpesvirus 8 infection in Ugandan children and their mothers. J Acquir Immune Defic Syndr *38*, 474-479.

Mbulaiteye, S.M., Pfeiffer, R.M., Engels, E.A., Marshall, V., Bakaki, P.M., Owor, A.M., Ndugwa, C.M., Katongole-Mbidde, E., Goedert, J.J., Biggar, R.J., *et al.* (2004). Detection of kaposi sarcoma-associated herpesvirus DNA in saliva and buffy-coat samples from children with sickle cell disease in Uganda. J Infect Dis *190*, 1382-1386.

Mbulaiteye, S.M., Pfeiffer, R.M., Whitby, D., Brubaker, G.R., Shao, J., and Biggar, R.J. (2003). Human herpesvirus 8 infection within families in rural Tanzania. J Infect Dis *187*, 1780-1785.

McGeoch, D.J., Rixon, F.J., and Davison, A.J. (2006). Topics in herpesvirus genomics and evolution. Virus Res *117*, 90-104.

Meade-Tollin, L.C., Way, D., and Witte, M.H. (1999). Expression of multiple matrix metalloproteinases and urokinase type plasminogen activator in cultured Kaposi sarcoma cells. Acta Histochem *101*, 305-316.

Meng, Y.X., Spira, T.J., Bhat, G.J., Birch, C.J., Druce, J.D., Edlin, B.R., Edwards, R., Gunthel, C., Newton, R., Stamey, F.R., *et al.* (1999). Individuals from North America, Australasia, and Africa are infected with four different genotypes of human herpesvirus 8. Virology *261*, 106-119.

Meredith, J.E., Jr., and Schwartz, M.A. (1997). Integrins, adhesion and apoptosis. Trends Cell Biol *7*, 146-150.

Mesri, E.A., Cesarman, E., and Boshoff, C. (2010). Kaposi's sarcoma and its associated herpesvirus. Nat Rev Cancer *10*, 707-719.

Mileo, A.M., Piombino, E., Severino, A., Tritarelli, A., Paggi, M.G., and Lombardi, D. (2006). Multiple interference of the human papillomavirus-16 E7 oncoprotein with the functional role of the metastasis suppressor Nm23-H1 protein. J Bioenerg Biomembr *38*, 215-225.

Milligan, S., Robinson, M., O'Donnell, E., and Blackbourn, D.J. (2004). Inflammatory cytokines inhibit Kaposi's sarcoma-associated herpesvirus lytic gene transcription in in vitro-infected endothelial cells. J Virol *78*, 2591-2596.

Mitra, S.K., Hanson, D.A., and Schlaepfer, D.D. (2005). Focal adhesion kinase: in command and control of cell motility. Nat Rev Mol Cell Biol *6*, 56-68.

Mizejewski, G.J. (1999). Role of integrins in cancer: survey of expression patterns. Proc Soc Exp Biol Med *222*, 124-138.

Montaner, S., Sodhi, A., Molinolo, A., Bugge, T.H., Sawai, E.T., He, Y., Li, Y., Ray, P.E., and Gutkind, J.S. (2003). Endothelial infection with KSHV genes in vivo reveals that vGPCR initiates Kaposi's sarcomagenesis and can promote the tumorigenic potential of viral latent genes. Cancer Cell *3*, 23-36.

Montaner, S., Sodhi, A., Servitja, J.-M., Ramsdell, A.K., Barac, A., Sawai, E.T., and Gutkind, J.S. (2004). The small GTPase Rac1 links the Kaposi sarcoma-associated herpesvirus vGPCR to cytokine secretion and paracrine neoplasia. Blood *104*, 2903-2911.

Moore, P.S., and Chang, Y. (1995). Detection of herpesvirus-like DNA sequences in Kaposi's sarcoma in patients with and without HIV infection. N Engl J Med *332*, 1181-1185.

Moore, P.S., Kingsley, L.A., Holmberg, S.D., Spira, T., Gupta, P., Hoover, D.R., Parry, J.P., Conley, L.J., Jaffe, H.W., and Chang, Y. (1996). Kaposi's sarcoma-associated herpesvirus infection prior to onset of Kaposi's sarcoma. AIDS *10*, 175-180.

Morris, M.A., Young, L.S., and Dawson, C.W. (2008). DNA tumour viruses promote tumour cell invasion and metastasis by deregulating the normal processes of cell adhesion and motility. Eur J Cell Biol *87*, 677-697.

Moses, A.V., Fish, K.N., Ruhl, R., Smith, P.P., Strussenberg, J.G., Zhu, L., Chandran, B., and Nelson, J.A. (1999). Long-term infection and transformation of dermal microvascular endothelial cells by human herpesvirus 8. J Virol *73*, 6892-6902.

Murakami, M., Lan, K., Subramanian, C., and Robertson, E.S. (2005). Epstein-Barr virus nuclear antigen 1 interacts with Nm23-H1 in lymphoblastoid cell lines and inhibits its ability to suppress cell migration. J Virol *79*, 1559-1568.

Naranatt, P.P., Akula, S.M., Zien, C.A., Krishnan, H.H., and Chandran, B. (2003). Kaposi's sarcoma-associated herpesvirus induces the phosphatidylinositol 3-kinase-PKC-zeta-MEK-ERK signaling pathway in target cells early during infection: implications for infectivity. J Virol *77*, 1524-1539.

Naranatt, P.P., Krishnan, H.H., Svojanovsky, S.R., Bloomer, C., Mathur, S., and Chandran, B. (2004). Host gene induction and transcriptional reprogramming in Kaposi's sarcoma-associated herpesvirus (KSHV/HHV-8)-infected endothelial, fibroblast, and B cells: insights into modulation events early during infection. Cancer Res *64*, 72-84.

Nguyen, B.P., Gil, S.G., and Carter, W.G. (2000). Deposition of laminin 5 by keratinocytes regulates integrin adhesion and signaling. J Biol Chem *275*, 31896-31907.

Nomizu, M., Utani, A., Beck, K., Otaka, A., Roller, P.P., and Yamada, Y. (1996). Mechanism of laminin chain assembly into a triple-stranded coiled-coil structure. Biochemistry *35*, 2885-2893.

Okina, E., Manon-Jensen, T., Whiteford, J.R., and Couchman, J.R. (2009). Syndecan proteoglycan contributions to cytoskeletal organization and contractility. Scand J Med Sci Sports *19*, 479-489.

Olsson, A.K., Dimberg, A., Kreuger, J., and Claesson-Welsh, L. (2006). VEGF receptor signalling - in control of vascular function. Nat Rev Mol Cell Biol *7*, 359-371.

Orenstein, J.M., Alkan, S., Blauvelt, A., Jeang, K.T., Weinstein, M.D., Ganem, D., and Herndier, B. (1997). Visualization of human herpesvirus type 8 in Kaposi's sarcoma by light and transmission electron microscopy. AIDS *11*, F35-45.

Oriel, J.D. (1997). Moritz Kaposi (1837-1902). Int J STD AIDS *8*, 715-717.

Pantanowitz, L., Moses, A.V., and Dezube, B.J. (2009). The inflammatory component of Kaposi sarcoma. Exp Mol Pathol *87*, 163-165.

Parkin, D.M. (2006). The global health burden of infection-associated cancers in the year 2002. Int J Cancer *118*, 3030-3044.

Parsons, J.T. (2003). Focal adhesion kinase: the first ten years. J Cell Sci *116*, 1409-1416.

Parsons, J.T., Horwitz, A.R., and Schwartz, M.A. (2010). Cell adhesion: integrating cytoskeletal dynamics and cellular tension. Nat Rev Mol Cell Biol *11*, 633-643.

Patarroyo, M., Tryggvason, K., and Virtanen, I. (2002). Laminin isoforms in tumor invasion, angiogenesis and metastasis. Semin Cancer Biol *12*, 197-207.

Pauk, J., Huang, M.L., Brodie, S.J., Wald, A., Koelle, D.M., Schacker, T., Celum, C., Selke, S., and Corey, L. (2000). Mucosal shedding of human herpesvirus 8 in men. N Engl J Med *343*, 1369-1377.

Pawar, S.C., Demetriou, M.C., Nagle, R.B., Bowden, G.T., and Cress, A.E. (2007). Integrin alpha6 cleavage: a novel modification to modulate cell migration. Exp Cell Res *313*, 1080-1089.

Pegtel, D.M., Subramanian, A., Sheen, T.S., Tsai, C.H., Golub, T.R., and Thorley-Lawson, D.A. (2005). Epstein-Barr-virus-encoded LMP2A induces primary epithelial cell migration and invasion: possible role in nasopharyngeal carcinoma metastasis. J Virol *79*, 15430-15442.

Penn, I. (1988). Secondary neoplasms as a consequence of transplantation and cancer therapy. Cancer Detect Prev *12*, 39-57.

Penn, I. (1991). Cancer in the immunosuppressed organ recipient. Transplant Proc *23*, 1771-1772.

Petzelbauer, P., Watson, C.A., Pfau, S.E., and Pober, J.S. (1995). IL-8 and angiogenesis: evidence that human endothelial cells lack receptors and do not respond to IL-8 in vitro. Cytokine *7*, 267-272.

Primo, L., Seano, G., Roca, C., Maione, F., Gagliardi, P.A., Sessa, R., Martinelli, M., Giraudo, E., di Blasio, L., and Bussolino, F. (2010). Increased expression of alpha6 integrin in endothelial cells unveils a proangiogenic role for basement membrane. Cancer Res *70*, 5759-5769.

Qian, L.-W., Xie, J., Ye, F., and Gao, S.-J. (2007). Kaposi's sarcoma-associated herpesvirus infection promotes invasion of primary human umbilical vein endothelial cells by inducing matrix metalloproteinases. J Virol *81*, 7001-7010.

Qin, Z., Dai, L., Toole, B., Robertson, E., and Parsons, C. (2011). Regulation of Nm23-H1 and cell invasiveness by Kaposi's sarcoma-associated herpesvirus. J Virol *85*, 3596-3606.

Rabinovitz, I., Nagle, R.B., and Cress, A.E. (1995). Integrin alpha 6 expression in human prostate carcinoma cells is associated with a migratory and invasive phenotype in vitro and in vivo. Clin Exp Metastasis *13*, 481-491.

Rabkin, C.S., Bedi, G., Musaba, E., Sunkutu, R., Mwansa, N., Sidransky, D., and Biggar, R.J. (1995). AIDS-related Kaposi's sarcoma is a clonal neoplasm. Clin Cancer Res *1*, 257-260.

Raghu, H., Sharma-Walia, N., Veettil, M.V., Sadagopan, S., and Chandran, B. (2009). Kaposi's sarcoma-associated herpesvirus utilizes an actin polymerization-dependent macropinocytic pathway to enter human dermal microvascular endothelial and human umbilical vein endothelial cells. J Virol *83*, 4895-4911.

Rappocciolo, G., Jenkins, F.J., Hensler, H.R., Piazza, P., Jais, M., Borowski, L., Watkins, S.C., and Rinaldo, C.R., Jr. (2006). DC-SIGN is a receptor for human herpesvirus 8 on dendritic cells and macrophages. J Immunol *176*, 1741-1749.

Rathinam, R., and Alahari, S.K. (2010). Important role of integrins in the cancer biology. Cancer Metastasis Rev *29*, 223-237.

Raza, A., Franklin, M.J., and Dudek, A.Z. (2010). Pericytes and vessel maturation during tumor angiogenesis and metastasis. Am J Hematol *85*, 593-598.

Regezi, J.A., MacPhail, L.A., Daniels, T.E., DeSouza, Y.G., Greenspan, J.S., and Greenspan, D. (1993). Human immunodeficiency virus-associated oral Kaposi's sarcoma. A heterogeneous cell population dominated by spindle-shaped endothelial cells. Am J Pathol *143*, 240-249.

Renne, R., Blackbourn, D., Whitby, D., Levy, J., and Ganem, D. (1998). Limited transmission of Kaposi's sarcoma-associated herpesvirus in cultured cells. J Virol *72*, 5182-5188.

Renwick, N., Dukers, N.H., Weverling, G.J., Sheldon, J.A., Schulz, T.F., Prins, M., Coutinho, R.A., and Goudsmit, J. (2002). Risk factors for human herpesvirus 8 infection in a cohort of drug users in the Netherlands, 1985-1996. J Infect Dis *185*, 1808-1812.

Restrepo, C.S., and Ocazionez, D. (2011). Kaposi's sarcoma: imaging overview. Semin Ultrasound CT MR *32*, 456-469.

Reynolds, L.P., Grazul-Bilska, A.T., and Redmer, D.A. (2000). Angiogenesis in the corpus luteum. Endocrine *12*, 1-9.

Rezaee, S.A., Cunningham, C., Davison, A.J., and Blackbourn, D.J. (2006). Kaposi's sarcoma-associated herpesvirus immune modulation: an overview. J Gen Virol *87*, 1781-1804.

Ridley, A.J., Schwartz, M.A., Burridge, K., Firtel, R.A., Ginsberg, M.H., Borisy, G., Parsons, J.T., and Horwitz, A.R. (2003). Cell migration: integrating signals from front to back. Science *302*, 1704-1709.

Rodriguez Fernandez, J.L., Geiger, B., Salomon, D., and Ben-Ze'ev, A. (1992). Overexpression of vinculin suppresses cell motility in BALB/c 3T3 cells. Cell Motil Cytoskeleton *22*, 127-134.

Rodriguez Fernandez, J.L., Geiger, B., Salomon, D., and Ben-Ze'ev, A. (1993). Suppression of vinculin expression by antisense transfection confers changes in cell morphology, motility, and anchorage-dependent growth of 3T3 cells. J Cell Biol *122*, 1285-1294.

Roovers, K., and Assoian, R.K. (2000). Integrating the MAP kinase signal into the G1 phase cell cycle machinery. Bioessays *22*, 818-826.

Rosenkilde, M.M., Kledal, T.N., Brauner-Osborne, H., and Schwartz, T.W. (1999). Agonists and inverse agonists for the herpesvirus 8-encoded constitutively active seven-transmembrane oncogene product, ORF-74. J Biol Chem *274*, 956-961.

Rousseau, S., Houle, F., Kotanides, H., Witte, L., Waltenberger, J., Landry, J., and Huot, J. (2000). Vascular endothelial growth factor (VEGF)-driven actin-based motility is mediated by VEGFR2 and requires concerted activation of stress-activated protein kinase 2 (SAPK2/p38) and geldanamycin-sensitive phosphorylation of focal adhesion kinase. J Biol Chem *275*, 10661-10672.

Rousseau, S., Houle, F., Landry, J., and Huot, J. (1997). p38 MAP kinase activation by vascular endothelial growth factor mediates actin reorganization and cell migration in human endothelial cells. Oncogene *15*, 2169-2177.

Ruocco, V., Ruocco, E., Schwartz, R.A., and Janniger, C.K. (2011). Kaposi sarcoma and quinine: a potentially overlooked triggering factor in millions of Africans. J Am Acad Dermatol *64*, 434-436.

Russo, J.J., Bohenzky, R.A., Chien, M.C., Chen, J., Yan, M., Maddalena, D., Parry, J.P., Peruzzi, D., Edelman, I.S., Chang, Y.*, et al.* (1996). Nucleotide sequence of the Kaposi sarcoma-associated herpesvirus (HHV8). Proc Natl Acad Sci U S A *93*, 14862-14867.

Sadagopan, S., Sharma-Walia, N., Veettil, M.V., Bottero, V., Levine, R., Vart, R.J., and Chandran, B. (2009). Kaposi's sarcoma-associated herpesvirus upregulates angiogenin during infection of human dermal microvascular endothelial cells, which induces 45S rRNA synthesis, antiapoptosis, cell proliferation, migration, and angiogenesis. J Virol *83*, 3342-3364.

Sadagopan, S., Sharma-Walia, N., Veettil, M.V., Raghu, H., Sivakumar, R., Bottero, V., and Chandran, B. (2007). Kaposi's sarcoma-associated herpesvirus induces sustained NF-kappaB activation during de novo infection of primary human dermal microvascular endothelial cells that is essential for viral gene expression. J Virol *81*, 3949-3968.

Said, J.W., Chien, K., Tasaka, T., and Koeffler, H.P. (1997). Ultrastructural characterization of human herpesvirus 8 (Kaposi's sarcoma-associated herpesvirus) in Kaposi's sarcoma lesions: electron microscopy permits distinction from cytomegalovirus (CMV). J Pathol *182*, 273-281.

Salcedo, R., Resau, J.H., Halverson, D., Hudson, E.A., Dambach, M., Powell, D., Wasserman, K., and Oppenheim, J.J. (2000). Differential expression and responsiveness of chemokine receptors (CXCR1-3) by human microvascular endothelial cells and umbilical vein endothelial cells. FASEB J *14*, 2055-2064.

Sarwar, N., Stebbing, J., and Bower, M. (2007). Translational review of AIDS-related Kaposi's sarcoma. Update on Caner Therapeutics *2*, 53-60.

Schalling, M., Ekman, M., Kaaya, E.E., Linde, A., and Biberfeld, P. (1995). A role for a new herpes virus (KSHV) in different forms of Kaposi's sarcoma. Nat Med *1*, 707-708.

Schraufstatter, I.U., Trieu, K., Zhao, M., Rose, D.M., Terkeltaub, R.A., and Burger, M. (2003). IL-8-mediated cell migration in endothelial cells depends on cathepsin B activity and transactivation of the epidermal growth factor receptor. J Immunol *171*, 6714-6722.

Schulte-Merker, S., Sabine, A., and Petrova, T.V. (2011). Lymphatic vascular morphogenesis in development, physiology, and disease. J Cell Biol *193*, 607-618.

Schulz, T.F. (2006). The pleiotropic effects of Kaposi's sarcoma herpesvirus. J Pathol *208*, 187-198.

Schwarzbauer, J. (1999). Basement membranes: Putting up the barriers. Curr Biol *9*, R242-244.

Sehgal, B.U., DeBiase, P.J., Matzno, S., Chew, T.L., Claiborne, J.N., Hopkinson, S.B., Russell, A., Marinkovich, M.P., and Jones, J.C. (2006). Integrin beta4 regulates migratory behavior of keratinocytes by determining laminin-332 organization. J Biol Chem *281*, 35487-35498.

Senger, D.R., Perruzzi, C.A., Streit, M., Koteliansky, V.E., de Fougerolles, A.R., and Detmar, M. (2002). The alpha(1)beta(1) and alpha(2)beta(1) integrins provide critical support for vascular endothelial growth factor signaling, endothelial cell migration, and tumor angiogenesis. Am J Pathol *160*, 195-204.

Serra-Pages, C., Kedersha, N.L., Fazikas, L., Medley, Q., Debant, A., and Streuli, M. (1995). The LAR transmembrane protein tyrosine phosphatase and a coiled-coil LAR-interacting protein co-localize at focal adhesions. EMBO J *14*, 2827-2838.

Serrels, B., Serrels, A., Brunton, V.G., Holt, M., McLean, G.W., Gray, C.H., Jones, G.E., and Frame, M.C. (2007). Focal adhesion kinase controls actin assembly via a FERM-mediated interaction with the Arp2/3 complex. Nat Cell Biol *9*, 1046-1056.

Sharma-Walia, N., Krishnan, H.H., Naranatt, P.P., Zeng, L., Smith, M.S., and Chandran, B. (2005). ERK1/2 and MEK1/2 induced by Kaposi's sarcoma-associated herpesvirus (human herpesvirus 8) early during infection of target cells are essential for expression of viral genes and for establishment of infection. J Virol *79*, 10308-10329.

Sharma-Walia, N., Naranatt, P.P., Krishnan, H.H., Zeng, L., and Chandran, B. (2004). Kaposi's sarcoma-associated herpesvirus/human herpesvirus 8 envelope glycoprotein gB induces the integrin-dependent focal adhesion kinase-Src-phosphatidylinositol 3-kinase-rho GTPase signal pathways and cytoskeletal rearrangements. J Virol *78*, 4207-4223.

Sheldon, H., Andre, M., Legg, J.A., Heal, P., Herbert, J.M., Sainson, R., Sharma, A.S., Kitajewski, J.K., Heath, V.L., and Bicknell, R. (2009). Active involvement of Robo1 and Robo4 in filopodia formation and endothelial cell motility mediated via WASP and other actin nucleation-promoting factors. FASEB J *23*, 513-522.

Singh, P., Carraher, C., and Schwarzbauer, J.E. (2010). Assembly of fibronectin extracellular matrix. Annu Rev Cell Dev Biol *26*, 397-419.

Sirianni, M.C., Uccini, S., Angeloni, A., Faggioni, A., Cottoni, F., and Ensoli, B. (1997). Circulating spindle cells: correlation with human herpesvirus-8 (HHV-8) infection and Kaposi's sarcoma. Lancet *349*, 255.

Sivakumar, R., Sharma-Walia, N., Raghu, H., Veettil, M.V., Sadagopan, S., Bottero, V., Varga, L., Levine, R., and Chandran, B. (2008). Kaposi's sarcoma-associated herpesvirus induces sustained levels of vascular endothelial growth factors A and C early during in vitro infection of human microvascular dermal endothelial cells: biological implications. J Virol *82*, 1759-1776.

Sixt, M., Engelhardt, B., Pausch, F., Hallmann, R., Wendler, O., and Sorokin, L.M. (2001). Endothelial cell laminin isoforms, laminins 8 and 10, play decisive roles in T cell recruitment across the blood-brain barrier in experimental autoimmune encephalomyelitis. J Cell Biol *153*, 933-946.

Skobe, M., Brown, L.F., Tognazzi, K., Ganju, R.K., Dezube, B.J., Alitalo, K., and Detmar, M. (1999). Vascular endothelial growth factor-C (VEGF-C) and its receptors KDR and flt-4 are expressed in AIDS-associated Kaposi's sarcoma. J Invest Dermatol *113*, 1047-1053.

Small, J.V., Geiger, B., Kaverina, I., and Bershadsky, A. (2002). How do microtubules guide migrating cells? Nat Rev Mol Cell Biol *3*, 957-964.

Smith, J.T., Elkin, J.T., and Reichert, W.M. (2006). Directed cell migration on fibronectin gradients: effect of gradient slope. Exp Cell Res *312*, 2424-2432.

Smith, J.T., Tomfohr, J.K., Wells, M.C., Beebe, T.P., Jr., Kepler, T.B., and Reichert, W.M. (2004). Measurement of cell migration on surface-bound fibronectin gradients. Langmuir *20*, 8279-8286.

Sodhi, A., Montaner, S., Patel, V., Zohar, M., Bais, C., Mesri, E.A., and Gutkind, J.S. (2000). The Kaposi's sarcoma-associated herpes virus G protein-coupled receptor up-regulates vascular endothelial growth factor expression and secretion through mitogen-activated protein kinase and p38 pathways acting on hypoxia-inducible factor 1alpha. Cancer Res *60*, 4873-4880.

Springer, T.A. (1995). Traffic signals on endothelium for lymphocyte recirculation and leukocyte emigration. Annu Rev Physiol *57*, 827-872.

Springer, T.A., and Wang, J.H. (2004). The three-dimensional structure of integrins and their ligands, and conformational regulation of cell adhesion. Adv Protein Chem *68*, 29-63.

Stanton, R.J., McSharry, B.P., Rickards, C.R., Wang, E.C., Tomasec, P., and Wilkinson, G.W. (2007). Cytomegalovirus destruction of focal adhesions revealed in a high-throughput Western blot analysis of cellular protein expression. J Virol *81*, 7860-7872.

Staskus, K.A., Zhong, W., Gebhard, K., Herndier, B., Wang, H., Renne, R., Beneke, J., Pudney, J., Anderson, D.J., Ganem, D.*, et al.* (1997). Kaposi's sarcoma-associated herpesvirus gene expression in endothelial (spindle) tumor cells. J Virol *71*, 715-719.

Streblow, D.N., Soderberg-Naucler, C., Vieira, J., Smith, P., Wakabayashi, E., Ruchti, F., Mattison, K., Altschuler, Y., and Nelson, J.A. (1999). The human cytomegalovirus chemokine receptor US28 mediates vascular smooth muscle cell migration. Cell *99*, 511-520.

Strieter, R.M., Polverini, P.J., Arenberg, D.A., and Kunkel, S.L. (1995). The role of CXC chemokines as regulators of angiogenesis. Shock *4*, 155-160.

Stupack, D.G., and Cheresh, D.A. (2002). ECM remodeling regulates angiogenesis: endothelial integrins look for new ligands. Sci STKE *2002*, pe7.

Su, I.-J., Hsu, Y.-S., Chang, Y.-C., and Wang, I.W. (1995). Herpesvirus-like DNA sequence in Kaposi's sarcoma from AIDS and non-AIDS patients in Taiwan. The Lancet *345*, 722-723.

Sumpio, B.E., Riley, J.T., and Dardik, A. (2002). Cells in focus: endothelial cell. Int J Biochem Cell Biol *34*, 1508-1512.

Sund, M., Xie, L., and Kalluri, R. (2004). The contribution of vascular basement membranes and extracellular matrix to the mechanics of tumor angiogenesis. APMIS *112*, 450-462.

Tabata, T., Kawakatsu, H., Maidji, E., Sakai, T., Sakai, K., Fang-Hoover, J., Aiba, M., Sheppard, D., and Pereira, L. (2008). Induction of an epithelial integrin alphavbeta6 in human cytomegalovirus-infected endothelial cells leads to activation of transforming growth factor-beta1 and increased collagen production. Am J Pathol *172*, 1127-1140.

Tanaka, K., Abe, M., and Sato, Y. (1999). Roles of extracellular signal-regulated kinase 1/2 and p38 mitogen-activated protein kinase in the signal transduction of basic fibroblast growth factor in endothelial cells during angiogenesis. Jpn J Cancer Res *90*, 647-654.

Tomar, A., and Schlaepfer, D.D. (2009). Focal adhesion kinase: switching between GAPs and GEFs in the regulation of cell motility. Curr Opin Cell Biol *21*, 676-683.

Touloumi, G., Hatzakis, A., Potouridou, I., Milona, I., Strarigos, J., Katsambas, A., Giraldo, G., Beth-Giraldo, E., Biggar, R.J., Mueller, N., *et al.* (1999). The role of immunosuppression and immune-activation in classic Kaposi's sarcoma. Int J Cancer *82*, 817-821.

Trus, B.L., Heymann, J.B., Nealon, K., Cheng, N., Newcomb, W.W., Brown, J.C., Kedes, D.H., and Steven, A.C. (2001). Capsid structure of Kaposi's sarcoma-associated herpesvirus, a gammaherpesvirus, compared to those of an alphaherpesvirus, herpes simplex virus type 1, and a betaherpesvirus, cytomegalovirus. J Virol *75*, 2879-2890.

Tsai, Y.H., Wu, M.F., Wu, Y.H., Chang, S.J., Lin, S.F., Sharp, T.V., and Wang, H.W. (2009). The M type K15 protein of Kaposi's sarcoma-associated herpesvirus regulates microRNA expression via its SH2-binding motif to induce cell migration and invasion. J Virol *83*, 622-632.

Tsuda, M., Matozaki, T., Fukunaga, K., Fujioka, Y., Imamoto, A., Noguchi, T., Takada, T., Yamao, T., Takeda, H., Ochi, F., *et al.* (1998). Integrin-mediated tyrosine phosphorylation of SHPS-1 and its association with SHP-2. Roles of Fak and Src family kinases. J Biol Chem *273*, 13223-13229.

Tull, S.P., Yates, C.M., Maskrey, B.H., O'Donnell, V.B., Madden, J., Grimble, R.F., Calder, P.C., Nash, G.B., and Rainger, G.E. (2009). Omega-3 Fatty acids and inflammation: novel interactions reveal a new step in neutrophil recruitment. PLoS Biol *7*, e1000177.

Tzu, J., and Marinkovich, M.P. (2008). Bridging structure with function: structural, regulatory, and developmental role of laminins. Int J Biochem Cell Biol *40*, 199-214.

Uccini, S., Scarpino, S., Ballarini, F., Soriani, A., Chilosi, M., Montesu, M.A., Masala, M.V., Cottoni, F., and Ruco, L. (2003). In situ study of chemokine and chemokine-receptor expression in Kaposi sarcoma. Am J Dermatopathol *25*, 377-383.

Uldrick, T.S., and Whitby, D. (2011). Update on KSHV epidemiology, Kaposi Sarcoma pathogenesis, and treatment of Kaposi Sarcoma. Cancer Lett *305*, 150-162.

Vart, R.J., Nikitenko, L.L., Lagos, D., Trotter, M.W.B., Cannon, M., Bourboulia, D., Gratrix, F., Takeuchi, Y., and Boshoff, C. (2007). Kaposi's sarcoma-associated herpesvirus-encoded interleukin-6 and G-protein-coupled receptor regulate angiopoietin-2 expression in lymphatic endothelial cells. Cancer Research *67*, 4042-4051.

Verma, S.C., and Robertson, E.S. (2003). Molecular biology and pathogenesis of Kaposi sarcoma-associated herpesvirus. FEMS Microbiol Lett *222*, 155-163.

Vernon, R.B., and Sage, E.H. (1995). Between molecules and morphology. Extracellular matrix and creation of vascular form. Am J Pathol *147*, 873-883.

Vieira, J., Huang, M.L., Koelle, D.M., and Corey, L. (1997). Transmissible Kaposi's sarcoma-associated herpesvirus (human herpesvirus 8) in saliva of men with a history of Kaposi's sarcoma. J Virol *71*, 7083-7087.

Vieira, J., O'Hearn, P., Kimball, L., Chandran, B., and Corey, L. (2001). Activation of Kaposi's sarcoma-associated herpesvirus (human herpesvirus 8) lytic replication by human cytomegalovirus. J Virol *75*, 1378-1386.

Vieira, J., and O'Hearn, P.M. (2004). Use of the red fluorescent protein as a marker of Kaposi's sarcoma-associated herpesvirus lytic gene expression. Virology *325*, 225-240.

Vinals, F., and Pouyssegur, J. (1999). Confluence of vascular endothelial cells induces cell cycle exit by inhibiting p42/p44 mitogen-activated protein kinase activity. Mol Cell Biol *19*, 2763-2772.

Visse, R., and Nagase, H. (2003). Matrix metalloproteinases and tissue inhibitors of metalloproteinases: structure, function, and biochemistry. Circ Res *92*, 827-839.

Wakeham, K., Webb, E.L., Sebina, I., Muhangi, L., Miley, W., Johnson, W.T., Ndibazza, J., Elliott, A.M., Whitby, D., and Newton, R. (2011). Parasite infection is associated with Kaposi's sarcoma associated herpesvirus (KSHV) in Ugandan women. Infect Agent Cancer *6*, 15.

Wang, F.Z., Akula, S.M., Pramod, N.P., Zeng, L., and Chandran, B. (2001). Human herpesvirus 8 envelope glycoprotein K8.1A interaction with the target cells involves heparan sulfate. J Virol *75*, 7517-7527.

Wang, H.W., Trotter, M.W., Lagos, D., Bourboulia, D., Henderson, S., Makinen, T., Elliman, S., Flanagan, A.M., Alitalo, K., and Boshoff, C. (2004a). Kaposi sarcoma herpesvirus-induced cellular reprogramming contributes to the lymphatic endothelial gene expression in Kaposi sarcoma. Nat Genet *36*, 687-693.

Wang, L., Wakisaka, N., Tomlinson, C.C., DeWire, S.M., Krall, S., Pagano, J.S., and Damania, B. (2004b). The Kaposi's sarcoma-associated herpesvirus (KSHV/HHV-8) K1 protein induces expression of angiogenic and invasion factors. Cancer Res *64*, 2774-2781.

Wegener, K.L., Basran, J., Bagshaw, C.R., Campbell, I.D., Roberts, G.C., Critchley, D.R., and Barsukov, I.L. (2008). Structural basis for the interaction between the cytoplasmic domain of the hyaluronate receptor layilin and the talin F3 subdomain. J Mol Biol *382*, 112-126.

Wei, Y., Yang, X., Liu, Q., Wilkins, J.A., and Chapman, H.A. (1999). A role for caveolin and the urokinase receptor in integrin-mediated adhesion and signaling. J Cell Biol *144*, 1285-1294.

Weis, S.M., and Cheresh, D.A. (2011). Tumor angiogenesis: molecular pathways and therapeutic targets. Nat Med *17*, 1359-1370.

Wen, K.W., and Damania, B. (2010). Kaposi sarcoma-associated herpesvirus (KSHV): molecular biology and oncogenesis. Cancer Lett *289*, 140-150.

Weninger, W., Partanen, T.A., Breiteneder-Geleff, S., Mayer, C., Kowalski, H., Mildner, M., Pammer, J., Sturzl, M., Kerjaschki, D., Alitalo, K.*, et al.* (1999). Expression of vascular

endothelial growth factor receptor-3 and podoplanin suggests a lymphatic endothelial cell origin of Kaposi's sarcoma tumor cells. Lab Invest *79*, 243-251.

Whitby, D., Luppi, M., Barozzi, P., Boshoff, C., Weiss, R.A., and Torelli, G. (1998). Human herpesvirus 8 seroprevalence in blood donors and lymphoma patients from different regions of Italy. J Natl Cancer Inst *90*, 395-397.

Winkler, E.A., Bell, R.D., and Zlokovic, B.V. (2011). Central nervous system pericytes in health and disease. Nat Neurosci *14*, 1398-1405.

Wolfenson, H., Henis, Y.I., Geiger, B., and Bershadsky, A.D. (2009). The heel and toe of the cell's foot: a multifaceted approach for understanding the structure and dynamics of focal adhesions. Cell Motil Cytoskeleton *66*, 1017-1029.

Wondimu, Z., Geberhiwot, T., Ingerpuu, S., Juronen, E., Xie, X., Lindbom, L., Doi, M., Kortesmaa, J., Thyboll, J., Tryggvason, K.*, et al.* (2004). An endothelial laminin isoform, laminin 8 (alpha4beta1gamma1), is secreted by blood neutrophils, promotes neutrophil migration and extravasation, and protects neutrophils from apoptosis. Blood *104*, 1859-1866.

Wu, L., Lo, P., Yu, X., Stoops, J.K., Forghani, B., and Zhou, Z.H. (2000). Three-dimensional structure of the human herpesvirus 8 capsid. J Virol *74*, 9646-9654.

Xie, J., Pan, H., Yoo, S., and Gao, S.J. (2005). Kaposi's sarcoma-associated herpesvirus induction of AP-1 and interleukin 6 during primary infection mediated by multiple mitogen-activated protein kinase pathways. J Virol *79*, 15027-15037.

Yakushko, Y., Hackmann, C., Gunther, T., Ruckert, J., Henke, M., Koste, L., Alkharsah, K., Bohne, J., Grundhoff, A., Schulz, T.F.*, et al.* (2011). Kaposi's sarcoma-associated herpesvirus bacterial artificial chromosome contains a duplication of a long unique-region fragment within the terminal repeat region. J Virol *85*, 4612-4617.

Ye, F.C., Blackbourn, D.J., Mengel, M., Xie, J.P., Qian, L.W., Greene, W., Yeh, I.T., Graham, D., and Gao, S.J. (2007). Kaposi's sarcoma-associated herpesvirus promotes angiogenesis by inducing angiopoietin-2 expression via AP-1 and Ets1. J Virol *81*, 3980-3991.

Yurchenco, P.D., Quan, Y., Colognato, H., Mathus, T., Harrison, D., Yamada, Y., and O'Rear, J.J. (1997). The alpha chain of laminin-1 is independently secreted and drives secretion of its beta- and gamma-chain partners. Proc Natl Acad Sci U S A *94*, 10189-10194.

Yurchenco, P.D., and Ruben, G.C. (1987). Basement membrane structure in situ: evidence for lateral associations in the type IV collagen network. J Cell Biol *105*, 2559-2568.

Zamir, E., and Geiger, B. (2001). Molecular complexity and dynamics of cell-matrix adhesions. J Cell Sci *114*, 3583-3590.

Zeng, Z.S., Cohen, A.M., and Guillem, J.G. (1999). Loss of basement membrane type IV collagen is associated with increased expression of metalloproteinases 2 and 9 (MMP-2 and MMP-9) during human colorectal tumorigenesis. Carcinogenesis *20*, 749-755.

Zhong, W., Wang, H., Herndier, B., and Ganem, D. (1996). Restricted expression of Kaposi sarcoma-associated herpesvirus (human herpesvirus 8) genes in Kaposi sarcoma. Proc Natl Acad Sci U S A *93*, 6641-6646.

Zhou, F.C., Zhang, Y.J., Deng, J.H., Wang, X.P., Pan, H.Y., Hettler, E., and Gao, S.J. (2002). Efficient infection by a recombinant Kaposi's sarcoma-associated herpesvirus cloned in a bacterial artificial chromosome: application for genetic analysis. J Virol *76*, 6185-6196.

Zhu, F.X., Chong, J.M., Wu, L., and Yuan, Y. (2005). Virion proteins of Kaposi's sarcoma-associated herpesvirus. J Virol *79*, 800-811.

Ziegler, J., Newton, R., Bourboulia, D., Casabonne, D., Beral, V., Mbidde, E., Carpenter, L., Reeves, G., Parkin, D.M., Wabinga, H., *et al.* (2003). Risk factors for Kaposi's sarcoma: a case-control study of HIV-seronegative people in Uganda. Int J Cancer *103*, 233-240.

Ziegler, J.L. (1993). Endemic Kaposi's sarcoma in Africa and local volcanic soils. Lancet *342*, 1348-1351.

Ziegler, J.L., Newton, R., Katongole-Mbidde, E., Mbulataiye, S., De Cock, K., Wabinga, H., Mugerwa, J., Katabira, E., Jaffe, H., Parkin, D.M., *et al.* (1997). Risk factors for Kaposi's sarcoma in HIV-positive subjects in Uganda. AIDS *11*, 1619-1626.